UNIVERSITY OF CALIFORNIA,
IRVINE

Elucidating the Mechanism of Action of Teixobactin

DISSERTATION

submitted in partial satisfaction of the requirements
for the degree of

DOCTOR OF PHILOSOPHY

in Chemistry

by

Hyunjun Yang

Dissertation Committee:
Professor James S. Nowick, Chair
Professor Gregory A. Weiss
Professor Vy M. Dong

2019

DEDICATION

To

my parents Nam Young Yang and Young Sil Yoo
my parents-in-law Seong Yun Lee and Song Sik Son
my wife Ahleum Lee
and
my two beautiful children Arthur (Ian) Yang and Elizabeth (Ina) Yang

I truly appreciate you all for your unconditional love and support.

TABLE OF CONTENTS

LIST OF FIGURES

LIST OF TABLES

LIST OF SCHEMES

ACKNOWLEDGMENTS

From the bottom of my heart, I appreciate you James for your immense energy and precious time you had put in to raise me as an adult in and out of your laboratory. I do not think I can describe this appreciation using words and pictures, and I challenge myself to give a try here.

My hook for peptide chemistry was during biochemistry class at University of Wisconsin-Madison, where Prof. David Nelson gave a lecture on solid-phase peptide synthesis. He got me thinking I could synthesize a whole protein with organic chemistry which was a cool feeling. I searched for a laboratory routinely synthesizing peptides and emailed Prof. Sam Gellman, who forwarded the emailed to Dr. Younghee Shin, who was kind enough to provide me with a position. Thank you Sam, for providing a top class environment for studying peptides, and Younghee, for providing me a solid hands-on training on SPPS. My time at Gellman group has become the blueprint of my PhD training. My hook for amyloidogenic peptides was from a seminar on amyloidogenic peptides given by Prof. David Eisenberg. Intrigued by the assembly, I asked Sam about stabilizing the protein through β-sheet peptide interaction and Sam right away printed three papers from Nowick laboratory and I was lucky enough to get into UC-Irvine for graduate chemistry program.

Thinking back five years ago, I walked into Nowick laboratory as a naïve but ambitious young man, who later married perfect woman, later had two beautiful children, and is now heading off to start a career that James paved every inch for. I am so sorry that you had to pave such a large amount and every inch of it. First of all, I appreciate James for being there for me whenever I had questions or findings. Conversation with James would excite me as I progress and was the energy source for doing science every day. Second of all, I appreciate your intellectual insights and your time to share what your thoughts are. In terms of research, there were a handful of times where I was in a dark room and James would pull out his magic green laser pointer and pin point where I need to go. I wish I could hide your magic green laser pointer in my pocket. Lastly, coping with my personality and style. Studying abroad alone at a young age, I have developed very straight forward and strong personality that sometimes maybe difficult to handle. You were never angry at me and were always supportive. Thank you. As I will be representing you and your laboratory, I will always act right and provide help in the areas that need help.

Thank you, colleagues. You all made coming to lab everyday fun. I want to especially thank Drs. Kevin Chen, Adam Kreutzer, and Michał Wierzbicki for their time listening to my random ideas and thoughts I had throughout my time in the Nowick lab. I also thank Derek Du Bois, Arthur Pishenko, Alexander Kvitsinski, and Max Lumetzberger for their time working with me.

I would like to appreciate my thesis committee Prof. Greg Weiss and Prof. Vy Dong. Prof. Weiss would ask me sharp and philosophical questions that left thoughts and insights for my next step forward. Prof. Dong would approach me with kindness and ask how I am doing in terms of life and research.

Thank you, Mom and Dad. My education since year 2000 was very expensive, and it is finally over. Your love, encouragement, and support have played an immeasurable role in getting me to this point.

I thank my wife, Ahleum, for always supporting, loving, and being the best wife and mother of our two children. Although we were not lavish and rich, I think we sailed smoothly in Irvine and I am always looking forward to sail the rest of my life with you. Thank you.

CURRICULUM VITAE

Hyunjun Yang

Department of Chemistry
1102 Natural Sciences 2
University of California Irvine
Irvine, CA 92697-2025

Email: peptidelinks@gmail.com

EDUCATIONS

Ph.D., Chemistry, University of California-Irvine, 2014–2019

B.S., Biochemistry, University of Wisconsin-Madison, 2008–2013

RESEARCH EXPERIENCES

2014–2019 Graduate Student Researcher with Professor and Department Chair James S. Nowick. *University of California-Irvine*.

2012–2014 Undergraduate Researcher with Professor Samuel H. Gellman. *University of Wisconsin-Madison*.

AWARDS

2019 Allergan Graduate Fellowship in Synthetic Organic Chemistry. *University of California, Irvine*

2019 American Peptide Symposium Peptide Science Poster Prize. *Monterey, CA*.

PROFESSIONAL MEMBERSHIPS

American Chemical Society
American Peptide Society

POSTERS AND TALKS

5. **Yang, H.**; Nowick, J. S. "Using X-ray Crystallographic Structure of a Teixobactin Derivative to Probe the Mechanism of Action of Teixobactin" Presented at the 26th American Peptide Symposium, Monterey, CA. June 26, 2019.
4. **Yang, H.**; Nowick, J. S. "Efforts to Elucidate the Mechanism of Action for Teixobactin to Design Next-Generation Teixobactin Analogues" Presented at the SCBC Symposium, Irvine, CA. July 27, 2018.
3. **Yang, H.**; Nowick, J. S. "Elucidation of the Teixobactin Pharmacophore" Presented at the Graduate Research Symposium, Irvine, CA. Feb 9, 2018.
2. **Yang, H.**; Du Bois, D. R.; Ziller, J. W.; Nowick, J. S. "X-ray Crystallographic Structures of Teixobactin Analogues" Presented at the 253rd National Meeting of the American Chemical Society, San Francisco, CA. April 2-6, 2017; paper MEDI 390.
1. **Yang, H.**; Chen, K. H.; Nowick, J. S. "Lipobactins: A New Class of Antibiotics Against Gram-Positive Bacteria" Presented at the 252nd National Meeting of the American Chemical Society, Philadelphia, PA. August 21-25, 2016; paper MEDI 352.

PATENTS

1. **Yang, H.**; Nowick, J. S. "Synthesis of Lipobactins and Teixobactin Analogues – New Antimicrobial Compositions against Gram-Positive Bacteria" WO2017181179A1.

PUBLICATIONS

4. **Yang, H.**; Pishenko, A. V.; Li, X. Y.; Nowick, J. S. "Design, Synthesis, and Study of Lactam and Ring-Expanded Analogues of Teixobactin" **2019**, *Submitted*.
3. **Yang, H.**; Wierzbicki, M.; Du Bois, D. R.; Nowick, J. S. "X-ray Crystallographic Structure Suggests Amyloid-Like Assembly May Be Critical to the Antibiotic Activity of Teixobactin" *J. Am. Chem. Soc.* **2018**, *140*, 14028–14032. doi: 10.1021/jacs.8b07709
2. **Yang, H.**; Du Bois, D. R.; Ziller, J. W.; Nowick, J. S. "X-ray Crystallographic Structure of a Teixobactin Analogue Reveals Key Interactions of the Teixobactin Pharmacophore" *Chem. Commun.* **2017**, *53*, 2772–2775. doi: 10.1039/c7cc00783c
1. **Yang, H.**; Chen, K. H.; Nowick, J. S. "Elucidation of Teixobactin Pharmacophore" *ACS Chem. Biol.* **2016**, *11*, 1823–1826. doi: 10.1021/acschembio.6b00295

ABSTRACT OF THE DISSERTATION

Elucidating the Mechanism of Action of Teixobactin
By

Hyunjun Yang

Doctor of Philosophy in Chemistry

University of California, Irvine

2019

Professor James S. Nowick, Chair

This dissertation work is centered on understanding the structure and mechanism of action of the peptide antibiotic, teixobactin. Each chapter shares the themes of understanding the molecular recognition and supramolecular assembly of teixobactin. Each chapter shares the approach of chemical design, organic synthesis, and solution-/solid-phase study.

Chapter 1 provides an overview of the field of teixobactin and provides context for the work described in this dissertation.

Chapter 2 explores an on-resin synthesis of teixobactin analogues to enable structure-activity relationship studies.

This chapter elucidates the teixobactin pharmacophore by comparing the arginine analogue of teixobactin Arg_{10}-teixobactin to seven homologues with varying structure and stereochemistry. The roles of the guanidinium group at position 10, the stereochemistry of the macrolactone ring, and the "tail" comprising residues 1–5 are investigated. The guanidinium group is not necessary for activity; Lys_{10}-teixobactin is more active than Arg_{10}-teixobactin against gram-positive bacteria in minimum inhibitory concentration (MIC) assays. The relative stereochemistry of the macrolactone ring is important; diastereomer L-Thr_8,Arg_{10}-teixobactin is inactive, and diastereomer D-*allo*-Ile_{11},Arg_{10}-teixobactin is less active. The macrolactone ring is critical; *seco*-Arg_{10}-teixobactin is inactive. The absolute stereochemistry is not important; the enantiomer *ent*-Arg_{10}-teixobactin is comparable in activity. The hydrophobic *N*-terminal tail is important; truncation of residues 1–5 results in loss of activity, and replacement of residues 1–5 with a dodecanoyl group partially restores activity. These findings pave the way for developing simpler homologues of teixobactin with enhanced pharmacological properties.

Chapter 3 explores the key interactions of the teixobactin pharmacophore using X-ray crystallography.

The X-ray crystallographic structure of a truncated teixobactin analogue reveals hydrogen-bonding and hydrophobic interactions and a cavity that binds a chloride anion. In the binding cavity, the carbonyl groups of D-Thr$_8$, Ala$_9$, Arg$_{10}$, and Ile$_{11}$ in the cyclic depsipeptide ring point upward, while the amide NH groups of Ala$_9$, Arg$_{10}$, and Ile$_{11}$ point toward the anion binding site. Mininmum inhibitory concentration (MIC) assays against Gram-positive bacteria correlate the observed structure with antibiotic activity.

Chapter 4 explores the supramolecular assembly and amyloid-like characteristic of teixobactin using gelation assay, ThT fluorescence assay, TEM, and X-ray crystallography.

This chapter describes the X-ray crystallographic structure of a derivative of the antibiotic teixobactin which suggests that supramolecular assembly through the formation of antiparallel β-sheets is integral to the antibiotic activity of teixobactin. An active derivative of teixobactin containing lysine in place of *allo*-enduracididine assembles to form amyloid-like fibrils, which are observed through a thioflavin T fluorescence assay and by transmission electron microscopy. A homologue, bearing an *N*-methyl substituent, to attenuate fibril formation, and an iodine atom, to facilitate X-ray crystallographic phase determination, crystallizes as double helices of β-sheets that bind sulfate anions. β-Sheet dimers are key subunits of these assemblies, with the *N*-terminal methylammonium group of one monomer and the *C*-terminal macrocycle of the other monomer binding each anion. These observations suggest a mechanism of action for teixobactin, in which the antibiotic assembles and the assemblies bind lipid II and related bacterial cell wall precursors on the surface of Gram-positive bacteria.

Chapter 5 explores the design, synthesis, and study two sets of teixobactin analogues providing further insights of supramolecular assembly and molecular recognition of teixobactin.

This paper describes the chemical synthesis, X-ray crystallography, and antibiotic activity assay of lactam teixobactin analogues and explores ring-expanded analogues of teixobactin with beta homo amino acids. Lactam teixobactin analogues containing all stereoisomers of azathreonine at position 8 is synthesized on a solid-support. In minimum inhibitory concentration (MIC) assay, D-aza-Thr$_8$,Arg$_{10}$-teixobactin exhibits 2–8 fold increase in activity when compared to the corresponding macrolactone Arg$_{10}$-teixobactin. Other stereoisomers of aza-threonine containing teixobactin are inactive. A dramatic 16-128 fold increase in the activity of teixobactin and teixobactin analogues is observed with the inclusion of a mild detergent 0.002% polysorbate 80 in broth during MIC assay. In the X-ray crystallographic structure of *N*-Me-D-Gln$_4$,D-aza-Thr$_8$,Arg$_{10}$-teixobactin, *N*-methyl variant of D-aza-Thr$_8$,Arg$_{10}$-teixobactin, reveals an amphipathic hydrogen-bonded antiparallel β-sheet dimer that bind chloride anions. In the binding site of chloride anion, the macrolactam amide NH groups of residues 8, 10, and 11, as well as, the extra amide NH group of the lactam ring hydrogen bond to the chloride anion. Teixobactin pharmacophore tolerates 13-membered ring expansion to 14-,15-, and 16-membered ring containing beta homo amino acids with retention of activity, but no enhancement of antibiotic activity is observed.

Chapter 1
Teixobactin, a new promising peptide antibiotic

Introduction

Antibiotic-resistant bacteria cause more than 2 million illnesses and 23,000 deaths in the US each year, with direct overall societal costs of about $20 billion and additional indirect societal costs of about $35 billion due to lost productivity (**Figure 1.1**).[1,2] Gram-positive pathogens — including methicillin-resistant *Staphylococcus aureus* (MRSA), vancomycin-resistant *Enterococci* (VRE), antibiotic-resistant *Streptococcus pneumoniae,* and four others — cause more than 65% and 87% of these illnesses and deaths. *Clostridium difficile* (*C. difficile*) causes more than 250,000 illnesses and 14,000 deaths per year. *Mycobacterium tuberculosis* causes tuberculosis and is one of the top ten causes of death worldwide.[3]

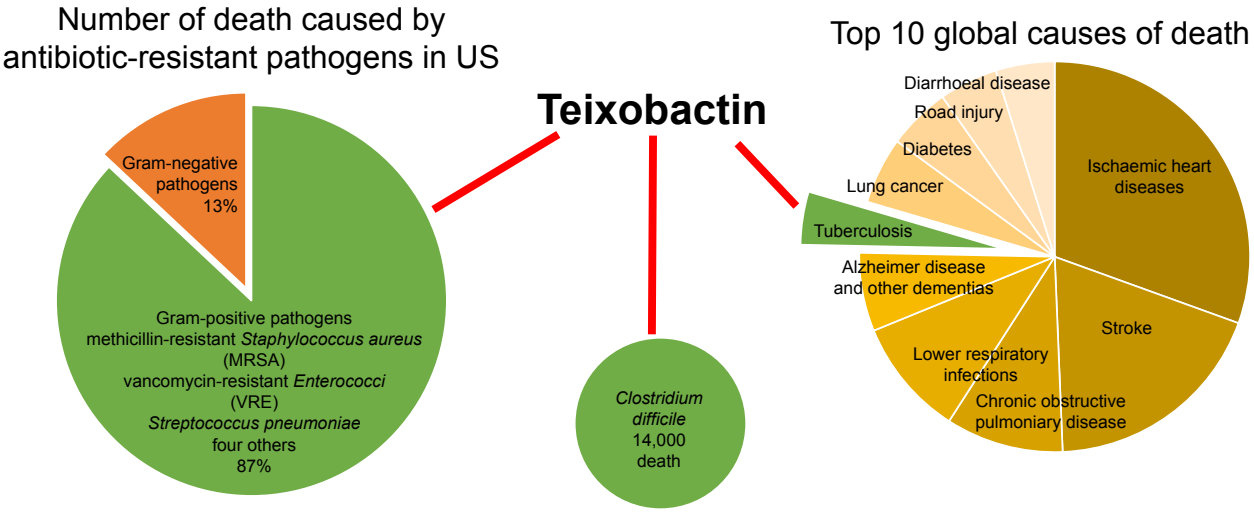

Figure 1.1. Deaths cause by antibiotic-resistant pathogens in US and pathogens in the world. Teixobactin is effective against Gram-positive and related pathogens shown in green.

The emergence of antibiotic resistance and the paucity of effective antibiotics against multidrug-resistant (MDR) Gram-positive pathogens demonstrates an unmet need for the development of new antibiotics that overcome these problems. However, the development of

new antibiotics has greatly dropped during the past three decades.[1] The dramatic attenuation of antibiotic advancement leaves the medical community with fewer options to treat the growing threat of antibiotic-resistant pathogens. In addition, bacterial resistance is even emerging against recently approved antibiotics, such as tigecycline (2005), doripenem (2007), and ceftaroline (2010).[4,5,6] The fight against bacterial pathogens is ongoing, and the new antibiotics will always be needed.

Antibiotic resistance among bacteria leads to increased human morbidity and mortality. Conventional *S. aureus* can be treated with oxacillin, a β-lactam antibiotic with excellent bactericidal activity. MRSA is generally treated by the intravenous administration of vancomycin, but clinical failure for such infections has been linked to poor bactericidal activity of the compound.[7,8] While daptomycin has excellent bactericidal activity, it cannot be used against common lung infections and has considerable toxicity. Low-level, but clinically significant resistance is common for both vancomycin and daptomycin, which presents an additional problem. The most advanced and promising approaches to antibiotic resistance are a therapeutic antibody that neutralizes MRSA alpha toxin (Medimmune/Astra Zeneca) and an antibody/rifamycin analog conjugate (Genentech/Roche).[9,10] Both are in clinical development, and both only target *S. aureus*.

Teixobactin

In 2015, co-investigator Kim Lewis and co-workers reported a new peptide antibiotic, teixobactin (**Figure 1.2**), which is naturally produced by the Gram-negative bacterium *Eleftheria terrae*.[11] Teixobactin has generated considerable excitement, because it kills Gram-positive bacteria without detectable resistance and is effective against bacteria that are resistant to other antibiotics.[12, 13, 14, 15] Pathogens susceptible to teixobactin include *Staphylococcus aureus*, *Streptococcus pneumoniae*, *Bacillus anthracis*, and *Mycobacterium tuberculosis* — the pathogens that cause staph infections, bacterial pneumonia, anthrax, and tuberculosis. In minimum inhibitory concentration (MIC) assays *in vitro*, teixobactin has shown remarkable potency (MIC=0.005–0.5 μg/mL) toward a wide variety of Gram-positive pathogens. In mice, teixobactin protects against death from MRSA at 0.2 mg/kg and is over an order of magnitude more effective than vancomycin, which requires 3 mg/kg to achieve equivalent protection. Single-dose studies in mice at 20 mg/kg initially revealed no evidence of toxicity. When dosed in mice to a serum concentration of 27 μg/mL, teixobactin remained at levels above the MIC in the bloodstream for 4 hours. *In vitro* studies revealed good stability toward rat liver microsomes and mouse, rat, human, and dog plasma.

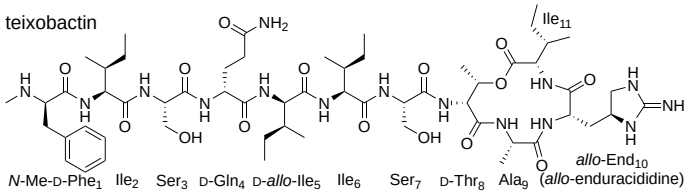

Figure 1.2. Teixobactin.

Teixobactin is a non-ribosomal undecapeptide containing a linear tail (residues 1–7) and a macrocyclic depsipeptide group (residues 8–11). It contains four D-amino acids and seven L-amino acids. The macrocyclic depsipeptide group is composed of D-Thr$_8$–Ala$_9$–*allo*-End$_{10}$–Ile$_{11}$

in which the *C*-terminal Ile_{11} and the hydroxy group of D-Thr_8 form an ester bond to close the 13-membered ring. Residue 10 is the non-proteinogenic amino acid *allo*-enduracididine (*allo*-End), a cyclic arginine analogue.

The mechanism of action of teixobactin is by inhibiting cell wall formation of Gram-positive bacteria, interrupting both the synthesis of peptidoglycan and the synthesis of teichoic acid, and ultimately causing bacterial cell lysis.[11,16] Teixobactin binds the highly conserved prenyl-pyrophosphate-saccharide regions of lipid II and related membrane-bound cell wall precursors (**Figure 1.3**).[17,18] These targets are extracellular and immutable, thus precluding the development of antibiotic resistance.

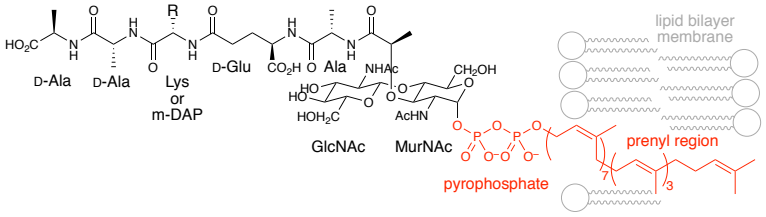

Figure 1.3. Lipid II illustrating the peptide, saccharide, pyrophosphate, and prenyl regions of the molecule anchored in the bacterial cell membrane.

Current efforts

Since the initial report of teixobactin in 2015, several research groups have worked to synthesize teixobactin and to elucidate its pharmacophore. Four total syntheses of teixobactin have been published.[19,20,21,22] A 10-step or a one-pot synthesis of *allo*-enduracididine suitable for preparing gram-quantities has also been reported.[23,22] Several groups have reported structure-activity relationship (SAR) studies of more than 120 teixobactin analogues in which *allo*-enduracididine at position 10 is replaced with arginine, lysine, or even isoleucine (**Figure 1.4**).[24,25,26,27,28,29,30,31,32,33,34,35,36,37,38,39,40,41,42,43,44,45,46] Collectively, these studies have revealed positions that tolerate mutation and have led to homologues that possess antibiotic activity on par with that of teixobactin *in vitro* and *in vivo* against MRSA and VRE.

Figure 1.4. Summary of structure-activity relationship studies of teixobactin. Green = good activity; Orange = moderate activity; Red = bad activity.

Most of these studies, however, have provided only a superficial understanding of the teixobactin pharmacophore, primarily providing insights into the roles of individual residues. A deeper understanding of teixobactin offers the possibility of learning from millions of years of evolution and holds the promise of designing next-generation teixobactin analogues that exploit the principles that are learned. A deeper understanding of the teixobactin pharmacophore will

pave the way for designing synthetic teixobactin-inspired analogues that are superior to teixobactin and have broader applications.

Limitations of teixobactin

In spite of its promise, it is not clear whether teixobactin will make it into the clinic. There are two main problems with teixobactin: (1) Ongoing studies by Lewis and co-workers in mice and rats have revealed nephrotoxicity. (2) Teixobactin forms a gel when dissolved in serum or buffer, which impedes its intravenous use at higher concentrations (**Figure 1.5A**). I have found that teixobactin and its active analogues behave like amyloidogenic peptides, forming fibrils that can be observed by transmission electron microscopy (TEM) and a lag time followed by the onset of fluorescence in a thioflavin T (ThT) fluorescence assay (**Figure 1.5B&C**).[47] The poor solubility and propensity to form a gel, as well as the nephrotoxicity, highlight the need for teixobactin analogues with improved properties. Overcoming either of these obstacles would be a significant advance toward realizing teixobactin's promise as a new antibiotic to treat Gram-positive pathogens such as MRSA. The remainder of this dissertation will focus on my effort to elucidate the mechanism of action of teixobactin which may facilitate strategic design of teixobactin analogues to realize the promise embedded in teixobactin.

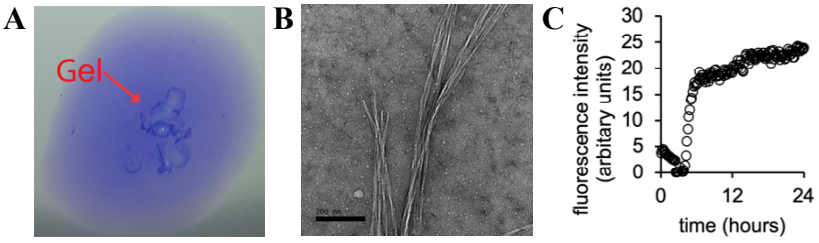

Figure 1.5. Amyloid-like properties of teixobactin. (A) Gelation of teixobactin in PBS buffer at pH 7.4, with crystal violet as a visual aid. (B) TEM image of teixobactin fibrils, ca. 8–10 nm in diameter. (C) ThT fluorescence assay of teixobactin.

References and Notes

1 http://www.cdc.gov/drugresistance/

2 Antibiotic resistance threats in the United States, 2013. U.S. Department of Health and Human Services Centers for Disease Control and Prevention. http://www.cdc.gov/drugresistance/threat-report-2013/pdf/ar-threats-2013-508.pdf

3 Global tuberculosis report, 2016. World Health Organization. http://apps.who.int/iris/bitstream/10665/250441/1/9789241565394-eng.pdf?ua=1

4 Chan, L. C.; Basuino, L.; Diep, B.; Hamilton, S.; Chatterjee, S. S.; Chambers, H. F. Ceftobiprole- and ceftaroline-resistant methicillin-resistant Staphylococcus aureus. *Antimicrob. Agents Chemother.* **2015**, *59*, 2960–2963.

5 Li, Y.; Lv, Y.; Xue, F.; Zheng, B.; Liu, J.; Zhang, J. Antimicrobial resistance surveillance of doripenem in China. *J. Antibiot.* **2015**, *68*, 496–500.

6 Sheng, Z. K.; Hu, F.; Wang, W.; Guo, Q.; Chen, Z.; Xu, X.; Zhu, D.; Wang, M. Mechanisms of tigecycline resistance among Klebsiella pneumoniae clinical isolates. *Antimicrob. Agents Chemother.* **2014**, *58*, 6982–6985.

7 Sakoulas, G.; Moise-Broder, P. A.; Schentag, J.; Forrest, A.; Moellering, R. C. Jr.; Eliopoulos, G. M. Relationship of MIC and bactericidal activity to efficacy of vancomycin for treatment of methicillin-resistant Staphylococcus aureus bacteremia. *J. Clin. Microbiol.* **2004**, *42*, 2398–2402.

8 Kollef, M. H. Limitations of vancomycin in the management of resistant staphylococcal infections. *Clin. Infect. Dis.* **2007**, *45*, 191–195.

9 Ruzin, A.; Wu, Y.; Yu, L.; Yu, X. Q.; Tabor, D. E.; Mok, H.; Tkaczyk, C.; Jensen, K.; Bellamy, T.; Roskos, L.; Esser, M. T.; Jafri, H. S. Characterisation of anti-alpha toxin antibody levels and colonisation status after administration of an investigational human monoclonal antibody, MEDI4893, against Staphylococcus aureus alpha toxin. *Clin. Transl. Immunology.* **2018**, *23*, 1009.

10 Lehar, S. M.; Pillow, T.; Xu, M.; Staben, L.; Kajihara, K. K.; Vandlen, R.; DePalatis, L.; Raab, H.; Hazenbos, W. L.; Morisaki, J. H.; Kim, J.; Park, S.; Darwish, M.; Lee, B. C.; Hernandez, H.; Loyet, K. M.; Lupardus, P.; Fong, R.; Yan, D.; Chalouni, C.; Luis, E.; Khalfin, Y.; Plise, E.; Cheong, J.; Lyssikatos, J. P.; Strandh, M.; Koefoed, K.; Andersen, P. S.; Flygare, J. A.; Wah Tan, M.; Brown, E. J.; Mariathasan, S. Novel antibody-antibiotic conjugate eliminates intracellular S. aureus. *Nature* **2015**, *527*, 323–328.

11 Ling, L. L.; Schneider, T.; Peoples, A. J.; Spoering, A. L.; Engels, I.; Conlon, B. P.; Mueller, A.; Schäberle, T. F.; Hughes, D. E.; Epstein, S.; Jones, M.; Lazarides, L.; Steadman, V. A.; Cohen, D. R.; Felix, C. R.; Fetterman, K. A.; Millett, W. P.; Nitti, A. G.; Zullo, A. M.; Chen, C.; Lewis, K. A new antibiotic kills pathogens without detectable resistance. *Nature* **2015**, *517*, 455–459. doi: 10.1038/nature14098.

12 Editorial. Reasons to be cheerful. *Nature*, **2015**, *517*, 121.

13 Ledford, H. Promising antibiotic discovered in microbial 'dark matter'. *Nature News* **2015**. doi:10.1038/nature.2015.16675.

14 Wright, G. Antibiotics: An irresistible newcomer. *Nature* **2015**, *517*, 442–444.

15 Kåhrström, C. T. Antimicrobials: a new drug for resistant bugs. *Nat. Rev. Microbiol.* **2015**, *13*, 126–127.

16 Homma, T.; Nuxoll, A.; Gandt, A. B.; Ebner, P.; Engels, I.; Schneider, T.; Götz, F.; Lewis, K.; Conlon, B. P. Dual Targeting of Cell Wall Precursors by Teixobactin Leads to Cell Lysis. *Antimicrob. Agents Chemother.* **2016**, *60*, 6510–6517.

17 Breukink, E.; de Kruijff, B. Lipid II as a target for antibiotics. *Nat. Rev. Drug Discov.* **2006**, *5*, 321–332.

18 de Kruijff, B.; van Dam, V.; Breukink, E. Lipid II: a central component in bacterial cell wall synthesis and a target for antibiotics. *Prostaglandins Leukot. Essent. Fatty Acids.* **2008**, *79*, 117–121.

19 Jin, K.; Sam, I. H.; Po, K. H. L.; Lin, D.; Ghazvini Zadeh, E. H.; Chen, S.; Yuan, Y.; Li, X. Total synthesis of teixobactin. *Nat. Commun.* **2016**, *7*, 12394.

20 Giltrap, A. M.; Dowman, L. J.; Nagalingam, G.; Ochoa, J. L.; Linington, R. G.; Britton, W. J.; Payne, R. J. Total Synthesis of Teixobactin. *Org. Lett.* **2016**, *18*, 2788–2791.

21 Liu, L.; Wu, S.; Wang, Q.; Zhang, M.; Wang, B.; He, G.; Chen, G. Total synthesis of teixobactin and its stereoisomers. *Org. Chem. Front.* **2018**, *5*, 1431–1435.

22 Zong, Y.; Fang, F.; Meyer, K. J.; Wang, L.; Ni, Z.; Gao, H.; Lewis, K.; Zhang, J.; Rao, Y. Gram-scale total synthesis of teixobactin promoting binding mode study and discovery of more potent antibiotics. *Nat. Commun.* **2019**, *10*, 3268.

23 Craig, W.; Chen, J.; Richardson, D.; Thorpe, R.; Yuan, Y. A Highly Stereoselective and Scalable Synthesis of L-allo-Enduracididine. *Org. Lett.* **2015**, *17*, 4620–4623.

24 Jad, Y. E.; Acosta, G. A.; Naicker, T.; Ramtahal, M.; El-Faham, A.; Govender, T.; Kruger, H. G.; de la Torre, B. G.; Albericio F. Synthesis and Biological Evaluation of a Teixobactin Analogue. *Org. Lett.* **2015**, *17*, 6182–6185.

25 Parmar, A.; Iyer, A.; Vincent, C. S.; Van Lysebetten, D.; Prior, S. H.; Madder, A.; Taylor, E. J.; Singh, I. Efficient total syntheses and biological activities of two teixobactin analogues. *Chem. Commun.* **2016**, *52*, 6060–6063.

26 Yang, H.; Chen, K. H.; Nowick, J. S. Elucidation of the Teixobactin Pharmacophore. *ACS Chem. Biol.* **2016**, *11*, 1823–1826.

27 Abdel Monaim, S. A. H.; Jad, Y. E.; Acosta, G. A.; Naicker, T.; Ramchuran, E. J.; El-Faham, A.; Govender, T.; Kruger, H. G.; de la Torre, B. G.; Albericio, F. Re-evaluation of the N-terminal substitution and the D-residues of teixobactin. *RSC Adv.* **2016**, *6*, 73827–73829.

28 Abdel Monaim, S. A. H.; Jad, Y. E.; Ramchuran, E. J.; El-Faham, A.; Govender, T.; Kruger, H. G.; de la Torre, B. G.; Albericio, F. Lysine Scanning of Arg(10)-Teixobactin: Deciphering the Role of Hydrophobic and Hydrophilic Residues. *ACS Omega* **2016**, *1*, 1262–1265.

29 Wu, C.; Pan, Z.; Yao, G.; Wang, W.; Fang, L.; Su, W. Synthesis and structure–activity relationship studies of teixobactin analogues. *RSC Adv.* **2017**, *7*, 1923–1926.

30 Parmar, A.; Prior, S. H.; Iyer, A.; Vincent, C. S.; Van Lysebetten, D.; Breukink, E.; Madder, A.; Taylor, E. J.; Singh, I. Defining the molecular structure of teixobactin analogues and understanding their role in antibacterial activities. *Chem. Commun.* **2017**, *53*, 2016–2019.

31 Yang, H.; Du Bois, D. R.; Ziller, J. W.; Nowick, J. S. X-ray crystallographic structure of a teixobactin analogue reveals key interactions of the teixobactin pharmacophore. *Chem. Commun.* **2017**, *53*, 2772–2775.

32 Jin, K.; Po, K. H. L.; Wang, S.; Reuven, J. A.; Wai, C. N.; Lau, H. T.; Chan, T. H.; Chen, S.; Li, X. Synthesis and structure-activity relationship of teixobactin analogues via convergent Ser ligation. *Bioorg. Med. Chem.* **2017**, *25*, 4990–4995.

33 Chen, K. H.; Le, S. P.; Han, X.; Frias, J. M.; Nowick, J. S. Alanine scan reveals modifiable residues in teixobactin. *Chem. Commun*. **2017**, *53*, 11357–11359.

34 Monaim, S. A. H. A.; Noki, S.; Ramchuran, E. J.; El-Faham, A.; Albericio, F.; Torre, B. G. Investigation of the N-Terminus Amino Function of Arg(10)-Teixobactin. *Molecules* **2017**, *22*, E1632.

35 Schumacher, C. E.; Harris, P. W. R.; Ding, X. B.; Krause, B.; Wright, T. H.; Cook, G. M.; Furkert, D. P.; Brimble, M. A. Synthesis and biological evaluation of novel teixobactin analogues. *Org. Biomol. Chem.* **2017**, *15*, 8755–8760.

36 Parmar, A.; Iyer, A.; Prior, S. H.; Lloyd, D. G.; Leng Goh, E. T.; Vincent, C. S.; Palmai-Pallag, T.; Bachrati, C. Z.; Breukink, E.; Madder, A.; Lakshminarayanan, R.; Taylor, E. J.; Singh, I. Teixobactin analogues reveal enduracididine to be non-essential for highly potent antibacterial activity and lipid II binding. *Chem. Sci.* **2017**, *8*, 8183–8192.

37 Jin, K.; Po, K. H. L.; Kong, W. Y.; Lo, C. H.; Lo, C. W.; Lam, H. Y.; Sirinimal, A.; Reuven, J. A.; Chen, S.; Li, X. Synthesis and antibacterial studies of teixobactin analogues with non-isostere substitution of enduracididine. *Bioorg. Med. Chem.* **2018**, *26*, 1062–1068.

38 Parmar, A.; Lakshminarayanan, R.; Iyer, A.; Mayandi, V.; Leng Goh, E. T.; Lloyd, D. G.; Chalasani, M. L. S.; Verma, N. K.; Prior, S. H.; Beuerman, R. W.; Madder, A.; Taylor, E. J.; Singh, I. Design and Syntheses of Highly Potent Teixobactin Analogues against Staphylococcus aureus, Methicillin-Resistant Staphylococcus aureus (MRSA), and

Vancomycin-Resistant Enterococci (VRE) in Vitro and in Vivo. *J. Med. Chem.* **2018**, *61*, 2009–2017.

39 Girt, G. C.; Mahindra, A.; Al Jabri, Z. J. H.; De Ste Croix, M.; Oggioni, M. R.; Jamieson, A. G. Lipopeptidomimetics derived from teixobactin have potent antibacterial activity against Staphylococcus aureus. *Chem. Commun.* **2018**, *54*, 2767–2770.

40 Guo, C.; Mandalapu, D.; Ji, X.; Gao, J.; Zhang, Q. Chemistry and Biology of Teixobactin. Chemistry. **2018**, *24*, 5406–5422.

41 Zong, Y.; Sun, X.; Gao, H.; Meyer, K. J.; Lewis, K.; Rao, Y. Developing Equipotent Teixobactin Analogues against Drug-Resistant Bacteria and Discovering a Hydrophobic Interaction between Lipid II and Teixobactin. *J. Med. Chem.* **2018**, *61*, 3409–3421.

42 Ng, V.; Kuehne, S. A.; Chan, W. C. Rational Design and Synthesis of Modified Teixobactin Analogues: In Vitro Antibacterial Activity against Staphylococcus aureus, Propionibacterium acnes and Pseudomonas aeruginosa. *Chemistry* **2018**, *24*, 9136–9147.

43 Mandalapu, D.; Ji, X.; Chen, J.; Guo, C.; Liu, W. Q.; Ding, W.; Zhou, J.; Zhang, Q. Thioesterase-Mediated Synthesis of Teixobactin Analogues: Mechanism and Substrate Specificity. *J. Org. Chem.* **2018**, *83*, 7271–7275.

44 Ramchuran, E. J.; Somboro, A. M.; Abdel Monaim. S. A. H.; Amoako, D. G.; Parboosing, R.; Kumalo, H. M.; Agrawal, N.; Albericio, F.; Torre, B. G.; Bester, L. A. In Vitro Antibacterial Activity of Teixobactin Derivatives on Clinically Relevant Bacterial Isolates. *Front. Microbiol.* **2018**, *9*, 1535.

45 Malkawi, R.; Iyer, A.; Parmar, A.; Lloyd, D. G.; Leng Goh, E. T.; Taylor, E. J.; Sarmad, S.; Madder, A.; Lakshminarayanan, R.; Singh, I. Cysteines and Disulfide-Bridged Macrocyclic Mimics of Teixobactin Analogues and Their Antibacterial Activity Evaluation against Methicillin-Resistant Staphylococcus Aureus (MRSA). *Pharmaceutics* **2018**, *10*, E183.

46 Gunjal, V. B.; Reddy, D. S. Total synthesis of Met10-teixobactin. *Tetrahedron Lett.* **2019**, *60*, 1909–1912.

47 Yang, H.; Wierzbicki, M.; Du Bois, D. R.; Nowick, J. S. X-ray Crystallographic Structure of a Teixobactin Derivative Reveals Amyloid-like Assembly. *J. Am. Chem. Soc.* **2018**, *140*, 14028–14032.

Chapter 2[a]
Elucidation of Teixobactin Pharmacophore

Introduction

At the beginning of 2015, a new antibiotic, teixobactin, was reported in *Nature*,[1] with great attention in the scientific press[2,3,4,5] and the popular press.[6] Teixobactin is a non-ribosomal undecapeptide containing a macrocyclic depsipeptide group (**Figure 2.1**). It contains four D-amino acids and seven L-amino acids, and the *C*-terminal Ile_{11} is cyclized onto the side chain of D-Thr_8 to form a 13-membered lactone. Residue 10 of teixobactin is the non-proteinogenic amino acid, L-*allo*-enduracididine (*allo*-End_{10}), which is a cyclic analogue of arginine. Teixobactin acts against Gram-positive bacteria by binding to prenyl-pyrophosphate-GlcNAc region of lipid II. This region is highly conserved in bacteria and cannot easily mutate to impart drug-resistance.[7,8] It is thus an attractive antibiotic target.

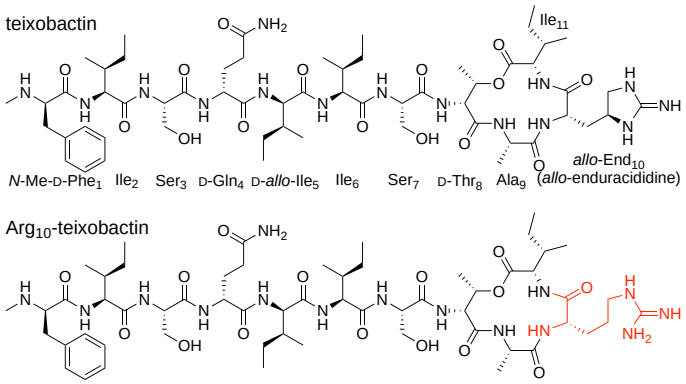

Figure 2.1. Structures of teixobactin and Arg_{10}-teixobactin.

Recently, Jad *et al*. and Parmar *et al*. reported syntheses of the arginine analogue of teixobactin Arg_{10}-teixobactin.[9,10] Both syntheses involve solid-phase peptide synthesis (SPPS) of

[a] This chapter is adapted from Yang, H.; Chen, K. H.; Nowick, J. S. *ACS Chem. Biol.* **2016**, *11*, 1823–1826.

a linear precursor on 2-chlorotrityl resin, followed by solution-phase macrolactamization to form the Ala$_9$–Arg$_{10}$ amide bond. The former synthesis requires both Fmoc and Alloc groups as orthogonal α-amino protecting groups; the latter requires Fmoc, Alloc, and trityl groups. Both syntheses introduce D-Thr$_8$ without protecting the alcohol group and *O*-acylate it before completing the *N*-terminal tail. Both sets of authors reported that Arg$_{10}$-teixobactin is about an order of magnitude less active against gram-positive bacteria than teixobactin in minimum inhibitory concentration (MIC) assays.[11,12,13]

Results and Discussion

In the current study, we set out to elucidate the teixobactin pharmacophore by synthesizing and evaluating a series of teixobactin homologues. We examine the roles of the guanidinium group at position 10, the stereochemistry of the macrolactone ring, and the "tail" comprising residues 1–5. We also report a simpler synthesis of teixobactin analogues and a simpler homologue, which we term lipobactin 1.

We synthesized Arg$_{10}$-teixobactin and other homologues by SPPS on 2-chlorotrityl resin, followed by solution-phase macrolactamization to form the Arg$_{10}$–Ile$_{11}$ amide bond (**Scheme 2.1**).[14,15,16,17] We used only Fmoc protecting groups to construct all of the amide bonds and carried D-Thr$_8$ through the entire synthesis without side chain protection. All homologues were prepared and studied as the trifluoroacetic acid (TFA) salts.

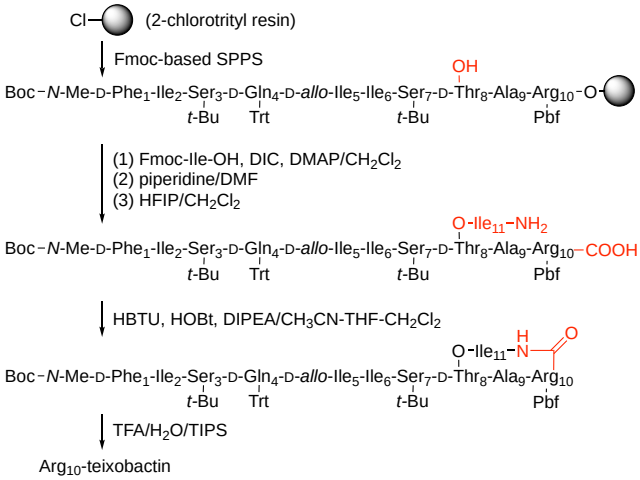

Scheme 2.1. Synthesis of Arg_{10}-teixobactin.

We began the synthesis by attaching Fmoc-Arg(Pbf)-OH to 2-chlorotrityl resin. Residues 9 through 1 were then introduced by standard Fmoc-based SPPS using HCTU as the coupling reagent. D-Thr_8 was introduced without a protecting group at the hydroxy position. No *O*-acylation of D-Thr_8 was observed in the subsequent rounds of SPPS. D-Thr_8 was then *O*-acylated with Fmoc-Ile-OH using DIC and DMAP.[18,19,20] Fmoc-deprotection, followed by cleavage from the resin with 20% hexafluoroisopropanol (HFIP) in CH_2Cl_2 afforded the linear precursor. Macrolactamization with HBTU and HOBt, followed by global deprotection with trifluoroacetic acid (TFA) and RP-HPLC purification afforded Arg_{10}-teixobactin. We also prepared a series of homologues using similar procedures (**Figure 2.2**).

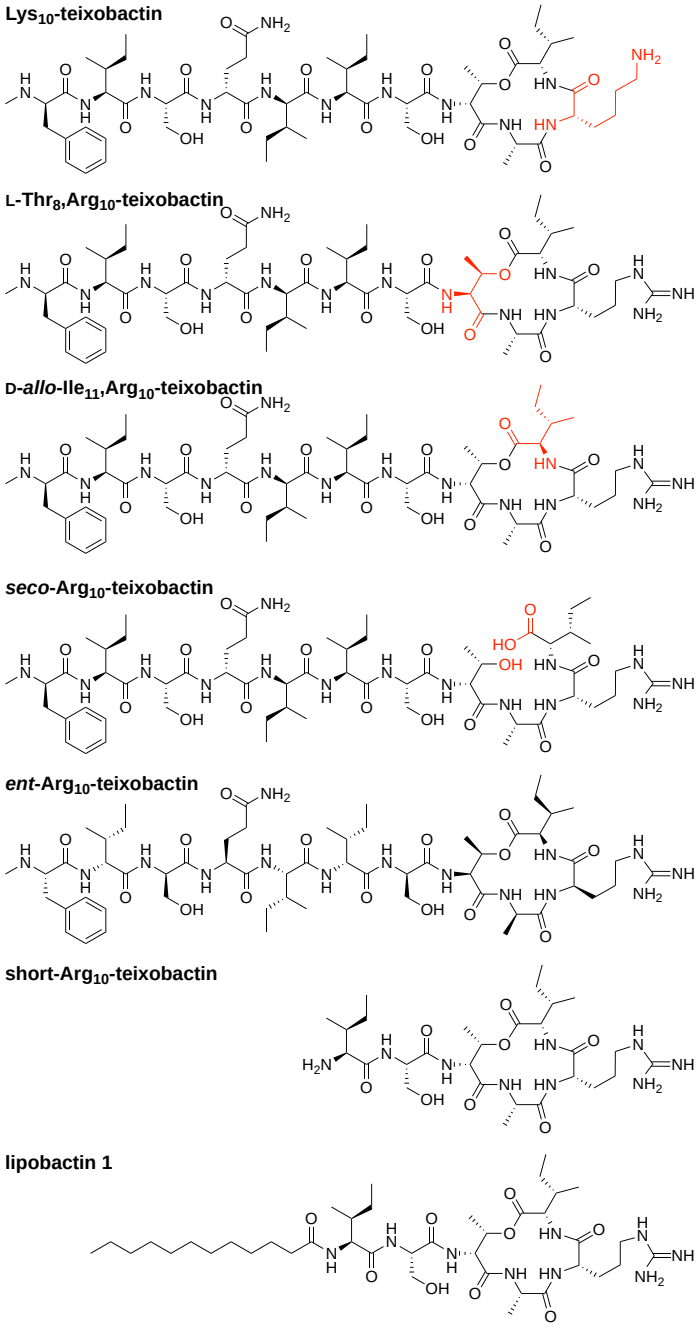

Figure 2.2. Structures of teixobactin homologues.

We investigated the antibiotic activity of Arg_{10}-teixobactin and homologues in MIC assays against four types of gram-positive bacteria. We used the antibiotic vancomycin as a positive control and the gram-negative bacteria *E. coli* as a negative control. We selected non-pathogenic

strains of bacteria to facilitate the safe and rapid screening of Arg_{10}-teixobactin and other homologues in a BSL-1 environment.

To explore the role of a guanidinium group in residue 10, we compared the MIC of Arg_{10}-teixobactin to Lys_{10}-teixobactin. The arginine residue serves as a surrogate for *allo*-enduracididine, which is not commercially available and has only been prepared by cumbersome multistep syntheses.[21,22,23,24,25] Arg_{10}-teixobactin gave MIC values of 1–4 μg/mL against the four gram-positive bacteria studied (**Table 2.1**). Although side-by-side comparison to an authentic sample of teixobactin was not possible, comparison to the original published values in related bacteria suggests that Arg_{10}-teixobactin is about an order of magnitude less active (**Table 2.1**). Surprisingly, Lys_{10}-teixobactin gave MIC values 2–4 times lower than Arg_{10}-teixobactin. While the MIC values for Lys_{10}-teixobactin are slightly higher than those reported for teixobactin, they are comparable to those of vancomycin (**Table 2.1**). This interesting finding indicates that the guanidinium group at position 10 is not necessary for activity and lays the foundation for the future discovery of homologues that lack *allo*-enduracididine and are even more potent.

Table 2.1. MIC of teixobactin homologues in μg/mL.

	Staphylococcus epidermidis ATCC 14990	*Streptococcus salivarius* ATCC 13419	*Enterococcus durans* ATCC 6056	*Bacillus subtilis* ATCC 6051	*Escherichia coli* ATCC 10798
Arg_{10}-teixobactin	1	1	4	2	>32
Lys_{10}-teixobactin	0.25	0.5	1	0.5	>32
L-Thr_8,Arg_{10}-teixobactin	>32	>32	>32	>32	>32
D-*allo*-Ile_{11},Arg_{10}-teixobactin	2	2	8	4	>32
seco-Arg_{10}-teixobactin	>32	>32	>32	>32	>32
ent-Arg_{10}-teixobactin	2	1	4	2	>32
short-Arg_{10}-teixobactin	>32	>32	>32	>32	>32
lipobactin 1	4	4	8	4	>32
vancomycin	0.5	0.5	0.5	1	>32
teixobactin[1]	0.08–0.3 various *Staphylococcus*[1]	0.02–0.15 various *Streptococcus*[1]	0.3–0.6 various *Enterococcu*[1]	0.02–0.6 various *Bacillus*[1]	25 *E. coli*[1]

To investigate the role of the macrolactone ring stereochemistry, we compared the diastereomer L-Thr_8,Arg_{10}-teixobactin and D-*allo*-Ile_{11},Arg_{10}-teixobactin to Arg_{10}-teixobactin. The former proved inactive (MIC > 32 μg/mL) against the Gram-positive bacteria, while the latter proved half as active (**Table 2.1**). Collectively, these results suggest that the ring stereochemistry and the conformation are important in teixobactin activity. *Seco*-Arg_{10}-texibobactin also proved inactive (MIC > 32 μg/mL), further supporting the importance of the cyclic depsipeptide structure (**Table 2.1**).

To further investigate the role of the macrolactone ring stereochemistry, we compared *ent*-Arg_{10}-teixobactin to Arg_{10}-teixobactin. *Ent*-Arg_{10}-teixobactin exhibits comparable activity to Arg_{10}-teixobactin. This exciting finding supports a model in which the amide NH groups on macrolactone ring bind to the achiral pyrophosphate group of lipid II through hydrogen-bonding interactions. This mode of binding has previously been reported in the NMR structure of the complex of nisin with lipid II (PDB 1WCO) and appears to occur for teixobactin as well.[26]

To investigate the role of the *N*-terminal tail, we truncated residues 1–5. The resulting short-Arg_{10}-teixobactin also proved inactive (MIC > 32 μg/mL). To investigate the possibility that the hydrophobic residues *N*-Me-D-Phe, Ile, and D-*allo*-Ile at positions 1, 2, and 5 help to anchor teixobactin into the plasma membrane, we replaced residues 1–5 with a dodecanoyl group.[27,28] The resulting homologue, lipobactin 1, proved only 2–4 times less active than Arg_{10}-teixobactin (**Table 2.1**). This finding confirms the importance of the hydrophobicity of the *N*-terminal tail and paves the way for further developing simpler homologues of teixobactin with enhanced pharmacological properties.

References and Notes

1 Ling, L. L.; Schneider, T.; Peoples, A. J.; Spoering, A. L.; Engels, I.; Conlon, B. P.; Mueller, A.; Schäberle, T. F.; Hughes, D. E.; Epstein, S.; Jones, M.; Lazarides, L.; Steadman, V. A.; Cohen, D. R.; Felix, C. R.; Fetterman, K. A.; Millett, W. P.; Nitti, A. G.; Zullo, A. M.; Chen, C.; Lewis, K. *Nature* **2015**, *517*, 455–459.

2 Editorial. *Nature* **2015**, *517*, 121.

3 Ledford, H. Promising antibiotic discovered in microbial 'dark matter'. *Nature News,* [Online], Jan 7, 2015. **2015**. http://www.nature.com/news/promising-antibiotic-discovered-in-microbial-dark-matter-1.16675 (accessed January 7, 2015).

4 Wright, G. *Nature* **2015,** *517*, 442–444.

5 Kahrstrom, C. T. *Nature Rev. Drug Discov.* **2015**, *14*, 94.

6 Grady, D. New Antibiotic Stirs Hope Against Resistant Bacteria. *The New York Times,* [Online], Jan 7, 2015. http://www.nytimes.com/2015/01/08/health/from-a-pile-of-dirt-hope-for-a-powerful-new-antibiotic.html?_r=0 (accessed January 7, 2015).

7 Breukink, E.; de Kruijff, B. *Nat. Rev. Drug Discov.* **2006**, *5*, 321–332.

8 de Kruijff, B.; van Dam, V.; Breukink, E. *Prostaglandins Leukot. Essent. Fatty Acids* **2008,** *79*, 117–121.

9 Jad, Y. E.; Acosta, G. A.; Naicker, T.; Ramtahal, M.; El-Faham, A.; Govender, T.;Kruger, H. G.;De la Torre, B. G.; Albericio, F. *Org. Lett.*, **2015**, *17*, 6182–6185.

10 Parmar, A.; Iyer, A.; Vincent, C. S.; Van Lysebetten, D.; Prior, S. H.; Madder, A.; Taylor, E. J.; Singh, I. *Chem. Commun.* **2016**, *52*, 6060–6063.

11 The MIC values reported in Table 2.1 of reference 9 appear to be in error, being reported as nM rather than μg/mL.

12 Wiegand, I.; Hilpert, K.; Hancock, R. E. *Nat. Protoc.* **2008**, *3*, 163–175.

13 CLSI. *Methods for Dilution Antimicrobial Susceptibility Tests for Bacteria That Grow Aerobically. Approved Standard—Ninth Edition*. CLSI document M07-A9. Wayne, PA: Clinical and Laboratory Standards Institute; 2012.

14 Davies, J. S. *J. Pept. Sci.* **2003,** *9*, 471–501.

15 Sarabia, F.; Chammaa, S.; Ruiz, A. S.; Ortiz, L. M.; Herrera, F. J. *Curr. Med. Chem.* **2004**, *11*, 1309–1332.

16 Lambert, J. N.; Mitchell, J. P.; Roberts, K. D. *J. Chem. Soc., Perkin Trans. 1* **2001**, 471–484.

17 White, C. J.; Yudin, A. K. *Nat. Chem.* **2011,** *3*, 509–524.

18 Neises, B.; Steglich, W. *Angew. Chem., Int. Ed. Engl.* **1978**, *17*, 522.

19 Kling, A.; Lukat, P.; Almeida, D. V.; Bauer, A.; Fontaine, E.; Sordello, S.; Zaburannyi, N.; Herrmann, J.; Wenzel, S. C.; Konig, C.; Ammerman, N. C.; Barrio, M. B.; Borchers, K.; Bordon-Pallier, F.; Bronstrup, M.; Coutemanche, G.; Gerlitz, M.; Geslin, M.; Hammann, P.;

Heinz, D. W.; Hoffmann, H.; Klieber, S.; Kohlmann, M.; Kurz, M.; Lair, C.; Matter, H.; Nuermberger, E.; Tyagi, S.; Fraisse, L.; Grosset, J. H.; Lagrange, S.; Muller, R. *Science* **2015**, *348*, 1106–1112.

20 Esterification with DIC and DMAP is known to epimerize amino acids. ^{1}H NMR analysis of the unpurified Arg_{10}-teixobactin, and comparison to an authentic sample of D-*allo*-Ile_{11},Arg_{10}-teixobactin, showed approximately 46% epimerization. HPLC purification of the crude product afforded Arg_{10}-teixobactin in approximately 95% diasteromeric purity.

21 Tsuji, S.; Kusumoto, S.; Shiba, T. *Chem. Lett.* **1975**, *12*, 1281–1284.

22 Sanière, L.; Leman, L.; Bourguignon, J.; Dauban, P.; Dodd, R. H. *Tetrahedron* **2004**, *60*, 5889–5897.

23 Möschwitzer, V. D.; Kariuki, B. M.; Redman, J. E. *Tetrahedron Lett.* **2013**, *54*, 4526–4528.

24 Olson, D. E.; Su, J. Y.; Robert, D. A.; Du Bois, J. *J. Am. Chem. Soc.* **2014**, *136*, 13506–13509.

25 Craig, W.; Chen, J.; Richardson, D.; Thorpe, R.; Yuan, Y. *Org. Lett*. **2015**, *17*, 4620–4623.

26 Hsu, S. T.; Breukink, E.; Tischenko, E.; Lutters M. A.; de Kruijff, B.; Kaptein, R.; Bonvin, A. M.; van Nuland N. A. *Nat. Struct. Mol. Biol.* **2004**, *11*, 963–937.

27 Straus, S. K.; Hancock, R. E. W. *Biochim. Biophys. Acta, Biomembr.* **2006**, *1758*, 1215–1223.

28 Steenbergen, J. N.; Alder, J.; Thorne, G. M.; Tally, F. P. *J. Antimicrob. Chemother.* **2005**, *55,* 283–288.

Supporting Information

Table of Contents

Materials and Methods:

Synthesis of Arg_{10}-teixobactin

Resin loading.[1] 2-Chlorotrityl chloride resin (300 mg, 1.2 mmol/g) was added to a 10 mL Bio-Rad Poly-Prep chromatography column. The resin was suspended in dry CH_2Cl_2 (10 mL) and allowed to swell for 30 min. The resin was loaded with a solution of Fmoc-Arg(Pbf)-OH (117 mg, 0.18 mmol, 0.50 equiv) and 2,4,6-collidine (300 μL) in dry CH_2Cl_2 (5 mL). The suspension was agitated for 12 h. The solution was drained, and the resin was washed with dry CH_2Cl_2 (3x). A mixture of CH_2Cl_2/MeOH/DIPEA (17:2:1, 8 mL) was added to the resin and agitated for 1 h to cap any unreacted resin sites. The solution was drained, and the resin was washed with dry CH_2Cl_2 (3x). The resin loading was determined to be 0.09 mmol [0.29 mmol/g, 48% loading] through UV analysis of the Fmoc cleavage product.

Peptide coupling. The loaded resin was suspended in dry DMF and transferred to a solid-phase peptide synthesis reaction vessel for automated peptide coupling with Fmoc-protected amino acid building blocks. The linear peptide was synthesized through the following cycles: *i*. Fmoc deprotection with 20% (v/v) piperidine in dry DMF (3 mL) for 10 min, *ii*. resin washing with dry DMF (3x), *iii*. coupling of amino acid (0.36 mmol, 4 equiv) with HCTU (142 mg, 0.36 mmol, 4 equiv) in 20% (v/v) 2,4,6-collidine in dry DMF (3 mL) for 20 min, and *iv.* resin washing with dry DMF (6x). For D-to-L and L-to-D amino acid couplings, the reaction time in step *iii* was increased to 1 h. After completing the linear synthesis, the resin was transferred to a 10 mL Bio-Rad Poly-Prep chromatography column. The resin was then washed with dry DMF (3x) and dry CH_2Cl_2 (3x).

Esterification. In a test tube, Fmoc-Ile-OH (303 mg, 0.90 mmol, 10 equiv) and diisopropylcarbodiimide (140 μL, 0.90 mmol, 10 equiv) were dissolved in dry CH_2Cl_2 (5 mL).

The resulting solution was filtered through 0.20 μm nylon filter, and then 4-dimethylaminopyridine (11 mg, 0.09 mmol, 1 equiv) was added to the filtrate. The resulting solution was transferred to the resin and was gently agitated for 1 h. The solution was drained and the resin was washed with dry CH_2Cl_2 (3x) and DMF (3x).

Fmoc deprotection and cleavage of the linear peptide from the resin. The Fmoc protecting group on Ile_{11} was removed by adding 20% piperidine in dry DMF (5 mL) for 30 min. The solution was drained, and the resin was washed with dry DMF (3x) and then with dry CH_2Cl_2 (3x). To cleave the peptide, the resin was treated with 20% hexafluoroisopropanol in dry CH_2Cl_2 (6 mL) followed by gentle agitation for 1 h. The filtrate was collected in a round-bottomed flask. The resin was washed with a second aliquot of 20% hexafluoroisopropanol (6 mL) and then washed with dry CH_2Cl_2 (3x). The filtrates were combined and concentrated under reduced pressure to afford a clear oil. The oil was placed under vacuum (≤ 10 mTorr) to remove any residual solvents.

Cyclization. The oil was dissolved in a mixture of CH_3CN/THF/CH_2Cl_2 (6:2:2, 10 mL). HBTU (195 mg, 0.54 mmol, 6 equiv) and HOBt (70 mg, 0.54 mmol, 6 equiv) were added to solution. The reaction mixture was stirred under nitrogen for 30 min. DIPEA (94 μL, 0.54 mmol, 6 equiv) was slowly added to the solution and the reaction mixture was stirred for 2 h. The mixture was concentrated under reduced pressure to afford the cyclized peptide as a white solid. The solid was placed under vacuum (≤ 10 mTorr) to remove any residual solvents.

Global deprotection and purification of Arg_{10}-teixobactin. The crude protected peptide was dissolved in a mixture of trifluoroacetic acid (TFA)/triisopropylsilane/H_2O (90:5:5, 10 mL) and stirred under nitrogen for 1 h. The resulting solution was then concentrated under reduced pressure to afford the deprotected peptide as a clear yellow oil. The oil was dissolved in 20%

(v/v) CH_3CN in water (5 mL) and centrifuged at 14,000 rpm for 5 min, and the solution was filtered through 0.20 μm nylon filter. The peptide was purified by reverse-phase HPLC with H_2O/CH_3CN (gradient elution of 20-50% CH_3CN w/ 0.1% TFA). Pure fractions analyzed by analytical HPLC and electrospray ionization (ESI) mass spectrometry were combined and lyophilized. Arg_{10}-teixobactin was isolated as the trifluoroacetic acid (TFA) salt of a 14.2 mg white powder (11.6 % yield based on resin loading).

Esterification with DIC and DMAP is known to epimerize amino acids. ^{1}H NMR analysis of the unpurified Arg_{10}-teixobactin, and comparison to an authentic sample of D-*allo*-Ile_{11},Arg_{10}-teixobactin, showed approximately 46% epimerization. HPLC purification of the crude product afforded Arg_{10}-teixobactin in approximately 95% diasteromeric purity.

The other teixobactin homologues were prepared using similar procedures. All teixobactin homologues were estimated to be at least 90% purity based on RP-HPLC and ^{1}H NMR analysis, with the exception of *ent*-Arg_{10}-teixobactin, which showed a 16 mol% impurity in the ^{1}H NMR spectrum. This impurity is suspected to arise from a stereoisomeric impurity at the L-*allo*-Ile_5 position, which could result from stereoisomeric impurity in the Fmoc-L-*allo*-Ile-OH that was used in the synthesis.

Table S2.1. Yield of teixobactin homologues.

homologue	yield (mg)	% yield	calcd. MW as TFA salt
Arg_{10}-teixobactin	14.2 mg	10.7%	1472.54 (·2 TFA)
Lys_{10}-teixobactin	14.2 mg	10.9%	1444.53 (·2 TFA)
L-Thr_8,Arg_{10}-teixobactin	4.7 mg	3.6%	1472.54 (·2 TFA)
D-*allo*-Ile_{11},Arg_{10}-teixobactin	13.2 mg	10.0%	1472.54 (·2 TFA)
seco-Arg_{10}-teixobactin	13.2 mg	9.8%	1490.56 (·2 TFA)
ent-Arg_{10}-teixobactin	11.5 mg	8.7%	1472.54 (·2 TFA)
short-Arg_{10}-teixobactin	9.7 mg	12.4%	869.81 (·2 TFA)
lipobactin 1	12.1 mg	14.1%	956.10 (·1 TFA)

NMR sample preparation and data processing

1D and 2D experiments of Arg_{10}-teixobactin and other homologues were performed at 2 mM concentration in DMSO-d_6 at 298K at 600 MHz. samples were prepared gravimetrically, based on the molecular weight of the corresponding trifluoracetate (TFA) salt. Spectra were referenced to residual DMSO-d_5. The data were collected with the TopSpin software and processed with the XwinNMR software.

Minimum inhibitory concentration (MIC) assay

MIC assays of Arg_{10}-teixobactin and other homologues were determined by using a broth microdilution method according to CLSI.[2] *Escherichia coli* (ATCC 10798), *Enterococcus durans* (ATCC 6056), *Streptococcus salivarius* (ATCC 13419), *Staphylococcus epidermidis* (ATCC 14990), *Bacillus subtilis* (ATCC 6051) were acquired as freeze-dried powders from ATCC.

Preparation of bacterial plate stocks. A portion of freeze-dried bacteria powder was removed with a sterile loop and suspended in 5 mL of Mueller-Hinton broth in a 14 mL polypropylene round-bottom culture tube. The mixture was incubated at 37 °C while shaking overnight. The mixture was streaked on Mueller-Hinton agar plates, and the plates were incubated at 37 °C overnight to allow colonies to grow. The plates were wrapped with Parafilm and stored for subsequent experiments.

Determination of bacterial concentration (CFU/mL). Five colonies from the bacterial plate stocks were transferred to a single 14 mL polypropylene round-bottom tube containing Mueller-Hinton broth (2 mL) and the mixture was incubated at 37 °C while shaking. As the turbidity of the cell suspension mixture visually increased, a 200 μL aliquot was transferred to a 96-well plate for OD_{600} measurement. The cell suspension mixture was diluted with Mueller-

Hinton broth to an OD_{600} of 0.075 as measured for a 200 µL sample in a 96-well plate (equivalent to a 0.5 McFarland standard). A 10 µL aliquot of the diluted cell suspension was diluted 1:1000 with Mueller-Hinton broth. A 10 µL aliquot of the 1:1000 diluted cell suspension mixture was further diluted 1:200 with Mueller-Hinton broth. A 100 µL aliquot of the resulting mixture was then streaked on a Mueller-Hinton agar plate (repeated four times). The agar plates were incubated at 37 °C overnight. The number of colonies on each agar plate was counted, and the average of four plates was used to back calculate the bacterial concentration (CFU/mL) at an OD_{600} of 0.075 as measured for a 200 µL sample in a 96-well plate (equivalent to a 0.5 McFarland standard).

Table S2.2. Bacterial concentration determination

Bacteria	Average number of colonies per plate	Concentration at a 0.5 McFarland standard[a]
Staphylococcus epidermidis ATCC 14990	5	1 x 10^7 CFU/mL
Streptococcus salivarius ATCC 13419	25	5 x 10^7 CFU/mL
Enterococcus durans ATCC 6056	32	6 x 10^7 CFU/mL
Bacillus subtilis ATCC 6051	25	5 x 10^7 CFU/mL
Escherichia coli ATCC 10798	24	5 x 10^7 CFU/mL

[a] OD_{600} of 0.075 as measured for a 200 µL sample in a 96-well plate

Preparing the peptide homologue stock. Solutions of vancomycin, Arg_{10}-teixobactin, and other teixobactin homologues were prepared gravimetrically by dissolving an appropriate amount of peptide in an appropriate volume of sterile DMSO to make 20 mg/mL stock solutions. The stock solutions were stored at -20 °C for subsequent experiments.

Preparing the minimum inhibitory concentration (MIC) assays. An aliquot of the 20 mg/mL peptide homologue stock solutions diluted 1:100 with Mueller-Hinton broth to make a 200 μg/mL. The resulting solution was further diluted to 64 μg/mL with Mueller-Hinton broth. A 200 μL aliquot of the 64 μg/mL solution was transferred to a 96-well plate. Two-fold serial dilutions were made with Mueller-Hinton broth across a 96-well plate to achieve a final volume of 100 μL in each well. The 100 μL serial diluted solutions had the following concentrations: 64, 32, 16, 8, 4, 2, 1, 0.5, 0.25, 0.125, and 0.06125 μg/mL.

Performing the minimum inhibitory concentration (MIC) assays. Five colonies from the bacterial plate stocks were selected and transferred to a single 14 mL polypropylene round-bottom tube that contained Mueller-Hinton broth (2 mL) and the mixture was incubated at 37 °C while shaking. As the turbidity of the cell suspension mixture visually increased, the mixture was diluted with Mueller-Hinton broth to OD_{600} of 0.075 as measured in a 96-well plate (equivalent to a 0.5 McFarland standard). Based on the previously determined CFU/mL (above), the diluted mixture was further diluted to 1 x 10^6 CFU/mL with Mueller-Hinton broth. A 100 μL aliquot of the 1 x 10^6 CFU/mL bacterial solution was added to each well in 96-well plates, resulting final bacteria concentration of 5 x 10^5 CFU/mL in each well. As 100 μL of bacteria were added to each well, peptide homologue solution was also diluted down to the following concentrations: 32, 16, 8, 4, 2, 1, 0.5, 0.25, 0.125, 0.0625, and 0.03125 μg/mL. The plate was covered with a lid and incubated at 37 °C for 16 h. The OD_{600} was measured using a 96-well UV/Vis plate reader (MultiSkan GO, Thermo Scientific). The MIC values were taken as the lowest concentration that had no bacteria growth. Each MIC assay was run in duplicate in three independent runs to ensure reproducibility.

HPLC, MS, 1D and 2D NMR spectrum of Arg_{10}-teixobactin and other homologues

Table S2.3. NMR data of Arg_{10}-teixobactin and other homologues.

teixobactin[3]

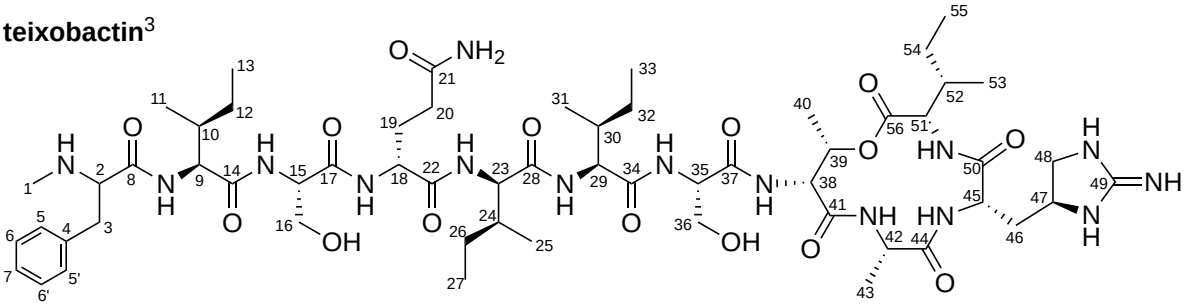

Arg_{10}-teixobactin

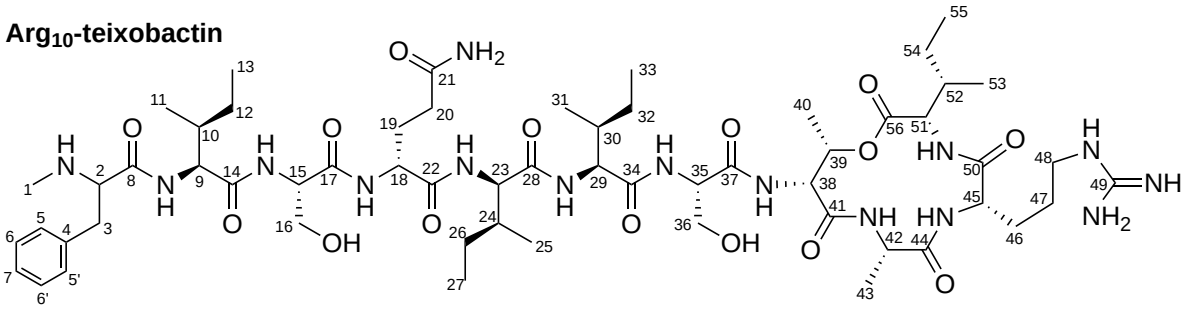

Lys_{10}-teixobactin

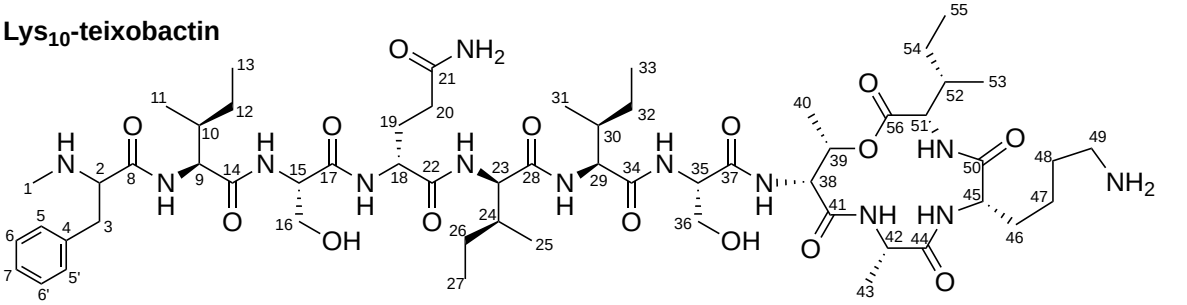

L-Thr_8,Arg_{10}-teixobactin

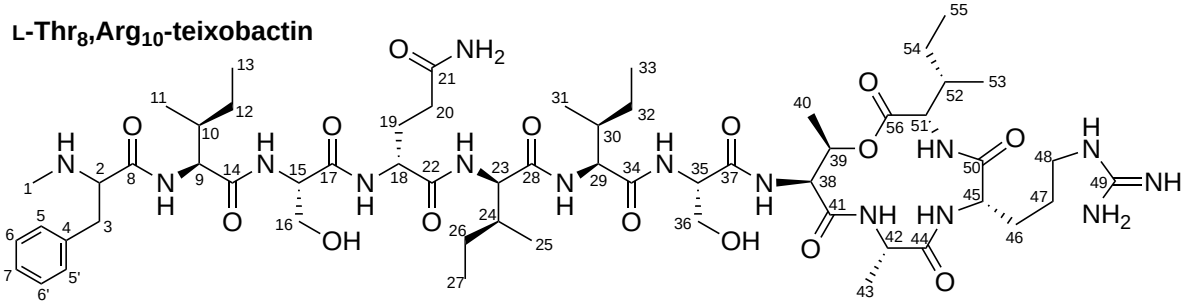

D-*allo*-Ile_{11},Arg_{10}-teixobactin

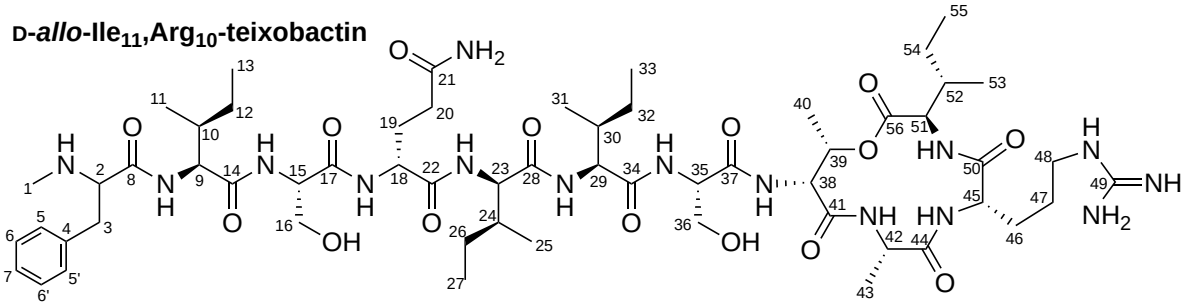

***seco*-Arg$_{10}$-teixobactin**

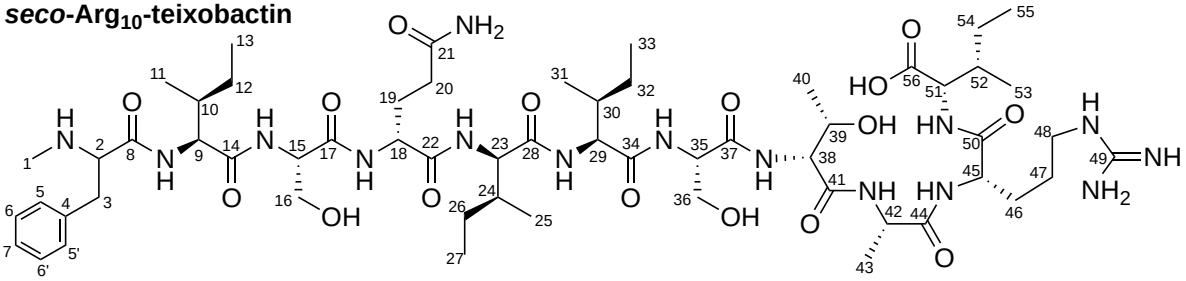

***ent*-Arg$_{10}$-teixobactin**

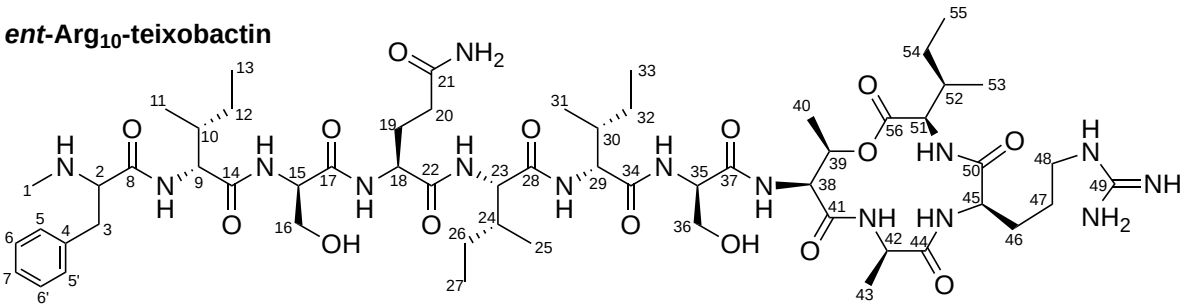

short-Arg$_{10}$-teixobactin

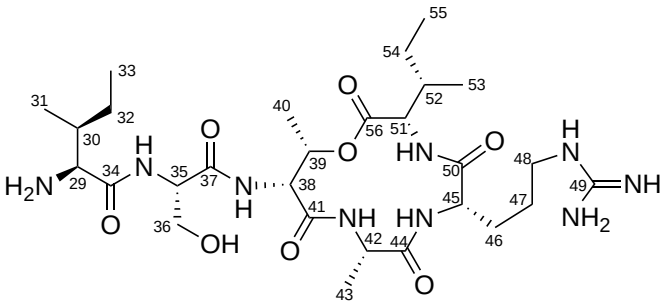

lipobactin 1

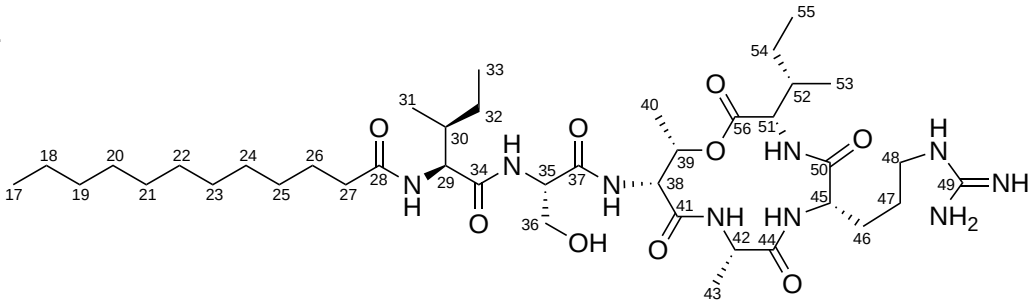

Homologue	Residue 1		1	2 2-NH	3		4	5	6	7	8
Teixobactin1	D-N-Me-Phe	2.50 (3H, br s)	4.21 (1H, dd, 9.4, 5.3)	(2H, 9.3, 9.0, v br s)	3.00 (1H, dd, 13.2, 5.3)	2.97 (1H, dd, 13.2, 9.4)	N/A	7.24 (2H, m)	7.31 (2H, m)	7.27 (1H, m)	N/A
Arg10-teixobactin	D-N-Me-Phe	2.46 (3H, br s)	4.17 (1H, m)	(2H, 9.04, 8.97, v br s)	3.15 (1H, dd, 13.2, 5.3)	3.11 (1H, m)	N/A	7.23 (2H, m)	7.31 (2H, m)	7.26 (1H, m)	N/A
Lys10-teixobactin	D-N-Me-Phe	2.46 (3H, br s)	4.18 (1H, m)	(2H, 9.04, 8.96, v br s)	3.10 (1H, dd, 13.2, 5.1)	2.97 (1H, dd, 13.2, 9.7)	N/A	7.22 (2H, m)	7.31 (2H, m)	7.26 (1H, m)	N/A
L-Thr8,Arg10-teixobactin	D-N-Me-Phe	2.38 (3H, br s)	4.16 (1H, m)	not observed	3.15 (1H, m)	2.94 (1H, m)	N/A	7.22 (2H, m)	7.31 (2H, m)	7.27 (1H, m)	N/A
D-allo-Ile11,Arg10-teixobactin	D-N-Me-Phe	2.46 (3H, br s)	4.16 (1H, m)	(2H, 9.05, 8.99, v br s)	3.11 (1H, m)	2.97 (1H, dd, 13.0, 9.4)	N/A	7.22 (2H, m)	7.31 (2H, m)	7.26 (1H, m)	N/A
seco-Arg10-teixobactin	D-N-Me-Phe	2.47 (3H, br s)	4.17 (1H, m)	(2H, 9.05, 8.99, v br s)	3.12 (1H, m)	2.97 (1H, dd, 13.2, 9.7)	N/A	7.22 (2H, m)	7.31 (2H, m)	7.26 (1H, m)	N/A
ent-Arg10-teixobactin	L-N-Me-Phe	2.46 (3H, br s)	4.17 (1H, m)	(2H, 9.04, 8.97, v br s)	3.15 (1H, m)	3.11 (1H, m)	N/A	7.23 (2H, m)	7.31 (2H, m)	7.26 (1H, m)	N/A
short-Arg10-teixobactin	N/A	N/A	N/A	N/A	N/A	N/A	N/A	N/A	N/A	N/A	N/A
lipobactin 1	N/A	N/A	N/A	N/A	N/A	N/A	N/A	N/A	N/A	N/A	N/A

Homologue	Residue 2		9 9-NH		10	11	12		13	14
Teixobactin1	Ile	4.12 (1H, dd, 7.8, 7.2)	8.43 (1H, d, 7.2)	1.56 (1H, m)	0.62 (1H, d, 6.7)4	0.76 (1H, m)	1.07 (1H, m)	0.66 (3H, t, 7.1)	N/A	
Arg10-teixobactin	Ile3	4.16 (1H, dd, 8, 7.4)	8.48 (1H, d, 8.4)	1.55 (1H, m)	0.59 (3H, d, 6.6)	0.73 (1H, m)	1.04 (1H, m)	0.63 (3H, t, 7.5)	N/A	
Lys10-teixobactin	Ile	4.15 (1H, m)	8.48 (1H, m)	1.53 (1H, m)	0.60 (3H, d, 6.6)	0.71 (1H, m)	1.04 (1H, m)	0.63 (3H, t, 7.1)	N/A	
L-Thr8,Arg10-teixobactin	Ile	4.14 (1H, m)	8.49 (1H, m)	1.54 (1H, m)	0.59 (3H, m)	0.73 (1H, m)	1.08 (1H, m)	0.63 (3H, m)	N/A	
D-allo-Ile11,Arg10-teixobactin	Ile	4.15 (1H, m)	8.49 (1H, d, 8.4)	1.53 (1H, m)	0.59 (3H, d, 6.6)	0.73 (1H, m)	1.04 (1H, m)	0.64 (3H, t, 7.3)	N/A	
seco-Arg10-teixobactin	Ile	4.13 (1H, t, 7.9)	8.47 (1H, d, 8.4)	1.54 (1H, m)	0.60 (3H, d, 6.6)	0.73 (1H, m)	1.05 (1H, m)	0.66 (3H, t, 7.1)	N/A	
ent-Arg10-teixobactin	D-Ile	4.16 (1H, m)	8.48 (1H, m)	1.55 (1H, m)	0.59 (3H, m)	0.73 (1H, m)	1.04 (1H, m)	0.63 (3H, t, 7.5)	N/A	
short-Arg10-teixobactin	N/A	N/A	N/A	N/A	N/A	N/A	N/A	N/A	N/A	
lipobactin 1	N/A	N/A	N/A	N/A	N/A	N/A	N/A	N/A	N/A	

Homologue	Residue 3		15 15-NH		16	16-OH	17
Teixobactin1	Ser	4.34 (1H, m)	7.88 (1H, d, 7.9)	3.57 (1H, dd, 10.8, 5.6)	3.63 (1H, dd, m)	Exchanged	N/A
Arg10-teixobactin	Ser	4.35 (1H, m)	8.04 (1H, d, 7.9)	3.54 (1H, dd, 10.1, 4.6)	3.58 (1H, dd, 10.1, 4.6)	Exchanged	N/A
Lys10-teixobactin	Ser	4.36 (1H, m)	8.05 (1H, d, 7.9)	3.54 (1H, m)	3.60 (1H, m)	Exchanged	N/A
L-Thr8,Arg10-teixobactin	Ser	4.37 (1H, m)	8.01 (1H, m)	3.57 (1H m)	3.61 (1H, m)	Exchanged	N/A
D-allo-Ile11,Arg10-teixobactin	Ser	4.35 (1H, m)	8.04 (1H, d, 7.9)	3.53 (1H, dd, 10.0, 4.8)	3.57 (1H, dd, 10.4, 5.9)	Exchanged	N/A
seco-Arg10-teixobactin	Ser	4.31 (1H, m)	8.04 (1H, d, 7.5)	3.52 (1H, m)	3.57 (1H, m)	Exchanged	N/A
ent-Arg10-teixobactin	D-Ser	4.35 (1H, m)	8.04 (1H, d, 7.9)	3.54 (1H, m)	3.58 (1H, m)	Exchanged	N/A
short-Arg10-teixobactin	N/A	N/A	N/A	N/A	N/A	N/A	N/A
lipobactin 1	N/A	N/A	N/A	N/A	N/A	N/A	N/A

Homologue	Residue 4		18 18-NH		19	20	21 21-NH			22
Teixobactin1	D-Gln	4.33 (1H, m)	7.85 (1H, d, 7.9)	2.10 (2H, m)	1.74 (1H, m)	1.92 (1H, m)	N/A	6.63 (1H, br s)	7.11 (1H, br s)	N/A
Arg10-teixobactin	D-Gln	4.32 (1H, m)	7.95 (1H, br)	2.09 (2H, m)	1.70 (1H, m)	1.85 (1H, m)	N/A	not observed	not observed	N/A
Lys10-teixobactin	D-Gln	4.33 (1H, m)	7.97 (1H, m)	2.09 (2H, m)	1.70 (1H, m)	1.87 (1H, m)	N/A	not observed	not observed	N/A
L-Thr8,Arg10-teixobactin	D-Gln	4.35 (1H, m)	7.95 (1H, m)	2.08 (2H, m)	1.70 (1H, m)	1.88 (1H, m)	N/A	not observed	not observed	N/A
D-allo-Ile11,Arg10-teixobactin	D-Gln	4.34 (1H, m)	7.95 (1H, d, 8.0)	2.07 (2H, dq, 9.2, 6.6)	1.69 (1H, m)	1.85 (1H, m)	N/A	not observed	not observed	N/A
seco-Arg10-teixobactin	D-Gln	4.34 (1H, m)	7.99 (1H, m)	2.08 (2H, m)	1.72 (1H, m)	1.89 (1H, m)	N/A	not observed	not observed	N/A
ent-Arg10-teixobactin	L-Gln	4.32 (1H, m)	7.95 (1H, br)	2.09 (2H, m)	1.70 (1H, m)	1.85 (1H, m)	N/A	not observed	not observed	N/A
short-Arg10-teixobactin	N/A	N/A	N/A	N/A	N/A	N/A	N/A	N/A	N/A	N/A
lipobactin 1	N/A	N/A	N/A	N/A	N/A	N/A	N/A	N/A	N/A	N/A

Homologue	Residue 5		23 23-NH		24	25	26		27	28
Teixobactin1	D-allo-Ile	4.36 (1H, m)	7.70 (1H, d, 8.8)	1.80 (2H, m)	0.82 (3H, m)	1.09 (1H, m)	1.32 (1H, m)	0.82 (3H, m)	N/A	
Arg10-teixobactin	D-allo-Ile3	4.37 (1H, m)	7.74 (1H, d, 9.1)	1.80 (1H, m)	0.84 (3H, m)	1.07 (1H, m)	1.30 (1H, m)	0.78 (3H, m)	N/A	
Lys10-teixobactin	D-allo-Ile	4.38 (1H, m)	7.74 (1H, d, 9.0)	1.78 (1H, m)	0.83 (3H, m)	1.07 (1H, m)	1.31 (1H, m)	0.77 (3H, t, 6.7)	N/A	
L-Thr8,Arg10-teixobactin	D-allo-Ile	4.39 (1H, m)	7.76 (1H, m)	1.78 (1H, m)	0.82 (3H, m)	1.06 (1H, m)	1.28 (1H, m)	0.77 (3H, m)	N/A	
D-allo-Ile11,Arg10-teixobactin	D-allo-Ile	4.38 (1H, m)	7.76 (1H, d, 9.0)	1.77 (1H, m)	0.82 (3H, m)	1.06 (1H, m)	1.28 (1H, m)	0.77 (3H, t, 6.6)	N/A	
seco-Arg10-teixobactin	D-allo-Ile	4.18 (1H, m)	7.87 (1H, d, 8.1)	1.80 (1H, m)	0.86 (3H, m)	1.20 (1H, m)	1.40 (1H)	0.77 (3H, m)	N/A	
ent-Arg10-teixobactin	L-allo-Ile	4.37 (1H, m)	7.74 (1H, d, 9.1)	1.80 (1H, m)	0.84 (3H, m)	1.07 (1H, m)	1.30 (1H, m)	0.78 (3H, m)	N/A	
short-Arg10-teixobactin	N/A	N/A	N/A	N/A	N/A	N/A	N/A	N/A	N/A	

Homologue	Residue 5	27-17
lipobactin 1	dodecanoyl	2.2-0.8 (23H, m)5

Homologue	Residue 6		29 29-NH		30	31	32		33	34
Teixobactin1	Ile	4.29 (1H, m)	7.78 (1H, d, 8.8)	1.83 (1H, m)	0.84 (3H, m)	1.11 (1H, m)	1.42 (1H, m)	0.85 (3H, m)	N/A	
Arg10-teixobactin	Ile3	4.21 (1H, m)	a7.97 (1H, br)	1.80 (1H, m)	0.84 (3H, m)	1.14 (1H, m)	1.41 (1H, m)	0.84 (3H, m)	N/A	
Lys10-teixobactin	Ile	4.21 (1H, m)	7.96 (1H, m)	1.80 (1H, m)	0.83 (3H, d, 6.3)	1.14 (1H, m)	1.4 (1H, m)	0.83 (3H, m)	N/A	
L-Thr8,Arg10-teixobactin	Ile	4. 29 (1H, m)	7.95 (1H, m)	1.76 (1H, m)	0.83 (3H, m)	1.09 (1H, m)	1.38 (1H, m)	0.81 (3H, m)	N/A	
D-allo-Ile11,Arg10-teixobactin	Ile	4.22 (1H, m)	7.91 (1H, d, 8.5)	1.75 (1H, m)	0.83 (3H, m)	1.10 (1H, m)	1.40 (1H, m)	0.82 (3H, t, 6.6)	N/A	
seco-Arg10-teixobactin	Ile	4.35 (1H, m)	8.00 (1H, m)	1.78 (1H, m)	0.84 (3H, m)	1.11 (1H, m)	1.40 (1H, m)	0.82 (3H, m)	N/A	
ent-Arg10-teixobactin	D-Ile	4.21 (1H, m)	7.97 (1H, br)	1.80 (1H, m)	0.84 (3H, m)	1.14 (1H, m)	1.41 (1H, m)	0.84 (3H, m)	N/A	
short-Arg10-teixobactin	Ile	3.72(1H, m)	8.08 (3H, br)	1.81 (1H, m)	0.91 (3H, d, 6.5)	1.17 (1H, m)	1.54 (1H, m)	0.86 (3H, t, 7.3)	N/A	
lipobactin 1	Ile	4.25 (1H, t, 8.2)	7.78 (1H, d, 8.2)	1.73 (1H, m)	0.85 (3H, m)	1.11 (1H, m)	1.43 (1H, m)	0.79 (3H, m)	N/A	

Homclogue	Residue 7		35 35-NH		36	36-OH	37
Teixobactin1	Ser	4.47 (1H, dt, 5.0, 5.2)	8.37 (1H, d, 5.2)	3.64 (1H, m)	3.80 (1H, dd, 10.8, 5.0)	Exchanged	N/A
Arg10-teixobactin	Ser	a4.31 (1H, m)	8.45 (1H, br)	3.67 (1H, m)	3.73 (1H, m)	Exchanged	N/A
Lys10-teixobactin	Ser	4.32 (1H, m)	8.48 (1H, m)	3.67 (1H, m)	3.74 (1H, m)	Exchanged	N/A
L-Thr8,Arg10-teixobactin	Ser	4.95 (1H, m)	8.25 (1H, m)	3.57 (1H, m)	3.61 (1H, m)	Exchanged	N/A
D-allo-Ile11,Arg10-teixobactin	Ser	4.24 (1H, m)	8.37 (1H, d, 4.4)	3.66 (1H, m)	3.69 (1H, m)	Exchanged	N/A
seco-Arg10-teixobactin	Ser	4.34 (1H, m)	8.18 (1H, d, 7.1)	3.57 (1H, m)	3.63 (1H, m)	Exchanged	N/A
ent-Arg10-teixobactin	D-Ser	4.31 (1H, m)	8.45 (1H, m)	3.67 (1H, m)	3.73 (1H, m)	Exchanged	N/A
short-Arg10-teixobactin	Ser	4.54 (1H, q, 5.6)	8.87 (1H, br)	3.69 (1H, m)	3.77 (1H, m)	Exchanged	N/A
lipobactin 1	Ser	4.36 (1H, q, 5.3)	8.58 (1H, br)	3.63 (1H, dd, 9.7, 6.0)	3.74 (1H, dd, 9.5, 5.1)	Exchanged	N/A

Homclogue	Residue 8		38 38-NH		39	40	41
Teixobactin1	D-Thr	4.64 (1H, dd, 9.5, 2.2)	N/A	5.36 (1H, dq, 2.2, 6.4)	1.13 (3H, d, 6.4)	N/A	
Arg10-teixobactin	D-Thr	4.61 (1H, m)	8.04 (1H, d, 8.2)	5.34 (1H, dq, 1.9, 5.7)	1.14 (3H, d, 6.4)	N/A	
Lys10-teixobactin	D-Thr	4.59 (1H, br)	8.06(1H, m)	5.36 (1H, m)	1.14 (3H, d, 6.4)	N/A	
L-Thr8,Arg10-teixobactin	D-Thr	4.62 (1H, m)	7.73 (1H, m)	4.81 (1H, m)	1.09 (3H, m)	N/A	
D-allo-Ile11,Arg10-teixobactin	D-Thr	4.63 (1H, m)	8.18 (1H, br)	5.33 (1H, m)	1.15 (3H, d, 6.4)	N/A	
seco-Arg10-teixobactin	D-Thr	4.19 (1H, m)	7.66 (1H, d, 8.07)	4.07 (1H, m)	1.02 (3H, d, 6.4))	N/A	
ent-Arg10-teixobactin	L-Thr	4.61 (1H, m)	8.04 (1H, d, 8.2)	5.34 (1H, m)	1.14 (3H, d, 6.4)	N/A	
short-Arg10-teixobactin	D-Thr	4.63 (1H, m)	8.18 (1H, br)	5.33 (1H, m)	1.15 (3H, d, 6.4)	N/A	
lipobactin 1	D-Thr	4.61 (1H, m)	8.25 (1H, br)	5.35 (1H, m)	1.11 (3H, d, 6.3)	N/A	

Homclogue	Residue 9		42 42-NH		43	44
Teixobactin1	Ala	3.97 (1H, dq, 5.1, 7.5)	8.05 (1H, d, 5.1)	1.34 (3H, d, 7.5)	N/A	
Arg10-teixobactin	Ala	3.94 (1H, dq, 5.4, 7.2)	8.08 (1H, br)	1.33 (3H, d, 7.2)	N/A	
Lys10-teixobactin	Ala	3.93 (1H, dq, 5.9 ,7.0)	8.10 (1H, m)	1.35 (3H, d, 7.2)	N/A	
L-Thr8,Arg10-teixobactin	Ala	4.50 (1H, m)	9.23 (1H, m)	1.38 (3H, m)	N/A	
D-allo-Ile11,Arg10-teixobactin	Ala	4.00 (1H, dq, 5.5, 7.2)	8.11 (1H, m)	1.35 (3H, d, 7.6)	N/A	
seco-Arg10-teixobactin	Ala	4.33 (1H, m)	7.81 (1H, d, 7.2)	1.21 (3H, d, 6.9)	N/A	
ent-Arg10-teixobactin	D-Ala	3.94 (1H, m)	8.08 (1H, br)	1.33 (3H, m)	N/A	
short-Arg10-teixobactin	Ala	3.98 (1H, quin, 6.5)	7.85 (1H, d, 5.1)	1.33 (3H, d, 7.2)	N/A	
lipobactin 1	Ala	3.92 (1H, dq, 5.7, 7.0)	8.15 (1H, br)	1.32 (3H, d, 7.3)	N/A	

Homclogue	Residue 10		45 45-NH		46		47	47-NH		48	48-NH		49 49-NH	50
Teixobactin1	End	4.38 (1H, m)	8.43 (1H, d, 9.1)	3.02 (2H, m)	N/A	3.90 (1H, m)	N/A	7.95 (1H, br s)	3.36 (1H, dd, 9.4, 7.7)	3.66 (1H, t, 9.4)	8.1 (1H, br s)	N/A	7.76 (2H, br s)	N/A
Arg10-teixobactin	Arg	4.31 (1H, m)	7.74 (1H, d, 8.7)	1.78 (1H, m)	1.65 (1H, m)	1.52 (1H, m)	1.44 (1H, m)	not observed	3.14 (2H, m)	N/A	not observed	N/A	7.60 (1H, m)	N/A
Lys10-teixobactin	Lys	4.31 (1H, m)	7.67 (1H, m)	1.75 (2H, m)5	N/A	1.35 (1H, m)5	1.28 (1H, m)5	N/A	1.65 (1H, m)5	1.57 (1H, m)5	N/A	2.79 (2H, q, 5.3)	7.67 (3H, br)	N/A
L-Thr8,Arg10-teixobactin	Arg	4.11 (1H, m)	8.86 (1H, m)	1.75 (1H, m)	1.54 (1H, m)	1.49 (1H, m)	1.37 (1H, m)	not observed	3.13 (2H, m)	N/A	not observed	N/A	7.61 (1H, m)	N/A
D-allo-Ile11,Arg10-teixobactin	Arg	4.35 (1H, m)	7.52 (1H, m)	1.87 (1H, m)	1.68 (1H, m)	1.46 (1H, m)	1.43 (1H, m)	not observed	3.13 (2H, m)	N/A	not observed	N/A	7.54 (1H, m)	N/A
seco-Arg10-teixobactin	Arg	4.36 (1H, m)	8.09 (1H, d, 7.8))	1.71 (1H, m)	1.68 (1H, m)	1.53 (1H, m)	1.49 (1H, m)	not observed	3.11 (2H, m)	N/A	not observed	N/A	7.46 (1H, t, 5.4))	N/A
ent-Arg10-teixobactin	D-Arg	4.31 (1H, m)	7.74 (1H, m)	1.78 (1H, m)	1.65 (1H, m)	1.52 (1H, m)	1.44 (1H, m)	not observed	3.14 (2H, m)	N/A	not observed	N/A	7.60 (1H, m)	N/A
short-Arg10-teixobactin	Arg	4.28 (1H, q, 6.9)	7.79 (1H, m)	1.78 (1H, m)	1.63 (1H, m)	1.52 (1H, m)	1.44 (1H, m)	7.57 (1H, t, 5.4)	3.13 (2H, m)	N/A	not observed	N/A	7.57 (1H, t, 5.4)	N/A
lipobactin 1	Arg	4.29 (1H, q, 7.2)	7.95 (1H, m)	1.79 (1H, m)	1.68 (1H, m)	1.52 (1H, m)	1.43 (1H, m)	7.58 (1H, t, 5.4)	3.13 (2H, m)	N/A	not observed	N/A	7.58 (1H, t, 5.4)	N/A

Homclogue	Residue 11		51 51-NH		52	53	54		55	56 56-COOH
Teixobactin1	Ile	4.03 (1H, t, 9.4)	8.01 (1H, d, 9.4)	1.77 (1H, m)	0.81 (3H, m)	0.77 (1H, m)	1.07 (1H, m)	0.82 (3H, m)	N/A	N/A
Arg10-teixobactin	Ile3	4.04 (1H, t, 9.7)	7.67 (1H, m)	1.72 (1H, m)	0.82 (3H, m)	1.11 (1H, m)	1.44 (1H, m)	0.82 (3H, m)	N/A	N/A
Lys10-teixobactin	Ile	4.03 (1H, t, 9.4)	7.67 (1H, m)	1.73 (1H, m)	0.83 (3H, m)	1.12 (1H, m)	1.45 (1H, m)	0.83 (3H, m)	N/A	N/A
L-Thr8,Arg10-teixobactin	Ile	4.42 (1H, m)	7.78 (1H m)	1.81 (1H, m)	0.76 (3H, m)	1.09 (1H, m)	1.28 (1H, m)	0.83 (3H, m)	N/A	N/A
D-allo-Ile11,Arg10-teixobactin	D-allo-Ile	4.42 (1H, dd, 8.8, 5.4)	7.21 (1H, m)	1.90 (1H, m)	0.78 (3H, d, 6.7)	1.08 (1H, m)	1.29 (1H,, m)	0.86 (3H, t, 7.6)	N/A	N/A
seco-Arg10-teixobactin	Ile	4.47 (1H, dd, 8.8, 4.7))	7.78 (1H, d, 9.1)	1.80 (1H, m)	0.77 (3H, m)	1.07 (1H, m)	1.27 (1H, m)	0.84 (3H, m)	N/A	12.61 (1H, br)
ent-Arg10-teixobactin	D-Ile	4.04 (1H, m)	7.67 (1H, m)	1.72 (1H, m)	0.82 (3H, m)	1.11 (1H, m)	1.44 (1H, m)	0.82 (3H, m)	N/A	N/A
short-Arg10-teixobactin	Ile	4.04 (1H, t, 9.7)	7.52 (1H, m)	1.69 (1H, m)	0.82 (3H, d, 6.5)	1.11 (1H, m)	1.42 (1H, m)	0.83 (3H, t, 7.3)	N/A	N/A
lipobactin 1	Ile	4.02 (1H, t, 9.8)	7.92 (1H, m)	1.76 (1H, m)	0.83 (3H, m)	1.12 (1H, m)	1.43 (1H, m)	0.81 (3H, m)	N/A	N/A

Arg_{10}-teixobactin : Mass spectrum and Analytical RP-HPLC

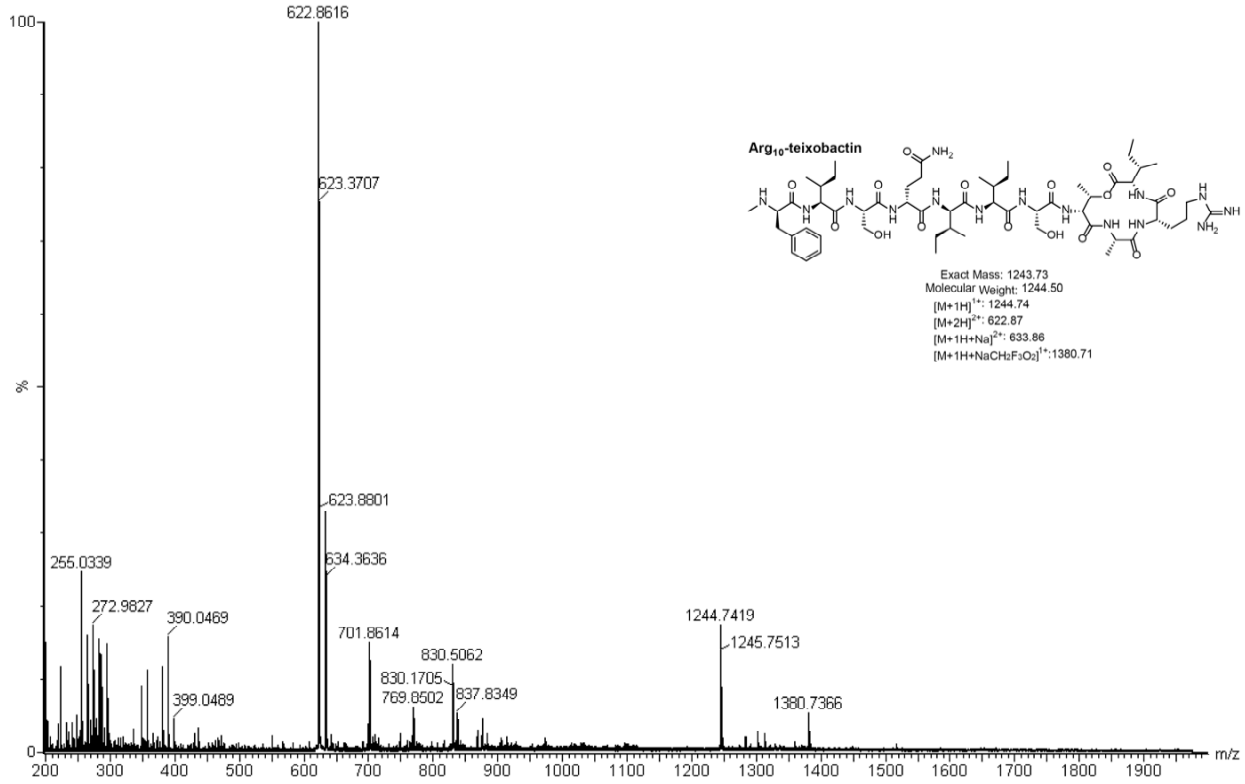

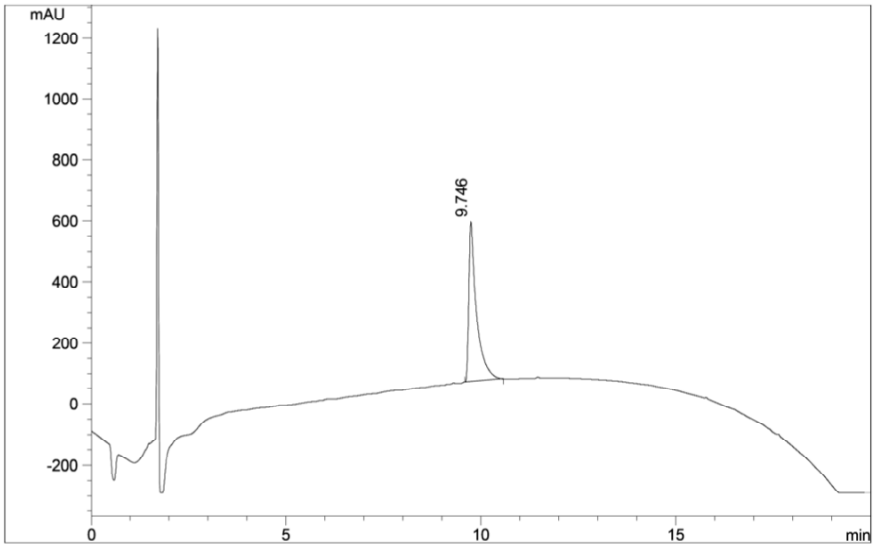

Signal 1:VWD1 A, Wavelength=214 nm

Peak #	RT [min]	Type	Width [min]	Area mAU*s	Height [mAU]	Area %
1	9.746	MM	0.226	7116.659	100.000	100.000

Arg_{10}-teixobactin : ^{1}H NMR spectrum in DMSO-*d6* (600 MHz)

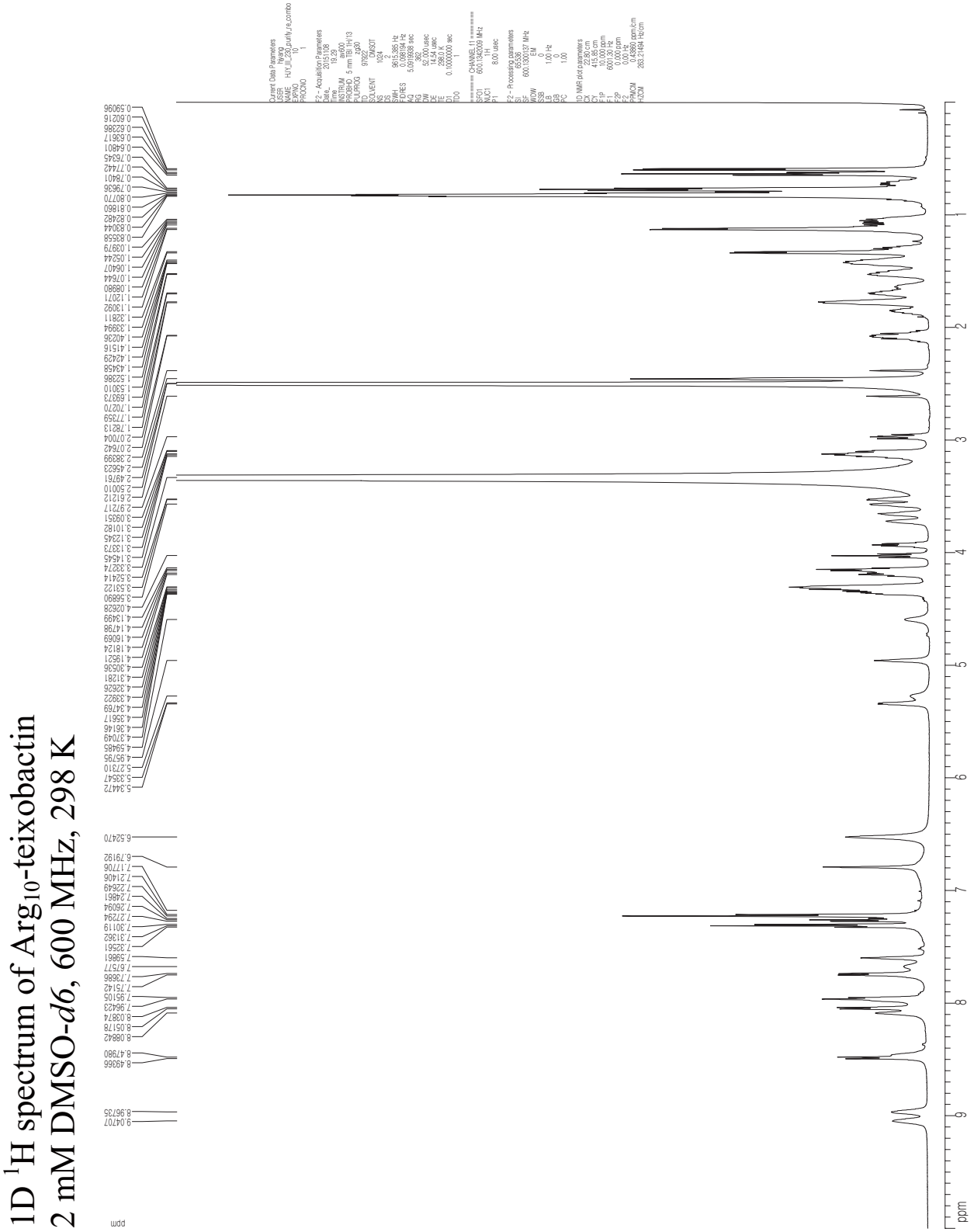

Arg_{10}-teixobactin : TOCSY spectrum in DMSO-*d6* (600 MHz)

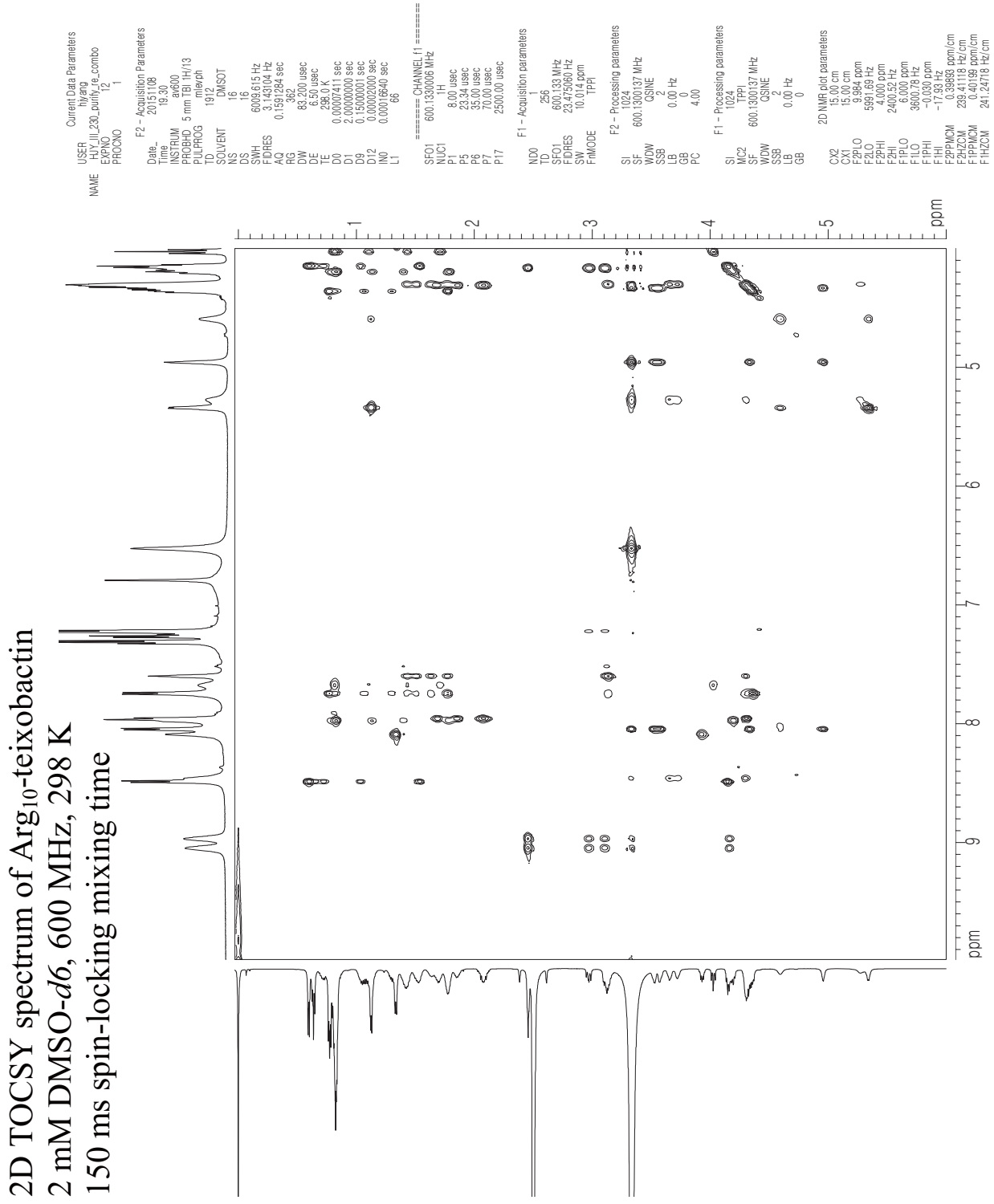

Arg_{10}-teixobactin : NOESY spectrum in DMSO-*d6* (500 MHz)

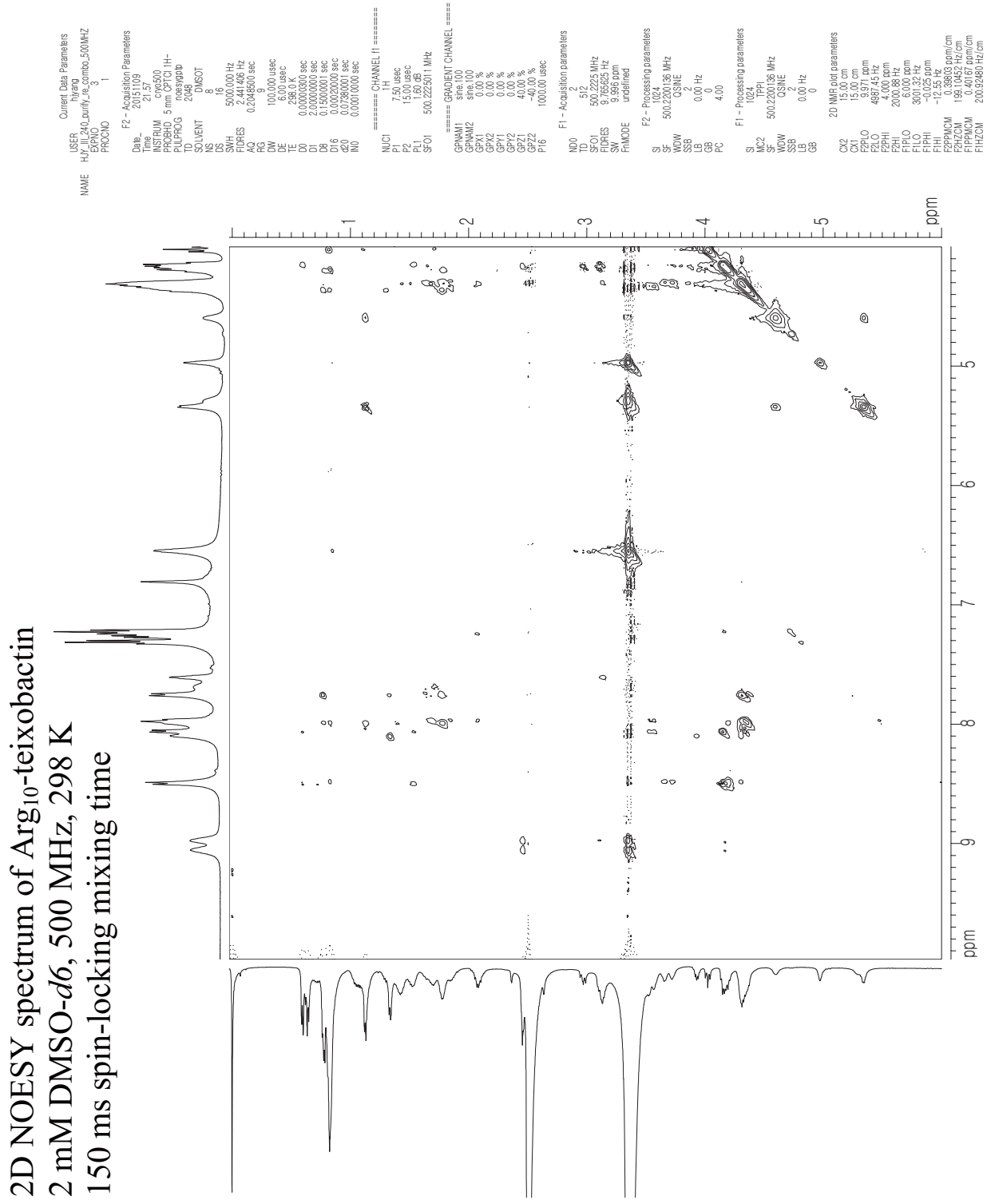

Lys_{10}-teixobactin : Mass spectrum and Analytical RP-HPLC

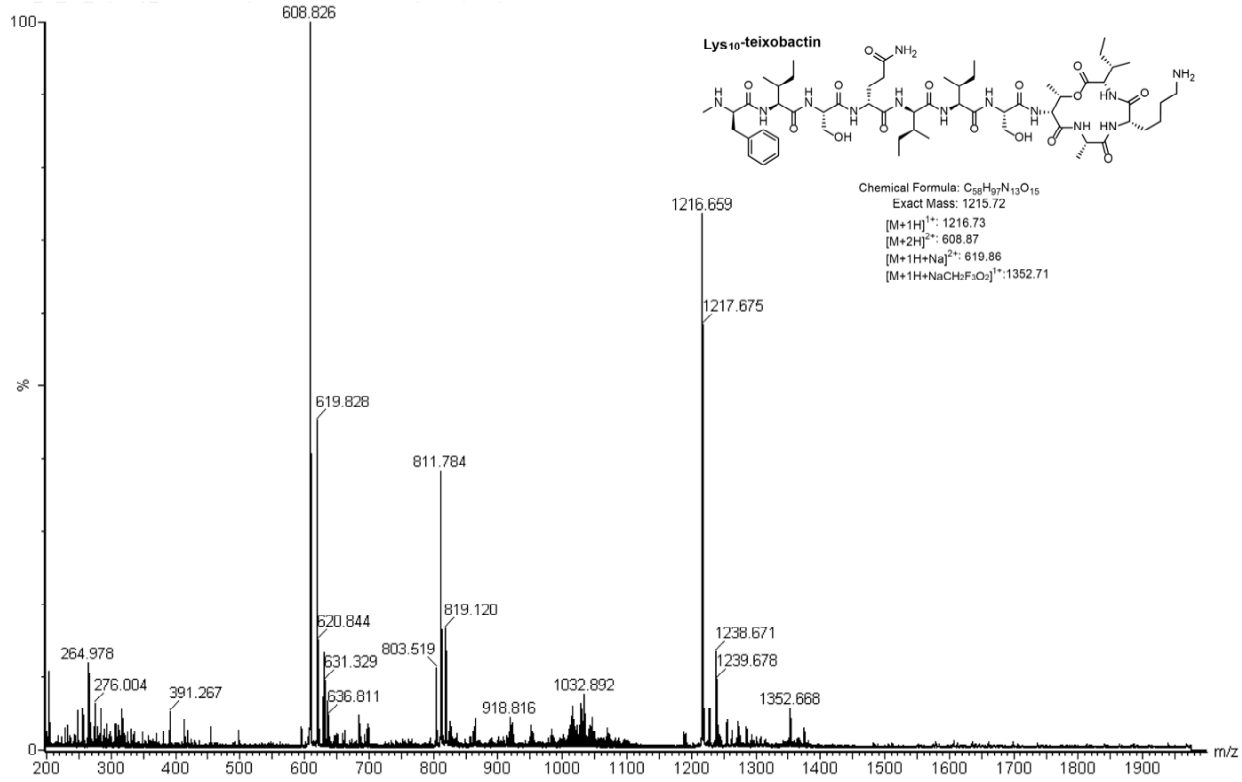

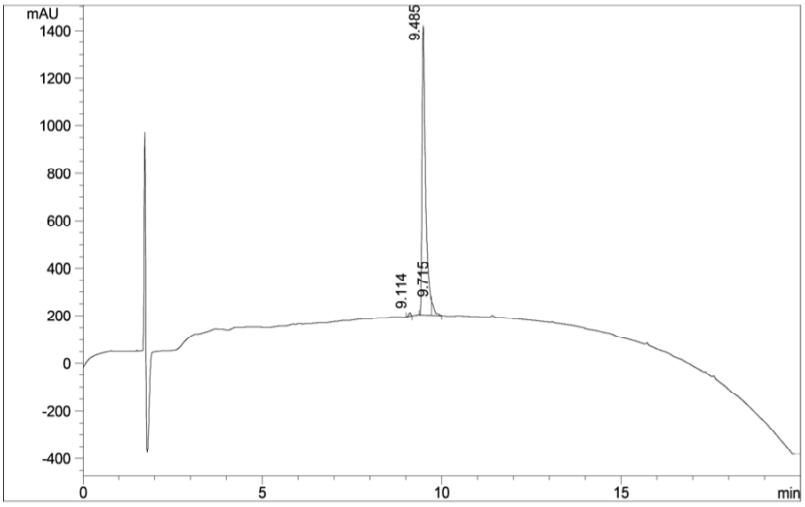

Signal 1:VWD1 A, Wavelength=214 nm

Peak #	RT [min]	Type	Width [min]	Area mAU*s	Height [mAU]	Area %
1	9.114	MM	0.068	62.311	1.187	0.725
2	9.485	MF	0.112	8234.027	94.222	95.857
3	9.715	FM	0.082	293.588	4.592	3.418

Lys$_{10}$-teixobactin : ^{1}H NMR spectrum in DMSO-*d6* (600 MHz)

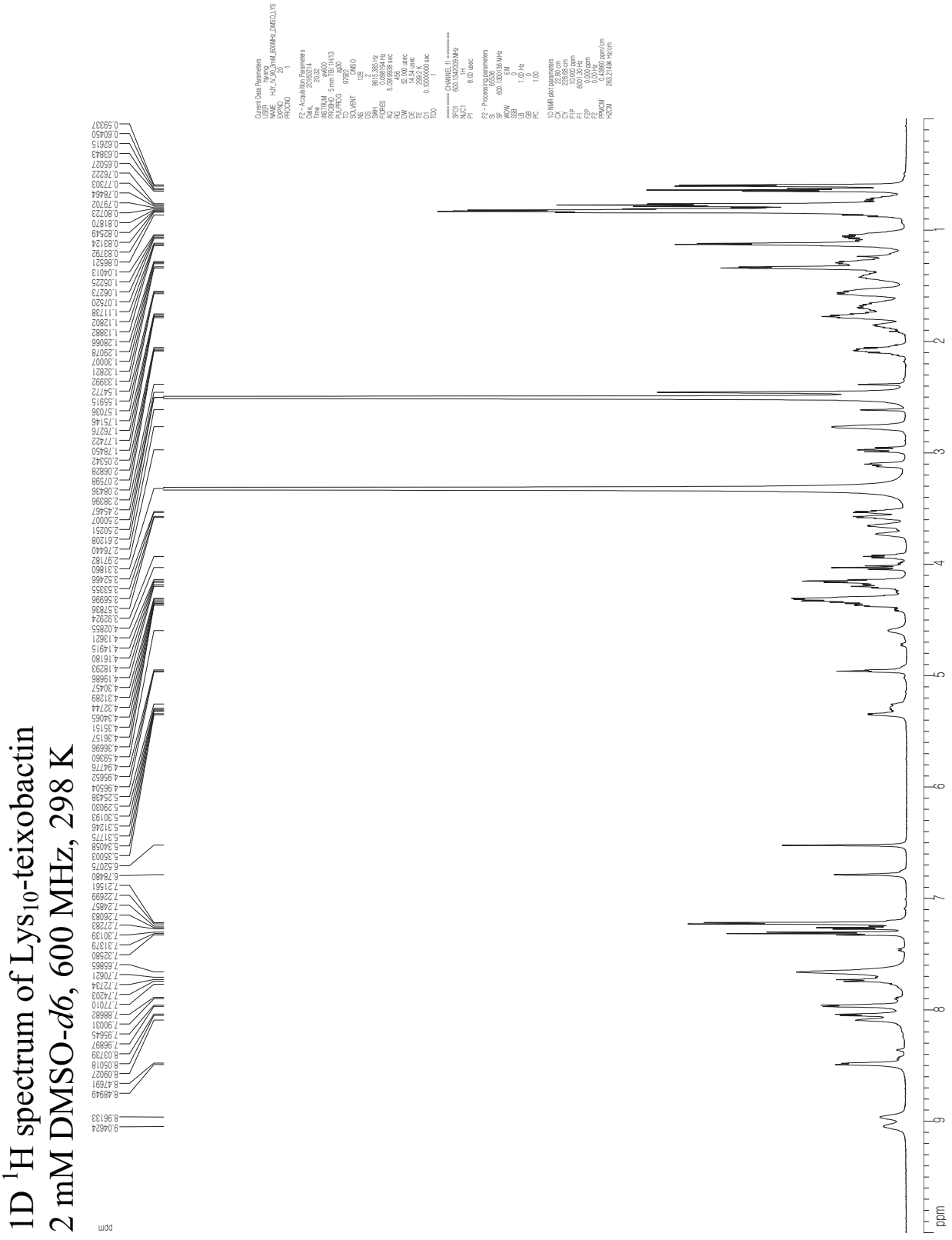

Lys$_{10}$-teixobactin : TOCSY spectrum in DMSO-*d6* (600 MHz)

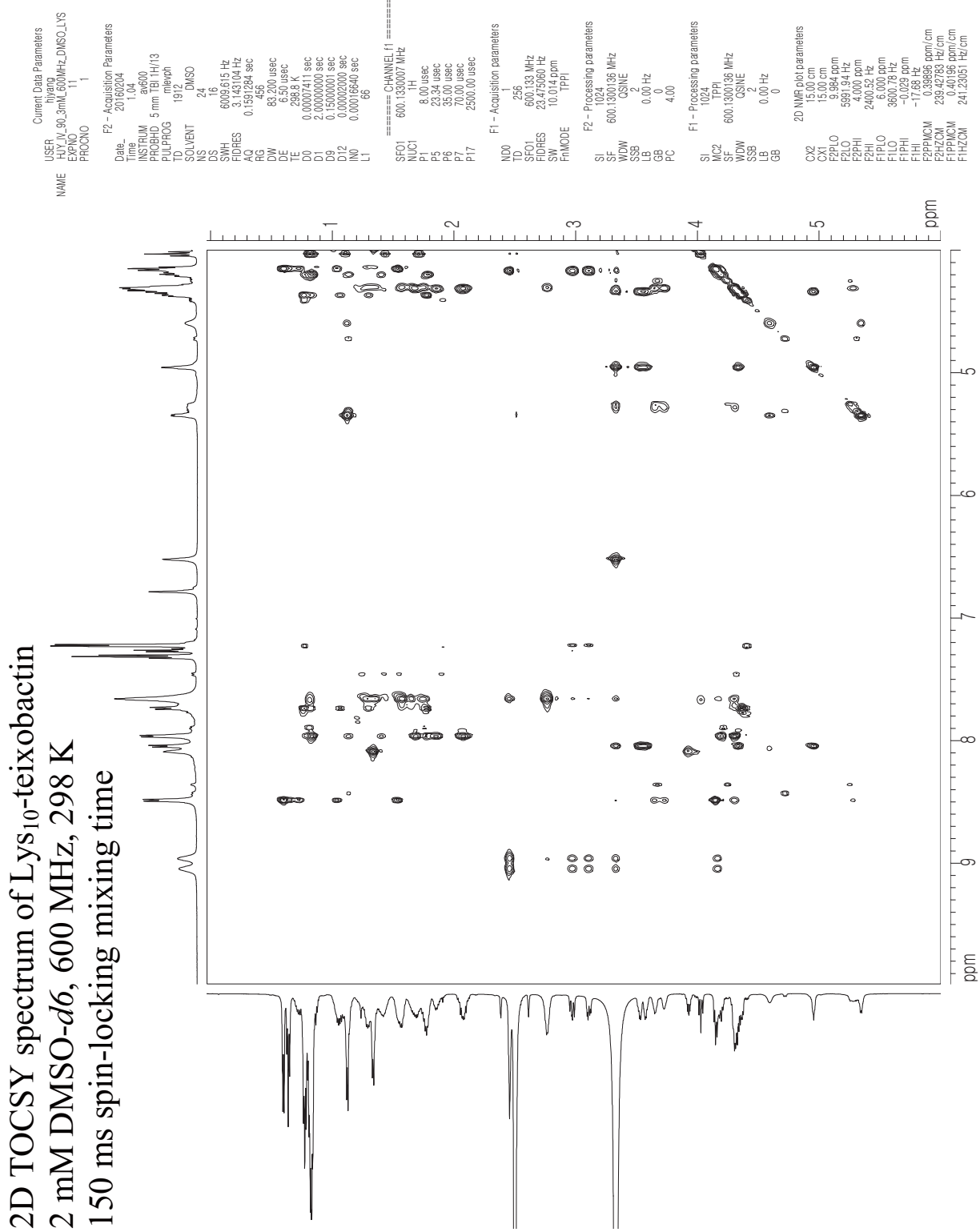

Lys$_{10}$-teixobactin : COSY spectrum in DMSO-*d6* (600 MHz)

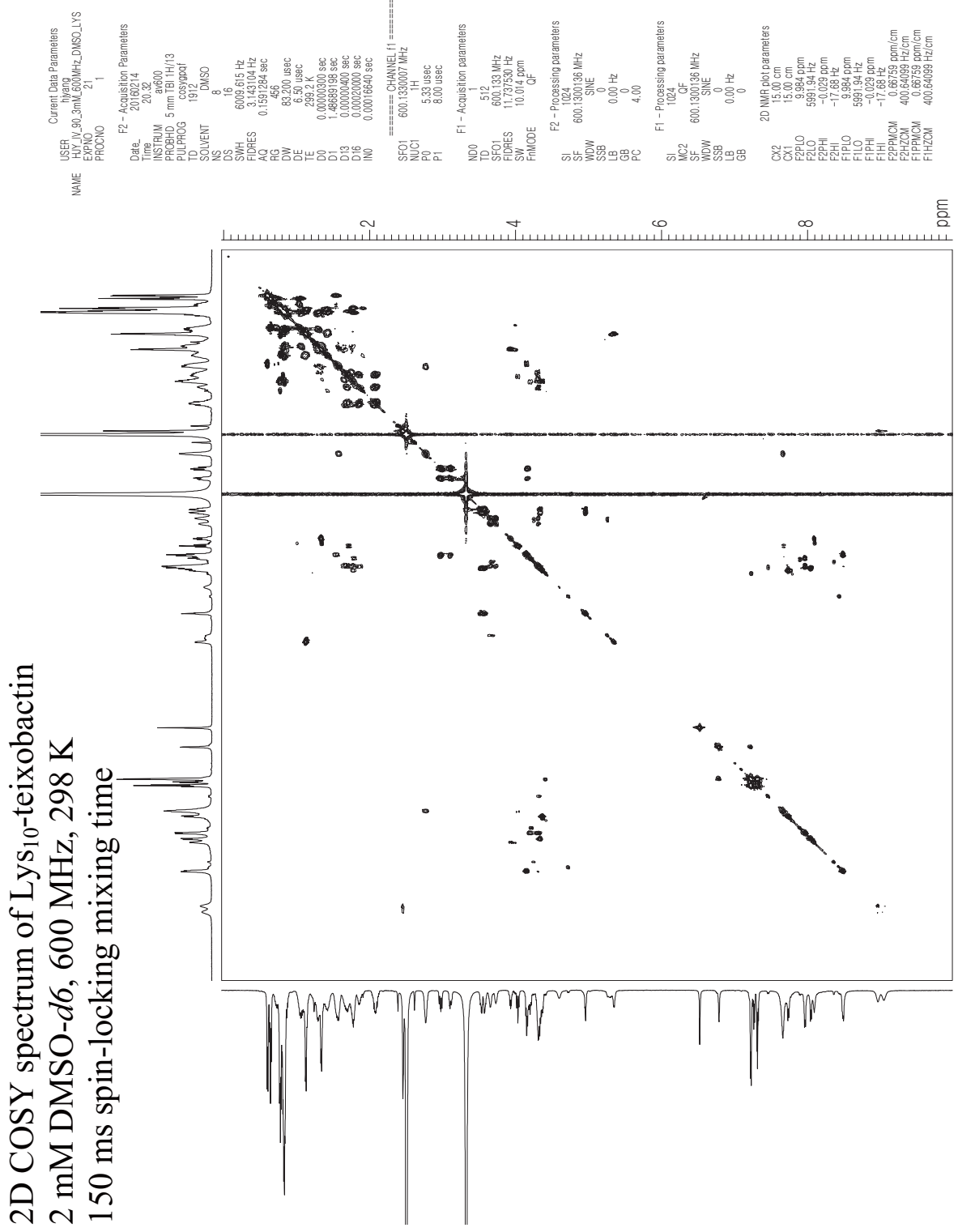

L-Thr$_8$-Arg$_{10}$-teixobactin : Mass spectrum and Analytical RP-HPLC

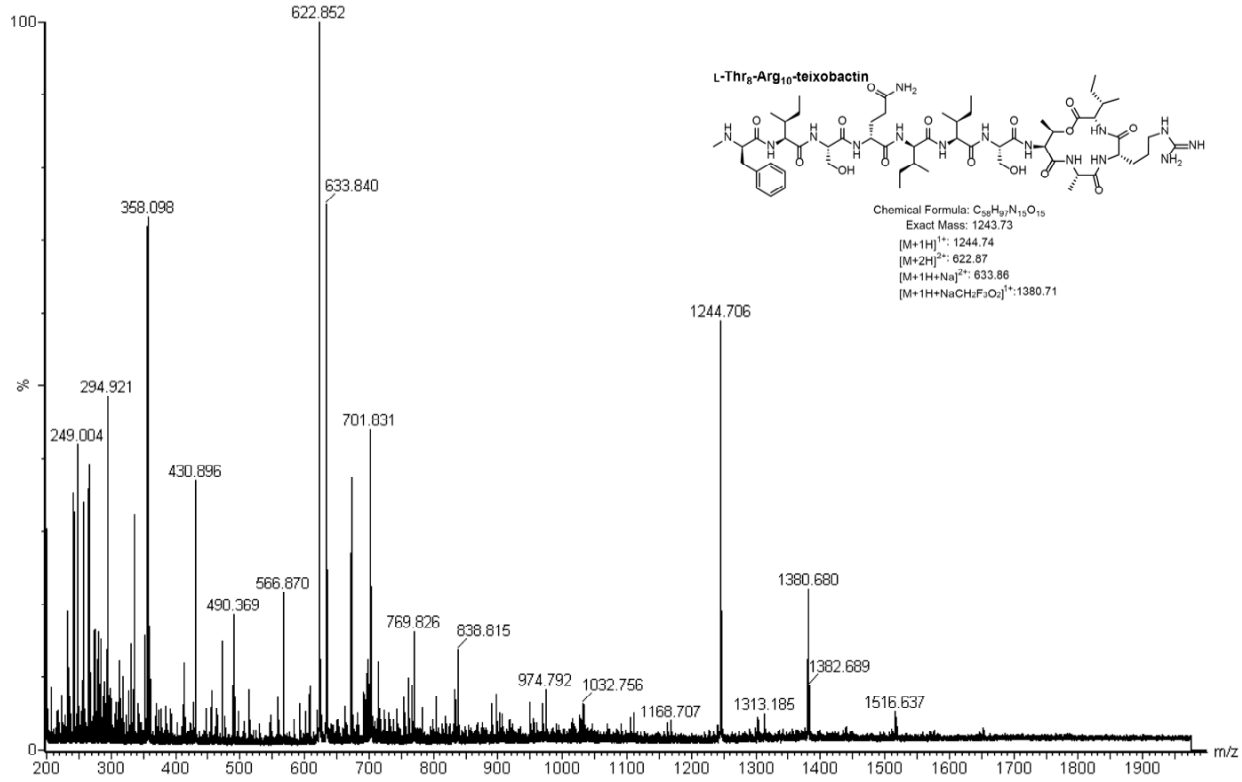

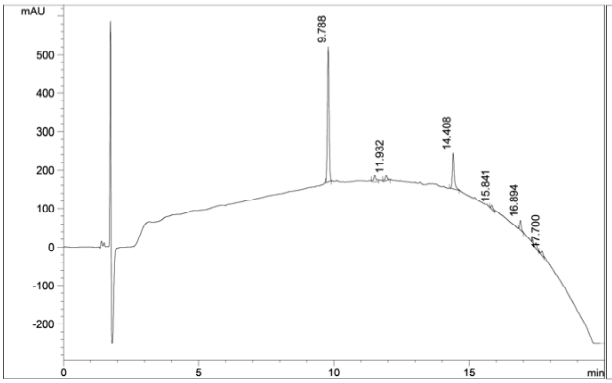

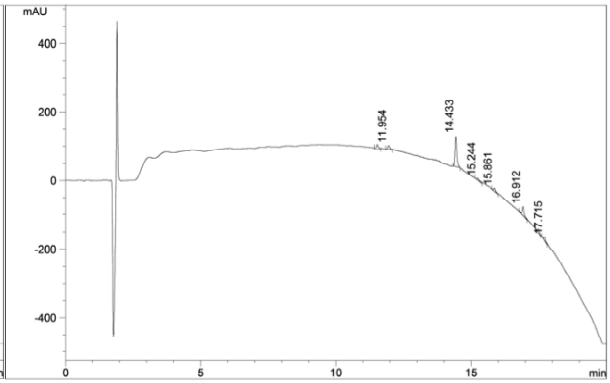

Signal 1:VWD1 A, Wavelength=214 nm

Peak #	RT [min]	Type	Width [min]	Area mAU*s	Height [mAU]	Area %
1	9.788	MM	0.073	1542.626	65.625	61.835
2	11.507	MM	0.110	111.939	3.134	4.487
3	11.932	MM	0.106	81.198	2.368	3.255
4	14.408	MM	0.081	453.000	17.359	18.158
5	15.841	MM	0.094	63.624	2.086	2.550
6	16.894	MM	0.065	96.093	4.561	3.852
7	17.472	MM	0.098	83.620	2.636	3.352
8	17.700	MM	0.087	62.655	2.231	2.511

Signal 1:VWD1 A, Wavelength=214 nm

Peak #	RT [min]	Type	Width [min]	Area mAU*s	Height [mAU]	Area %
1	11.529	MM	0.109	89.495	7.706	9.963
2	11.954	MM	0.100	72.988	6.848	8.125
3	14.433	MM	0.073	389.539	49.873	43.365
4	15.244	MM	0.137	41.289	2.837	4.597
5	15.861	MM	0.093	54.164	5.489	6.030
6	16.912	MM	0.087	138.678	15.043	15.438
7	17.491	MM	0.093	64.065	6.430	7.132
8	17.715	MM	0.078	48.057	5.774	5.350

L-Thr$_8$-Arg$_{10}$-teixobactin : ^{1}H NMR spectrum in DMSO-*d6* (600 MHz)

1D ^{1}H spectrum of L-Thr,Arg$_{10}$-teixobactin
2 mM DMSO-*d6*, 600 MHz, 298 K

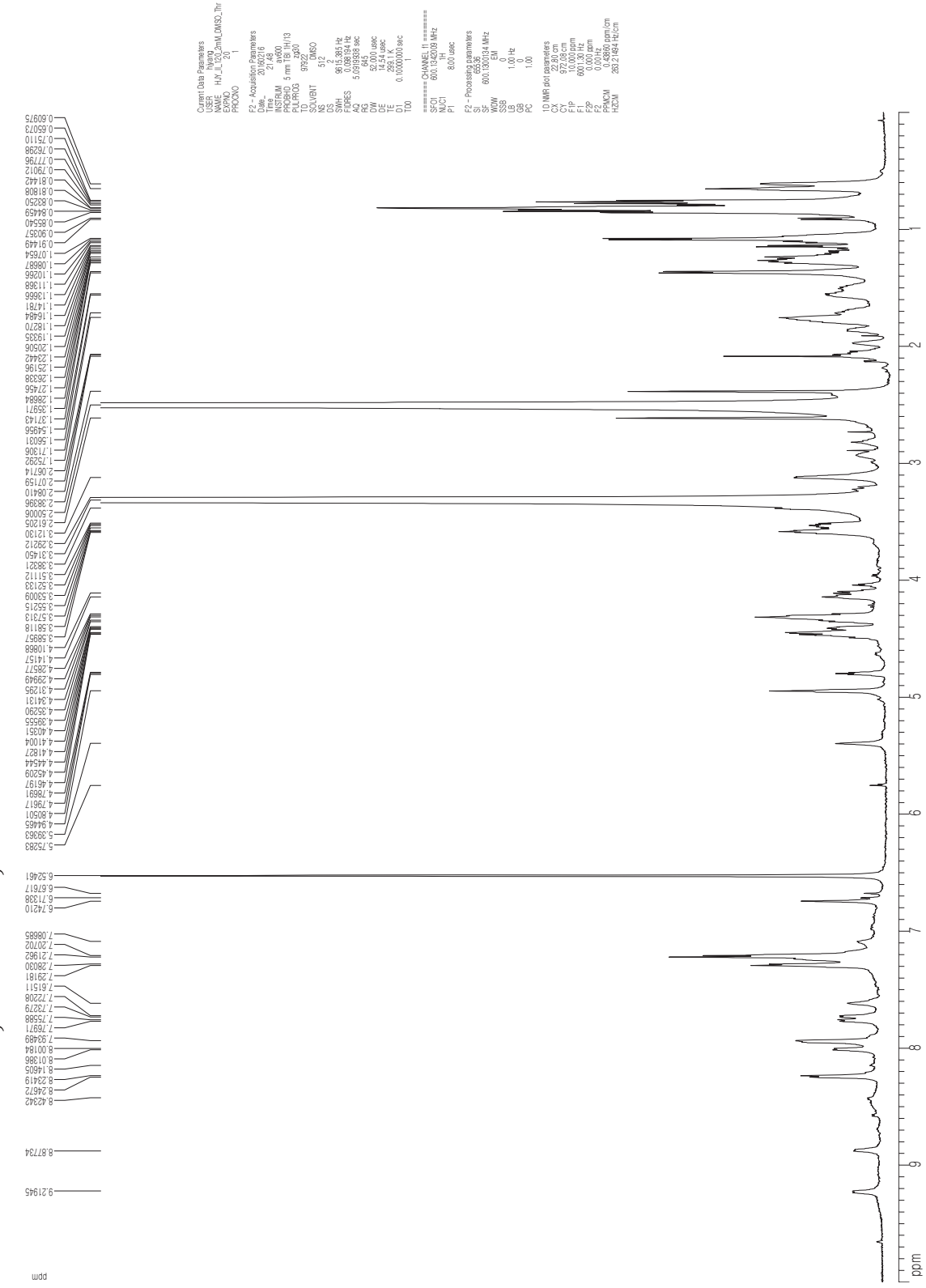

L-Thr$_8$-Arg$_{10}$-teixobactin : TOCSY spectrum in DMSO-*d6* (600 MHz)

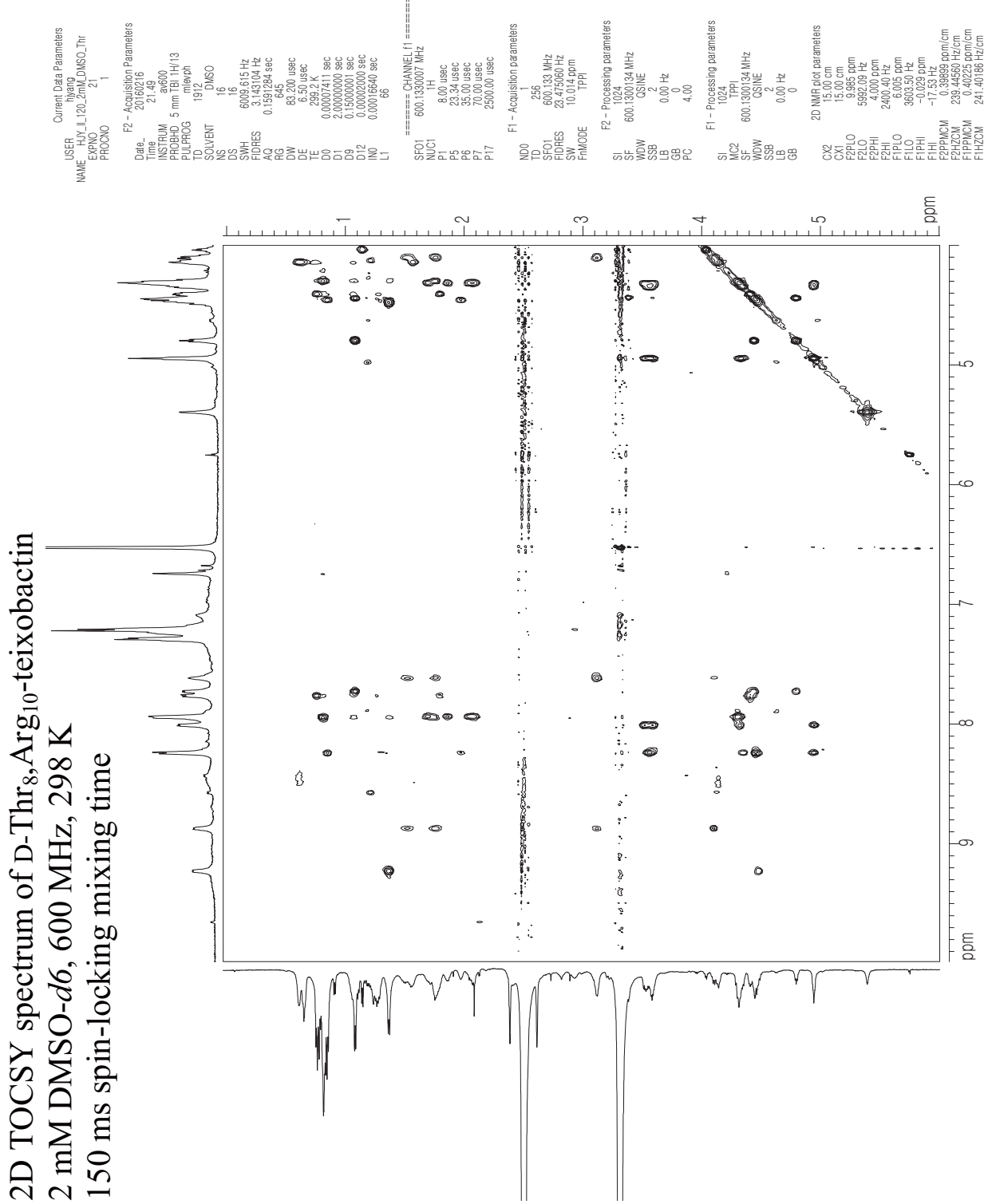

D-*allo*-Ile$_{11}$-Arg$_{10}$-teixobactin : Mass spectrum and Analytical RP-HPLC

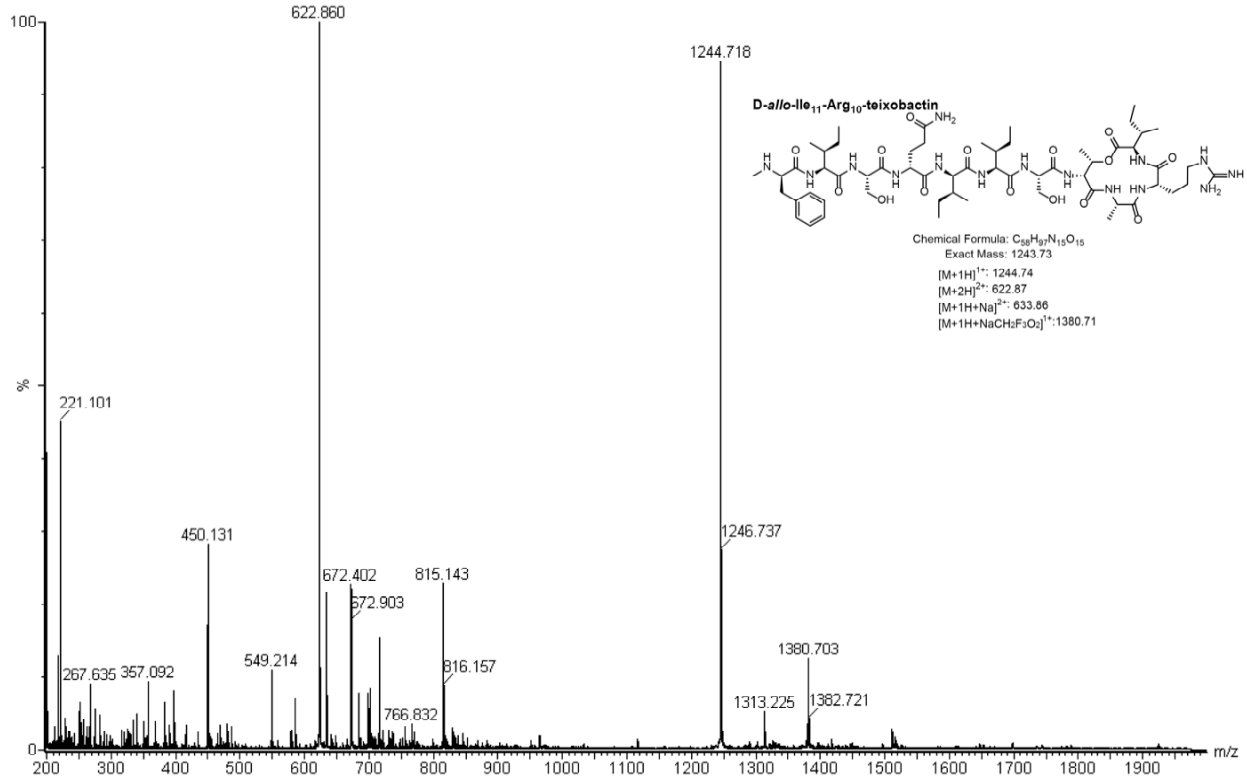

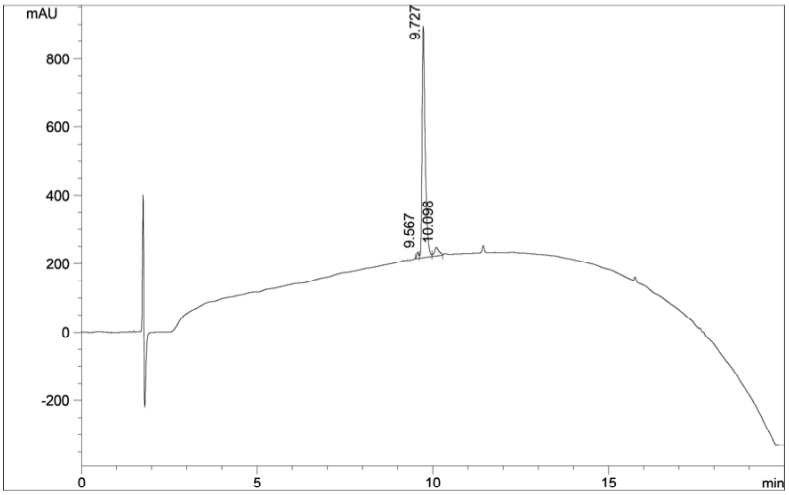

Signal 1:VWD1 A, Wavelength=214 nm

Peak #	RT [min]	Type	Width [min]	Area mAU*s	Height [mAU]	Area %
1	9.567	MF	0.066	72.238	2.511	1.631
2	9.727	FM	0.101	4115.366	93.954	92.932
3	10.098	FM	0.157	240.780	3.534	5.437

D-*allo*-Ile$_{11}$-Arg$_{10}$-teixobactin : ^{1}H NMR spectrum in DMSO-*d6* (600 MHz)

1D ^{1}H spectrum of D-*allo*-Ile$_{11}$,Arg$_{10}$-teixobactin
2 mM DMSO-*d6*, 600 MHz, 298 K

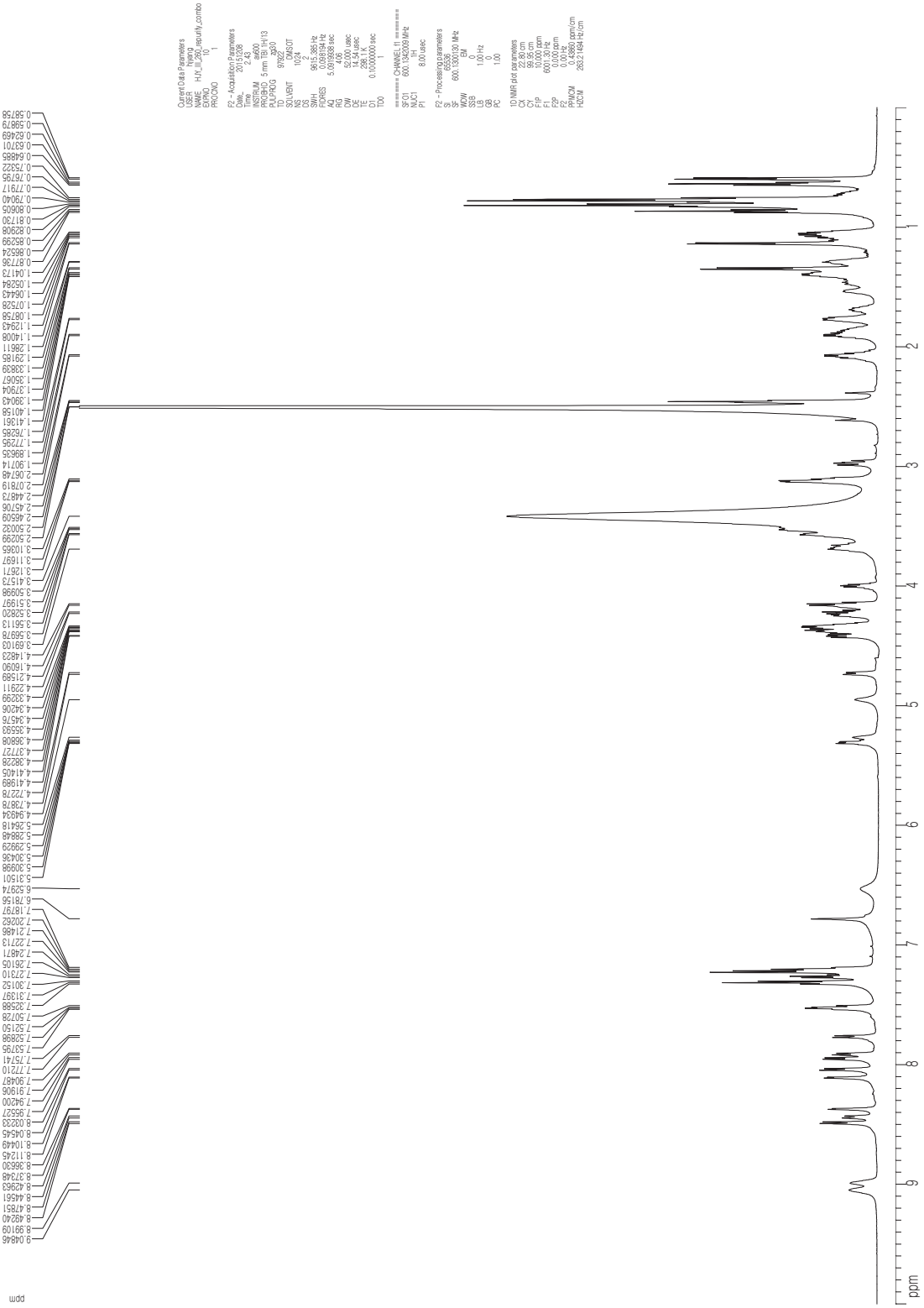

D-*allo*-Ile$_{11}$-Arg$_{10}$-teixobactin : TOCSY spectrum in DMSO-*d6* (600 MHz)

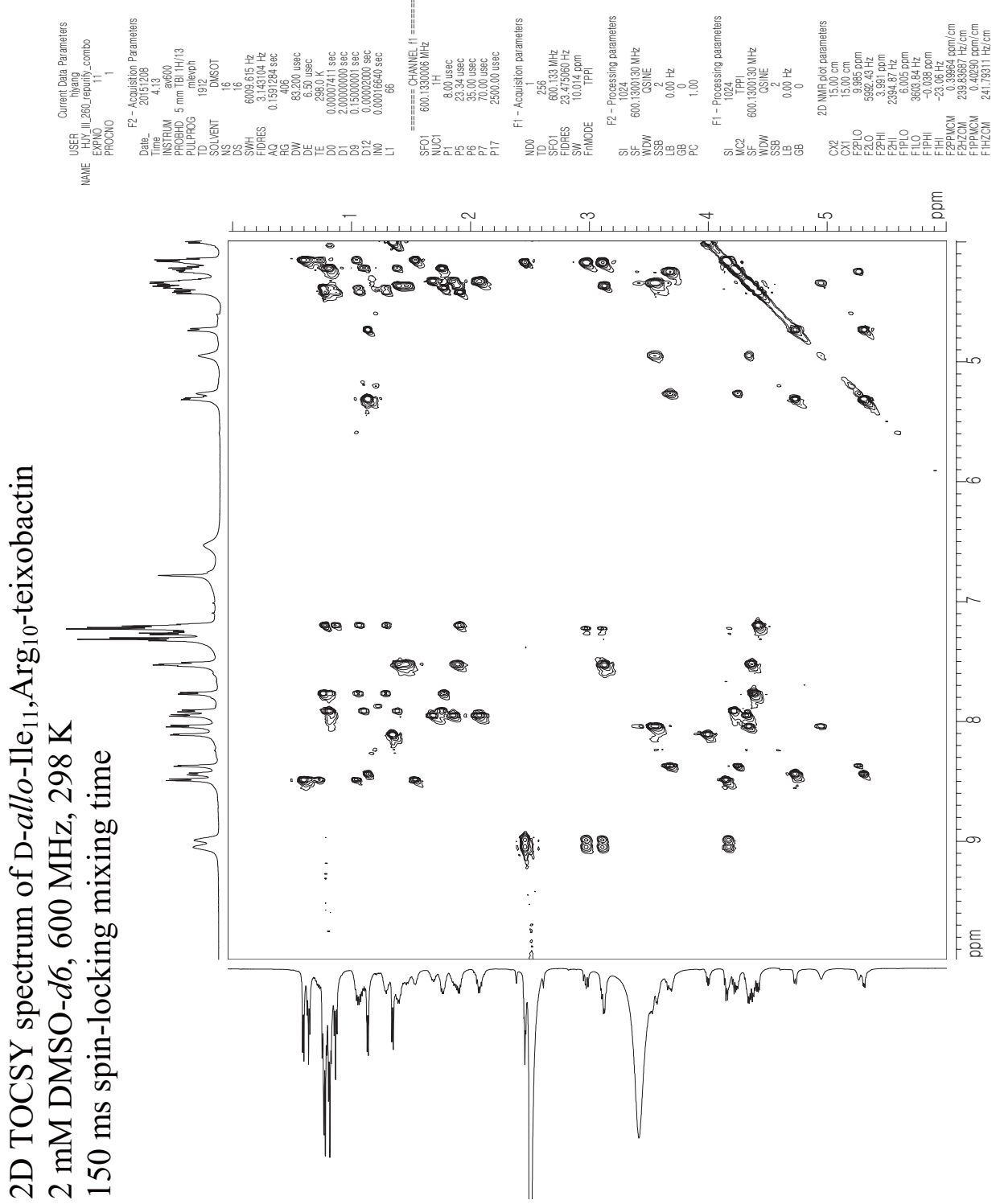

***seco*-Arg$_{10}$-teixobactin** : Mass spectrum and Analytical RP-HPLC

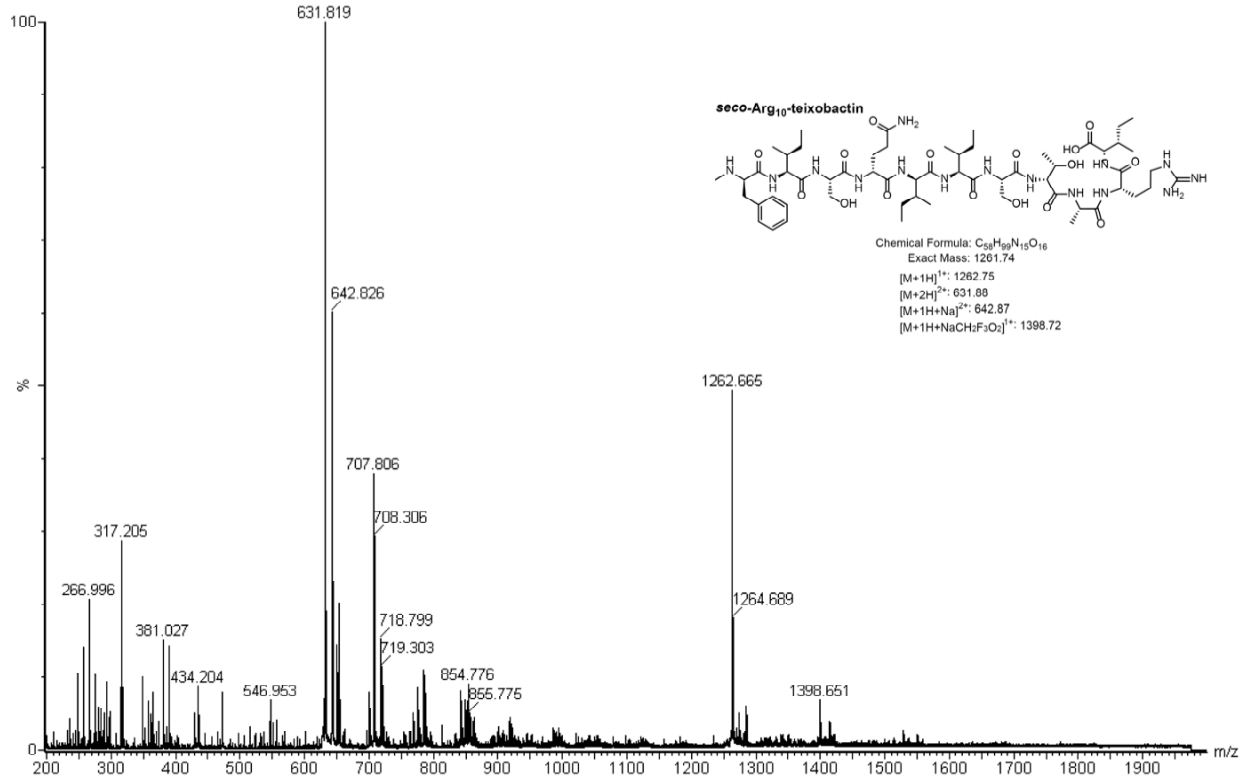

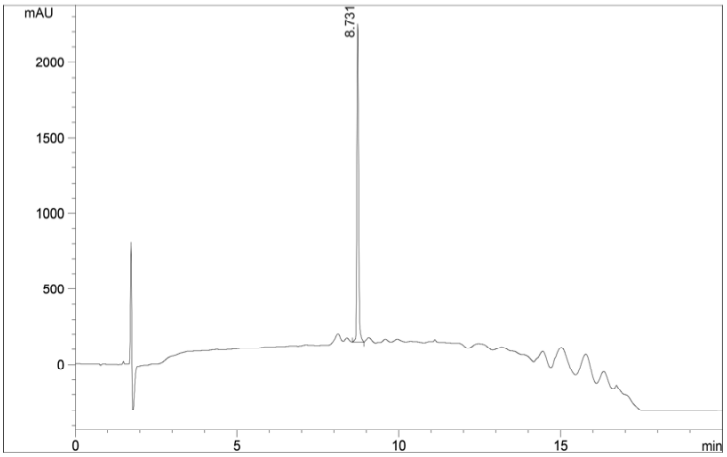

Signal 1:VWD1 A, Wavelength=214 nm

Peak #	RT [min]	Type	Width [min]	Area mAU*s	Height [mAU]	Area %
1	8.731	MM	0.062	7911.522	100.000	100.000

***seco*-Arg$_{10}$-teixobactin** : ^{1}H NMR spectrum in DMSO-*d6* (600 MHz)

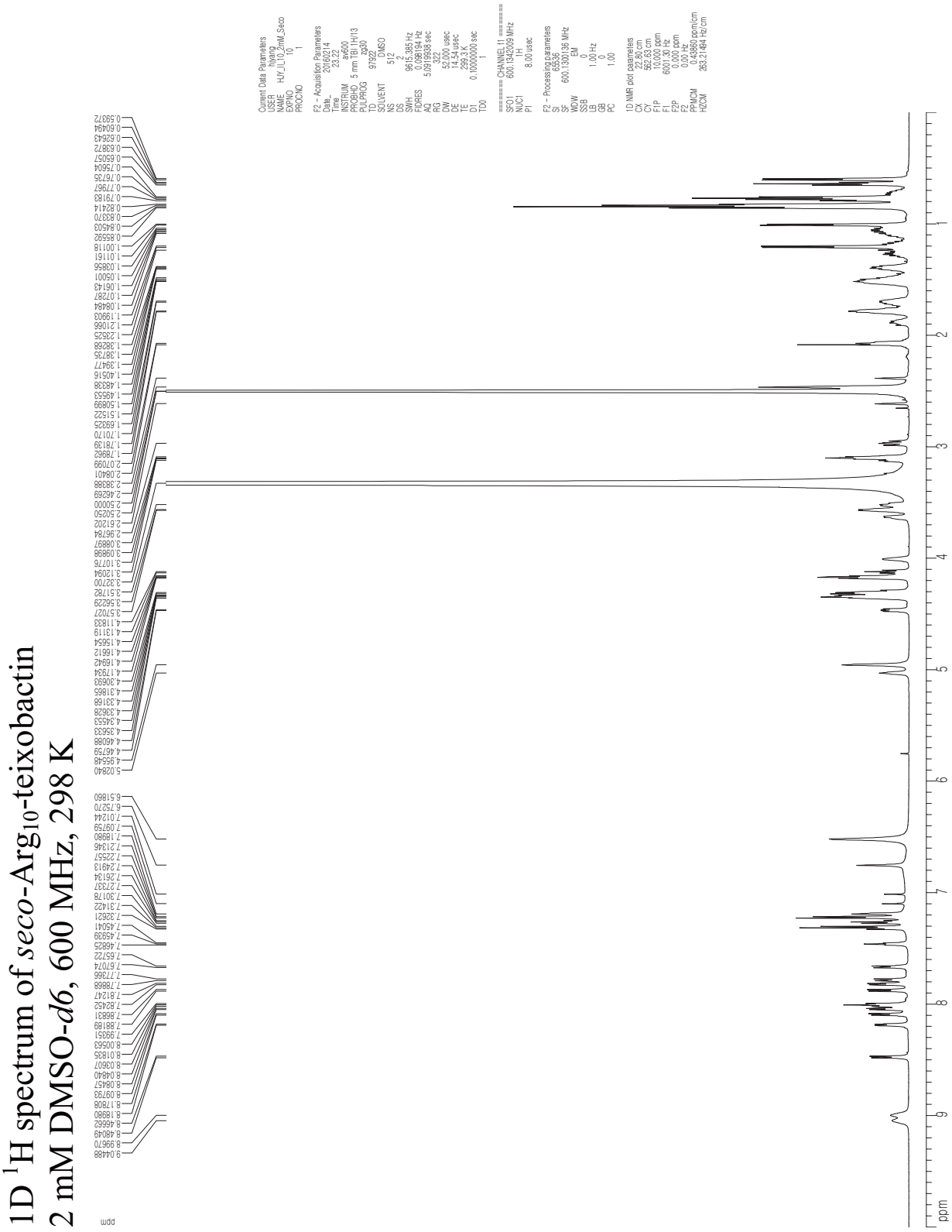

***seco*-Arg$_{10}$-teixobactin** : TOCSY spectrum in DMSO-*d6* (600 MHz)

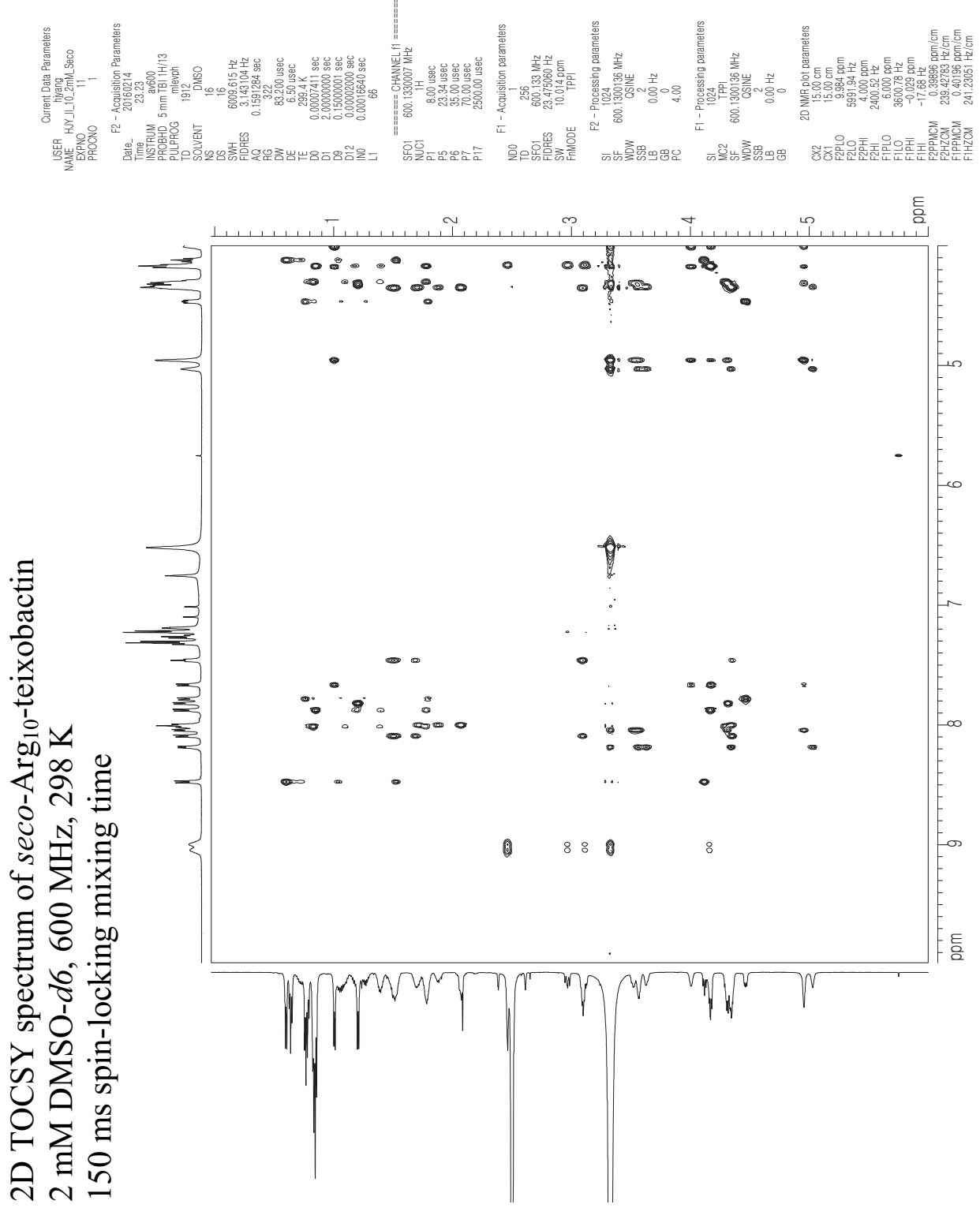

***ent*-Arg$_{10}$-teixobactin** : Mass spectrum and Analytical RP-HPLC

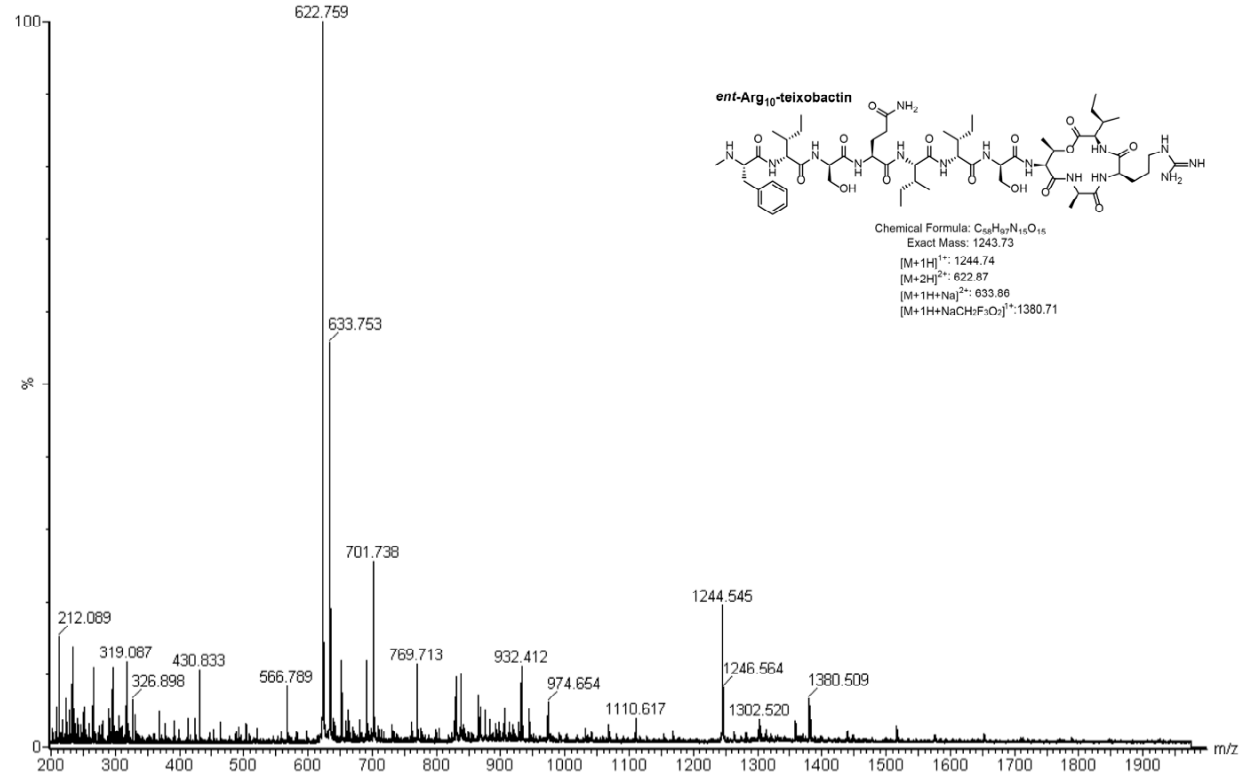

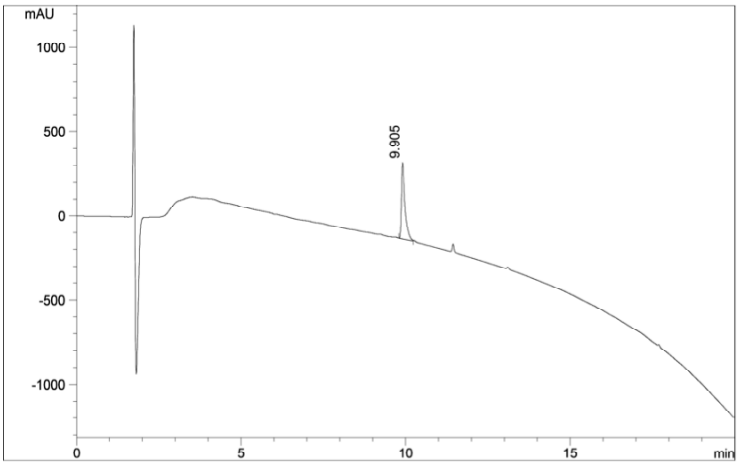

Signal 1:VWD1 A, Wavelength=214 nm

Peak #	RT [min]	Type	Width [min]	Area mAU*s	Height [mAU]	Area %
1	9.905	MM	0.126	3460.172	100.000	100.000

***ent*-Arg$_{10}$-teixobactin** : ^{1}H NMR spectrum in DMSO-*d6* (600 MHz)

1D ^{1}H spectrum of *ent*-Arg$_{10}$-teixobactin
2 mM DMSO-*d6*, 600 MHz, 298 K

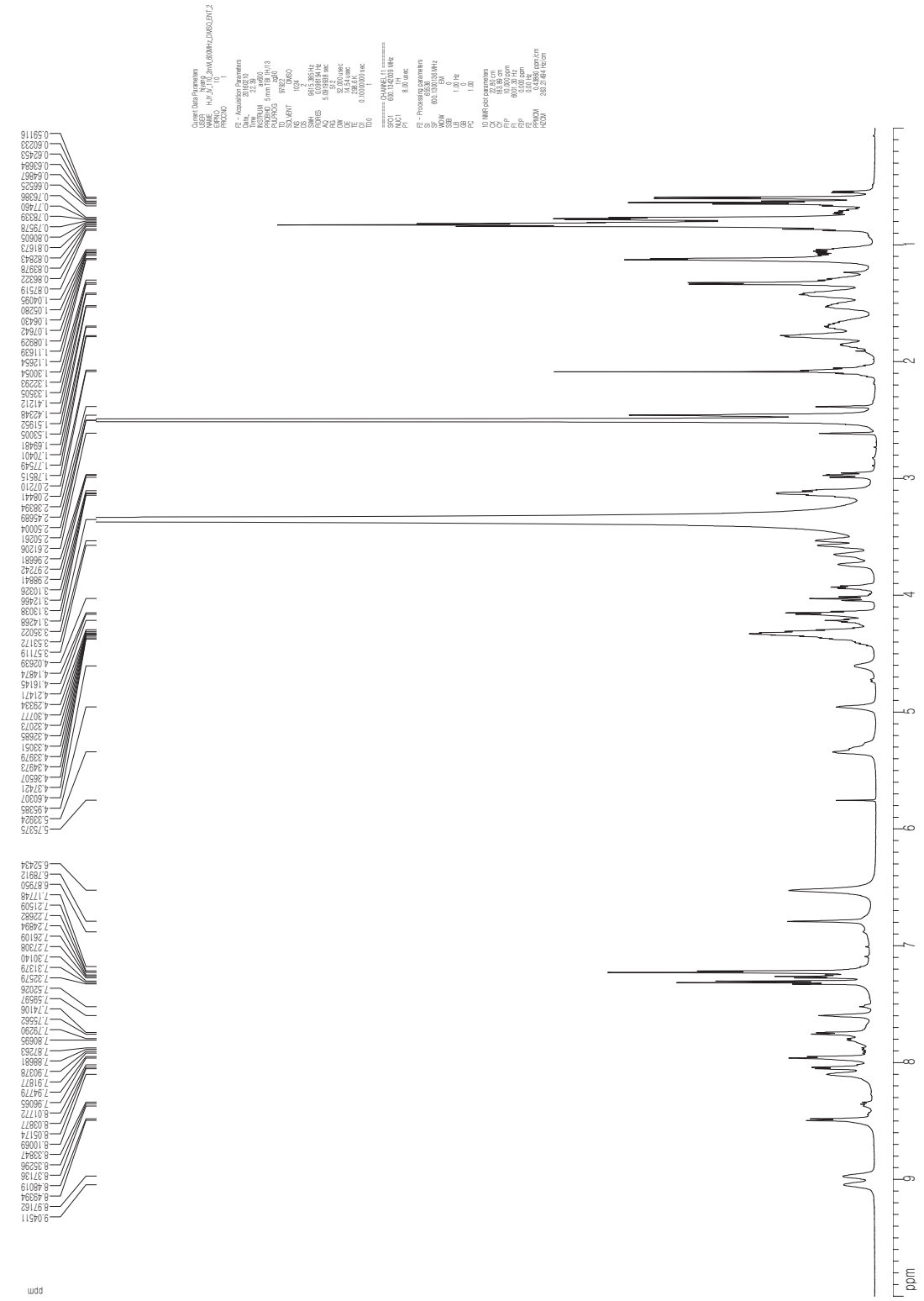

***ent*-Arg$_{10}$-teixobactin** : TOCSY spectrum in DMSO-*d6* (600 MHz)

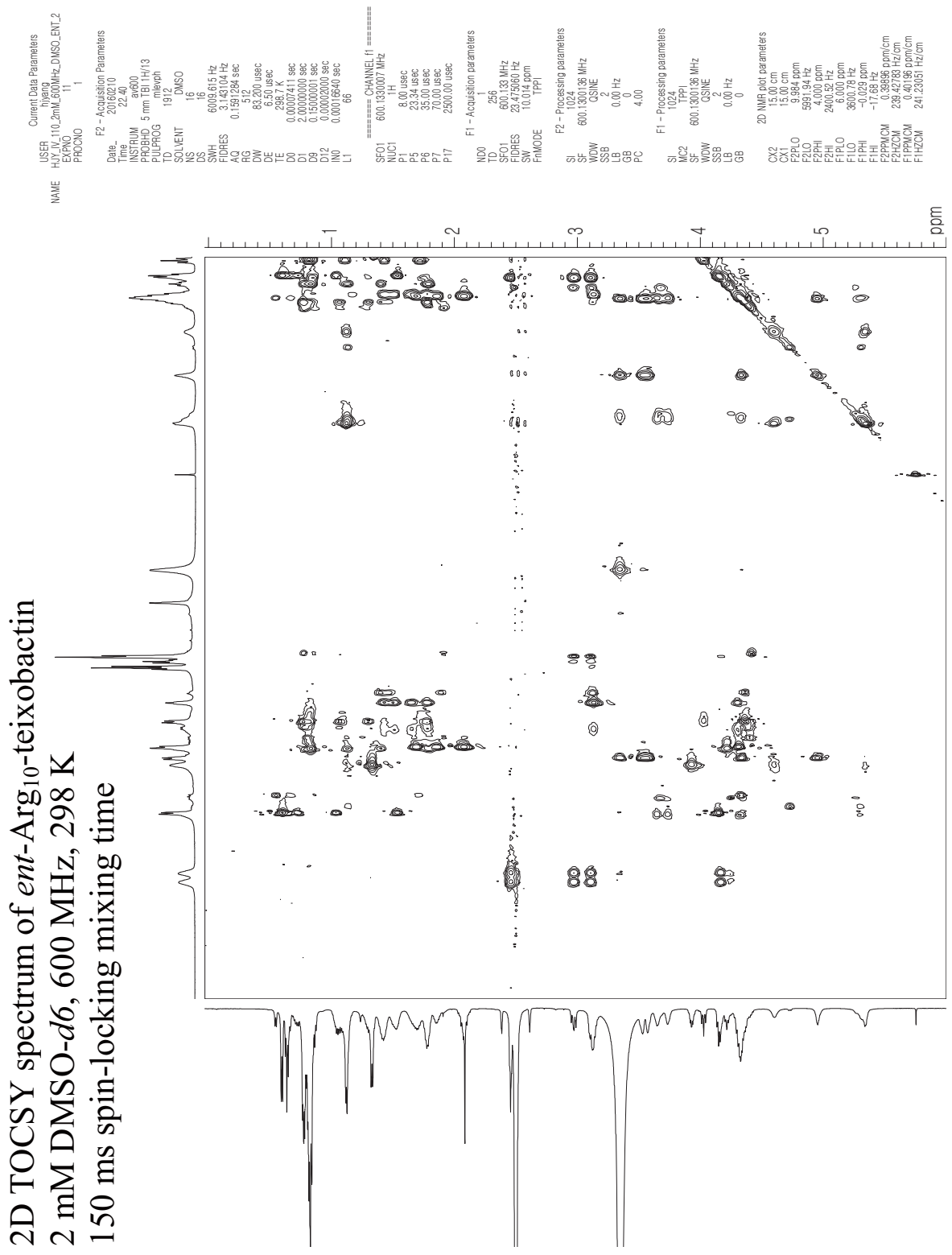

short-Arg$_{10}$-teixobactin : Mass spectrum and Analytical RP-HPLC

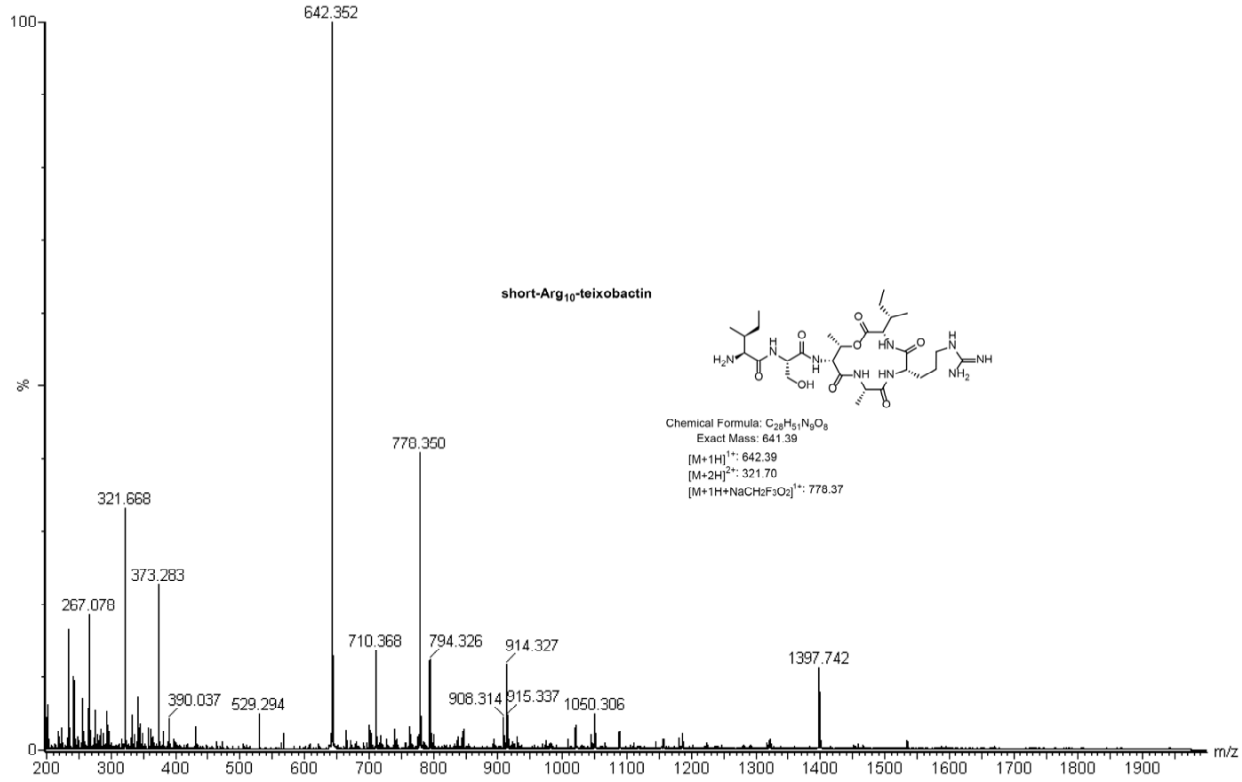

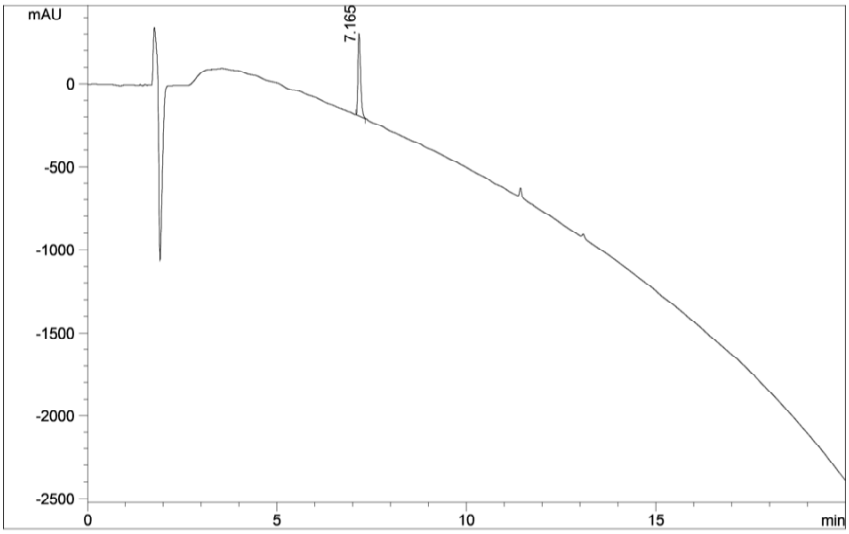

Signal 1:VWD1 A, Wavelength=214 nm

Peak #	RT [min]	Type	Width [min]	Area mAU*s	Height [mAU]	Area %
1	7.165	MM	0.080	2382.848	100.000	100.000

short-Arg$_{10}$-teixobactin : ^{1}H NMR spectrum in DMSO-*d6* (600 MHz)

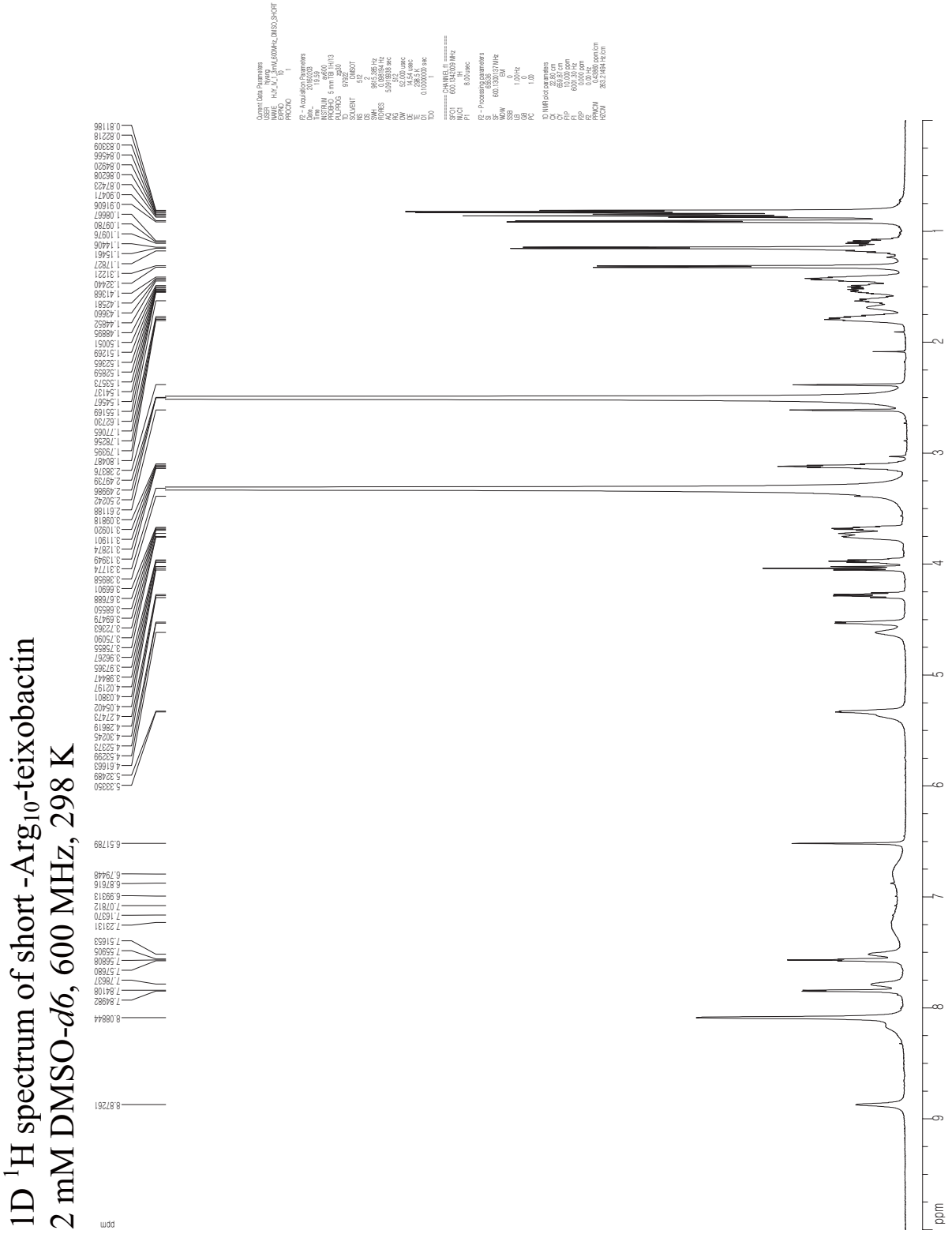

short-Arg$_{10}$-teixobactin : TOCSY spectrum in DMSO-*d6* (600 MHz)

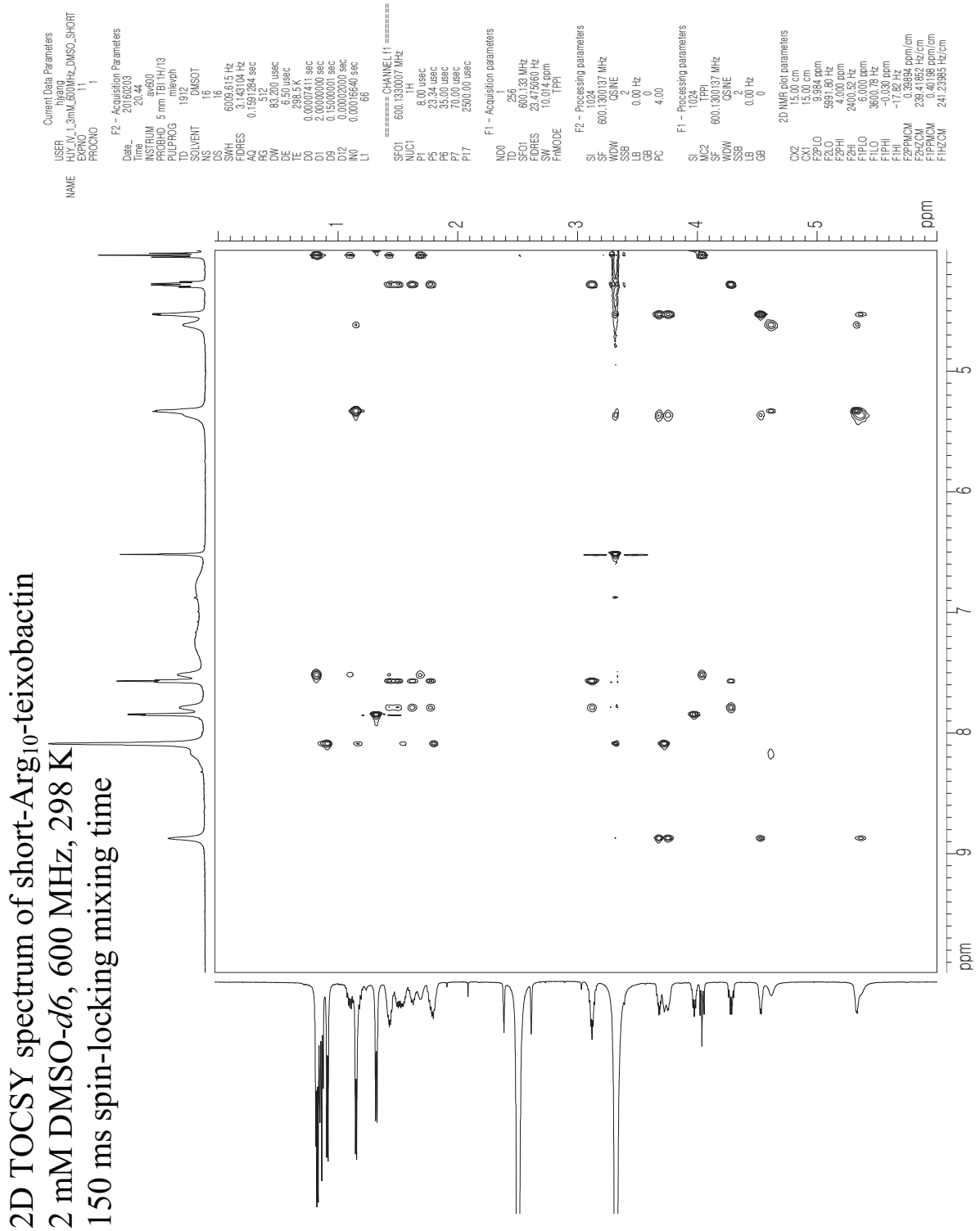

lipobactin 1 : Mass spectrum and Analytical RP-HPLC

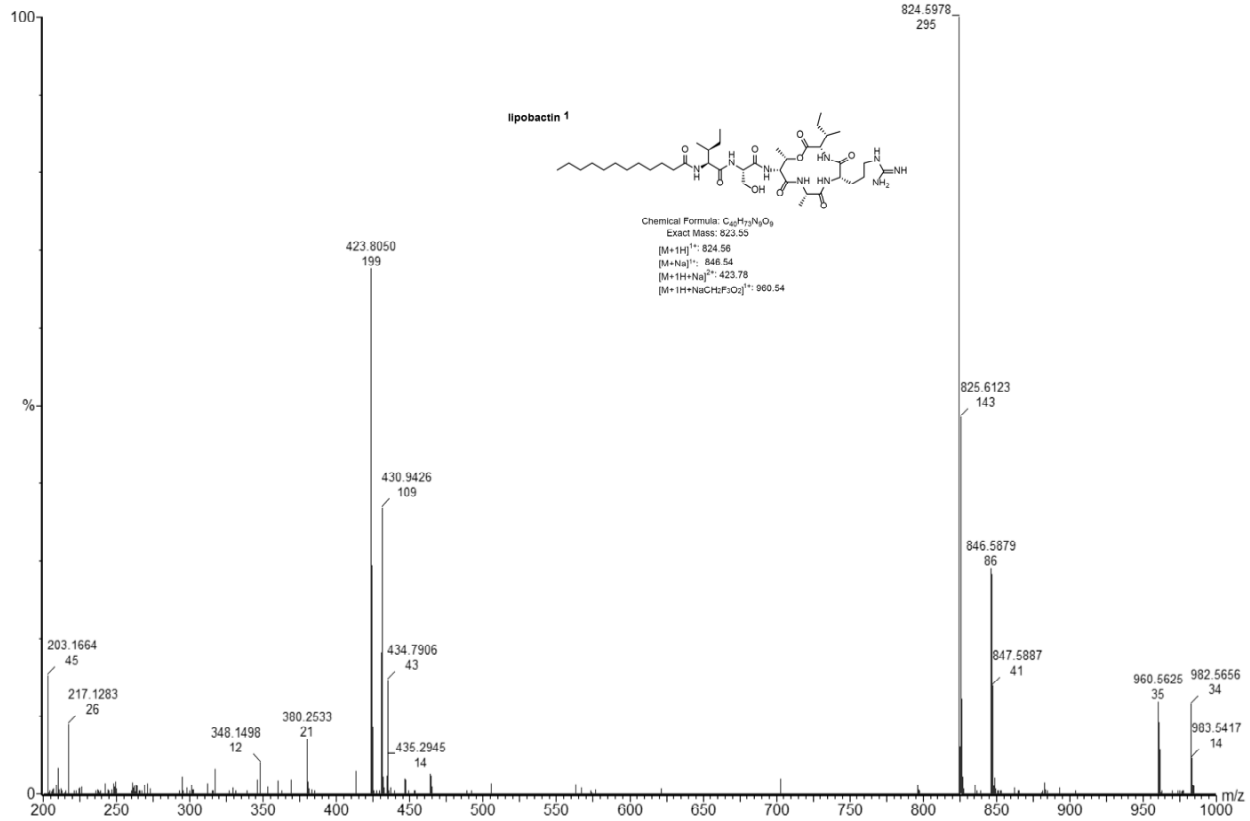

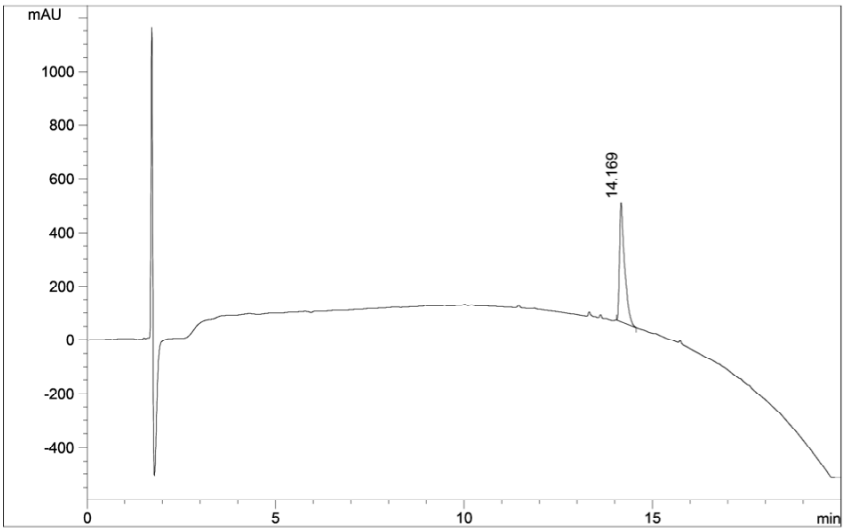

Signal 1:VWD1 A, Wavelength=214 nm

Peak #	RT [min]	Type	Width [min]	Area mAU*s	Height [mAU]	Area %
1	14.169	MM	0.157	4159.424	100.000	100.000

lipobactin 1 : ^{1}H NMR spectrum in DMSO-*d6* (600 MHz)

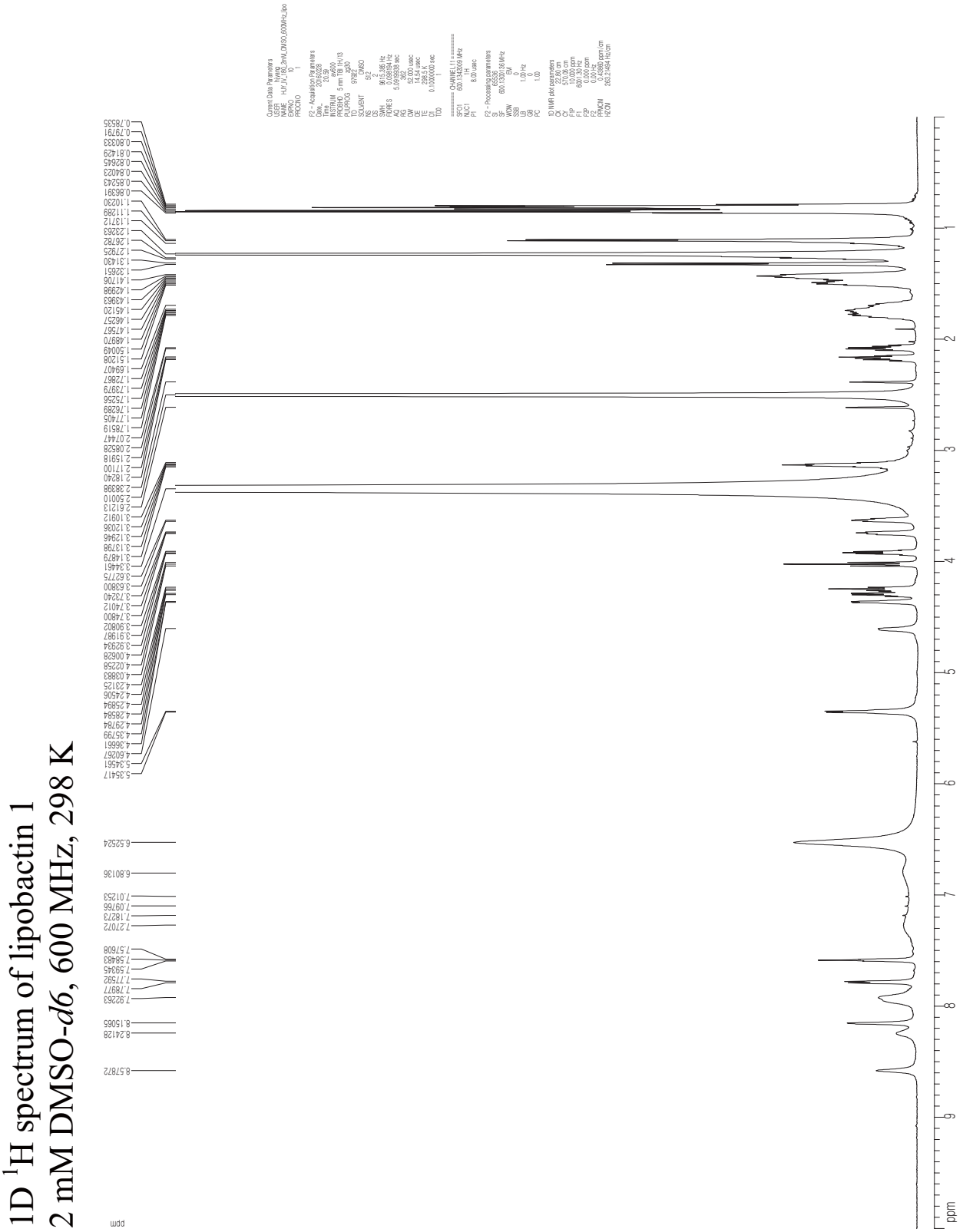

lipobactin 1 : TOCSY spectrum in DMSO-*d6* (600 MHz)

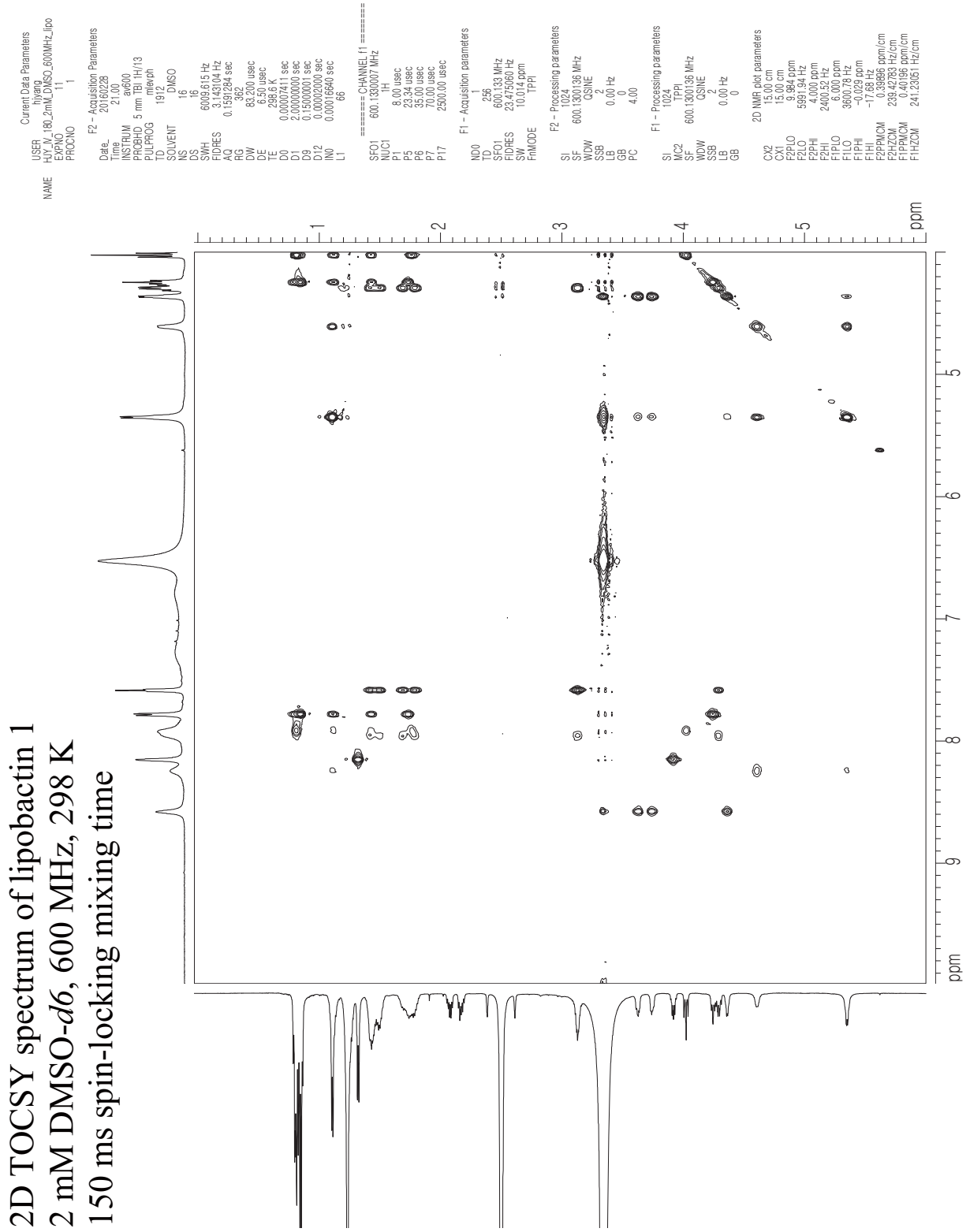

lipobactin 1 : COSY spectrum in DMSO-*d6* (600 MHz)

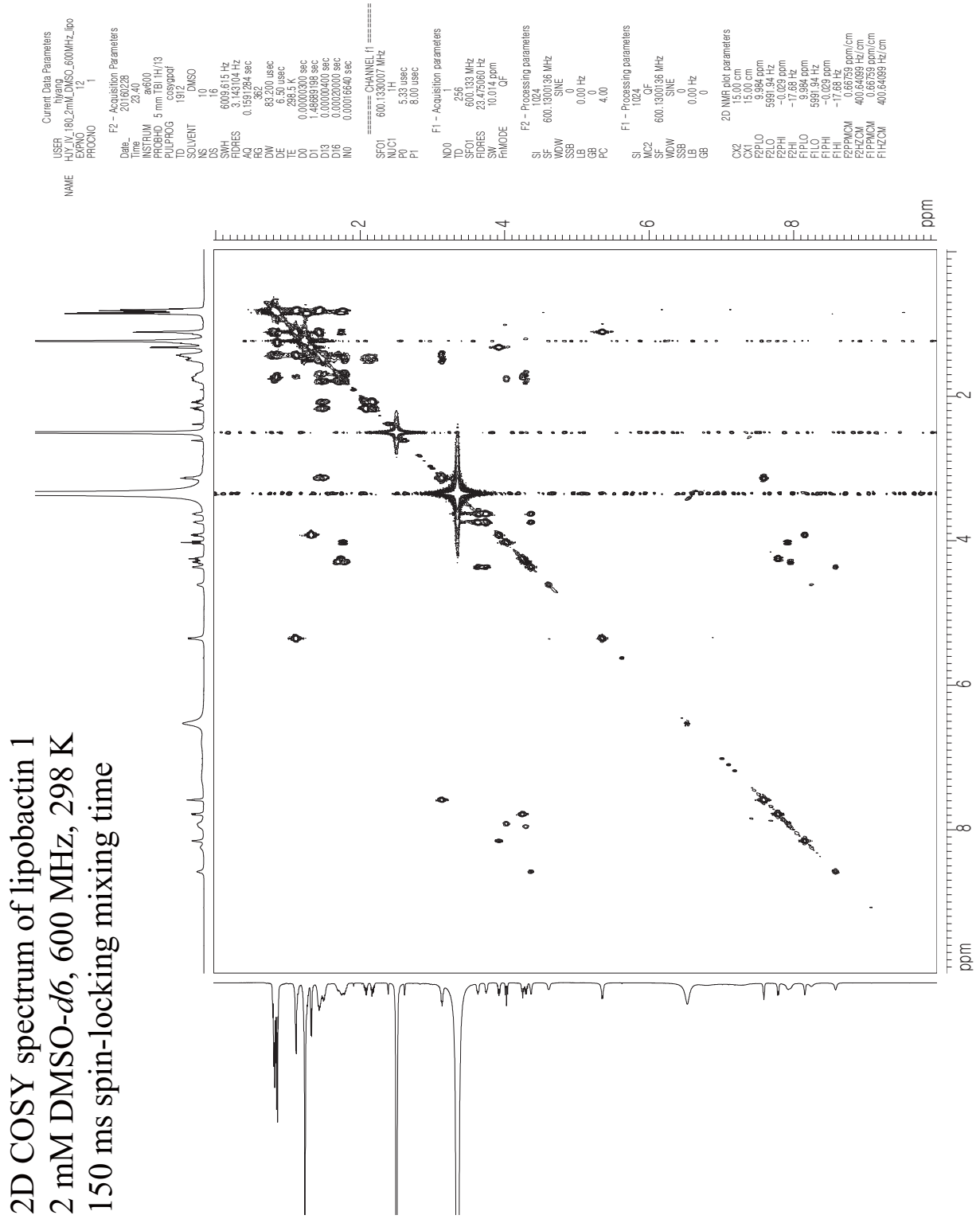

References and Notes

1 Spencer, R.; Li, H.; Nowick, J. S. *J. Am. Chem. Soc.* **2014**, *136*, 5595–5598.

2 CLSI. *Methods for Dilution Antimicrobial Susceptibility Tests for Bacteria That Grow Aerobically. Approved Standard—Ninth Edition*. CLSI document M07-A9. Wayne, PA: Clinical and Laboratory Standards Institute; 2012.

3 Ling, L. L.; Schneider, T.; Peoples, A. J.; Spoering, A. L.; Engels, I.; Conlon, B. P.; Mueller, A.; Schäberle, T. F.; Hughes, D. E.; Epstein, S.; Jones, M.; Lazarides, L.; Steadman, V. A.; Cohen, D. R.; Felix, C. R.; Fetterman, K. A.; Millett, W. P.; Nitti, A. G.; Zullo, A. M.; Chen, C.; Lewis, K. *Nature* **2015**, *517*, 455–459.

4 Peak assignments for Ile residues 2, 6, and 11 and D-*allo*-Ile residue 7 on Arg10-teixobactin were corroborated by NOESY.

5 The integration of position 11 reported in reference 3 (*Nature* **2015**, *517*, 455–459.) appears to be an error, being reported as 1H rather than 3H.

6 Assigned peaks were corroborated by COSY.

Chapter 3[a]
X-ray Crystallographic Structure of a Teixobactin Analogue Reveals Key Interactions of the Teixobactin Pharmacophore

Introduction

The antibiotic teixobactin—first reported in 2015—kills Gram-positive bacteria without detectable resistance and offers promise against rising resistance in pathogens such as methicillin-resistant *Staphylococcus aureus* (MRSA).[1,2] In reflection of this promise, the initial report has been cited more than 500 times. Teixobactin is a non-ribosomal cyclic undecadepsipeptide and contains the rare amino acid *allo*-enduracididine at position 10.[3] Teixobactin inhibits cell wall formation in Gram-positive bacteria by binding to lipid II and related peptidoglycan precursors.

Since the initial publication, multiple research groups have worked to synthesize teixobactin and to elucidate its pharmacophore. Two reports of the total synthesis of teixobactin have been published,[4,5] as well as the third describing the synthesis of the cyclic depsipeptide ring.[6] A 10-step synthesis of *allo*-enduracididine suitable for preparing gram-quantities has also been reported.[7] Several research groups have reported structure-activity relationship studies of Arg_{10}-teixobactin (**Figure 3.1**) and related homologues in which arginine is used as a surrogate for *allo*-enduracididine.[8,9,10,11,12,13] Very recently, Singh *et al.* reported NMR-based structures and structure-activity-relationships of Arg_{10}-teixobactin and its diastereomers at positions 1, 4, 5, and 8.[14]

We recently reported the elucidation of the teixobactin pharmacophore, describing syntheses and structure-activity studies of a variety of teixobactin homologues.[10] On the basis of these data, we proposed a model in which the amide NH groups of the cyclic depsipeptide ring

[a] Yang, H.; Du Bois, D. R.; Ziller, J. W.; Nowick, J. S. *Chem. Commun.* **2017**, *53*, 2772–2775.

bind to the pyrophosphate group of lipid II through hydrogen-bonding interactions, in a fashion similar to the binding of nisin to lipid II (PDB 1WCO).[15] We further proposed that the hydrophobic residues *N*-Me-D-Phe, Ile, and D-*allo*-Ile at positions 1, 2, and 5 help anchor teixobactin to the plasma membrane and demonstrated that residues 1–5 could be replaced with a lipid group. The resulting homologue lipobactin 1 (dodecanoyl-Δ_{1-5}-Arg_{10}-teixobactin) is only 2-4 times less active than Arg_{10}-teixobactin (**Figure 3.1**).

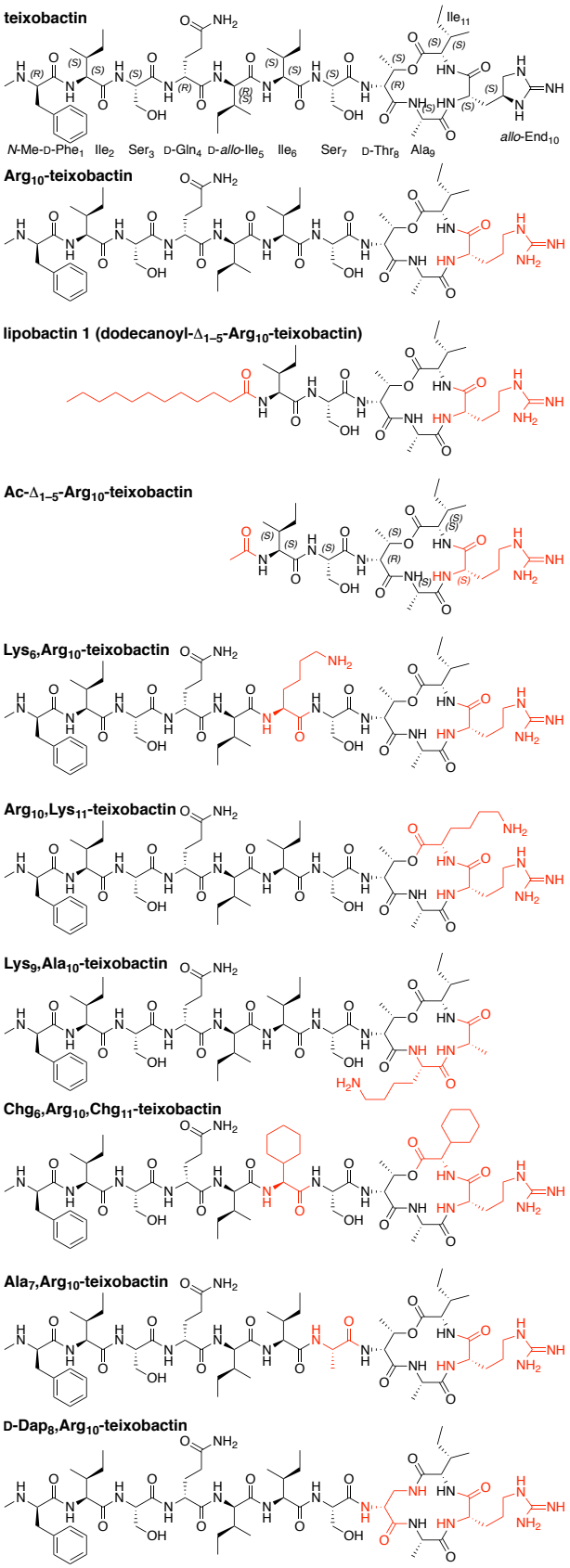

Figure 3.1. Structures of teixobactin and homologues.

Results and Discussion

In the current study, we report the X-ray crystallographic structure of a truncated version of lipobactin 1 in which the dodecanoyl group is replaced with an acetyl group, Ac-Δ_{1-5}-Arg_{10}-teixobactin (**Figure 3.1**). In attempting to crystallize this homologue with inorganic pyrophosphate anions, we instead obtained a complex with chloride anion and observe that the chloride anion coordinates to three amide NH groups of the cyclic depsipeptide ring, the amide NH group of Ser_7, and the guanidinium group of Arg_{10}. Here we describe the X-ray crystallographic structure of Ac-Δ_{1-5}-Arg_{10}-teixobactin as the hydrochloride salt and relate the observed structure to changes in activity upon mutation of Arg_{10}-teixobactin.

We began our efforts to crystallize the teixobactin pharmacophore by screening Arg_{10}-teixobactin in 864 conditions in a 96-well plate format using crystallization kits from Hampton Research (PEG/Ion, Index, and Crystal Screen). Initial efforts to screen Arg_{10}-teixobactin for crystallization were thwarted by the propensity of the peptide to form a gel at concentrations as low as 5 mg/mL used for screening. Truncation by removal of residues 1–5 (Δ_{1-5}-Arg_{10}-teixobactin) eliminated the propensity to form a gel but afforded no crystals. We postulated that a monocationic homologue would better crystallize than the dicationic homologue and were gratified that Ac-Δ_{1-5}-Arg_{10}-teixobactin afforded crystals suitable for X-ray crystallography. Only conditions containing chloride anion afforded suitable crystals. Attempts to crystallize with inorganic pyrophosphate anions, with HCl being used to adjust the pH of the pyrophosphate buffer, still afforded the chloride salt. The X-ray crystallographic structure shows Ac-Δ_{1-5}-Arg_{10}-teixobactin as the hydrochloride salt (**Figure 3.2**).[16]

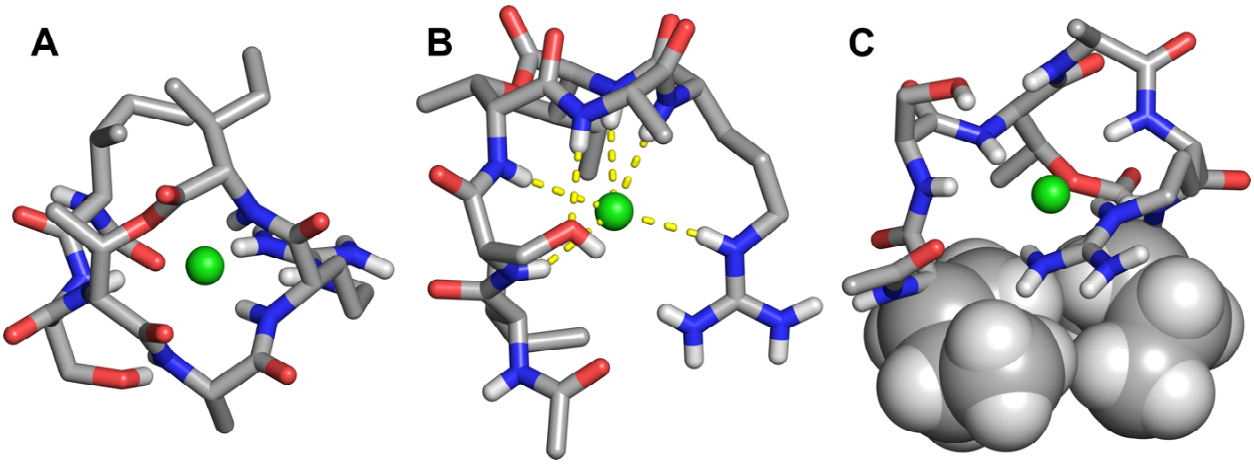

Figure 3.2 X-ray crystallographic structure of Ac-Δ_{1-5}-Arg_{10}-teixobactin as the hydrochloride salt. (A) Top view. (B) Side view. (C) Rotated side view, in which the side chains of Ile_6 and Ile_{11} are shown as spheres. Hydrogens attached to carbons that are shown as sticks are omitted for clarity. Water of crystallization (1.5 H_2O per molecule of peptide) is not shown.

In the X-ray crystallographic structure, the carbonyl groups of D-Thr_8, Ala_9, Arg_{10}, and Ile_{11} in the cyclic depsipeptide ring point upward, while the amide NH groups of Ala_9, Arg_{10}, and Ile_{11} point downward (**Figure 3.2B**). The α-amino group of D-Thr_8 and the attached residues (Ser_7 and Ile_6), run downward at almost a right angle to the cyclic depsipeptide ring. The side chain of Arg_{10} also runs downward. The side chains of Ala_9 and Ile_{11}, as well as the methyl group of D-Thr_8 point outward from the cyclic depsipeptide ring (**Figure 3.2A**). The amide NH group of Ala_9 hydrogen bonds to the oxygen atom of the hydroxy group of Ser_7. The side chains of Ile_6 and Ile_{11} are in loose contact, suggesting a hydrophobic interaction (**Figure 3.2C**). The methyl group of D-Thr_8 sits near the Ile_6 and Ile_{11} side chains, creating a hydrophobic patch.

The amide NH groups of Arg_{10} and Ile_{11} in the cyclic depsipeptide ring, as well as the amide NH groups of Ser_7 and D-Thr_8 and the guanidinium group of Arg_{10}, hydrogen bond to the chloride anion (**Figure 3.2B**). This mode of interaction is similar to that of nisin with the pyrophosphate group of lipid II.[15] We envision that the binding cavity of teixobactin and its

analogues may be able to adjust to accommodate larger anions, including the pyrophosphate group of lipid II and other related peptidoglycan precursors.

To explore the roles of the hydrophobic residues at positions 6, 9, and 11, we mutated each of these residues to lysine and compared the activity of the resulting homologues to that of Arg_{10}-teixobactin in minimum inhibitory concentration (MIC) assays in four types of Gram-positive bacteria. Mutation of either Ile_6 or Ile_{11} to lysine results in loss of activity, while mutation of Ala_9 to lysine does not (**Table 3.1**).[17] These data suggest that the hydrophobicity of Ile_6 and Ile_{11} is important in teixobactin activity, while that of Ala_9 is not. The outward pointing geometry of the Ala_9 side chain, coupled with the activity of Lys_9,Arg_{10}-teixobactin, suggest that the 9-position should allow functionalization to provide other modified homologous of teixobactin that are active.

To further explore the role of hydrophobicity at positions 6 and 11 and the contact between the Ile_6 and Ile_{11} side chains, we mutated both of these residues to cyclohexylglycine (Chg). Cyclohexylglycine may be thought of as a homologue of isoleucine, in which two carbons have been added to the sec-butyl side chain to form a cyclohexane ring. The resulting homologue, Chg_6,Arg_{10},Chg_{11}-teixobactin, has slightly greater activity than Arg_{10}-teixobactin, with three of the four measured MIC values in the Gram-positive bacteria lower by a factor of two (**Table 3.1**). This finding suggests that hydrophobicity or hydrophobic contact at positions 6 and 11 is important in the activity of teixobactin.

To explore the hydrogen bond between the amide NH group of Ala_9 and side chain of Ser_7, we mutated Ser_7 to alanine. The resulting homologue, Ala_7,Arg_{10}-teixobactin, shows greatly diminished activity (**Table 3.1**).[18] This finding supports the importance of this hydrogen bond in the activity of teixobactin.

The hydrogen bonding of the depsipeptide ring to the chloride anion (**Figure 3.2**) suggests the possibility of increasing the activity of teixobactin homologues by strengthening the complexation with the pyrophosphate group of lipid II. To explore this idea, we mutated D-Thr$_8$ to D-diaminopropionic acid (D-Dap). The mutation of D-Thr$_8$ to D-Dap replaces the lactone oxygen atom with an amide NH group, but also results in the loss of the threonine methyl group. The resulting homologue, D-Dap$_8$,Arg$_{10}$-teixobactin, shows comparable activity to Arg$_{10}$-teixobactin (**Table 3.1**). Direct comparison of these two homologues is hampered, because two factors are changed at one time in making this mutation. A reasonable interpretation of this observation is that enhanced activity from replacing the lactone oxygen atom with an NH group is offset by the increased conformational flexibility of the ring associated with removal of the D-Thr$_8$ methyl group.

Table 3.1. MIC values of teixobactin homologues in μg/mL.[a]

	Staphylococcus epidermidis ATCC 14990	*Streptococcus salivarius* ATCC 13419	*Enterococcus durans* ATCC 6056	*Bacillus subtilis* ATCC 6051	*Escherichia coli* ATCC 10798
Arg$_{10}$-teixobactin	1	1	4	2	>32
lipobactin 1	4	4	8	4	>32
Ac-Δ$_{1–5}$-Arg$_{10}$-teixobactin	>32	>32	>32	>32	>32
Lys$_6$,Arg$_{10}$-teixobactin	>32	>32	>32	>32	>32
Arg$_{10}$,Lys$_{11}$-teixobactin	>32	>32	>32	>32	>32
Lys$_9$,Arg$_{10}$-teixobactin	1	1	4	1	>32
Chg$_6$,Arg$_{10}$,Chg$_{11}$-teixobactin	1	0.5	2	1	>32
Ala$_7$,Arg$_{10}$-teixobactin	32	16	>32	32	>32
D-Dap$_8$,Arg$_{10}$-teixobactin	2	1	4	1	>32
vancomycin	0.5	0.5	0.5	1	>32
teixobactin	0.06	0.03	0.5	0.06	>32

[a] All teixobactin homologues were prepared and studied as the trifluoroacetate salts. The *Staphylococcus*, *Streptococcus*, *Enterococcus*, and *Bacillus* species are non-pathogenic (BSL-1) Gram-positive bacteria. The *E. coli* serves as a Gram-negative control. Vancomycin and teixobactin serve as positive controls.

Conclusion

The studies described here demonstrate how the X-ray crystallographic structure of a truncated teixobactin analogue can reveal key interactions of teixobactin. The structure reveals a 13-membered cyclic depsipeptide ring in which the amide groups and ester group of residues 8–11 align. The amide NH groups of residues 10 and 11, in conjunction with those of residues 7 and 8 and the guanidinium side chain of residue 10, create a cavity that can bind an anion. The hydrophobic side chains at positions 6 and 11 are required for activity, whereas that at position 9 is not. The hydrogen bond between Ser_7 and Ala_9 is also important for activity. The teixobactin pharmacophore tolerates the amide substitution of lactone oxygen in the ring. Figure 3.3 summarizes these findings. We are now using the X-ray crystallographic structure and structure-activity relationships that we have observed to design teixobactin homologues with better pharmacological properties.

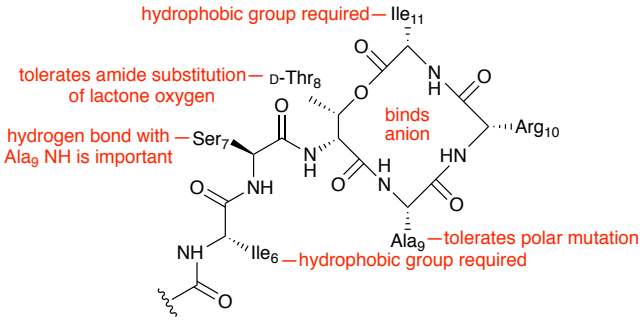

Figure 3.3. Summary of key findings.

References and Notes

1 Ling, L. L.; Schneider, T.; Peoples, A. J.; Spoering, A. L.; Engels, I.; Conlon, B. P.; Mueller, A.; Schäberle, T. F.; Hughes, D. E.; Epstein, S.; Jones, M.; Lazarides, L.; Steadman, V. A.; Cohen, D. R.; Felix, C. R.; Fetterman, K. A.; Millett, W. P.; Nitti, A. G.; Zullo, A. M.; Chen, C.; Lewis, K. A new antibiotic kills pathogens without detectable resistance. *Nature* **2015**, *517*, 455–459.

2 Homma, T.; Nuxoll, A.; Gandt, A. B.; Ebner, P.; Engels, I.; Schneider, T.; Götz, F.; Lewis, K.; Conlon, B. P. Dual Targeting of Cell Wall Precursors by Teixobactin Leads to Cell Lysis. *Antimicrob. Agents Chemother.* **2016**, *60*, 6510–6517.

3 Atkinson, D. J.; Naysmith, B. J.; Furkert, D. P.; Brimble, M. A. Enduracididine, a rare amino acid component of peptide antibiotics: Natural products and synthesis. *Beilstein J. Org. Chem.* **2016**, *12*, 2325–2342.

4 Jin, K.; Sam, I. H.; Po, K. H. L.; Lin, D.; Ghazvini Zadeh, E. H.; Chen, S.; Yuan, Y.; Li, X. Total synthesis of teixobactin. *Nat. Commun.* **2016**, *7*, 12394.

5 Giltrap, A. M.; Dowman, L. J.; Nagalingam, G.; Ochoa, J. L.; Linington, R. G.; Britton, W. J.; Payne, R. J. Total Synthesis of Teixobactin. *Org. Lett.* **2016**, *18*, 2788–2791.

6 Dhara, S.; Gunjal, V. B.; Handore, K. L.; Reddy, D. S. Solution-Phase Synthesis of the Macrocyclic Core of Teixobactin. *Eur. J. Org. Chem.* **2016**, *25*, 4289–4293.

7 Craig, W.; Chen, J.; Richardson, D.; Thorpe, R.; Yuan, Y. A Highly Stereoselective and Scalable Synthesis of L-allo-Enduracididine. *Org. Lett.* **2015**, *17*, 4620–4623.

8 Jad, Y. E.; Acosta, G. A.; Naicker, T.; Ramtahal, M.; El-Faham, A.; Govender, T.; Kruger, H. G.; de la Torre, B. G.; Albericio F. Synthesis and Biological Evaluation of a Teixobactin Analogue. *Org. Lett.* **2015**, *17*, 6182–6185.

9 Parmar, A.; Iyer, A.; Vincent, C. S.; Van Lysebetten, D.; Prior, S. H.; Madder, A.; Taylor, E. J.; Singh, I. Efficient total syntheses and biological activities of two teixobactin analogues. *Chem. Commun.* **2016**, *52*, 6060–6063.

10 Yang, H.; Chen, K. H.; Nowick, J. S. Elucidation of the Teixobactin Pharmacophore. *ACS Chem. Biol.* **2016**, *11*, 1823–1826.

11 Abdel Monaim, S. A. H.; Jad, Y. E.; Acosta, G. A.; Naicker, T.; Ramchuran, E. J.; El-Faham, A.; Govender, T.; Kruger, H. G.; de la Torre, B. G.; Albericio, F. Re-evaluation of the N-terminal substitution and the D-residues of teixobactin. *RSC Adv.* **2016**, *6*, 73827–73829.

12 Abdel Monaim, S. A. H.; Jad, Y. E.; Ramchuran, E. J.; El-Faham, A.; Govender, T.; Kruger, H. G.; de la Torre, B. G.; Albericio, F. Lysine Scanning of Arg(10)-Teixobactin: Deciphering the Role of Hydrophobic and Hydrophilic Residues. *ACS Omega* **2016**, *1*, 1262–1265.

13 Wu, C.; Pan, Z.; Yao, G.; Wang, W.; Fang, L.; Su, W. Synthesis and structure–activity relationship studies of teixobactin analogues. *RSC Adv.* **2017**, *7*, 1923–1926.

14 Parmar, A.; Prior, S. H.; Iyer, A.; Vincent, C. S.; Van Lysebetten, D.; Breukink, E.; Madder, A.; Taylor, E. J.; Singh, I. Defining the molecular structure of teixobactin analogues and understanding their role in antibacterial activities. *Chem. Commun.* **2017**, *53*, 2016–2019.

15 Hsu, S. T.; Breukink, E.; Tischenko, E.; Lutters, M. A.; de Kruijff, B.; Kaptein, R.; Bonvin, A. M.; Nuland, N. A. The nisin-lipid II complex reveals a pyrophosphate cage that provides a blueprint for novel antibiotics. *Nat. Struct. Mol. Biol.* **2004**, *11*, 963–967.

16 The crystallographic coordinates were deposited in the Cambridge Crystallographic Data Centre (CCDC), deposition number CCDC 1523518.

17 Albericio *et al.* recently reported that Lys_6,Arg_{10}-teixobactin and Arg_{10},Lys_{11}-teixobactin are inactive against Gram-positive bacteria, and that Lys_9,Arg_{10}-teixobactin is less active than Arg_{10}-teixobactin. For details, see reference 12.

18 Su *et al.* recently reported that Ala_7,Arg_{10}-teixobactin is substantially less active than Arg_{10}-teixobactin. For details, see reference 13.

Supporting Information

Table of Contents

Materials and Methods

General information

Methylene chloride (CH_2Cl_2) was passed through alumina under argon prior to use. Amine-free *N,N*-dimethylformamide (DMF) was purchased from Alfa Aesar. Fmoc-D-*allo*-Ile-OH was purchased from Santa Cruz Biotechnology. Other protected amino acids were purchased from CHEM-IMPEX. Preparative reverse-phase HPLC was performed on a Beckman Gold Series P instrument equipped with an Agilent Zorbax SB-C18 column. Analytical reverse-phase HPLC was performed on either an Agilent 1200 or an Agilent 1260 Infinity II instrument, both equipped with a Phenomonex Aeris PEPTIDE 2.6μ XB-C18 column. HPLC grade acetonitrile (MeCN) and deionized water (18 MΩ) containing 0.1% trifluoroacetic acid (TFA) were used as solvents for both preparative and analytical reverse-phase HPLC. Deionized water (18 MΩ) was obtained from a Barnstead NANOpure Diamond water purification system. All teixobactin homologues were prepared and studied as the trifluoroacetate salts.

Synthesis of teixobactin homologues

Ac-$\Delta_{1\text{-}5}$-Arg_{10}-teixobactin and other teixobactin homologues were synthesized as the trifluoroacetate salts following procedures we have previously reported.[1] Dry DMF was used instead of a mixture of MeCN/THF/CH_2Cl_2 for the cyclization step. For the acetylation reaction, glacial acetic acid (3.0 μL, 0.90 mmol, 10 equiv) was coupled with coupling reagent HCTU (142 mg, 0.46 mmol, 4 equiv) in 20% (v/v) collidine in dry DMF (5 mL). For the synthesis of D-Dap_8,Arg_{10}-teixobactin, Fmoc-D-Dap(Alloc)-OH was used instead of Fmoc-D-Thr-OH, and the Alloc protecting group was deprotected using $Pd(PPh_3)_4$ (0.10 equiv) and $PhSiH_3$ (20 equiv) in CH_2Cl_2 prior to the esterification step.[2]

MIC assays of teixobactin homologues

MIC assays of Ac-$\Delta_{1\text{-}5}$-Arg_{10}-teixobactin and other teixobactin homologues were performed following procedures we have previously reported.[1]

Crystallization of Ac-$\Delta_{1\text{-}5}$-Arg_{10}-teixobactin[3]

Ac-$\Delta_{1\text{-}5}$-Arg_{10}-teixobactin was dissolved in 0.1 M $Na_4P_2O_7$ (sodium pyrophosphate) at pH 7.00 (adjusted with HCl and NaOH) to make a 10 mg/mL stock solution. Crystallization conditions were screened using the hanging-drop vapor-diffusion method with three crystallization kits (Hampton Index, PEG/Ion, and Crystal Screen) in 96-well plates. Using a TTP LabTech Mosquito® liquid handling instrument, three 150-nL hanging drops with differing ratios of peptide to well solution (1:1, 1:2, and 2:1 peptide/well solution) were made per condition in each 96-well plate, for a total of 864 experiments. Crystals of Ac-$\Delta_{1\text{-}5}$-Arg_{10}-teixobactin grew rapidly (~24 h) with a well solution of 0.2 M ammonium tartrate dibasic and 20% polyethylene glycol 3,350. Crystallization conditions were further optimized using a 4x6 matrix Hampton VDX 24-well plate, varying the concentration of ammonium tartrate dibasic (0.12, 0.16, 0.20, 0.24, 0.28, and 0.32 M) in the columns and the concentration of polyethylene glycol 3,350 (10, 15, 20, and 25%) in the rows. The 0.24 M ammonium tartrate dibasic and 20% polyethylene glycol 3,350 condition afforded colorless parallelogram-shaped crystals suitable for X-ray diffraction.

X-ray crystallographic data collection, data processing, and structure determination

A colorless crystal of approximate dimensions 0.030 x 0.130 x 0.200 mm was mounted in a cryoloop and transferred to a Bruker SMART APEX II diffractometer. The APEX2[4] program package was used to determine the unit-cell parameters and for data collection (180 sec/frame scan time for a sphere of diffraction data). The raw frame data was processed using SAINT[5] and

SADABS[6] to yield the reflection data file. Subsequent calculations were carried out using the SHELXTL[7] program. The diffraction symmetry was 2/*m* and the systematic absences were consistent with the monoclinic space groups *C*2, *Cm* and *C*2/*m*. It was later determined that space group *C*2 was correct.

The structure was solved by direct methods and refined on F^2 by full-matrix least-squares techniques. The analytical scattering factors[8] for neutral atoms were used throughout the analysis. Hydrogen atoms were either located from a difference-Fourier map and refined (x,y,z and U_{iso}) or were included using a riding model. There were 1.5 molecules of water solvent present per formula-unit. One water molecule was located on a twofold rotation axis. Water hydrogen atoms were refined with d(O-H) = 0.85Å.

At convergence, wR2 = 0.0878 and Goof = 1.016 for 520 variables refined against 7914 data (0.80Å), R1 = 0.0424 for those 6389 data with $I > 2.0\sigma(I)$. The absolute structure was assigned by refinement of the Flack parameter.[9]

There was a single residual (1.23e^-) present in the final difference-Fourier map. It was not possible to determine the nature of the residual. The SQUEEZE[10] routine in the PLATON[11] program package was used to account for the electrons associated with the solvent accessible voids.

Definitions:

$wR2 = [\Sigma[w(F_o^2-F_c^2)^2] / \Sigma[w(F_o^2)^2]]^{1/2}$

$R1 = \Sigma||F_o|-|F_c|| / \Sigma|F_o|$

$Goof = S = [\Sigma[w(F_o^2-F_c^2)^2] / (n-p)]^{1/2}$ where n is the number of reflections and p is the total number of parameters refined.

The thermal ellipsoid plot is shown at the 50% probability level.

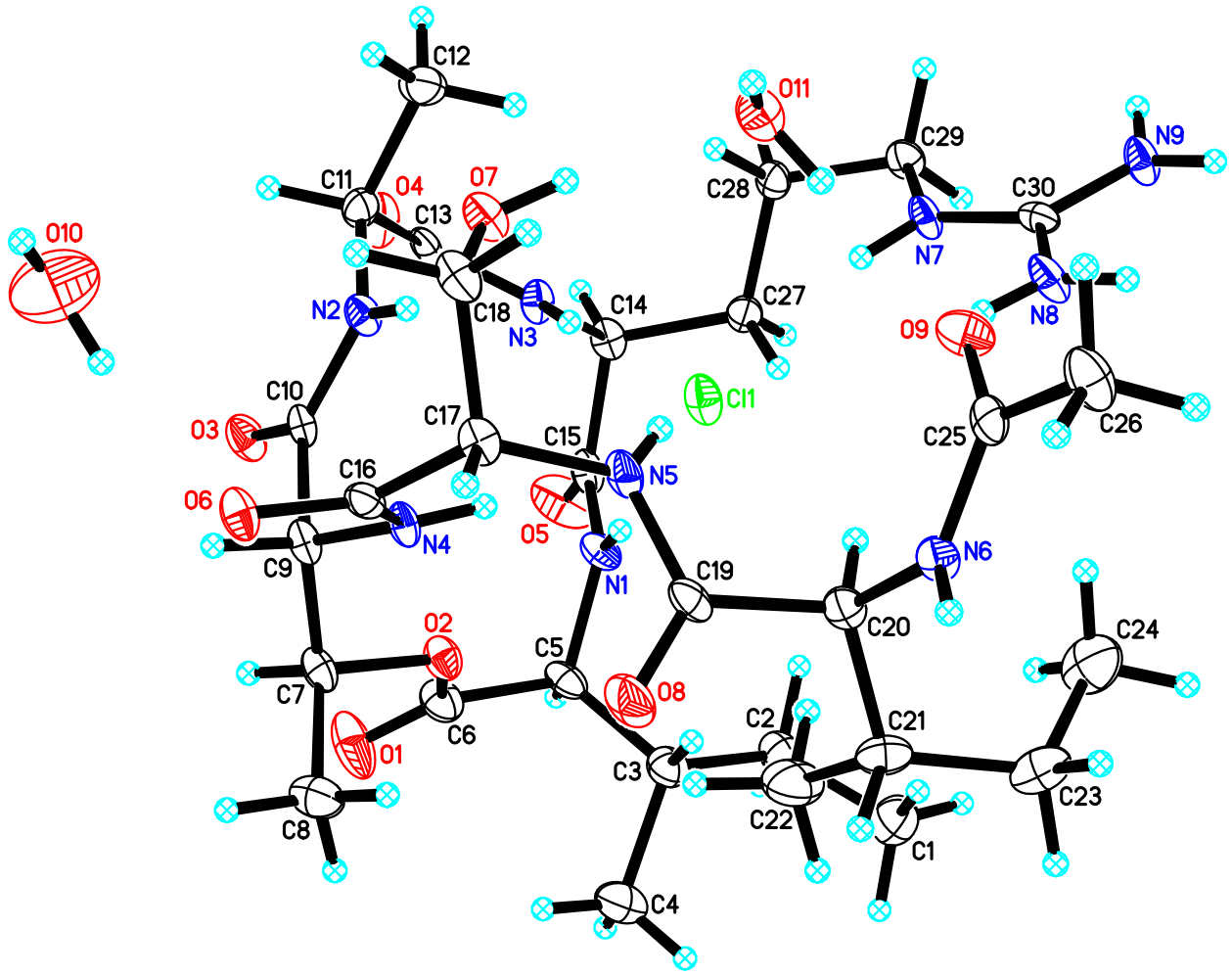

Table S3.1. Crystal data and structure refinement for Ac-$\Delta_{1\text{-}5}$-Arg_{10}-teixobactin.

Empirical formula	C_{30} H_{54} Cl N_9 O_9 •1.5(H_2O)	
Formula weight	747.29	
Temperature	88(2) K	
Wavelength	0.71073 Å	
Crystal system	Monoclinic	
Space group	*C*2	
Unit cell dimensions	a = 19.376(3) Å	α= 90°.
	b = 12.405(2) Å	β= 94.809(3)°.
	c = 16.135(3) Å	γ = 90°.
Volume	3864.5(12) $Å^3$	
Z	4	
Density (calculated)	1.284 Mg/m^3	
Absorption coefficient	0.163 mm^{-1}	
F(000)	1604	
Crystal color	colorless	
Crystal size	0.200 x 0.130 x 0.030 mm^3	
Theta range for data collection	1.951 to 26.393°	
Index ranges	$-24 \leq h \leq 24$, $-15 \leq k \leq 15$, $-20 \leq l \leq 20$	
Reflections collected	21510	
Independent reflections	7914 [R(int) = 0.0477]	
Completeness to theta = 25.500°	100.0 %	
Absorption correction	Semi-empirical from equivalents	
Max. and min. transmission	0.8620 and 0.8121	
Refinement method	Full-matrix least-squares on F^2	
Data / restraints / parameters	7914 / 4 / 520	
Goodness-of-fit on F^2	1.016	
Final R indices [I>2sigma(I) = 6389 data]	R1 = 0.0424, wR2 = 0.0811	
R indices (all data, 0.80 Å)	R1 = 0.0625, wR2 = 0.0878	
Absolute structure parameter	0.04(4)	
Largest diff. peak and hole	0.193 and -0.348 $e.Å^{-3}$	

Figure S3.1. ^{1}H and TOCSY NMR spectra of Ac-$\Delta_{1\text{-}5}$-Arg_{10}-teixobactin.

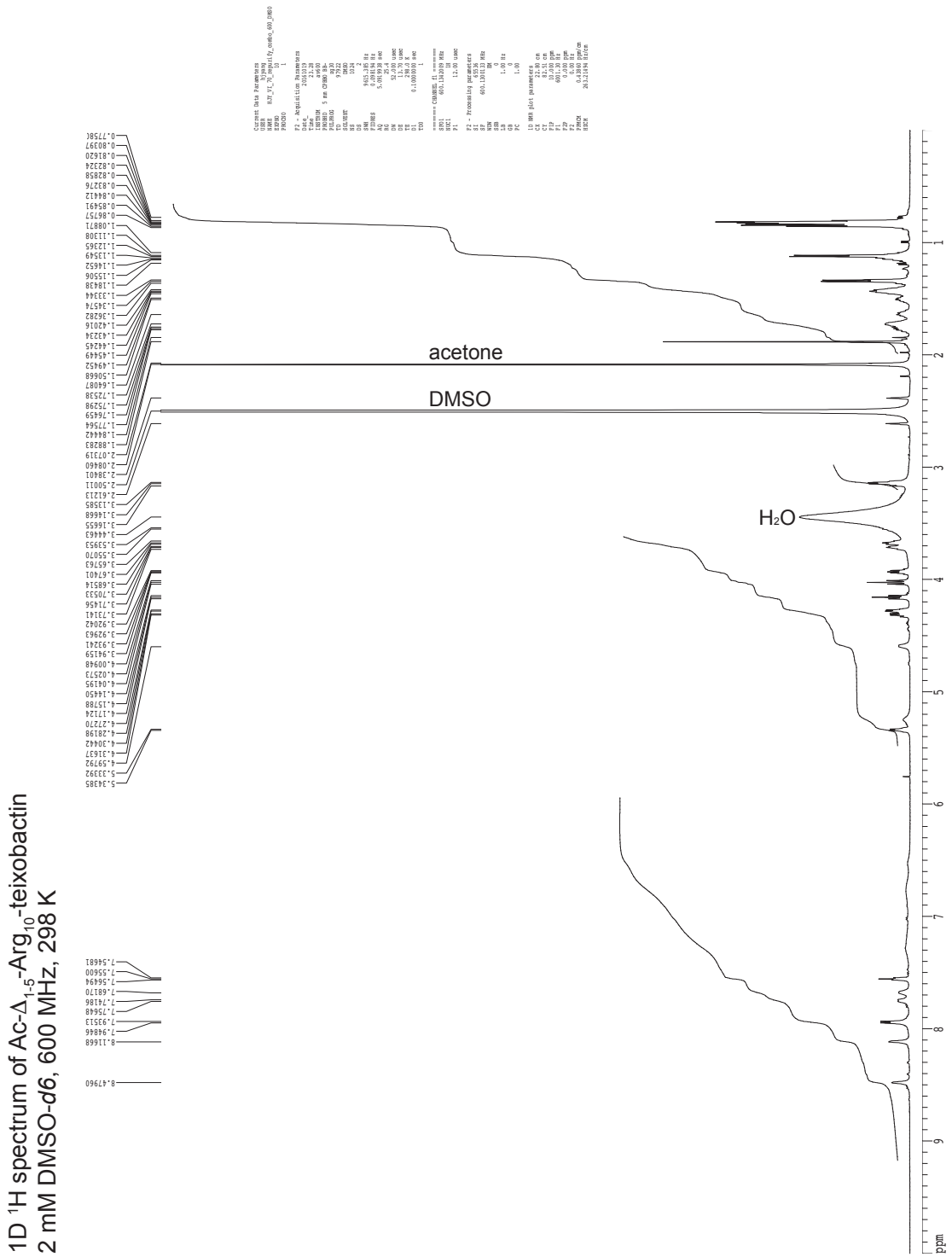

TOCSY spectrum of Ac-$\Delta_{1\text{-}5}$-Arg_{10}-teixobactin
2 mM DMSO-*d6*, 600 MHz, 298 K
150 ms spin-lock mixing time

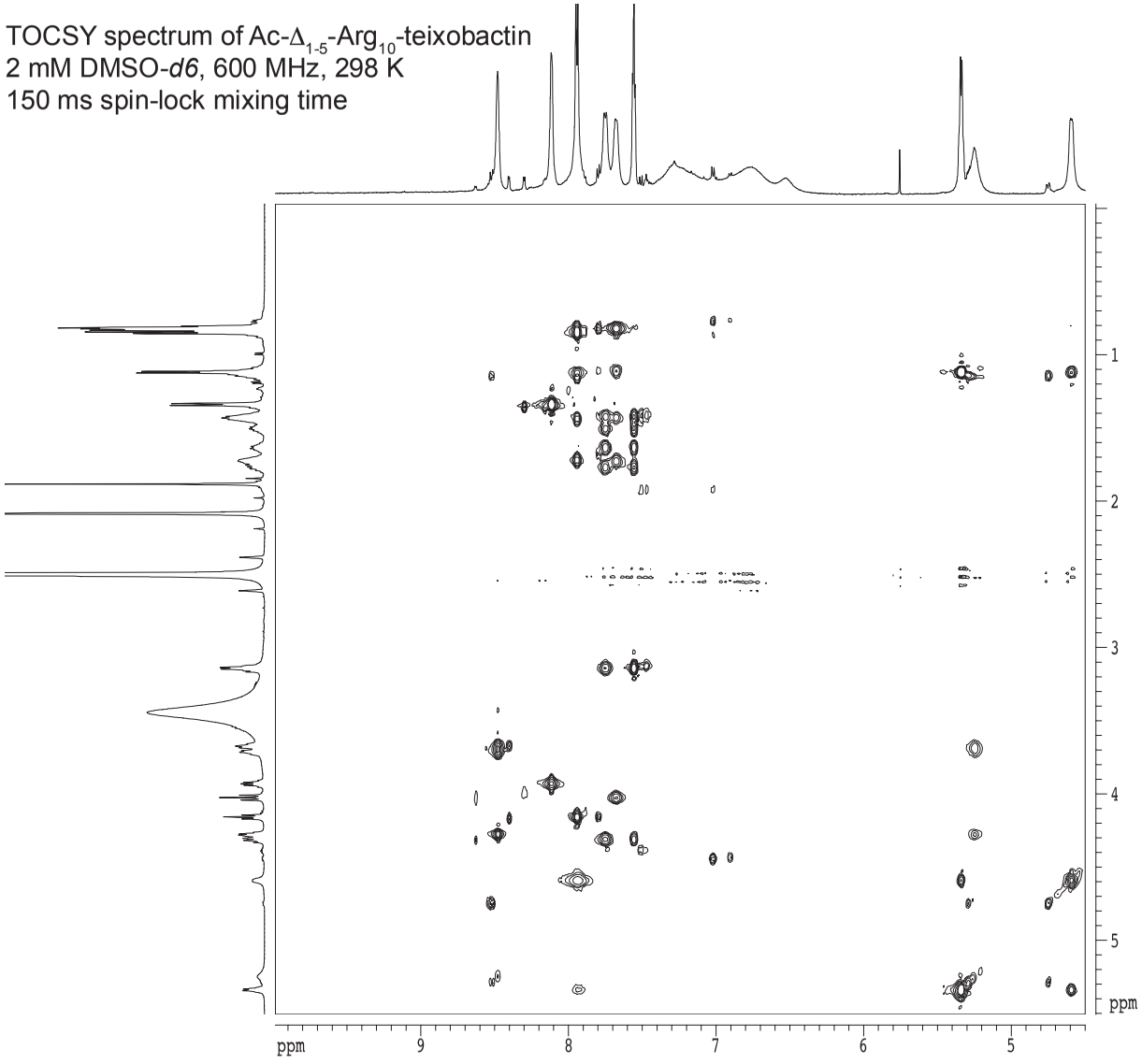

Current Data Parameters

	USER	hjyang
NAME		HJY_VI_70_repurify_combo_600_DMSO
	EXPNO	11
	PROCNO	1

F2 - Acquisition Parameters

Date_	20161019
Time	23.30
INSTRUM	av600
PROBHD	5 mm CPBBO BB-
PULPROG	mlevph
TD	1912
SOLVENT	DMSO
NS	32
DS	16
SWH	6009.615 Hz
FIDRES	3.143104 Hz
AQ	0.1591284 sec
RG	25.4
DW	83.200 usec
DE	10.00 usec
TE	298.0 K
D0	0.00007156 sec
D1	2.00000000 sec
D9	0.15000001 sec
D12	0.00002000 sec
IN0	0.00016640 sec
L1	90

======= CHANNEL f1 =======

SFO1	600.1330007 MHz
NUC1	1H
P1	12.00 usec
P5	16.67 usec
P6	25.00 usec
P7	50.00 usec
P17	2500.00 usec

F1 - Acquisition parameters

ND0	1
TD	256
SFO1	600.133 MHz
FIDRES	23.475060 Hz
SW	10.014 ppm
FnMODE	TPPI

F2 - Processing parameters

SI	1024
SF	600.1300133 MHz
WDW	QSINE
SSB	2
LB	0.00 Hz
GB	0
PC	1.00

F1 - Processing parameters

SI	1024
MC2	TPPI
SF	600.1300133 MHz
WDW	QSINE
SSB	2
LB	0.00 Hz
GB	0

2D NMR plot parameters

CX2	15.00 cm
CX1	15.00 cm
F2PLO	9.985 ppm
F2LO	5992.24 Hz
F2PHI	4.499 ppm
F2HI	2699.86 Hz
F1PLO	5.506 ppm
F1LO	3304.34 Hz
F1PHI	-0.029 ppm
F1HI	-17.38 Hz
F2PPMCM	0.36574 ppm/cm
F2HZCM	219.49181 Hz/cm
F1PPMCM	0.36900 ppm/cm
F1HZCM	221.44806 Hz/cm

Ac-$\Delta_{1\text{-}5}$-Arg$_{10}$-teixobactin

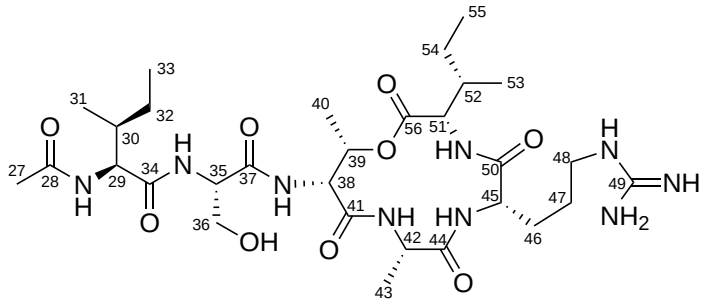

Table S3.2. NMR data of Ac-$\Delta_{1\text{-}5}$-Arg$_{10}$-teixobactin.

	Ac	27	1.88 (3H, s)	Residue 9	Ala	42	3.90 (1H, qd, 7.5, 5.6)
		28	N/A			42-NH	8.12 (1H, m)
Residue 6	Ile	29	4.16 (1H, t, 8.2)			43	1.34 (3H, d, 7.5)
		29-NH	7.94 (1H, d, 8.0)			44	N/A
		30	1.75 (1H, m)	Residue 10	Arg	45	4.30 (1H, m)
		31	0.85 (3H, m)			45-NH	7.75 (1H, m)
		32	1.14 (1H, m)			46	1.78 (1H, m)
			1.44 (1H, m)				1.65 (1H, m)
		33	0.81 (3H, m)			47	1.52 (1H, m)
		34	N/A				1.43 (1H, m)
Residue 7	Ser	35	4.28 (1H, q, 5.7)			47-NH	not observed
		35-NH	8.48 (1H, m)			48	3.14 (2H, m)
		36	3.72 (1H, m)			48-NH	7.56 (1H, t, 5.4)
			3.67 (1H, m)			49	N/A
		36-OH	5.25 (1H, br)			49-NH	not observed
		37	N/A			50	N/A
Residue 8	D-Thr	38	4.59 (1H, m)	Residue 11	Ile	51	4.03 (1H, t, 9.5)
		38-NH	7.94 (1H, m)			51-NH	7.68 (1H, m)
		39	5.34 (1H, m)			52	1.73 (1H, m)
		40	1.12 (3H, d, 6.2)			53	0.82 (3H, m)
		41	N/A			54	1.43 (1H, m)
							1.11 (1H, m)
						55	0.83 (3H, m)
						56	N/A

HPLC Traces and Mass Spectra of Teixobactin Homologues

Ac-$\Delta_{1\text{-}5}$-Arg$_{10}$-teixobactin : Analytical RP-HPLC and mass spectrum

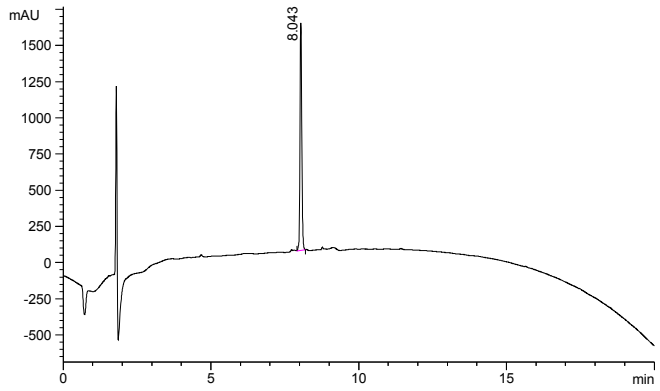

Signal 1:VWD1 A, Wavelength=214 nm

Peak #	RT [min]	Type	Width [min]	Area mAU*s	Height [mAU]	Area %
1	8.043	MM	0.071	6722.876	100.000	100.000

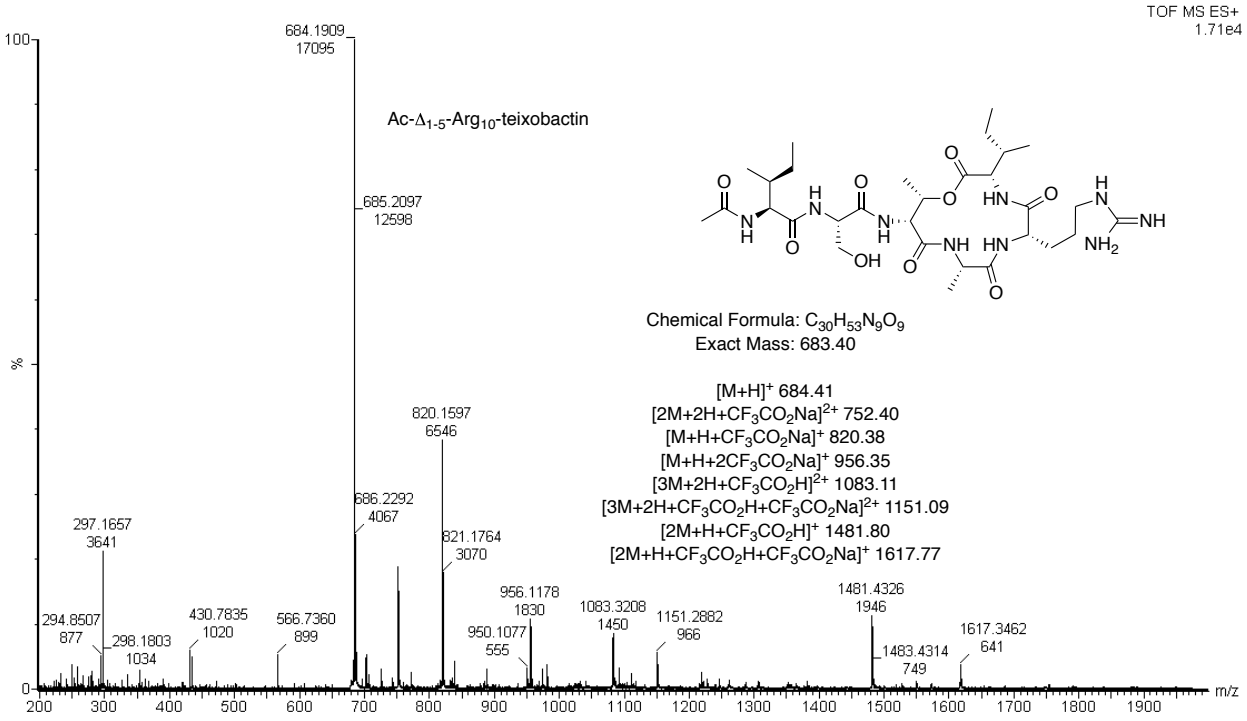

Lys_6,Arg_{10}-teixobactin : Analytical RP-HPLC and mass spectrum

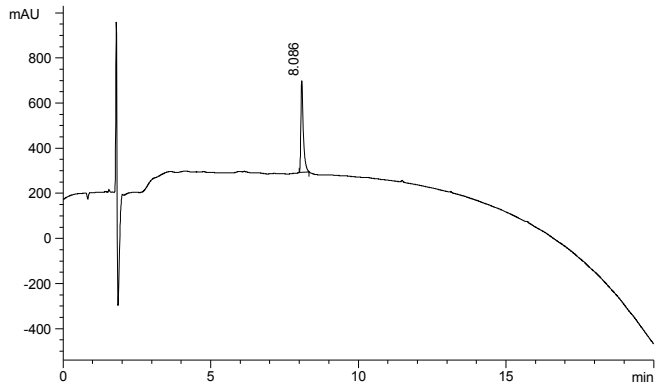

Signal 1:VWD1 A, Wavelength=214 nm

Peak #	RT [min]	Type	Width [min]	Area mAU*s	Height [mAU]	Area %
1	8.086	MM	0.094	2297.094	100.000	100.000

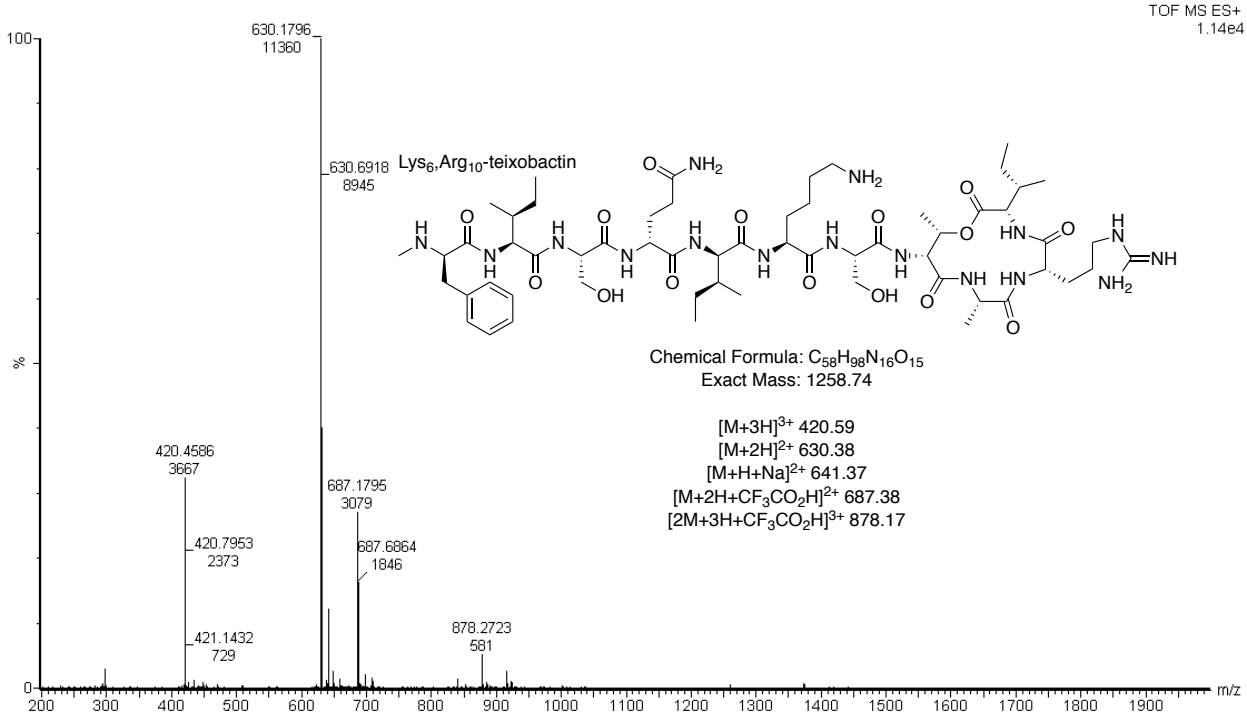

Chemical Formula: $C_{58}H_{98}N_{16}O_{15}$
Exact Mass: 1258.74

$[M+3H]^{3+}$ 420.59
$[M+2H]^{2+}$ 630.38
$[M+H+Na]^{2+}$ 641.37
$[M+2H+CF_3CO_2H]^{2+}$ 687.38
$[2M+3H+CF_3CO_2H]^{3+}$ 878.17

Arg_{10},Lys_{11}-teixobactin : Analytical RP-HPLC and mass spectrum

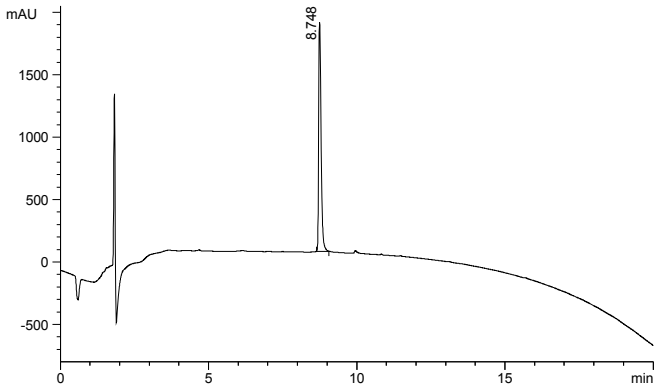

Signal 1:VWD1 A, Wavelength=214 nm

Peak #	RT [min]	Type	Width [min]	Area mAU*s	Height [mAU]	Area %
1	8.748	MM	0.095	10503.242	100.000	100.000

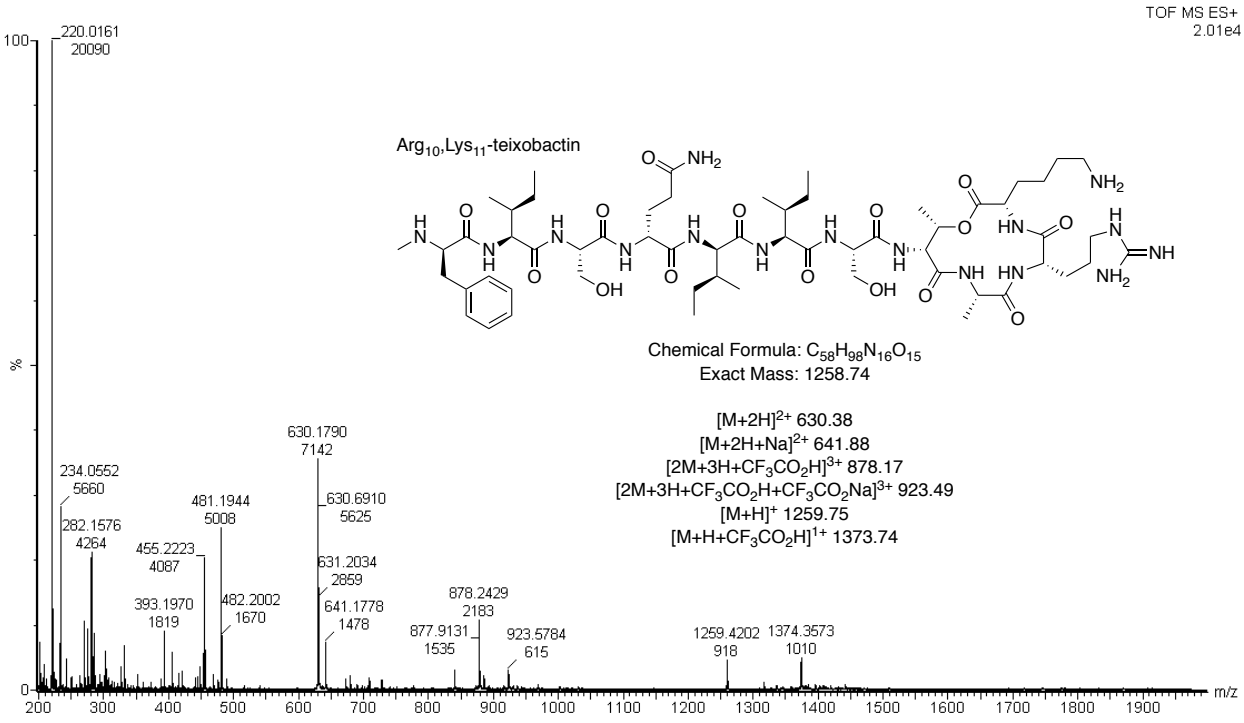

Arg_{10},Lys_{11}-teixobactin

Chemical Formula: $C_{58}H_{98}N_{16}O_{15}$
Exact Mass: 1258.74

$[M+2H]^{2+}$ 630.38
$[M+2H+Na]^{2+}$ 641.88
$[2M+3H+CF_3CO_2H]^{3+}$ 878.17
$[2M+3H+CF_3CO_2H+CF_3CO_2Na]^{3+}$ 923.49
$[M+H]^{+}$ 1259.75
$[M+H+CF_3CO_2H]^{1+}$ 1373.74

Lys$_9$,Arg$_{10}$-teixobactin : Analytical RP-HPLC and mass spectrum

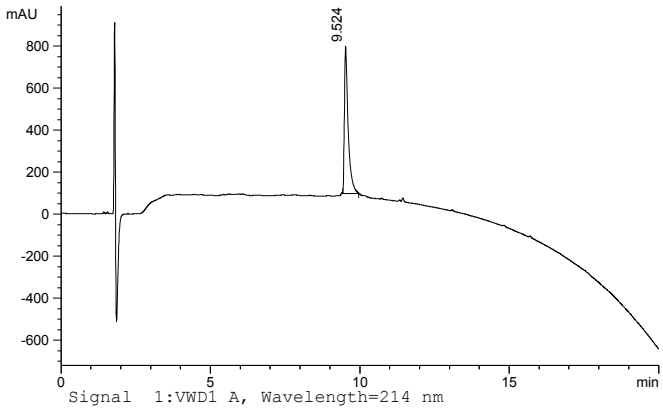

Peak #	RT [min]	Type	Width [min]	Area mAU*s	Height [mAU]	Area %
1	9.524	MM	0.144	6068.178	100.000	100.000

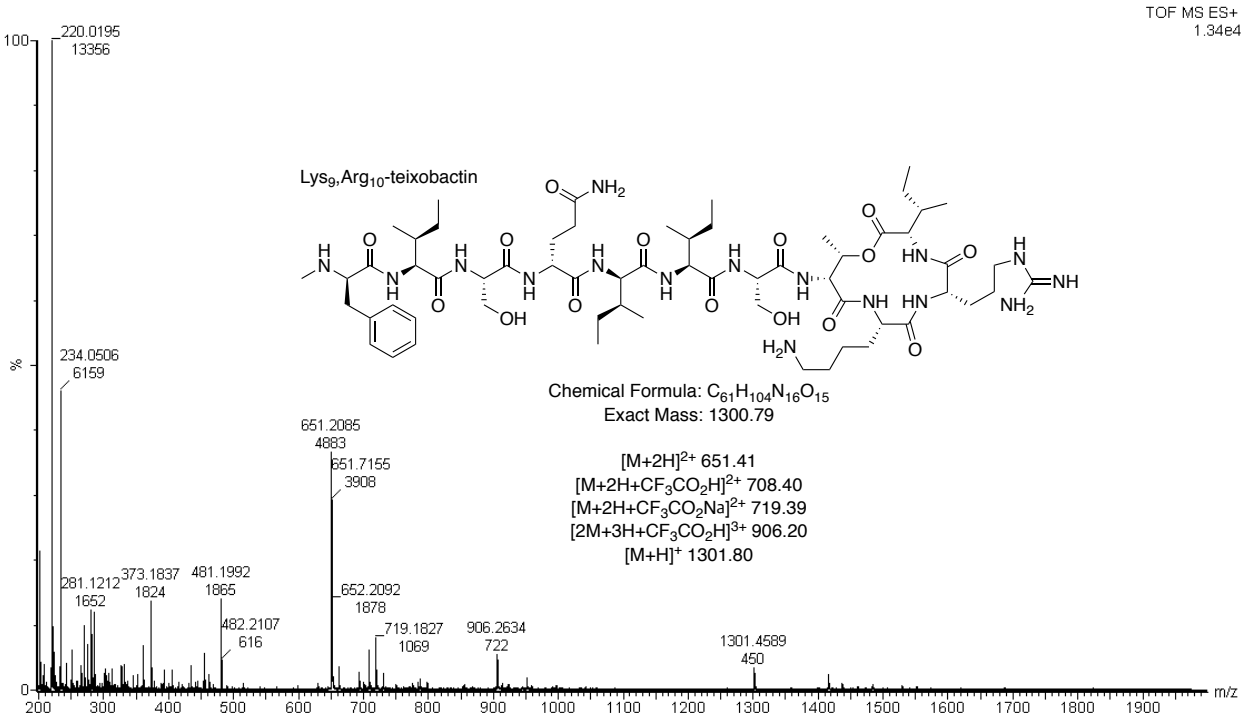

Chg_6,Arg_{10},Chg_{11}-teixobactin : Analytical RP-HPLC and mass spectrum

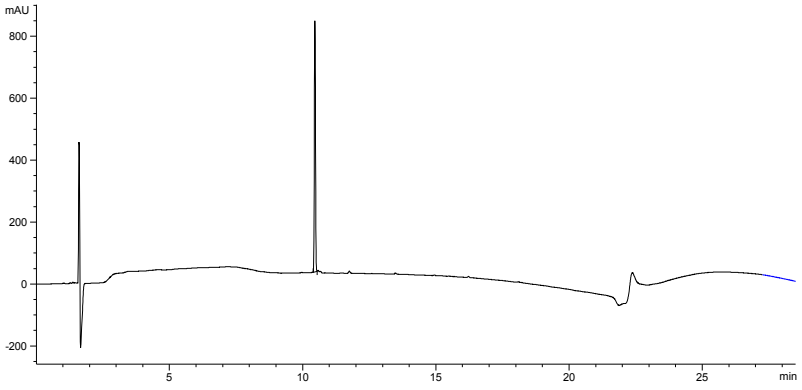

Signal 1: MWD1 A, Sig=214,4 Ref=off

Peak #	RetTime [min]	Type	Width [min]	Area [mAU*s]	Area %	Name
1	10.461	MM	0.0468	2296.97607	100.0000	?

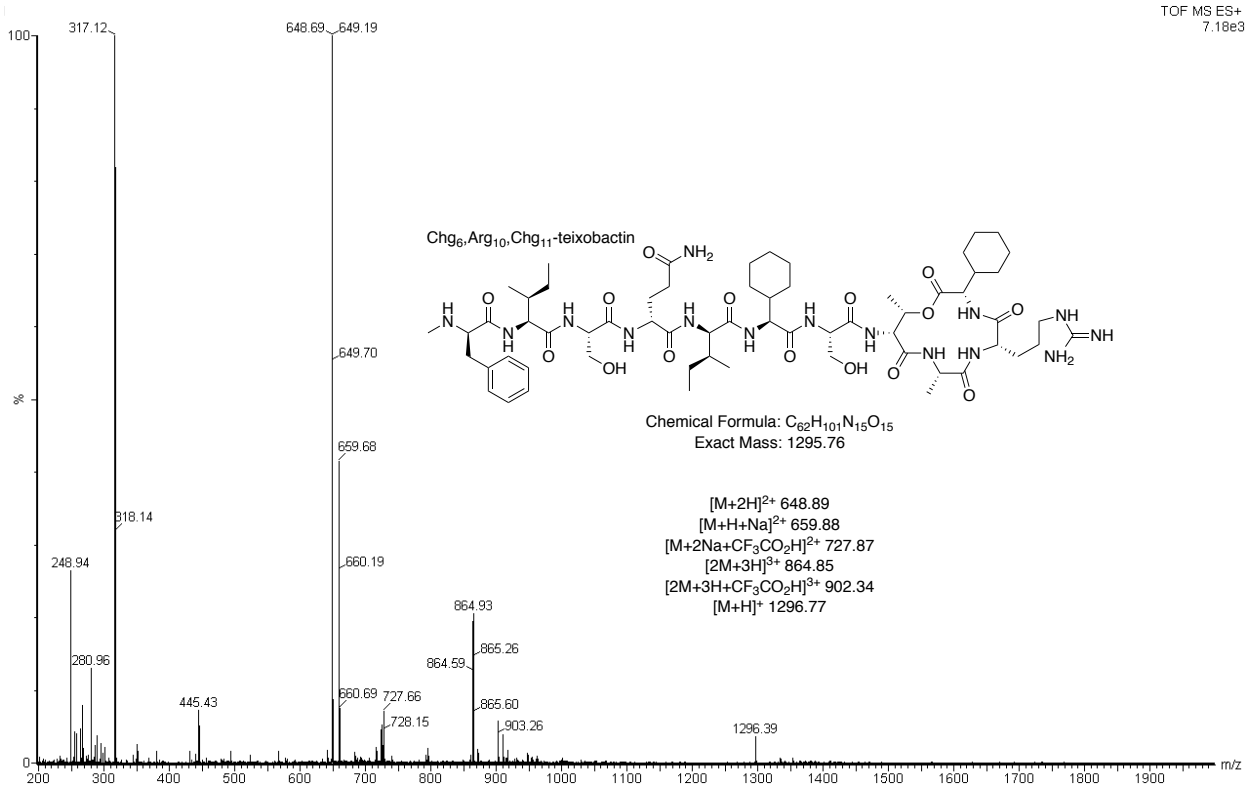

Chg_6,Arg_{10},Chg_{11}-teixobactin

Chemical Formula: $C_{62}H_{101}N_{15}O_{15}$
Exact Mass: 1295.76

$[M+2H]^{2+}$ 648.89
$[M+H+Na]^{2+}$ 659.88
$[M+2Na+CF_3CO_2H]^{2+}$ 727.87
$[2M+3H]^{3+}$ 864.85
$[2M+3H+CF_3CO_2H]^{3+}$ 902.34
$[M+H]^{+}$ 1296.77

Ala$_7$,Arg$_{10}$-teixobactin : Analytical RP-HPLC and mass spectrum

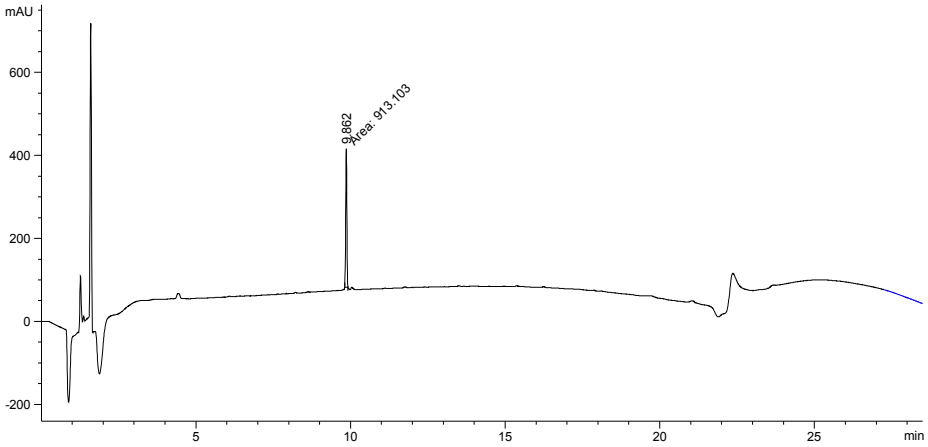

Signal 1: MWD1 A, Sig=214,4 Ref=off

Peak #	RetTime [min]	Type	Width [min]	Area [mAU*s]	Height [mAU]	Area %
1	9.862	MM	0.0452	913.10345	336.54343	100.0000

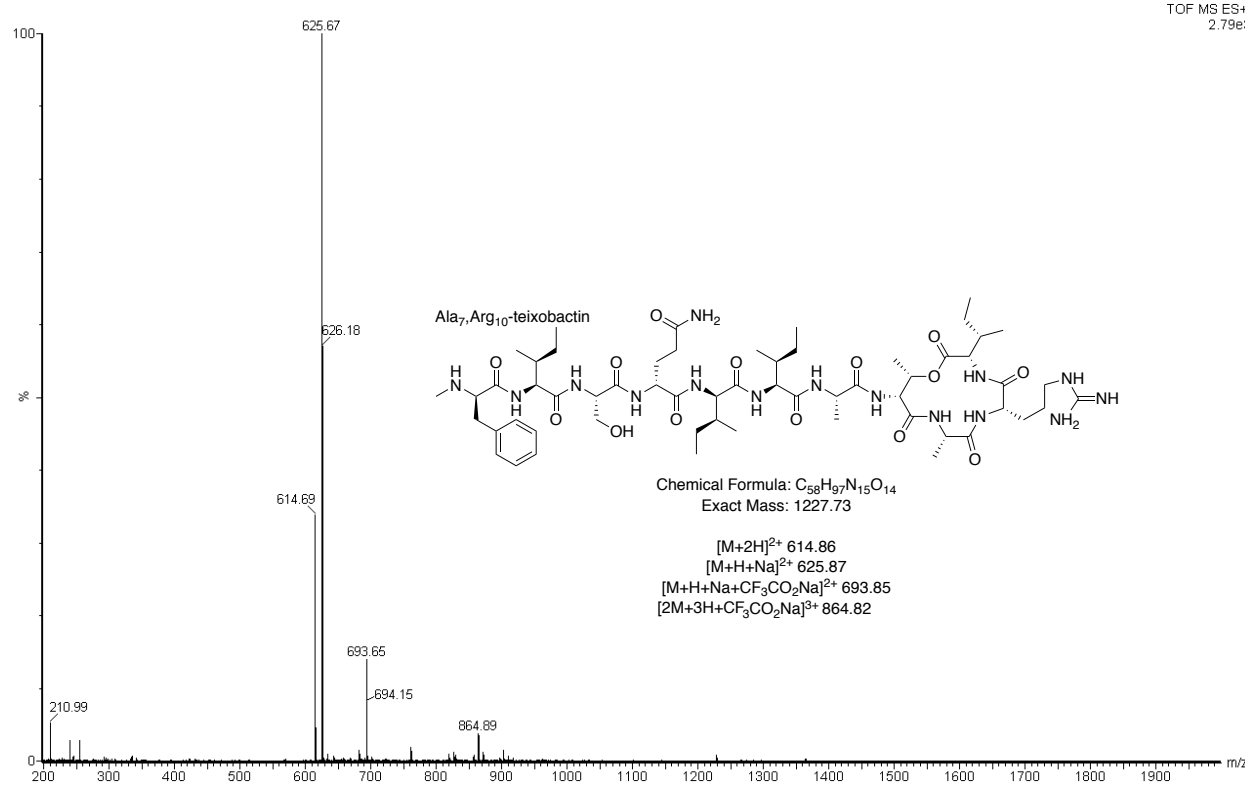

D-Dap$_8$,Arg$_{10}$-teixobactin : Analytical RP-HPLC and mass spectrum

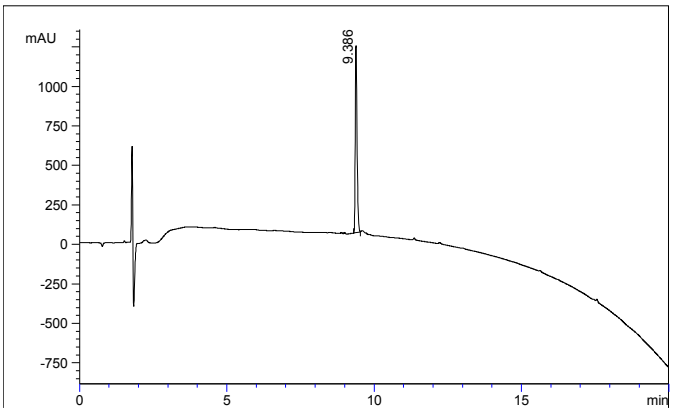

Signal 1:VWD1 A, Wavelength=214 nm

Peak #	RT [min]	Type	Width [min]	Area mAU*s	Height [mAU]	Area %
1	9.386	MM	0.070	5032.440	100.000	100.000

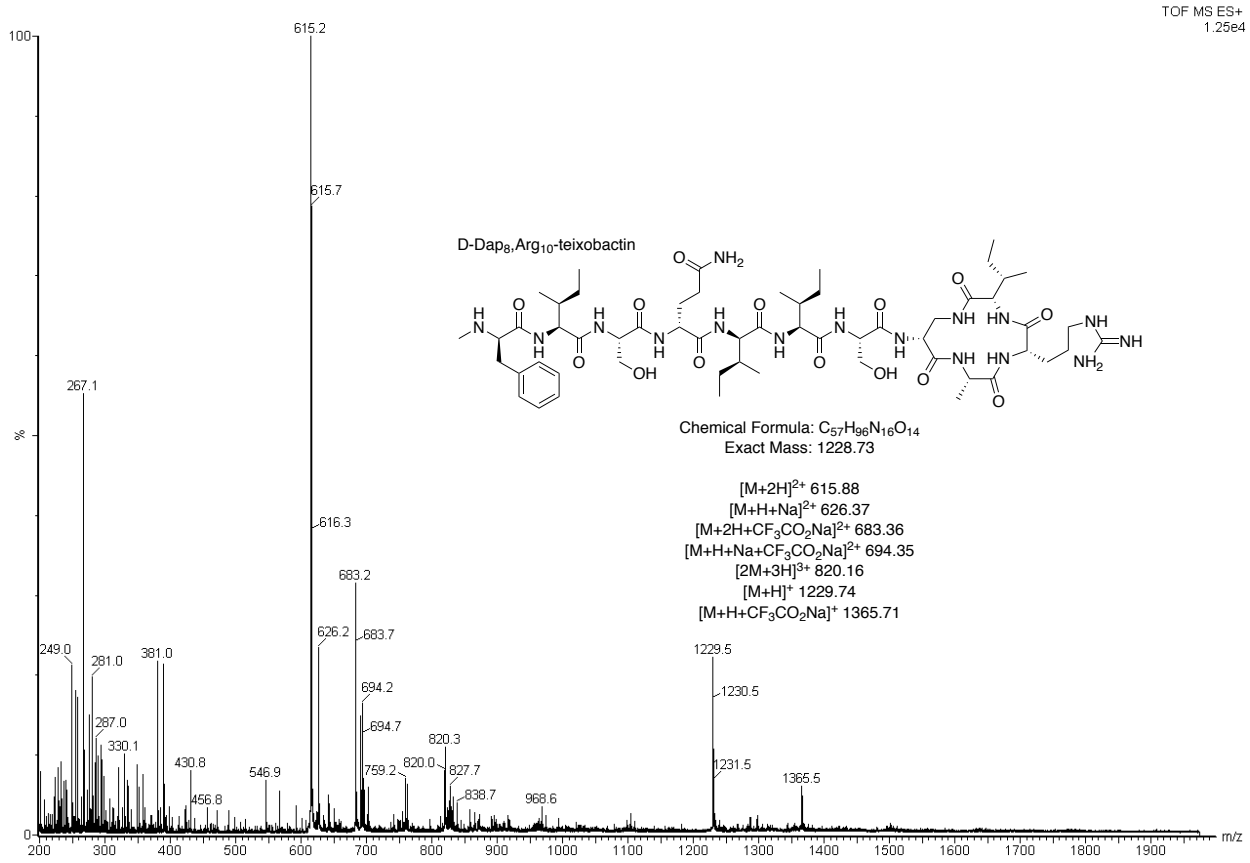

D-Dap$_8$,Arg$_{10}$-teixobactin

Chemical Formula: $C_{57}H_{96}N_{16}O_{14}$
Exact Mass: 1228.73

$[M+2H]^{2+}$ 615.88
$[M+H+Na]^{2+}$ 626.37
$[M+2H+CF_3CO_2Na]^{2+}$ 683.36
$[M+H+Na+CF_3CO_2Na]^{2+}$ 694.35
$[2M+3H]^{3+}$ 820.16
$[M+H]^{+}$ 1229.74
$[M+H+CF_3CO_2Na]^{+}$ 1365.71

References and Notes

1 Yang, H.; Chen, K. H.; Nowick, J. S. *ACS Chem. Biol.* **2016**, *11*, 1823–1826.

2 Thieriet, N.; Alsina, J.; Giralt, E.; Guibé, F.; Albericio, F. *Tetrahedron Lett.* **1999**, *38*, 7275–7278.

3 The procedure in this section is adapted from and in some cases taken verbatim from Spencer, R. K.; Kreutzer, A. G.; Salveson, P. J.; Li, H.; Nowick, J. S. *J. Am. Chem. Soc.* **2015**, *137*, 6304–6311 and Kreutzer, A. G.; Yoo, S.; Spencer, R. K.; Nowick, J. S. *J. Am. Chem. Soc.* **2017**, *139*, 966–975.

4 APEX2 Version 2014.11-0, Bruker AXS, Inc.; Madison, WI 2014.

5 SAINT Version 8.34a, Bruker AXS, Inc.; Madison, WI 2013.

6 G. M. Sheldrick, SADABS, Version 2014/5, Bruker AXS, Inc.; Madison, WI 2014.

7 G. M. Sheldrick, SHELXTL, Version 2014/7, Bruker AXS, Inc.; Madison, WI 2014.

8 International Tables for Crystallography 1992, Vol. C., Dordrecht: Kluwer Academic Publishers.

9 Parsons, S.; Flack, H. D.; Wagner, T. *Acta Cryst.* **2013**, *B69*, 249–259.

10 Spek, A.L. *Acta Cryst.* **2015**, *C71*, 9–19.

11 Spek, A. L. *Acta. Cryst.* **2009**, *D65*, 148–155.

Chapter 4[a]
X-ray Crystallographic Structure of a Teixobactin Derivative Reveals Amyloid-Like Assembly

Introduction

The peptide antibiotic teixobactin has been the subject of intensive research efforts for its promise of addressing antibiotic-resistant Gram-positive pathogens such as MRSA and VRE (**Figure 4.1**).[1,2,3,4,5,6,7,8,9] Teixobactin is thought to bind highly conserved prenyl-pyrophosphate-saccharide regions of lipid II and related membrane-bound cell wall precursors.[1] Here we describe the first X-ray crystallographic structure of a full-length teixobactin analogue, which reveals an amphipathic amyloid-like assembly that acts as a multivalent receptor for sulfate anions. This crystallographic structure suggests a working model for the mechanism of action of teixobactin in which teixobactin forms fibrils or smaller assemblies that bind to the pyrophosphate groups of lipid II and related cell wall precursors on the bacterial cell membrane and thus disrupt cell wall biosynthesis. These findings should be of value both in understanding the mechanism of action of teixobactin and in rationally designing new antibiotics that target lipid II and related cell wall precursors.

[a] Yang, H.; Wierzbicki, M.; Du Bois, D. R.; Nowick, J. S. *J. Am. Chem. Soc.* **2018**, *140*, 14028–14032.

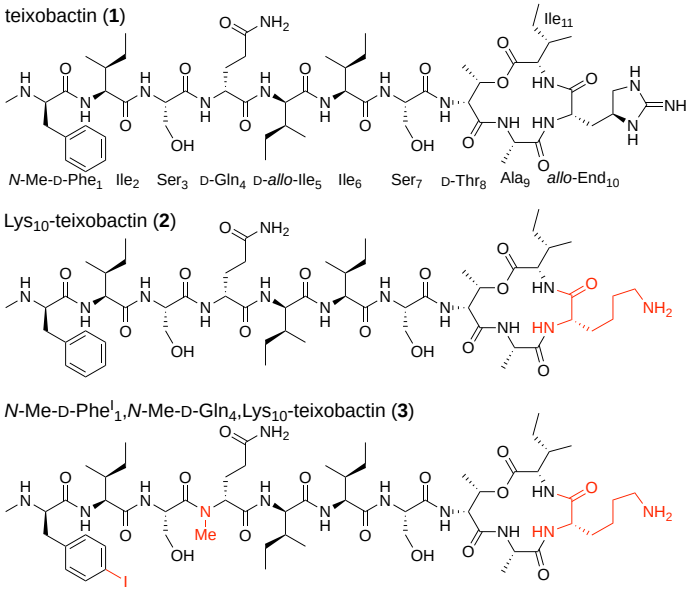

Figure 4.1. Teixobactin (**1**), Lys_{10}-teixobactin (**2**), and *N*-Me-D-Phe^{I}_{1},*N*-Me-D-Gln_4,Lys_{10}-teixobactin (**3**).

While studying structure-activity relationships among teixobactin analogues, we have observed that teixobactin and analogues with good antibiotic activity (low MIC values) form gels, while analogues with poor activity (high MIC values) do not (**Figure 4.2**).[10] For example, Lys_{10}-teixobactin (**2**), a homologue of teixobactin in which *allo*-enduracididine at position 10 is replaced with lysine (**Figure 4.1**), has an MIC of 0.5-1.0 μg/mL against *S. aureus* and forms a gel in PBS buffer, while D-Ala_5,Lys_{10}-teixobactin (MIC≥16 μg/mL) does not.[10] This observation suggested that supramolecular assembly of teixobactin analogues could be involved in antibiotic activity.

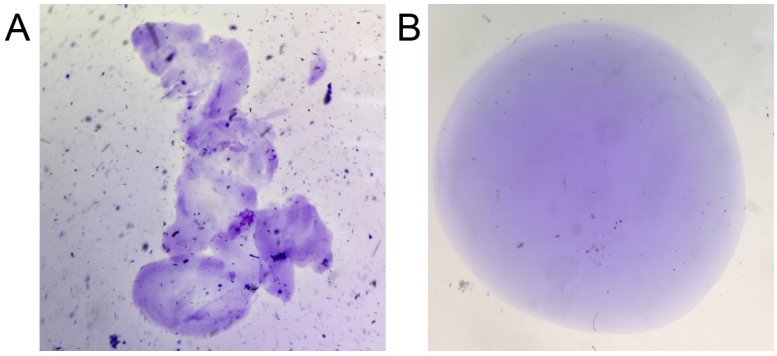

Figure 4.2. Solubility assays of (A) Lys_{10}-teixobactin (**2**) and (B) *N*-Me-D-Phe^{I}_{1},*N*-Me-D-Gln_4,Lys_{10}-teixobactin (**3**). 1 µL of 20 mg/mL solution of peptide in DMSO was added to 20 µL of PBS buffer at pH 7.4 containing a small amount of crystal violet to aid in visualization.

Results and Discussion

We began exploring the supramolecular assembly of teixobactin and its analogues by performing thioflavin T (ThT) fluorescence assays and transmission electron microscopy (TEM) studies upon Lys_{10}-teixobactin. When we incubated Lys_{10}-teixobactin with PBS buffer and ThT and monitored fluorescence, we observed a lag phase of ca. 1 day, followed by an increase in fluorescence (**Figure 4.3A**).[11] This behavior is a hallmark of amyloidogenic peptides and proteins. To further explore the assemblies that formed, we performed TEM studies. TEM images of the aggregated Lys_{10}-teixobactin revealed amyloid-like fibrils (**Figure 4.3B**). The fibrils range from individual or paired filaments, ca. 8 nm across, through bundles of filaments ca. 100-200 nm in diameter.

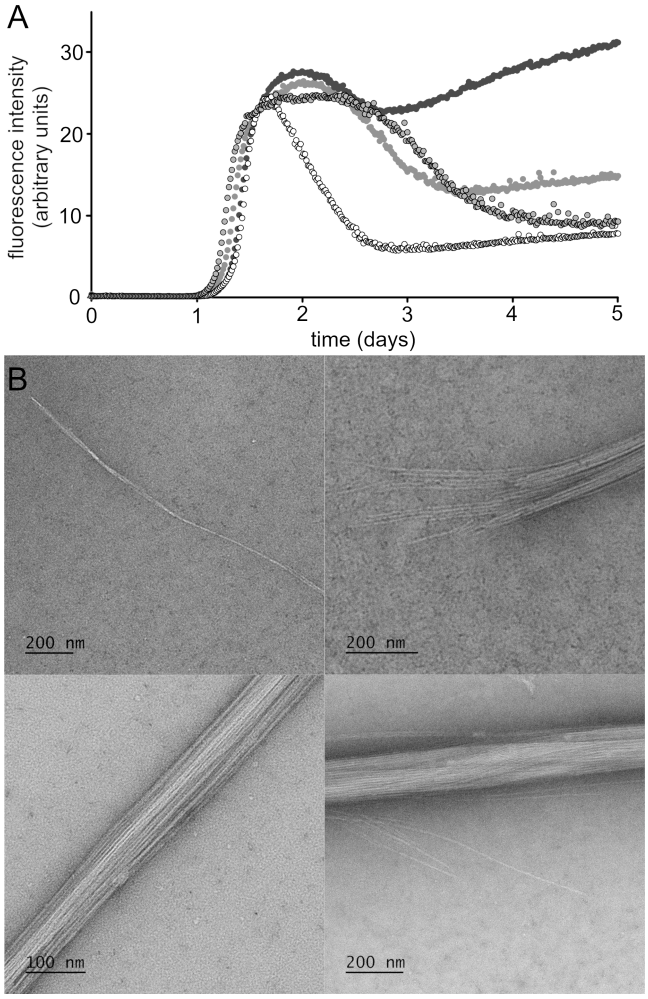

Figure 4.3. (A) ThT fluorescence assay of Lys_{10}-teixobactin (**2**, four replicate runs with 120 μM peptide in PBS buffer at pH 7.4). (B) TEM images of the fibrils formed by Lys_{10}-teixobactin (**2**).

To further study teixobactin supramolecular assembly, we turned to X-ray crystallography. Although we had successfully crystallized a truncated teixobactin analogue containing only residues 6–11, all efforts to crystallize full-length teixobactin analogues failed, giving only amorphous aggregates.[12] We postulated that *N*-methylation of the peptide backbone would attenuate the aggregation and permit the growth of crystals.[13,14] We discovered that *N*-methylation of D-Gln_4 indeed facilitated crystallization. We also incorporated an iodine atom in *N*-Me-D-Phe_1 to give *N*-methyl-*p*-iodo-D-phenylalanine (*N*-Me-D-Phe^{I}_1), to permit determination

of the X-ray crystallographic phases.[15,16] **Figure 4.1** illustrates the structure of the resulting teixobactin analogue **3**, a homologue of Lys_{10}-teixobactin (**2**). Teixobactin analogue **3** does not form a gel and exhibits only modest activity against *S. aureus* (MIC=16 μg/mL).

We began our crystallization efforts by screening teixobactin analogue **3** in 864 conditions in a 96-well plate format using crystallization kits from Hampton Research (PEG/Ion, Index, and Crystal Screen). Rectangular rod-shaped crystals grew in conditions containing sulfate salts (Li_2SO_4, $MgSO_4$, Na_2SO_4, K_2SO_4, $(NH_4)_2SO_4$) and polyethylene glycol (PEG) 3,350. With further optimization in a 24-well plate format, 0.19 M Na_2SO_4 and 15% PEG 3,350 afforded crystals suitable for X-ray diffraction. Four X-ray diffraction datasets were acquired at the Stanford Synchrotron Radiation Lightsource (SSRL) at a wavelength of 2.07 Å. The datasets were processed using XDS[17] and merged using BLEND[18]. The structure was solved by single-wavelength anomalous diffraction (SAD) phasing using the iodine anomalous signal from *N*-Me-D-Phe^{I}_1. The structure was refined with REFMAC5[19] in the $P2_12_12_1$ space group at 2.20 Å resolution. The asymmetric unit contains 32 crystallographically independent teixobactin analogue molecules, as well as 32 sulfate anions and 53 ordered water molecules.

The 32 molecules of teixobactin analogue **3** form a double helix of β-sheet fibrils in which each fibril is composed of 16 peptide molecules. Each fibril may be thought of as comprising hydrogen-bonded dimers. **Figure 4.4** illustrates the structure of a representative hydrogen-bonded dimer. In the dimer, two molecules of teixobactin analogue **3** come together to form an antiparallel β-sheet in which Ile_2 hydrogen bonds with Ile_6, *N*-Me-D-Gln_4 pairs with *N*-Me-D-Gln_4, and Ile_6 hydrogen bonds with Ile_2. The *N*-methyl groups of the two *N*-Me-D-Gln_4 residues tilt upward, allowing the β-sheet to form in spite of the disruption of the hydrogen-bonding pattern. As a result, the β-sheet has four hydrogen bonds instead of six hydrogen bonds.

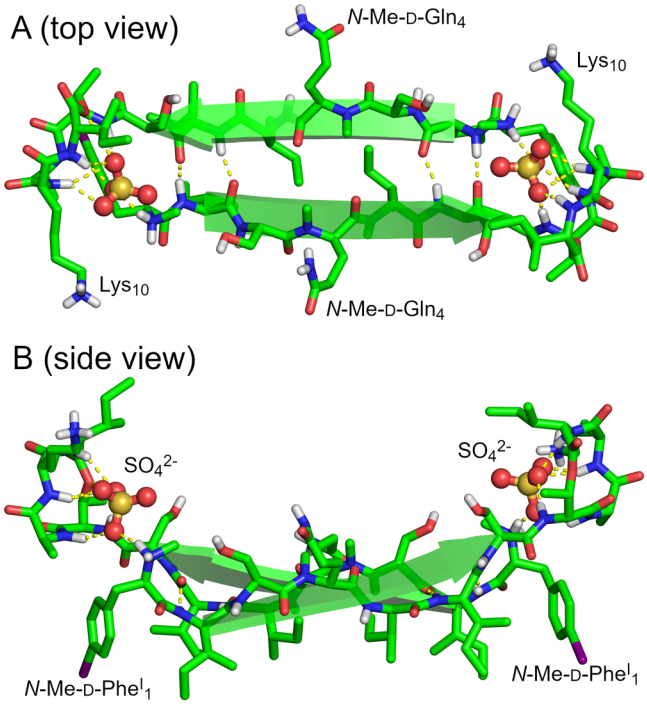

Figure 4.4. X-ray crystallographic structure of a representative dimer of *N*-Me-D-Phe$^{I}_{1}$,*N*-Me-D-Gln$_4$,Lys$_{10}$-teixobactin (**3**). (A) Top view. (B) Side view.

In the X-ray crystallographic structure, the dimer acts as a receptor for two sulfate anions. The amide NH groups of the macrocyclic ring of each monomer subunit act in conjunction with the *N*-terminus of the other monomer subunit to bind each sulfate anion. Each sulfate anion hydrogen bonds to the amide NH groups of D-Thr$_8$, Ala$_9$, Lys$_{10}$, and Ile$_{11}$ of one monomer subunit and the methylammonium group of the *N*-Me-D-Phe$^{I}_{1}$ of the other subunit. The β-sheet dimer is amphipathic: the side chains of *N*-Me-D-Phe$^{I}_{1}$, Ile$_2$, D-*allo*-Ile$_5$, and Ile$_6$ create a hydrophobic surface, and the side chains of Ser$_3$, *N*-Me-D-Gln$_4$, and Ser$_7$, as well as the *N*-terminal methylammonium group, create a hydrophilic surface. The macrocyclic rings and the sulfate anions lie above the hydrophilic surface.

Sixteen molecules of teixobactin analogue **3** assemble to form each β-sheet fibril (**Figure 4.5**). The molecules assemble in an antiparallel fashion to form an extended amphiphilic β-sheet,

with the hydrophobic residues on one face and hydrophilic residues on the other face. At each β-sheet interface between the dimers, Ser_3 hydrogen bonds with Ser_7, D-*allo*-Ile_5 hydrogen bonds with D-*allo*-Ile_5, and Ser_7 hydrogen bonds with Ser_3. Each dimer interface is thus shifted by two residues, which results in an offset fibril structure.[20] (In an aligned fibril structure, *N*-Me-D-Phe^{I}_1 would hydrogen bond with Ser_7, Ser_3 would hydrogen bond with D-*allo*-Ile_5, D-*allo*-Ile_5 would hydrogen bond with Ser_3, and Ser_7 would hydrogen bond with *N*-Me-D-Phe^{I}_1.)

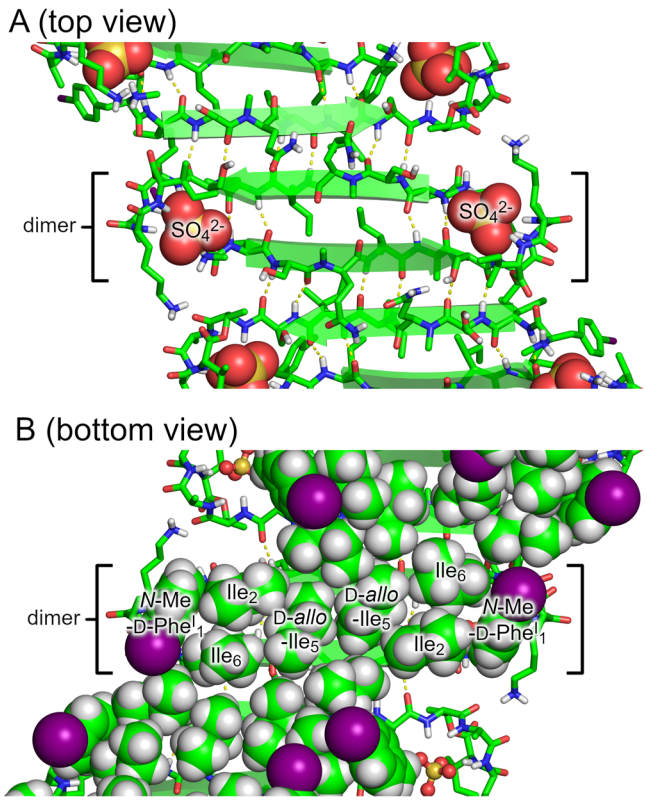

Figure 4.5. β-Sheet fibril formed by *N*-Me-D-Phe^{I}_1,*N*-Me-D-Gln_4,Lys_{10}-teixobactin (**3**). (A) Top view. (B) Bottom view with hydrophobic side chains shown as spheres.

Two β-sheet fibrils wrap around each other to form a right-handed double helix of β-sheets, with the hydrophobic surfaces in the interior and the hydrophilic surfaces on the exterior (**Figure 4.6**). Each double helix contains 32 molecules of teixobactin analogue **3** and

corresponds to the asymmetric unit. The double helices are discrete structures in the crystal lattice and are not part of extended superstructures. The double helix is ca. 9 nm in length and ca. 4 nm in diameter in the middle, tapering to ca. 2 nm at the two ends. The ends of the double helix are closed, but the middle has a central cavity of ca. 1 nm in diameter and ca. 5 nm in length that is surrounded by the hydrophobic side chains of *N*-Me-D-Phe$^{I}_{1}$, Ile$_2$, D-*allo*-Ile$_5$, and Ile$_6$ (**Figure 4.7**). The ordered water molecules surround the hydrophilic exterior of the double helix.

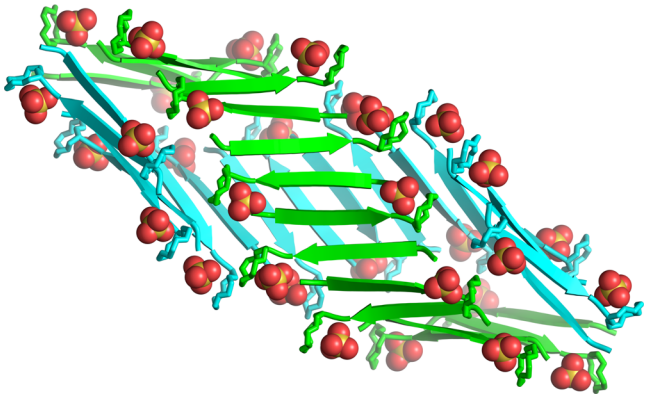

Figure 4.6. Double helix of β-sheet fibrils formed by *N*-Me-D-Phe$^{I}_{1}$,*N*-Me-D-Gln$_4$,Lys$_{10}$-teixobactin (**3**). Sulfate anions are shown as spheres.

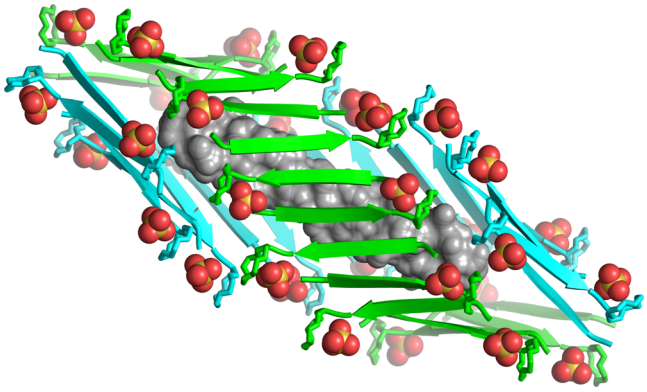

Figure 4.7. Double helix of β-sheet fibrils formed by *N*-Me-D-Phe$^{I}_{1}$,*N*-Me-D-Gln$_4$,Lys$_{10}$-teixobactin (**3**) illustrating the central cavity (grey surface).

The X-ray crystallographic structure of the discrete double helix of β-sheets formed by teixobactin analogue **3** suggests a molecular model for the assembly of teixobactin analogue **2**

into the filaments and fibrils observed by TEM (**Figure 4.3**). In this model, teixobactin analogue **2** assembles to form extended networks of β-sheet fibrils, which wrap around each other to form extended double helices of β-sheets. **Figure 4.8** illustrates this model. Unlike the discrete structures formed by *N*-methylated analogue **3**, these double helices persist for many hundreds of nanometers and contain thousands of molecules. These fibrils further wrap or bundle together to form the fibrils and bundles observed by TEM. Although the *N*-methyl group in teixobactin analogue **3** does not prevent β-sheet formation, it impedes the formation of extended fibrils by reducing the stability of the β-sheets that form.

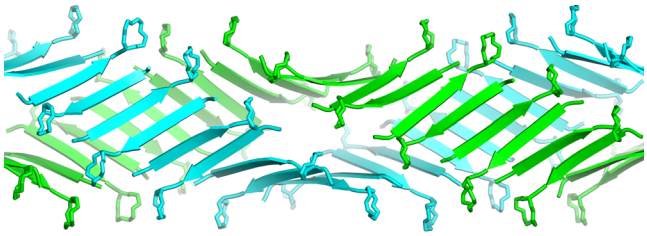

Figure 4.8. Crystallographically based molecular model of an extended double helix of β-sheet fibrils formed by teixobactin analogue **2** and observed by TEM (**Figure 4.3**).

The amphipathic assembly formed by teixobactin analogue **3** explains many of the previously reported structure-activity relationships in teixobactin analogues.[10,21,22] Our laboratory has previously reported that substituting residues 1, 2, 5, 6, and 7 with L- or D-alanine dramatically reduces or eliminates the antibiotic activity of Lys_{10}-teixobactin, while substituting residues 3 and 4 with L- or D-alanine has much smaller effects upon activity.[10] Similar effects have been observed upon replacement of residues 2–7 with L- or D-lysine.[21] The densely packed hydrophobic surface formed by residues 1, 2, 5, and 6 on the interior of the double helix of β-sheet fibrils (**Figure 4.5B**) explains why mutating any of these bulky hydrophobic residues to L- or D- alanine or lysine disrupts supramolecular assembly and causes loss of activity. The

hydrophilic side chains of residues 3 and 4 are on the hydrophilic exterior of the double helix of β-sheet fibrils (**Figure 4.5A**) and are substantially more tolerant of substitution. The hydrophilic side chain of residue 7 is also on the hydrophilic exterior of the double helix of β-sheet fibrils, however the X-ray crystallographic structure does not appear to explain the loss of activity upon mutating this residue to Ala or Lys. Additional studies have reported that substituting L-amino acids for D-amino acids at residues 1, 4, and 5 in Arg_{10}-teixobactin also dramatically reduces or eliminates antibiotic activity.[22] Each of these stereochemical mutations disrupts the amphipathic β-sheet formed by residues 1–7 and causes loss of antibiotic activity.

The X-ray crystallographic structure of teixobactin analogue **3**, in conjunction with the observation that Lys_{10}-teixobactin (**2**) forms amyloid-like fibrils, suggest that supramolecular assembly may be involved in the antibiotic activity of teixobactin. We thus propose a working model for the antibiotic activity of teixobactin in which teixobactin forms dimers, higher-order assemblies, or fibrils through antiparallel β-sheet interactions.[23] The dimers or dimer subunits create binding sites for the pyrophosphate groups of lipid II and related membrane-bound cell wall precursors, perhaps adhering strongly to the surface through contacts with multiple lipid molecules.[24] In the binding site, the amide NH groups of residues 8–11 of one teixobactin molecule in the dimer and the *N*-terminus of the other teixobactin molecule interact with each bound pyrophosphate group. In teixobactin (**1**), the guanidinium group of *allo*-End_{10} may make additional contacts to the pyrophosphate group.

This model shares a number of features in common with those observed for other antibiotics that target lipid II and related cell wall precursors, including ramoplanin and nisin.[25,26] Ramoplanin forms fibrils with lipid II analogues, and supramolecular assembly through the formation of antiparallel β-sheet dimers is thought to be important in its mechanism of

action.[27,28,29,30,31] Nisin binds the pyrophosphate group of lipid II by means of a pyrophosphate cage formed by amide NH groups in and adjacent to the 16-membered lanthionine A ring.[32,33]

Conclusion

The unique pattern of hydrophobicity and stereochemistry of residues 1–7 of teixobactin makes fibril formation possible. By having evolved a D-L-L-D-D-L-L pattern of stereochemistry with a hydrophobic-hydrophobic-hydrophillic-hydrophilic-hydrophobic-hydrophobic-hydrophilic pattern of side chains, *Eleftheria terrae* has achieved an amyloidogenic non-ribosomal peptide that can assemble to form amphiphilic β-sheets and amyloid-like fibrils that can bind oxyanions. On the basis of our crystal structure, we have proposed a working model for the mechanism of action of teixobactin involving the formation of β-sheet dimers or higher-order supramolecular assemblies. We further recognize that the crystallographic observation of supramolecular assembly[34,35] and its potential involvement in antibiotic activity[36,37] does not assure its biological relevance.[38,39] We envision the model put forth here to be worthy of further study and anticipate reporting these studies in due course.

References and Notes

1 Ling, L. L.; Schneider, T.; Peoples, A. J.; Spoering, A. L.; Engels, I.; Conlon, B. P.; Mueller, A.; Schäberle, T. F.; Hughes, D. E.; Epstein, S.; Jones, M.; Lazarides, L.; Steadman, V. A.; Cohen, D. R.; Felix, C. R.; Fetterman, K. A.; Millett, W. P.; Nitti, A. G.; Zullo, A. M.; Chen, C.; Lewis, K. A new antibiotic kills pathogens without detectable resistance. *Nature* **2015**, *517*, 455–459.

2 Homma, T.; Nuxoll, A.; Gandt, A. B.; Ebner, P.; Engels, I.; Schneider, T.; Götz, F.; Lewis, K.; Conlon, B. P. Dual Targeting of Cell Wall Precursors by Teixobactin Leads to Cell Lysis. *Antimicrob. Agents Chemother.* **2016**, *60*, 6510–6517.

3 Zong, Y.; Sun, X.; Gao, H.; Meyer, K. J.; Lewis, K.; Rao, Y. Developing Equipotent Teixobactin Analogues against Drug-Resistant Bacteria and Discovering a Hydrophobic Interaction between Lipid II and Teixobactin. *J. Med. Chem.* **2018**, *61*, 3409–3421.

4 Jin, K.; Sam, I. H.; Po, K. H. L.; Lin, D.; Ghazvini Zadeh, E. H.; Chen, S.; Yuan, Y.; Li, X. Total synthesis of teixobactin. *Nat. Commun.* **2016**, *7*, 12394.

5 Parmar, A.; Lakshminarayanan, R.; Iyer, A.; Mayandi, V.; Leng Goh, E. T.; Lloyd, D. G.; Chalasani, M. L. S.; Verma, N. K.; Prior, S. H.; Beuerman, R. W.; Madder, A.; Taylor, E. J.; Singh, I. Design and Syntheses of Highly Potent Teixobactin Analogues against *Staphylococcus aureus*, Methicillin-Resistant *Staphylococcus aureus* (MRSA), and Vancomycin-Resistant Enterococci (VRE) *in Vitro* and *in Vivo*. *J. Med. Chem.* **2018**, *61*, 2009–2017.

6 Abdel Monaim, S. A. H.; Jad, Y. E.; El-Faham, A.; de la Torre, B. G.; Albericio, F. Teixobactin as a scaffold for unlimited new antimicrobial peptides: SAR study. *Bioorganic Med. Chem.* **2018**, *26*, 2788–2796.

7 Yang, H.; Chen, K. H.; Nowick, J. S. Elucidation of the Teixobactin Pharmacophore. *ACS Chem. Biol.* **2016**, *11*, 1823–1826.

8 Kåhrström, C. T. Antimicrobials: A new drug for resistant bugs. *Nat. Rev. Microbiol.* **2015**, *13*, 126–127.

9 Wen, P.; Vanegas, J. M.; Rempe, S. B.; Tajkhorshid. E. Probing Key Elements of Teixobactin-Lipid II Interactions in Membrane. *Chem. Sci.* **2018,** *9*, 6997–7008.

10 Chen, K. H.; Le, S. P.; Han, X.; Frais, J. M.; Nowick, J. S. Alanine scan reveals modifiable residues in teixobactin. *Chem. Commun.* **2017**, *53*, 11357–11359.

11 Upon further incubation, the fluorescence declines variably. This subsequent change in fluorescence may reflect further reorganization of the amyloid-like fibrils that form, such as assembly into the bundles of filaments that are observed by TEM.

12 Yang, H.; Du Bois, D. R.; Ziller, J. W.; Nowick, J. S. X-ray crystallographic structure of a teixobactin analogue reveals key interactions of the teixobactin pharmacophore. *Chem. Commun.* **2017**, *53*, 2772–2775.

13 Spencer, R.; Li, H.; Nowick, J. S. X-ray Crystallographic Structures of Trimers and Higher-Order Oligomeric Assemblies of a Peptide Derived from Aβ17–36. *J. Am. Chem. Soc.* **2014**, *136*, 5595–5598.

14 Spencer, R. K.; Kreutzer, A. G.; Salveson, P. J.; Li, H.; Nowick, J. S. X-ray Crystallographic Structures of Oligomers of Peptides Derived from β2-Microglobulin. *J. Am. Chem. Soc.* **2015**, *137*, 6304–6311.

15 Richardson, M. B.; Brown, D. B.; Vasquez, C. A.; Ziller, J. W.; Johnston, K. M.; Weiss, G. A. Synthesis and Explosion Hazards of 4-Azido-l-phenylalanine. *J. Org. Chem.* **2018**, *83*, 4525–4536.

16 Malkov, A. V.; Stončius, S.; MacDougall, K, N.; Mariani, A.; McGeoch, G. D.; Kočovský, P. Formamides derived from N-methyl amino acids serve as new chiral organocatalysts in the enantioselective reduction of aromatic ketimines with trichlorosilane. *Tetrahedron* **2006**, *62*, 264–284.

17 Kabsch, W. XDS. *Acta Crystallogr., Sect. D: Biol. Crystallogr.* **2010**, *66*, 125−132.

18 Foadi, J.; Aller, P.; Alguel, Y.; Cameron, A.; Axford, D.; Owen, R. L.; Armour, W.; Waterman, D. G.; Iwata, S.; Evans, G. Clustering procedures for the optimal selection of data sets from multiple crystals in macromolecular crystallography. *Acta Crystallogr., Sect. D: Biol. Crystallogr.* **2013**, *69*, 1617−1632.

19 Murshudov, G. N.; Vagin, A. A.; Dodson, E. J. Refinement of macromolecular structures by the maximum-likelihood method. *Acta Crystallogr., Sect. D: Biol. Crystallogr.* **1997**, *53*, 240−255.

20 Sangwan, S.; Zhao, A.; Adams, K. L.; Jayson, C. K.; Sawaya, M. R.; Guenther, E. L.; Pan, A. C.; Ngo, J.; Moore, D. M.; Soriaga, A. B.; Do, T. D.; Goldschmidt, L.; Nelson, R.; Bowers, M. T.; Koehler, C. M.; Shaw, D. E.; Novitch, B. G.; Eisenberg, D. S. Atomic structure of a toxic, oligomeric segment of SOD1 linked to amyotrophic lateral sclerosis (ALS). *Proc. Natl. Acad. Sci. U.S.A.* **2017**, *114*, 8770−8775.

21 Abdel Monaim, S. A. H.; Jad, Y. E.; Ramchuran, E. J.; El-Faham, A.; Govender, T.; Kruger, H. G.; de la Torre, B. G.; Albericio, F. Lysine Scanning of Arg10−Teixobactin: Deciphering the Role of Hydrophobic and Hydrophilic Residues. *ACS Omega* **2016**, *1*, 1262−1265.

22 Parmar, A.; Prior, S. H.; Iyer, A.; Vincent, C. S.; Van Lysebetten, D.; Breukink, E.; Madder, A.; Taylor, E. J.; Singh, I. Defining the molecular structure of teixobactin analogues and understanding their role in antibacterial activities. *Chem. Commun.* **2017**, *53*, 2016−2019.

23 Lewandowski et al. have concurrently reported NMR-based structural studies of teixobactin in aqueous and membranelike environments, both with and without lipid II and lipid II analogues. [Öster, C.; Walkowiak, G. P.; Hughes, D. E.; Spoering, A. L.; Peoples, A. J.; Catherwood, A. C.; Tod, J. A.; Lloyd, A. J.; Herrmann, T.; Lewis, K.; Dowson, C.; Lewandowski, J. R. Structural studies suggest aggregation as one of the modes of action for teixobactin. *Chem. Sci.* **2018**, *Accepted Manuscript* (DOI: 10.1039/C8SC03655A)] These studies indicate that teixobactin, in the presence of lipid II, rapidly aggregates and the residues 2–6 rearrange from random coil like conformation to a more extended β-strand like conformation.

24 A 2:1 teixobactin:lipid II binding stoichiometry was reported in the original 2015 *Nature* paper on teixobactin (reference 1). The crystallographic observation of putative pyrophosphate binding sites created by dimers could potentially support either a 2:1 or a 2:2 teixobactin:lipid II stoichiometry, depending on how the binding of one molecule of lipid II to the dimer affects the accessibility of the other site of the dimer.

25 Breukink, E.; de Kruijff, B. Lipid II as a target for antibiotics. *Nat. Rev. Drug Discov.* **2006**, *5*, 321–332.

26 de Kruijff, B.; van Dam, V.; Breukink, E. Lipid II: a central component in bacterial cell wall synthesis and a target for antibiotics. *Prostaglandins Leukot. Essent. Fatty Acids* **2008**, *79*, 117–121.

27 Lo, M. C.; Men, H.; Branstrom, A.; Helm, J.; Yao, N.; Goldman, R.; Walker, S. A new mechanism of action proposed for ramoplanin. *J. Am. Chem. Soc.* **2000**, *122*, 3540−3541.

28 Lo, M. C.; Helm, J. S.; Sarngadharan, G.; Pelczer, I.; Walker, S. A new structure for the substrate-binding antibiotic ramoplanin. *J. Am. Chem. Soc.* **2001**, *123*, 8640−8641.

29 Hu, Y.; Helm, J. S.; Chen, L.; Ye, X.-Y.; Walker, S. Ramoplanin inhibits bacterial transglycosylases by binding as a dimer to lipid II. *J. Am. Chem. Soc.* **2003**, *125*, 8736−8737.

30 Walker, S.; Chen, L.; Hu, Y.; Rew, Y.; Shin, D.; Boger, D. L. Chemistry and biology of ramoplanin: a lipoglycodepsipeptide with potent antibiotic activity. *Chem. Rev.* **2005**, *105*, 449−476.

31 Hamburger, J. B.; Hoertz, A. J.; Lee, A.; Senturia, R. J.; McCafferty, D. G.; Loll, P. J.; A crystal structure of a dimer of the antibiotic ramoplanin illustrates membrane positioning and a potential Lipid II docking interface. *Proc. Natl. Acad. Sci. U.S.A.* **2009**, *106*, 13759−13764.

32 Hsu, S. T.; Breukink, E.; Tischenko, E.; Lutters, M. A.; de Kruijff, B.; Kaptein, R.; Bonvin, A. M.; Nuland, N. A. The nisin-lipid II complex reveals a pyrophosphate cage that provides a blueprint for novel antibiotics. *Nat. Struct. Mol. Biol.* **2004**, *11*, 963−967.

33 Watson, J. D.; Milner-White, E. J. A novel main-chain anion-binding site in proteins: The nest. A particular combination of phi, psi values in successive residues gives rise to anion-binding sites that occur commonly and are found often at functionally important regions. *J. Mol. Biol.* **2002**, *315*, 171–182.

34 Sheldrick, G. M.; Jones, P. G.; Kennard, O.; Williams, D. H.; Smith, G. A. Structure of vancomycin and its complex with acetyl-D-alanyl-D-alanine. *Nature* **1978**, *271*, 223–225.

35 Schäfer, M.; Schneider, T. R.; Sheldrick, G. M. Crystal structure of vancomycin. *Structure* **1996**, *4*, 1509–1515.

36 Sharman, G. J.; Try, A. C.; Dancer, R. J.; Cho, Y. R.; Staroske, T.; Bardsley, B.; Maguire, A. J.; Cooper, M. A.; O'Brie, D. P.; Williams. D. H. The Roles of Dimerization and Membrane Anchoring in Activity of Glycopeptide Antibiotics against Vancomycin-Resistant Bacteria. *J. Am. Chem. Soc.* **1997**, *119*, 12041–12047.

37 Cooper, M. A.; Williams, D. H. Binding of glycopeptide antibiotics to a model of a vancomycin-resistant bacterium. *Chem. Biol.* **1999**, *6*, 891–899.

38 Ge, M.; Chen, Z.; Onishi, H. R.; Kohler, J.; Silver, L. L.; Kerns, R.; Fukuzawa, S.; Thompson, C.; Kahne, D. Vancomycin Derivatives That Inhibit Peptidoglycan Biosynthesis Without Binding d-Ala-d-Ala. *Science* **1999**, *284*, 507–511.

39 Kahne, D.; Leimkuhler, C.; Lu, W.; Walsh, C. Glycopeptide and Lipoglycopeptide Antibiotics. *Chem. Rev.* **2005**, *105*, 425–448.

Supporting Information

Table of contents

Supplemental Figures and Table

Table S4.1. MIC values of teixobactin analogues in µg/mL.

	Staphylococcus aureus ATCC 29213	*Staphylococcus epidermidis* ATCC 14990	*Bacillus subtilis* ATCC 6051	*Escherichia coli* ATCC 10798
Lys_{10}-teixobactin (**2**)[a]	1	0.5	1	>32
N-Me-D-Phe^{I}_{1},*N*-Me-D-Gln_4,Lys_{10}-teixobactin (**3**)[a]	16	16	8	>32

[a] Trifluoroacetic acid (TFA) salts.

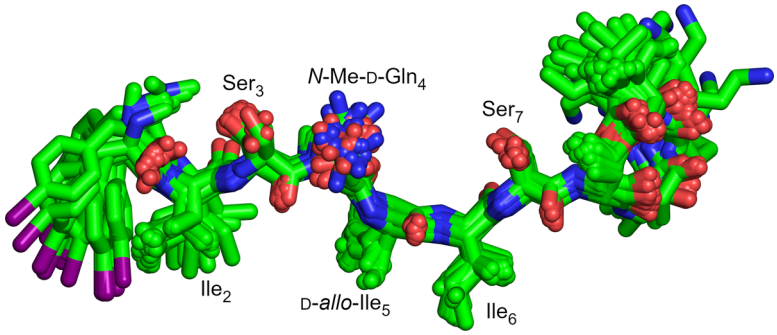

Figure S4.1. Overlay of the 32 crystallographically independent molecules of *N*-Me-D-Phe^{I}_{1},*N*-Me-D-Gln_4,Lys_{10}-teixobactin (**3**).

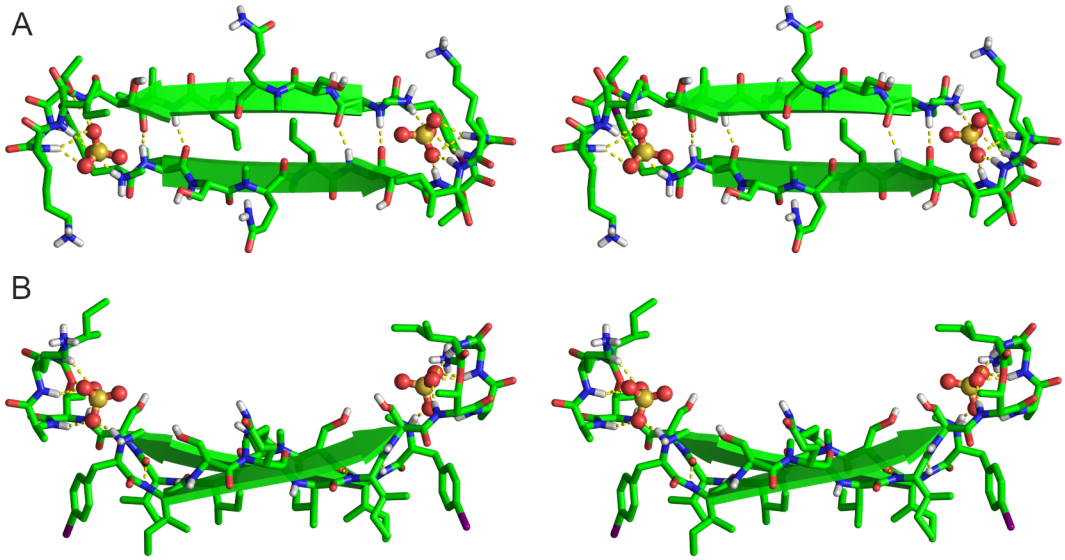

Figure S4.2. Wall-eye stereo view of the X-ray crystallographic structure of a representative dimer of *N*-Me-D-Phe^{I}_{1},*N*-Me-D-Gln_4,Lys_{10}-teixobactin (**3**). (A) Top view. (B) Side view.

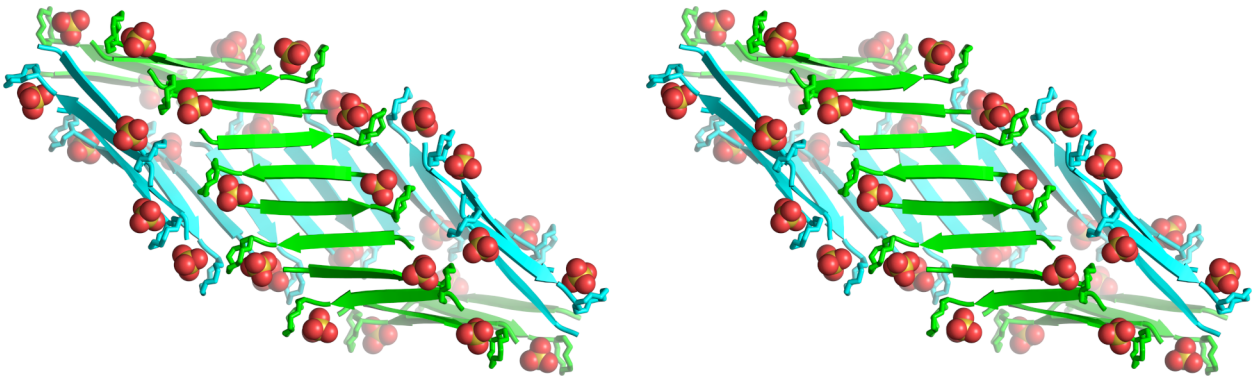

Figure S4.3. Wall-eye stereo view of the double helix of β-sheet fibrils formed by *N*-Me-D-Phe$^{I}_{1}$,*N*-Me-D-Gln$_4$,Lys$_{10}$-teixobactin (**3**). Sulfate anions are shown as spheres.

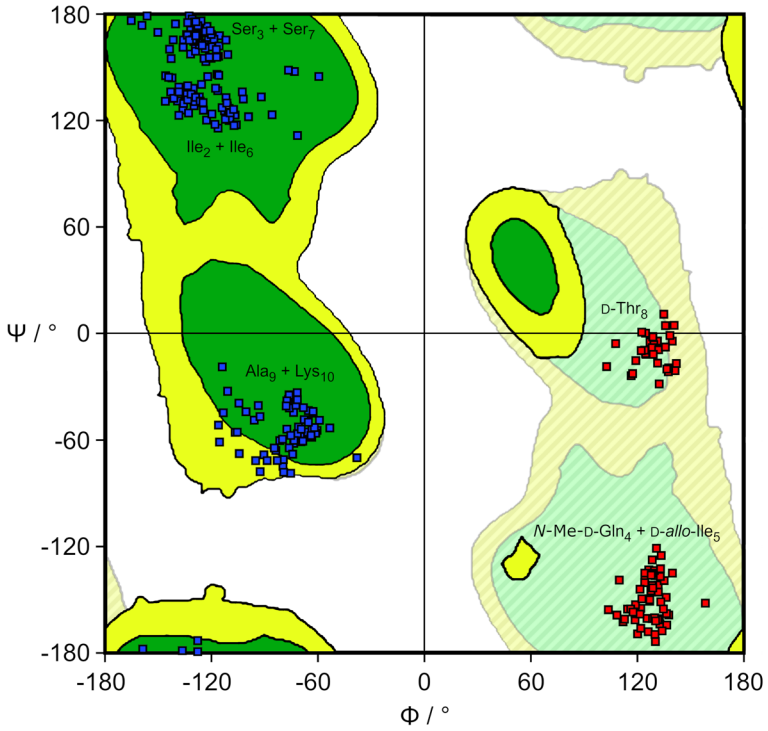

Figure S4.4. Ramachandran plot illustrating the ϕ and φ angles of residues 2–10 of the 32 independent molecules of *N*-Me-D-Phe$^{I}_{1}$,*N*-Me-D-Gln$_4$,Lys$_{10}$-teixobactin (**3**). The dark green regions correspond to preferred dihedral angles for L-peptides and proteins; the yellow-green regions correspond to allowed regions for L-peptides and proteins; the pale green and yellow regions correspond to preferred and allowed dihedral angles for D-peptides and proteins.

Materials and Methods

General information

Methylene chloride (CH_2Cl_2) was passed through alumina under argon prior to use. Amine-free *N*,*N*-dimethylformamide (DMF) was purchased from Alfa Aesar. Fmoc-D-*allo*-Ile-OH was purchased from Santa Cruz Biotechnology. Fmoc-*N*-Me-D-Gln(Trt)-OH was purchased from Alabiochem Tech. Other protected amino acids were purchased from CHEM-IMPEX. Preparative reverse-phase HPLC was performed on a Rainin Dynamax instrument equipped with an Agilent Zorbax SB-C18 column. Analytical reverse-phase HPLC was performed on an Agilent 1260 Infinity II instrument equipped with a Phenomonex Aeris PEPTIDE 2.6μ XB-C18 column. HPLC grade acetonitrile (MeCN) and deionized water (18 MΩ) containing 0.1% trifluoroacetic acid (TFA) were used as solvents for both preparative and analytical reverse-phase HPLC. Deionized water (18 MΩ) was obtained from a Barnstead NANOpure Diamond water purification system. Teixobactin analogues **2** and **3** were prepared and studied as the trifluoroacetate salts.

Synthesis of Lys_{10}-teixobactin (2) and *N*-Me-D-Phe^{I}_1,*N*-Me-D-Gln_4,Lys_{10}-teixobactin (3)

Lys_{10}-teixobactin (**2**) and *N*-Me-D-Phe^{I}_1,*N*-Me-D-Gln_4,Lys_{10}-teixobactin (**3**) were synthesized as the trifluoroacetate salts using procedures we have previously reported.[1] Dry DMF was used instead of a mixture of MeCN/THF/CH_2Cl_2 for the cyclization step. In the synthesis of *N*-Me-D-Phe^{I}_1,*N*-Me-D-Gln_4,Lys_{10}-teixobactin (**3**), Boc-*N*-Me-D-Phe^{I}_1-OH was used instead of Boc-*N*-Me-D-Phe_1-OH. Coupling of Fmoc-Ser_3(tBu)-OH after *N*-Me-D-Gln_4 was performed using 4 equiv Fmoc-Ser_3(tBu)-OH with coupling reagent HATU (4 equiv), HOAt (4 equiv) in 20% (v/v) collidine in dry DMF (5 mL) for 12 h.

Minimum inhibitory concentration (MIC) assay of teixobactin analogues

MIC assays of teixobactin analogues **2** and **3** were performed using procedures we have previously reported.[1]

Solubility assay

Solubility assays of teixobactin analogues **2** and **3** were performed using procedures we have previously reported.[2]

Thioflavin T (ThT) fluorescence assay

Preparation of buffered ThT solution. The ThT solution was freshly prepared before use. A solution of 20 μM ThT was prepared in a 1x PBS buffer at pH 7.4 (5 mL). The solution was filtered through a 0.2-micron syringe filter. The concentration of ThT in the solution was determined using a UV-vis spectrophotometer (ε = 36000 M-1 cm-1 at 412 nm) and adjusted to 20 μM.

ThT fluorescence assay. ThT fluorescence assays were conducted in 96-well plates (96 Well Optical Bottom Black, Polymer base, NUNC, Rochester, NY, USA). A 200-μL aliquot of ThT solution in PBS (above) was transferred to each of four wells of 96-well plate. A 1.73-μL aliquot of a 20 mg/mL solution of Lys_{10}-teixobactin in DMSO was added to each well to give 119 uM Lys_{10}-teixobactin and 20 μM ThT in PBS. The 96-well plate was sealed with adhesive plate sealers. The plate was immediately inserted into a Varioskan LUX multimode microplate reader (Thermo Fisher Scientific) and incubated at 37°C while shaking (1200 rpm, high shaking force) and monitoring fluorescence (444 nm excitation, 480 nm emission, 12 nm slit width) every 20 min over 5 days using the bottom-read mode.

Transmission electron microscopy (TEM) imaging

Sample preparation. Lys_{10}-teixobactin in DMSO (10 mg/mL concentration) was diluted to 100 μM with PBS buffer at pH 7.4. The solution was incubated at 37 ºC over 72 h with shaking. A TEM grid (Formvar/carbon film on 400 mesh copper) was treated by glow discharge using a Leica EM ACE200 vacuum coater (Leica Microsystems, Buffalo Grove, IL, USA). A 5-μL aliquot of the Lys_{10}-teixobactin solution was applied to the TEM grid. After 15 sec, the solution was wicked away with filter paper and the grid was immediately washed with two 200-μL aliquots of distilled H_2O. The distilled H_2O was wicked away with filter paper and the grid was immediately stained with 2% uranyl acetate in H_2O (5 μL) for 15 sec. The remaining solution was wicked away from the grid with filter paper.

TEM Imaging. TEM images of Lys_{10}-teixobactin were taken with a JEM-2100F transmission electron microscope (JEOL, Peabody, MA, USA) at 200 kV with an electron dose of approximately 15 e^-/A^2. The microscope was equipped with Gatan K2 Summit direct electron detector (Gatan, Pleasanton, CA, USA) at 15,000x or 25,000x magnification. The sample was cooled at liquid nitrogen temperature through the cryostage. Contrast and brightness of the images were adjusted as appropriate.

Crystallization of *N*-Me-D-Phe$^{I}_{1}$,*N*-Me-D-Gln$_4$,Lys$_{10}$-teixobactin (3)

N-Me-D-Phe$^{I}_{1}$,*N*-Me-D-Gln$_4$,Lys$_{10}$-teixobactin (**3**) was dissolved in 0.2 micron syringe filtered NANOpure H_2O (10 mg/mL). Crystallization conditions were screened by screening in a 96-well plate format using three crystallization kits from Hampton Research (PEG/Ion, Index, and Crystal Screen). Each well was loaded with 100 µL of a different mother liquor solution from the kits. The hanging drops were set up using a TTP Labtech Mosquito® liquid handling instrument. Hanging drops were made by combining an appropriate volume of teixobactin analogue **3** with an appropriate volume of well solution to create three 150-nL hanging drops with 1:1, 1:2, and 2:1 peptide:well solution. Rectangular rod-shaped crystals grew in all conditions that contained sulfate salts (Li_2SO_4, $MgSO_4$, Na_2SO_4, K_2SO_4, $(NH_4)_2SO_4$) and polyethylene glycol (PEG) 3,350.

Crystal growth was optimized using conditions containing Na_2SO_4. In the optimization, the Na_2SO_4 and PEG 3,350 concentrations were varied across the 4x6 matrix of a Hampton VDX 24-well plate to afford crystals suitable for X-ray diffraction. The hanging drops for these optimizations were prepared on glass slides by combining 1 or 2 µL of teixobactin solution with 1 or 2 µL of well solution in ratios of 1:1, 2:1, and 1:2. Crystals that formed were checked for diffraction using a Rigaku Micromax-007 HF diffractometer with a Cu anode at 1.54 Å. Through these optimization studies the following conditions were selected: 0.19 M Na_2SO_4 and 15% PEG 3,350.[*] No cryoprotectant was used other than the PEG 3,350 already present in the drop.

[*] These conditions afforded multiple crystals that diffracted to 3 or 4 Å, but only one crystal that diffracted to 2 Å. All of the crystals had comparable unit cell dimensions, but the crystal for which the dataset (below) was collected gave the best diffraction data. After collecting data needed to obtain anomalous signal at 6 keV, the crystal had degraded to a point where it was no longer possible to collect adequate data at higher energy (ca. 12 keV).

X-ray crystallographic data collection, data processing, and structure determination

Data collection was performed with the Blu-Ice software[3] at Stanford Synchrotron Radiation Lightsource using BL 9-2 beamline at a wavelength of 2.06633 Å. The rotation method was employed and four sets of 360 images each were collected at a 0.5º rotation interval (a total of two complete rotations). The four sets were processed separately with XDS[4], and the resulting datasets were merged with BLEND[5]. The structure was solved with SAD phasing implemented in the Hybrid Substructure Search (HySS)[6] module of the Phenix suite[7]. Iodine atoms of the *N*-Me-D-Phe$^{I}_{1}$ residues were used as sources of the anomalous signal. The initial electron density maps were generated using the substructure coordinates as initial positions in Autosol[8]. The structure was then refined with REFMAC5[9] under CCP4[10] using Coot[11] for model building. All B-factors were refined isotropically and riding hydrogen atoms coordinates were generated geometrically. The bond length, angles, and torsions restraints for unnatural amino acids (*N*-Me-D-Phe^{I}, *N*-Me-D-Gln, and D-*allo*-Ile) were generated with AceDRG[12] under CCP4.

Table S4.2. Crystallographic properties, crystallization conditions, data collection, and model refinement statistics for teixobactin analogue **3**

	Teixobactin analogue **3**
PDB ID	6E00
space group	$P2_12_12_1$
a, b, c (Å)	47.5, 69.4, 115.4
α, β, γ (˚)	90, 90, 90
peptides per asymmetric unit	32
crystallization conditions	0.19 M Na_2SO_4, 15% PEG 3,350
Data collection	
wavelength (Å)	2.06633
resolution (Å)	39.21 - 2.20 (2.279 - 2.200)
total reflections	479611 (24317)
unique reflections	17797 (1370)
Multiplicity	21.20 (15.1)
completeness (%)	93.36 (67.87)
mean I/σ	8.8 (1.48)
R_{merge}	0.339 (1.314)
$R_{measure}$	0.348 (1.36)
$CC_{1/2}$	0.991 (0.467)
CC*	0.998 (0.798)
Refinement	
R_{work}	0.211 (0.216)
R_{free}	0.246 (0.294)
number of non-hydrogen atoms per ASU	3037
RMS_{bonds}	0.011
RMS_{angles}	1.880
Ramachandran favored (%)	100
Ramachandran outliers (%)	0
clashscore	6
average B-factor	20.2

Synthesis of Boc-*N*-Me-D-Phe^{I}-OH from D-phenylalanine (D-Phe-OH)

Boc-*N*-Me-D-Phe^{I}-OH was synthesized from D-Phe-OH in the following steps: first to Boc-D-Phe^{I}-OH following Richardson et al. *J. Org. Chem.* **2018**, *83*, 4525-4536 and then to Boc-*N*-Me-D-Phe^{I}-OH following Malkov et al. *Tetrahedron* **2006**, *62*, 264-284.[13,14] The yields were not optimized as the products were synthesized and used from the first batch of synthesis.

D-Phe^{I}-OH.[13] D-Phenylalanine (3.0 g, 18.2 mmol), $NaIO_3$ (0.82 g, 7.26 mmol), and I_2 (1.84 g, 7.26 mmol) were dissolved in a mixture of 18.2 mL glacial acetic acid and 2.18 mL concentrated H_2SO_4. The mixture was heated to 70 °C and stirred under nitrogen for 24 h. $NaIO_4$ (116.6 mg, 0.544 mmol) was added and the mixture was heated to 70 °C with stirring under nitrogen for 24 h. The mixture was concentrated by rotary evaporator to ca. 15 mL. The residue was dissolved with H_2O (50 mL) and transferred to a separatory funnel. The mixture was washed with Et_2O (2 x 50 mL) and then with CH_2Cl_2 (50 mL). The aqueous phase was transferred to an Erlenmeyer flask and cooled to 0 °C on an ice bath. The pH was adjusted to 7.0 by slowly adding 5 M aq KOH with stirring (ca. 25 mL of 5 M aq KOH was used). A white solid precipitated and was isolated by filtration with a Büchner funnel. The solid was transferred to an Erlenmeyer flask and dissolved in 50% EtOH solution (20 mL). The mixture was heated to 85 °C in an oil bath. 20-mL aliquots of boiling 50% EtOH were added repeatedly until a clear yellow solution was obtained. (ca. 125 mL of boiling 50% EtOH was used). The hot solution was filtered through glass wool and was left for 12 h at room temperature to achieve crystallization. The resulting crystals were collected by Büchner funnel filtration and was washed with 50 mL of ice cold 50% EtOH solution. The solid was placed under vacuum (≤ 100 mTorr) to remove any residual solvents. The yield of D-Phe^{I}-OH was 1.98 g (38% yield).

Boc-D-Phe^{I}-OH.[13] D-Phe^{I}-OH (2.0 g, 6.9 mmol) and Boc_2O (2.4g, 11.0 mmol) were dissolved in a mixture of MeOH (3.5 mL), H_2O (3.5 mL), and Et_3N (2.4 mL). The mixture was heated to 55 °C under nitrogen with stirring for 16 h. The mixture was concentrated by rotary evaporator and the resulting residue was dried under vacuum (≤ 100 mTorr). The residue was dissolved in EtOAc (30 mL) and cooled to 0 °C on an ice bath. The mixture was added to a separatory funnel containing 250 mM aq HCl (50 mL) and shaken vigorously for 15 s. The organic phase was collected, and the pH of the aqueous phase was adjusted to pH 1 with 1 M aq HCl. The aqueous phase was extracted with EtOAc (2 x 20 mL) and then organic phases were combined, washed with 250 mM aq HCl in saturated aqueous NaCl solution (30 mL), dried with $MgSO_4$, then filtered through Celite. The filtrate was evaporated by rotary evaporator and the residue was dried under vacuum (≤ 100 mTorr) to give a white foam. The product was recrystallized by suspending in 30 mL of hot hexane with stirring and adding hot Et_2O in 2-mL aliquots until a clear yellow solution was obtained (ca. 60 mL Et_2O added). The solution was transferred to a beaker and boiled until the volume read ca. 30 mL. The product was crystallized by cooling the solution on an ice bath and isolated by filtration using a Büchner funnel. The crystals were washed with cold hexane. The yield of Boc-D-Phe^{I}-OH was 1.71 g (65% yield).

Boc-N-Me-D-Phe^{I}-OH.[14] Boc-D-Phe^{I}-OH (1.71 g, 4.4 mmol) and MeI (2.74 mL, 44 mmol) were dissolved in THF (20 mL) at 0 °C and then NaH (60% dispersion in mineral oil, 1.76 g in oil, 44 mmol) was slowly added. The mixture was stirred at room temperature for 24 h under nitrogen. The mixture was quenched with H_2O (15 mL) and EtOAc (10 mL) was added. The solvents were evaporated by rotary evaporator and the residue was dried under vacuum (≤ 100 mTorr). The residue was dissolved in H_2O (300 mL) and transferred to a separatory funnel. The solution was washed with EtOAc (150 mL) and the aqueous solution was collected and

acidified to pH 3.5 with 5% citric acid. The suspension was extracted with EtOAc (200 mL) and the organic phase was washed with saturated aq NaCl (50 mL), H_2O (50 mL), and then dried with $MgSO_4$, and filtered through a Büchner funnel filtration. The resulting solution was evaporated by rotary evaporator and the residue was dried placed under vacuum (≤ 100 mTorr) to yield 0.78 g of Boc-*N*-Me-D-Phe^{I}-OH (44% yield). MS (negative ion mode) calcd for $C_{15}H_{19}INO_4^-$ $[M - H]^-$ m/z 404.04, found 404.88. Boc-*N*-Me-D-Phe^{I}-OH was used for solid-phase peptide synthesis without further purification.

Figure S4.7. ^{1}H NMR of Boc-N-Me-D-Phe^{I}-OH.

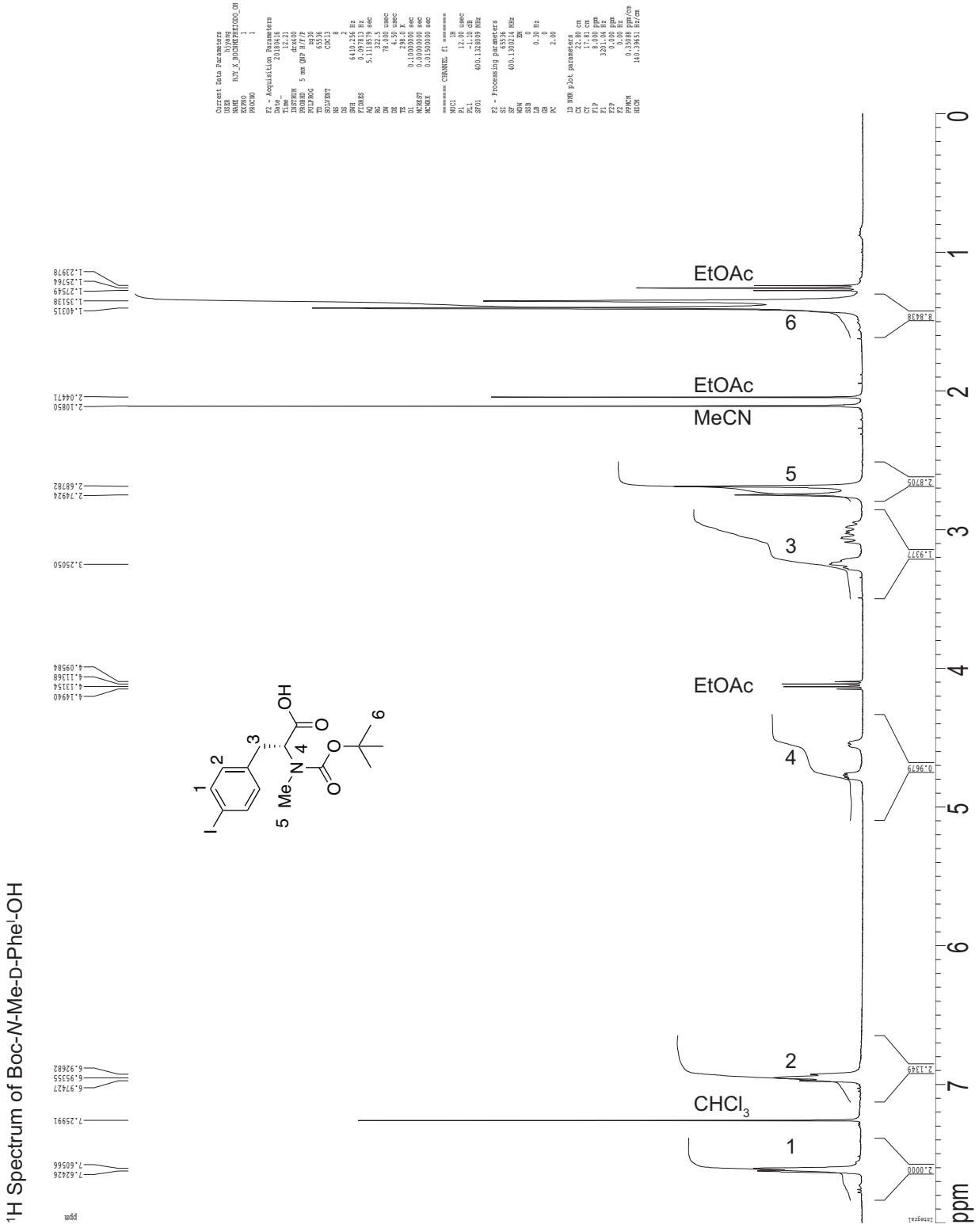

^{1}H Spectrum of Boc-*N*-Me-D-Phe^{I}-OH

HPLC trace and mass spectrum of *N*-Me-D-Phe$^{I}_{1}$,*N*-Me-D-Gln$_4$,Lys$_{10}$-teixobactin (**3**)

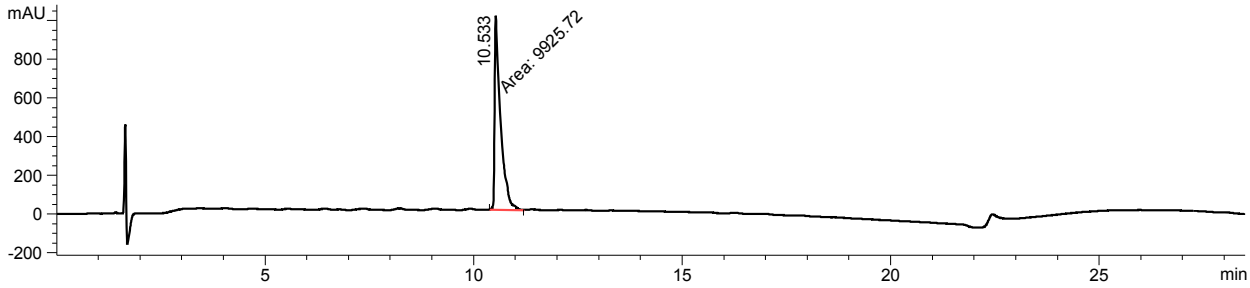


```
=====================================================================
                        Area Percent Report
=====================================================================

Sorted By             :      Signal
Signal 1: MWD1 A, Sig=214,4 Ref=off
Inj Volume : 20.000 µl

Peak RetTime Type  Width     Area      Height     Area
  #   [min]        [min]   [mAU*s]     [mAU]       %
----|-------|----|-------|----------|----------|--------|
   1  10.533 MM    0.1644 9925.71680 1006.51044 100.0000

Totals :                  9925.71680 1006.51044
```

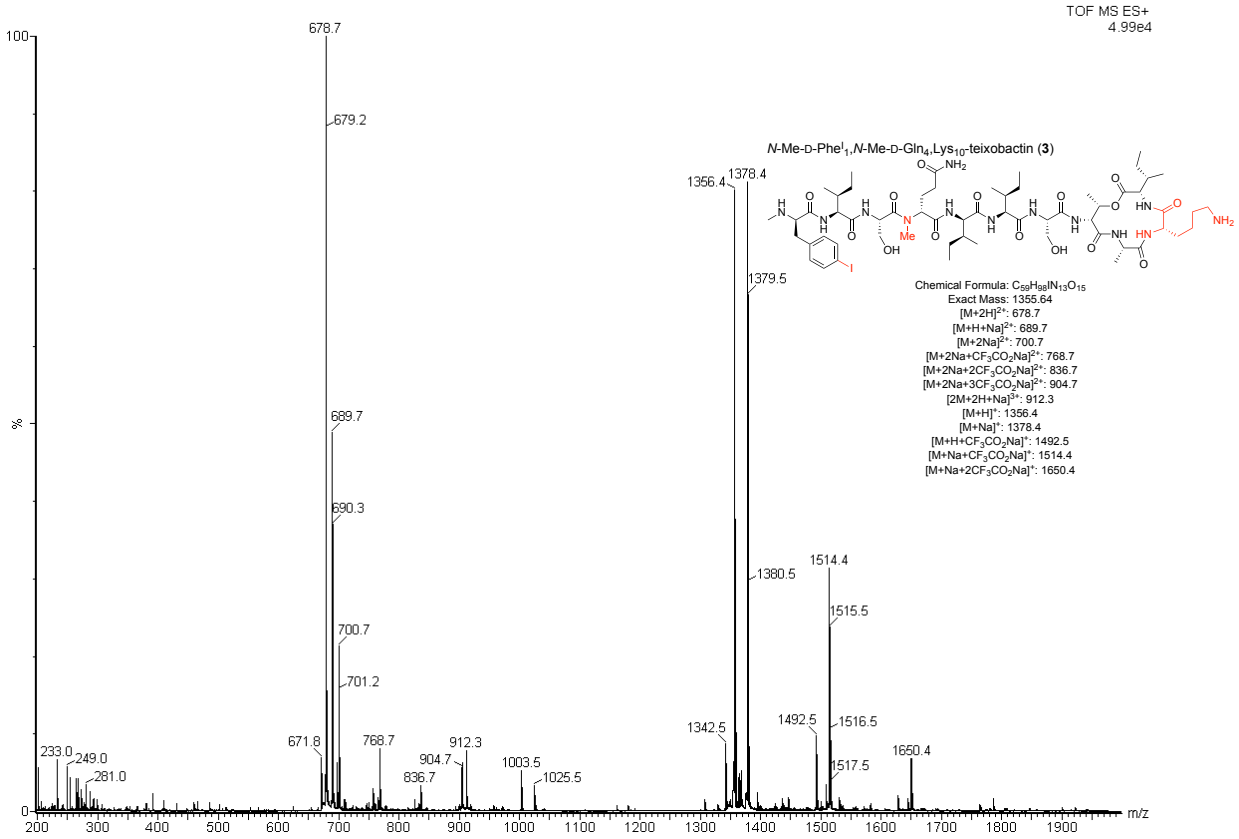

References and Notes

1 Yang, H.; Chen, K. H.; Nowick, J. S. *ACS Chem. Biol.* **2016**, *11*, 1823-1826.

2 Chen, K. H.; Le, S. P.; Han, X.; Frais, J. M.; Nowick, J. S. *Chem. Commun.* **2017**, *53*, 11357–11359.

3 McPhillips, T. M.; McPhillips, S. E.; Chiu, H. J.; Cohen, A. E.; Deacon, A. M.; Ellis, P. J.; Garman, E.; Gonzalez, A.; Sauter, N. K.; Phizackerley, R. P.; Soltis, S. M.; Kuhn, P. J. Synchrotron Rad. **2002**, *9*, 401–406.

4 Kabsch, W. Acta *Crystallogr., Sect. D: Biol. Crystallogr.* **2010**, *66*, 125–132.

5 Foadi, J.; Aller, P.; Alguel, Y.; Cameron, A.; Axford, D.; Owen, R. L.; Armour, W.; Waterman, D. G.; Iwata, S.; Evans, G. *Acta Crystallogr., Sect. D: Biol. Crystallogr.* **2013**, *69*, 1617–1632.

6 Grosse-Kunstleve, R. W.; Adams, P. D. *Acta Crystallogr., Sect. D: Biol. Crystallogr.* **2003**, *59*, 1966–1973.

7 Adams, P. D.; Afonine, P. V.; Bunkoczi, G.; Chen, V. B.; Davis, I. W.; Echols, N.; Headd, J. J.; Hung, L. W.; Kapral, G. J.; Grosse-Kunstleve, R. W.; McCoy, A. J.; Moriarty, N. W.; Oeffner, R.; Read, R. J.; Richardson, D. C.; Richardson, J. S.; Terwilliger, T. C.; Zwart, P. H. *Acta Crystallogr., Sect. D: Biol. Crystallogr.* **2010**, *66*, 213–221.

8 Terwilliger, T. C.; Adams, P. D.; Read, R. J.; McCoy, A. J.; Moriarty, N. W.; Grosse-Kunstleve, R. W.; Afonine, P. V.; Zwart, P. H.; Hung L. W. *Acta Crystallogr., Sect. D: Biol. Crystallogr.* **2009**, *65*, 582–601.

9 Murshudov, G. N.; Vagin, A. A.; Dodson, E. J. *Acta Crystallogr., Sect. D: Biol Crystallogr.* **1997**, *53*, 240–255.

10 Winn, M. D.; Ballard, C. C.; Cowtan, K. D.; Dodson, E. J.; Emsley, P.; Evans, P. R.; Keegan, R. M.; Krissinel, E. B.; Leslie, A. G. W.; McCoy, A.; McNicholas, S. J.; Murshudov, G. N.; Pannu, N. S.; Potterton, E. A.; Powell, H. R.; Read, R. J.; Vagin, A.; Wilson, K. S. *Acta Crystallogr., Sect. D: Biol Crystallogr.* **2011**, *67*, 235–242.

11 Emsley, P.; Lohkamp, B.; Scott, W. G.; Cowtan, K. *Acta Crystallogr., Sect. D: Biol. Crystallogr.* **2010**, *66*, 486–501.

12 Long, F.; Nicholls, R. A.; Emsley, P.; Gražulis, S.; Merkys, A.; Vaitkus, A.; Murshudov, G. N. *Acta Crystallogr., Sect. D: Biol. Crystallogr.* **2017**, *73*, 112–122.

13 Richardson, M. B.; Brown, D. B.; Vasquez, C. A.; Ziller, J. W.; Johnston, K. M.; Weiss, G. A. *J. Org. Chem.* **2018**, *83*, 4525-4536.

14 Malkov, A. V.; Stončius, S.; MacDougall, K, N.; Mariani, A.; McGeoch, G. D.; Kočovský, P. *Tetrahedron* **2006**, *62*, 264-284.

Chapter 5
Design, Synthesis, and Study of Lactam and Ring-Expanded Analogues of Teixobactin

Introduction

Teixobactin is a new class of peptide antibiotic against Gram-positive bacteria that inhibits cell-wall formation, interrupting both the synthesis of peptidoglycan and the synthesis of teichoic acid, and ultimately causing bacterial cell lysis.[1,2] Teixobactin is thought to bind the highly conserved prenyl-pyrophosphate-saccharide regions of lipid II and related membrane-bound cell-wall precursors, and thus precluding the development of antibiotic resistance.[3] Furthermore, these targets are extracellular and represent the bottleneck of peptidoglycan synthesis. Teixobactin exhibits remarkable antibiotic activity against all important Gram-positive pathogens including methicillin-resistant *Staphylococcus aureus* (MRSA), drug-resistant *Streptococcus pneumonia*, and vancomycin-resistant *Enterococci* (VRE).

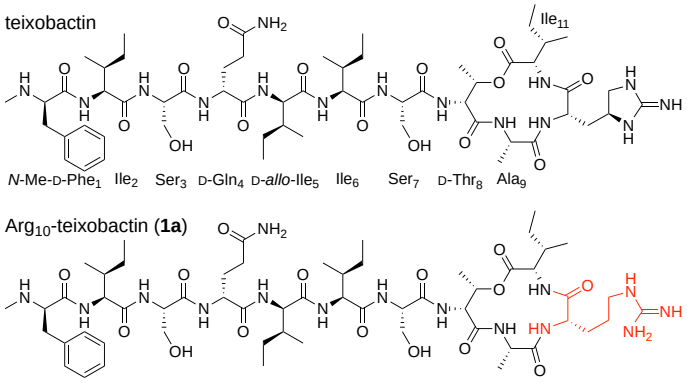

Teixobactin is a non-ribosomal undecapeptide containing a linear tail (residues 1–7) and a macrocyclic ring (residues 8–11). It contains four D-amino acids at positions 1, 4, 5, and 8, namely *N*-Me-D-Phe$_1$, D-Gln$_4$, D-*allo*-Ile$_5$, and D-Thr$_8$, and seven L-amino acids at positions 2, 3,

6, 7, 9, 10, and 11. The tail represents a unique pattern of D-L-L-D-D-L-L of stereochemistry with a hydrophobic–hydrophobic–hydrophilic–hydrophilic–hydrophobic–hydrophobic–hydrophilic pattern of side chains. The macrocyclic ring is composed of D-Thr_8–Ala_9–*allo*-End_{10}–Ile_{11} in which the *C*-terminal Ile_{11} and the hydroxy group of D-Thr_8 form an ester bond to close the 13-membered ring. Residue 10 is the rare amino acid *allo*-enduracididine (*allo*-End_{10}), a cyclic arginine analogue.[4]

We recently reported the X-ray crystallographic structure of a teixobactin analogue.[5] The analogue forms hydrogen-bonded antiparallel β-sheet dimers that bind sulfate anions (**Figure 5.1A**). In the X-ray crystallographic structure, the three NH groups of the macrolactone ring form three hydrogen bonds to each sulfate anion (**Figure 5.1B**). The lactone ring oxygen points toward the bound anion but is unable to form a hydrogen bond. The *N*-terminal ammonium group of the second monomer subunit of the dimer also hydrogen bonds to the sulfate anion. The dimers further assemble to form a double-helix of β-sheet fibrils. The binding of the sulfate anions suggests how teixobactin might bind to the anionic pyrophosphate group of lipid II and related cell-wall precursors, and thus inhibit cell wall biosynthesis.[5,6]

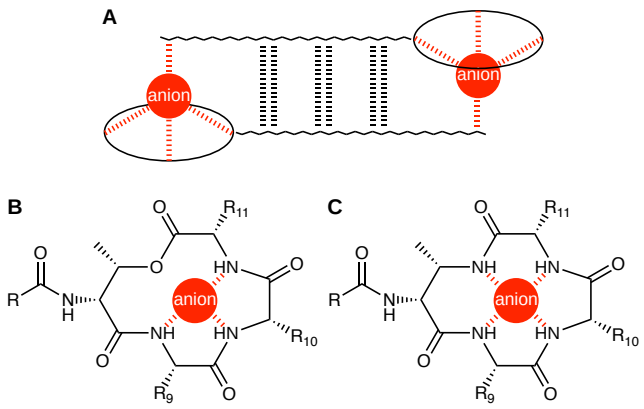

Figure 5.1. Proposed working model for mechanism of action of teixobactin (A). Coordination of an anion by the teixobactin macrolactone ring (B). Hypothesized coordination of an anion by an azateixobactin macrolactam ring (C).

The current paper begins by exploring the hypothesis that replacement of the lactone ring oxygen with an NH group will allow the resulting macrolactam ring to better bind anions by forming an additional hydrogen bond to the bound anion (**Figure 5.1C**).[7] We report a synthesis of macrolactam derivatives of teixobactin that contain D-aza-threonine at position 8 and find that a lactam derivative of teixobactin is 4-8 times more active as the corresponding lactone. We then explore whether the 13-membered macrocyclic ring composed of residues 8–11 is optimal for binding pyrophosphate group by expanding the ring with β-homo amino acids and find that teixobactin pharmacophore tolerates ring expansion of 14-, 15-, and 16-membered rings with retention of activity. Through these studies we further elucidate the role of macrocyclic ring in the teixobactin pharmacophore.

Results and Discussion

Solid-Phase Syntheses of Lactam Teixobactin Analogues Containing Aza-Threonine at Position 8. We had previously reported a synthetic route to teixobactin homologues through solid-phase peptide synthesis (SPPS) on 2-chlorotrityl resin followed by solution-phase

macrolactamization.[8] In this route, D-Thr$_8$ is introduced without a protecting group at the hydroxy position. Because D-aza-threonine is not commercially available in a suitably protected form, we envisioned adapting this route by incorporating D-*allo*-Thr at position 8 and converting it to D-aza-threonine on the solid support by an S$_N$2 displacement reaction.

We tested this approach using the tripeptide Boc-Ala-D-*allo*-Thr-Gln(Trt) on 2-chlorotrityl resin and found that conversion of the D-*allo*-Thr residue to the mesylate and then to the azide proceeded with elimination to form the corresponding dehydropeptide (**Scheme 5.1**). We hypothesized that the elimination reaction could be avoided by introducing the azide group before elongating the peptide chain (**Scheme 5.1**). Because Fmoc protecting group is labile to azide, we first converted the Fmoc group on D-*allo*-Thr to an Alloc protecting group on resin to give Alloc-D-*allo*-Thr-Gln(Trt) dipeptide on resin. This dipeptide could be converted to the mesylate and then to Alloc-D-azido-Thr-Gln(Trt) on resin by treating with triethylamine and mesyl chloride in dichloromethane, followed sodium azide in a mixture of 15-crown-5 and DMF. Alloc deprotection with Pd(Ph$_3$)$_4$ and phenylsilane liberated the α-amino group of D-azido-threonine for subsequent SPPS. This sequence of steps proceeded cleanly, and afforded the tripeptide Boc-Ala-D-azido-Thr-Gln(Trt)-OH in greater than 90% conversion by HPLC analysis.

\

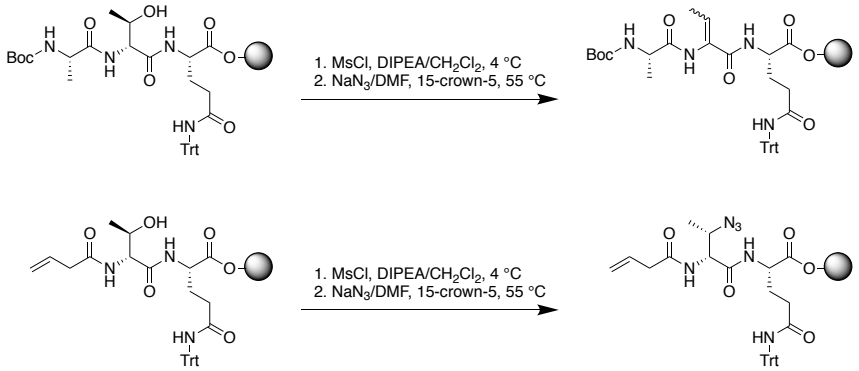

Scheme 5.1. Model system to study the D-aza-threonine synthesis on solid-support.

Reduction of the azide group of the resin bound Boc-Ala-D-azido-Thr-Gln(Trt) to an amino group proved challenging. Treatment with stannous chloride ($SnCl_2$, PhSH, DIPEA)[9] resulted approximately 60% conversion after four treatments of reducing cocktail; Staudinger reduction (Ph_3P and H_2O/THF)[10] stalled at the imino-phosphorane intermediate, and no hydrolysis to the amine was observed even at high temperatures (50 °C) in various mixtures of solvents. Saneyoshi *et al.* reported a derivative of triphenylphosphine, triphenylphosphine-2-carboxamide (Ph_2P-*o*-$C_6H_4CONH_2$), in which a phenyl ring of triphenylphosphine contains an ortho-carboxamide group to facilitate the hydrolysis of the imino-phosphorane intermediate by providing anchimeric assistance.[11] When we used triphenylphosphine-2-carboxamide in our model system, we observed good conversion from the azido group to the amino group.

We applied the conditions that we developed to the synthesis of D-aza-Thr_8,Arg_{10}-teixobactin (**2a**). The synthesis began by attaching Fmoc-Ala-OH to 2-chlorotrityl resin. Fmoc-D-*allo*-Thr-OH was then introduced by standard Fmoc-based SPPS using HCTU as the coupling reagent. The Fmoc group was removed by treatment with 20% piperidine in DMF and the *N*-terminus was protected with allyl chloroformate. The hydroxy group on D-*allo*-Thr_8 was then converted to a mesyl group with methanesulfonyl chloride and to an azide group with sodium azide. The Alloc protecting group was removed with tetrakis(triphenylphosphine)palladium(0) and phenylsilane, and residues 7 through 1 were introduced by SPPS. The azide group on D-azido-Thr_8 was reduced to the corresponding amine with triphenylphosphine-2-carboxamide and H_2O. Residues 11 and 10 were then introduced by SPPS. Fmoc deprotection followed by cleavage from the resin with 20% hexafluoroisopropanol (HFIP) in CH_2Cl_2 afforded the protected acyclic precursor. Macrolactamization with HBTU and HOBt, followed by global deprotection with trifluoroacetic acid (TFA), RP-HPLC purification, and lyophilization, afforded

13.5 mg of D-aza-Thr$_8$,Arg$_{10}$-teixobactin (**2a**) with ≥95% purity, from a 0.15 mmol scale synthesis.

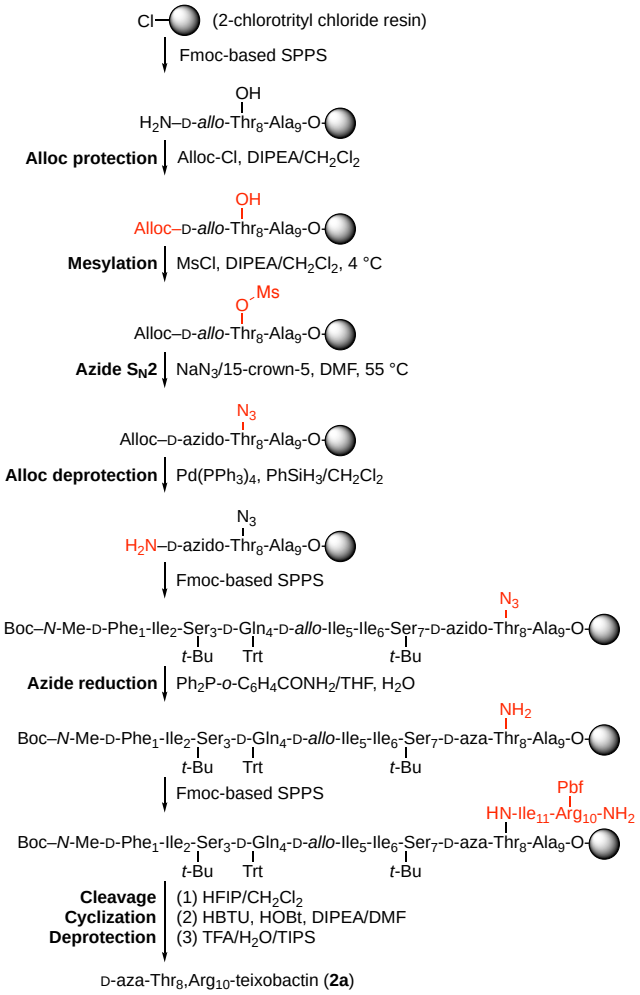

Scheme 5.2. Synthesis of aza-D-Thr$_8$,Arg$_{10}$-teixobactin (**2a**).

This synthetic route proved versatile and also allowed us to prepare the three diastereomeric analogues, aza-D-*allo*-Thr$_8$,Arg$_{10}$-teixobactin (**2b**), aza-L-Thr$_8$,Arg$_{10}$-teixobactin (**2c**), and aza-L-*allo*-Thr$_8$,Arg$_{10}$-teixobactin (**2d**). Replacing D-*allo*-threonine with D-threonine afforded aza-D-*allo*-threonine; replacing D-*allo*-threonine with L-*allo*-threonine afforded aza-L-

threonine, and replacing D-*allo*-threonine with L-threonine afforded aza-L-*allo*-threonine. The mesylation, azide SN2 displacement, and azide reduction reactions of the diastereomers all proceeded with similar conversion efficiencies and permitted the synthesis of teixobactin analogues containing all stereoisomers of aza-threonines, **2a–2d** (**Figure 5.2**). The purification of teixobactin analogues containing the L-aza-threonine stereoisomers (**2c** and **2d**) proved especially difficult, however, as the crude peptides after global deprotection formed gels in acetonitrile-water mixtures, thus limiting the amount of peptide that could be injected in preparative HPLC.

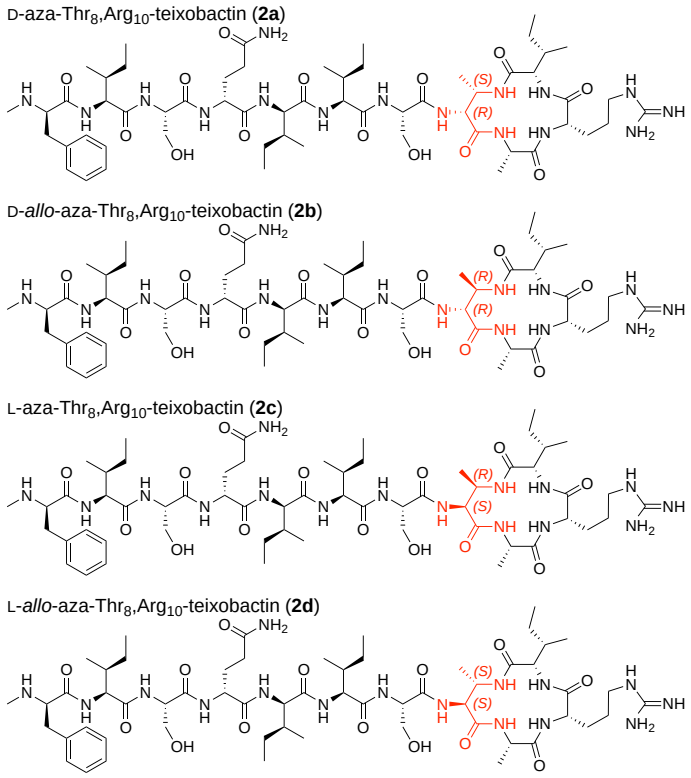

Figure 5.2. D-aza-Thr$_8$,Arg$_{10}$-teixobactin (2**a**), aza-D-*allo*-Thr$_8$,Arg$_{10}$-teixobactin (**2b**), aza-L-Thr$_8$,Arg$_{10}$-teixobactin (**2c**), and aza-L-*allo*-Thr$_8$,Arg$_{10}$-teixobactin (**2d**).

Minimum Inhibitory Concentration (MIC) Assay of Lactam Teixobactin Analogues. We assessed the antibiotic activity of D-aza-Thr$_8$,Arg$_{10}$-teixobactin (**2a**) and related stereoisomer

analogues (**2b–2d**) in minimum inhibitory concentration (MIC) assays against three Gram-positive bacteria (**Table 5.1**). We used the teixobactin and vancomycin as a positive control and the Gram-negative bacterium *E. coli* as a negative control. The MIC values of D-aza-Thr_8,Arg_{10}-teixobactin (**2a**) is 0.5-1 μg/mL across three Gram-positive bacteria, which is 2 times more potent than Arg_{10}-teixobactin (**1a**).[12,13,6] Teixobactin analogues containing other stereoisomers of aza-threonine (**2b–2d**) were inactive (MIC >32 μg/mL).

Table 5.1. MIC values of teixobactin and teixobactin analogues (μg/mL).

	Staphylococcus aureus ATCC 29213	*Staphylococcus epidermidis* ATCC 14990	*Bacillus subtilis* ATCC 6051	*Escherichia coli* ATCC 10798
Arg_{10}-teixobactin (**1a**)	2	1	2	>32
aza-D-Thr_8,Arg_{10}-teixobactin (**2a**)	1	0.5	1	>32
aza-D-*allo*-Thr_8,Arg_{10}-teixobactin (**2b**)		>32	>32	>32
aza-L-Thr_8,Arg_{10}-teixobactin (**2c**)		>32	>32	>32
aza-L-*allo*-Thr_8,Arg_{10}-teixobactin (**2d**)		>32	>32	>32
teixobactin	0.25	0.25	0.25-0.5	>32
vancomycin	0.25	0.25	0.5	>32

Effect of Polysorbate 80 on Antibiotic Activity. In the original report of teixobactin, the authors describe the use of the mild detergent polysorbate 80 at 0.002% concentration in their MIC assays.[1] Having always performed our MIC assays without polysorbate 80, we decided to investigate the effect of polysorbate 80 on the MIC values of azateixobactin analogue **2a**. When we performed the MIC assay with broth containing 0.002% polysorbate 80, the MIC values decreased from 0.5–1 μg/mL to 0.008–0.03 μg/mL, a dramatic 16–128-fold increase in activity (**Table 5.2**). We also observe a similar decrease in the MIC of teixobactin, from 0.25–0.5 μg/mL to < 0.008 μg/mL, the lowest concentration tested. In contrast, we observe only a modest two-fold decrease in the MIC of vancomycin.[14] We observe a similar but slightly smaller increase in

the activity of teixobactin analogue **1a** with 0.002% polysorbate 80. Thus, azateixobactin analogue **2a** proved 4–8 times more active than teixobactin analogue **1a** in the presence of 0.002% polysorbate 80.

Table 5.2. MIC values of teixobactin and teixobactin analogues (μg/mL) with 0.002% polysorbate 80.

	Staphylococcus aureus ATCC 29213	*Staphylococcus epidermidis* ATCC 14990	*Bacillus subtilis* ATCC 6051	*Escherichia coli* ATCC 10798
Arg_{10}-teixobactin (**1a**)	0.06	0.13	0.06	>8
aza-D-Thr_8,Arg_{10}-teixobactin (**2a**)	0.008	0.03	0.016	>8
teixobactin	<0.008	<0.008	<0.008	>8
vancomycin	0.125	0.25	0.25	>8

The authors of the original teixobactin report suggest that polysorbate 80 prevents the binding of the antibiotic to plastic surfaces.[15] We favor a different explanation, because of the modest effect of polysorbate 80 on the activity of vancomycin. Having observed that teixobactin and its analogues form gels and amyloid-like fibrils upon addition to buffer or culture media,[16,5] we believe that inclusion of polysorbate 80 in the broth helps solubilize the gels or inhibit fibril formation, and thus increases the bioavailability and activity of teixobactin and its analogues.

X-ray Crystallographic Structure of *N*-Me-D-Gln_4,D-aza-Thr_8,Arg_{10}-teixobactin (3a). To assess the effect of the additional amide NH group on the structure of azateixobactin analogues, we turned to X-ray crystallography. We had previously found that *N*-methylation of the peptide backbone of D-Gln_4 facilitated crystallization of a teixobactin analogue by attenuating its propensity to form a gel.[5] In the current study we utilized this finding and synthesized *N*-Me-D-Gln_4,D-aza-Thr_8,Arg_{10}-teixobactin (**3a**).[17]

N-Me-D-Gln$_4$,D-aza-Thr$_8$,Arg$_{10}$-teixobactin (**3a**)

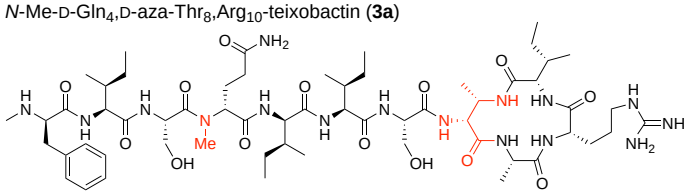

We screened *N*-Me-D-Gln$_4$,D-aza-Thr$_8$,Arg$_{10}$-teixobactin (**3a**) for crystallization in 864 conditions in a 96-well plate format using crystallization kits from Hampton Research (PEG/Ion, Index, and Crystal Screen). Hexagonal prism-shaped crystals grew in conditions containing polyethylene glycol (PEG) and chloride salts. With further optimization in a 24-well plate format, 0.16 M $CaCl_2$, 0.1 M HEPES Na pH 7.00, 24% PEG 400 afforded crystals suitable for X-ray diffraction. Three X-ray diffraction data sets were acquired at the Advanced Light Source (ALS) at a wavelength of 1.77 Å (7000 eV). The data sets were processed using XDS[18] and merged using BLEND.[19] The structure was solved by single-wavelength anomalous diffraction (SAD) phasing using the chloride anomalous signal. The structure was refined with PHENIX[20] in the $P3_221$ space group at 2.10 Å resolution. The asymmetric unit contains one *N*-Me-D-Gln$_4$,D-aza-Thr$_8$,Arg$_{10}$-teixobactin (**3a**) molecule, as well as one chloride anion and four ordered water molecules. We refined the *N*-methyl terminus (*N*-Me-D-Phe$_1$) as the free base, rather than as the methyl ammonium ion, to reflect that only a single chloride anion was identified in the asymmetric unit, thus balancing the positive charge of the arginine side chain. We found no electron density or voids in the lattice that could account for an additional anion.

The X-ray crystallographic structure reveals an amphipathic hydrogen-bonded antiparallel β-sheet dimer that bind chloride anions (**Figure 5.3**). Residues 1–7 form the dimerization interface and create an amphipathic antiparallel β-sheet containing both D and L residues. In the binding site of chloride anion, the macrolactam amide NH groups of residues 8,

10, and 11, as well as, the extra amide NH group of the lactam ring hydrogen bond to the chloride anion. The amide NH group of Ala$_9$ hydrogen bonds to the hydroxy group of Ser$_7$.[21]

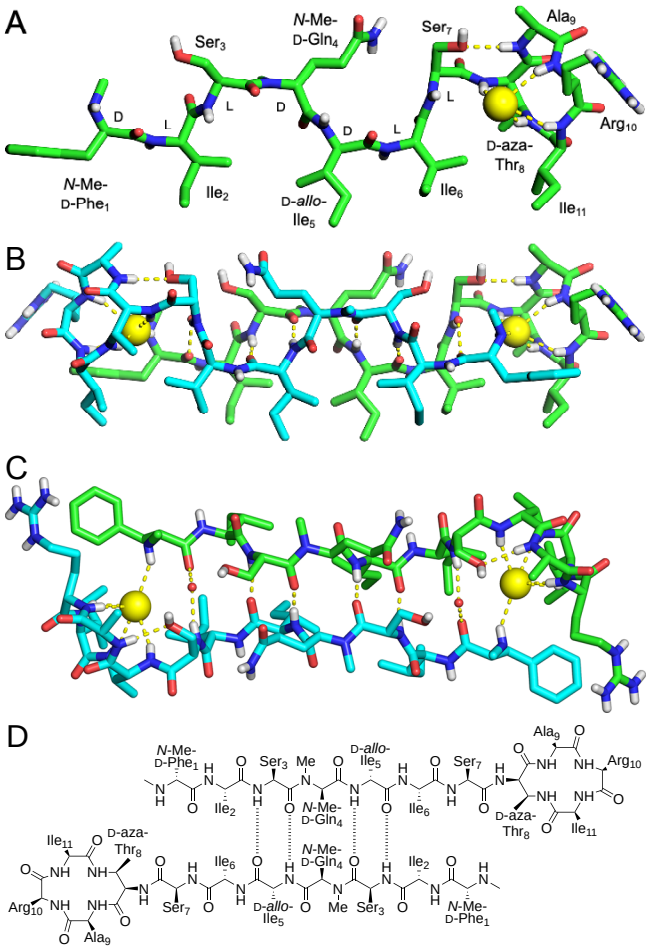

Figure 5.3. X-ray crystallographic structure of *N*-Me-D-Gln$_4$,D-aza-Thr$_8$,Arg$_{10}$-teixobactin (**3a**) binding chloride anion. (A) Monomer. (B and C) Dimer side and top views with two water molecules shown as non-bonded spheres. (D) Alignment of the dimer assembly. Four water molecules are omitted for visual clarity.

In the antiparallel β-sheet assembly, the sidechains of hydrophobic residues *N*-Me-D-Phe$_1$, Ile$_2$, D-*allo*-Ile$_5$, Ile$_6$, and Ile$_{11}$ as well as the β-methyl group of D-aza-Thr$_8$ make hydrophobic face, and the sidechains of hydrophilic residues Ser$_3$, *N*-Me-D-Gln$_4$, Ser$_7$, and Arg$_{10}$, as well as the *N*-methylamine terminus make hydrophilic face. The *N*-methyl group of *N*-Me-D-Gln$_4$ points outward from the dimer, thus blocking further assembly. The antiparallel β-sheet

dimer brings the *N*-methylamine terminus of each monomer subunit into proximity of the macrolactam ring of the other monomer subunit and allows each methylamine group to hydrogen bond to a chloride anion.

The X-ray crystallographically structure of azateixobactin analogue **2a** reveals a mode of antiparallel β-sheet assembly distinct from that which we had previously reported.[5] In our previous X-ray crystallographic antiparallel β-sheet dimer, the residues 1–7 also create an amphipathic dimerization interface (**Figure 5.4**). The antiparallel β-sheet dimer assembly also brings each *N*-terminus into the proximity of the binding site and allows each *N*-terminus to hydrogen bond to the anion. However, there are three significant differences between the current antiparallel β-sheet dimer (**2a**) and our previously reported antiparallel β-sheet dimer: (1) The dimerization interfaces involve opposite edges of the β-sheets. In the current structure, residues 3 and 5 form hydrogen-bonded pairs; in our previously reported structure, residues 2 and 6 form hydrogen-bonded pairs (**Figures 5.3D and 5.4D**). (2) The psi and phi angles of Ser_7 differ dramatically between the two structures, thus rotating the macrocycle toward the dimerization interface of each structure. (3) The dimer in the current structure binds two chloride anions, while the dimer in our previously reported structure binds two sulfate anions. Although the details of the crystallographic structures of the previous and current dimers differ, both structures are consistent with the model shown in **Figure 5.1A**.

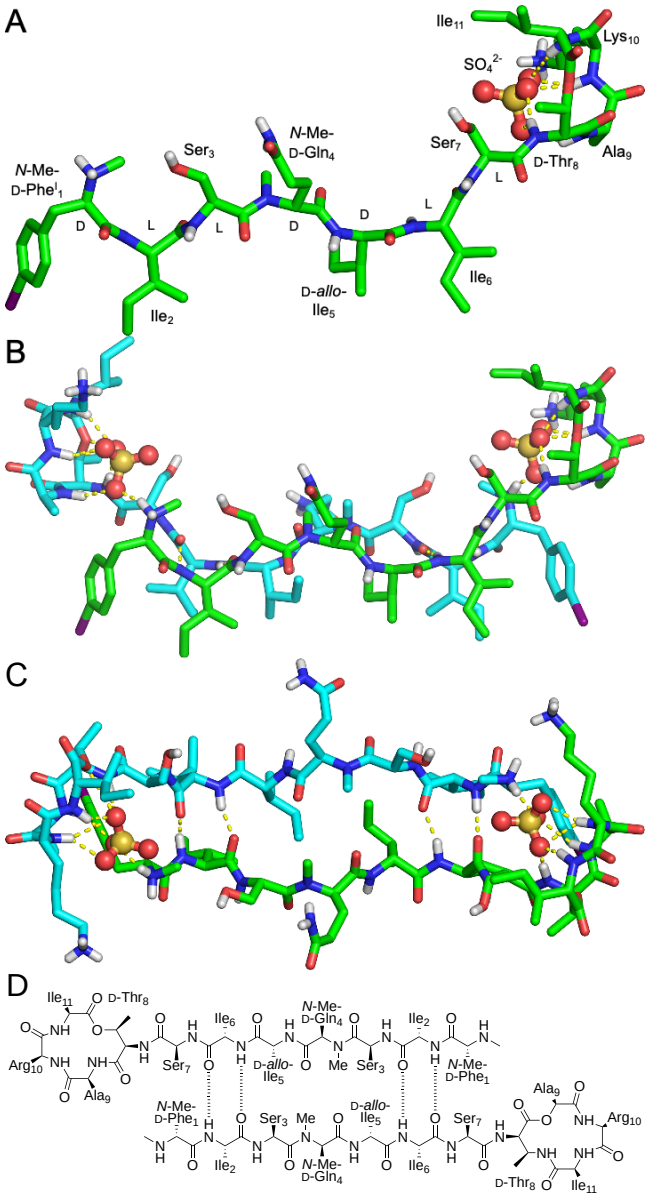

Figure 5.4. X-ray crystallographic structure of the *N*-Me-D-Phe$^{I}_{1}$,*N*-Me-D-Gln$_4$,Lys$_{10}$-teixobactin binding sulfate anion (PDB 6E00). (A) Monomer. (B) Side view. (C) Top view. (D) Alignment of the dimer assembly.

Ring-expanded Teixobactin Analogues.

The 13-membered macrolactone ring of teixobactin is substantially smaller than that of many other cyclic depsipeptide antibiotics that bind lipid II,[22] including ramoplanin[23] (49-

membered macrolactone), lysobactin/katanosin B[24] (28-membered macrolactone), and plusbacin A3 [25] (28-membered macrolactone). Our X-ray crystallographic structures of teixobactin analogues bound to chloride and sulfate anions suggest that a larger ring might allow teixobactin analogues to better accommodate the larger polyphosphate group of lipid II and related cell-wall precursors. Inspired by our X-ray crystallographic structures and the larger macrolactone rings of other antibiotics, we set out to explore the effect of the teixobactin macrolactone ring size upon antibiotic activity. In this section, we expand the 13-membered macrolactone ring to 14-, 15-, and 16-membered macrolactone rings with β^3-homo amino acids.

We synthesized seven ring-expanded teixobactin analogues containing 1–3 β^3-homo amino acids at positions 9, 10, and 11 (**Figure 5.5**) and assessed their activity in MIC assays (**Table 5.3**). Six out of seven ring-expanded teixobactin analogues exhibited activity against Gram-positive bacteria, indicating teixobactin pharmacophore tolerates ring expansion. β^3h-Arg_{10}-teixobactin (**5**) and β^3h-Arg_{10},β^3h-Ile_{11}-teixobactin (**9**) exhibit comparable activity to Arg_{10}-teixobactin. Molecular modeling studies suggest that the ring expanded analogues are more flexible and that the NH groups of the rings are less well aligned to bind anions (**Figures S5.3 and S5.4**). Collectively, the MIC and molecular modeling studies suggest that the 13-membered ring of teixobactin may provide an optimal balance of size and preorganization for lipid II binding.

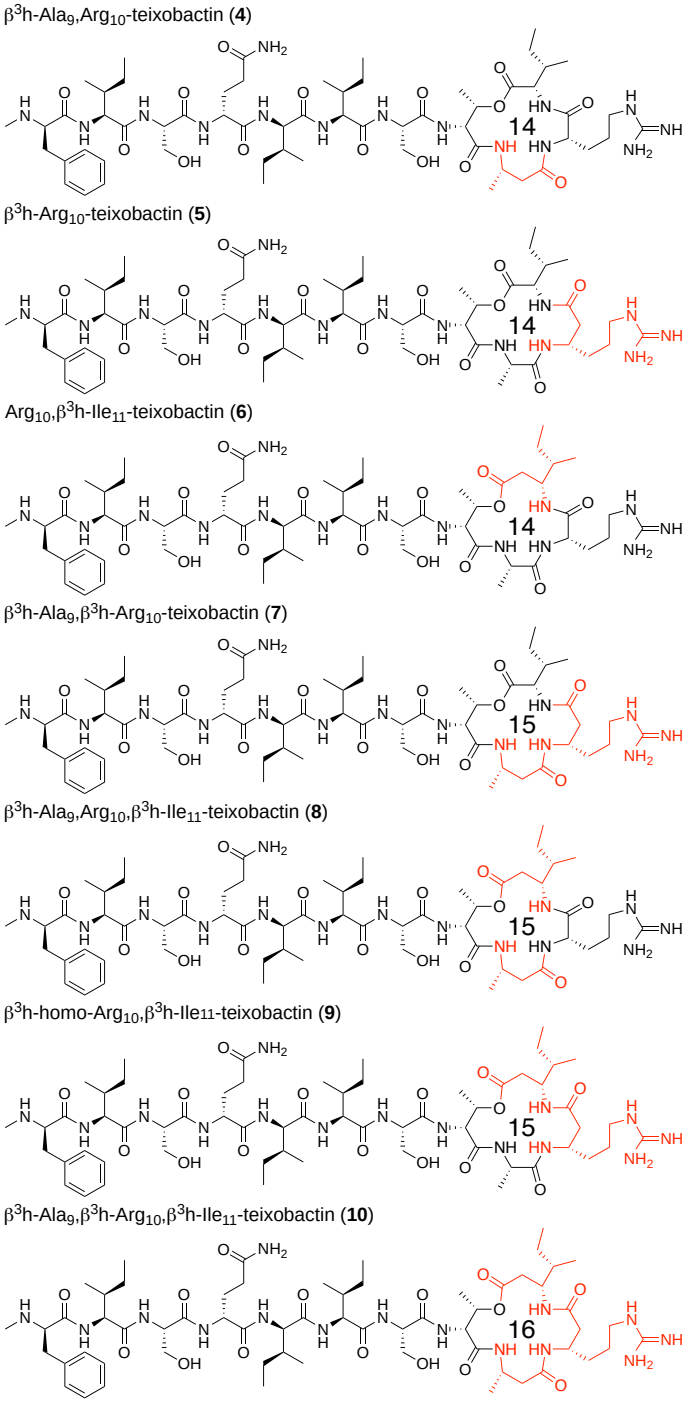

Figure 5.5. Structures of 14-, 15-, and 16-membered ring-expanded teixobactin analogues containing β^3-homo amino acids at positions 9, 10, and 11.

Table 5.3. MIC values of ring-expanded teixobactin analogues in μg/mL.

Ring size		*Staphylococcus aureus* ATCC 29213	*Staphylococcus epidermidis* ATCC 14990	*Bacillus subtilis* ATCC 6051	*Escherichia coli* ATCC 10798
13	Arg_{10}-teixobactin (**1a**)	2	1	2	>32
14	β^3h-Ala,Arg_{10}-teixobactin (**4**)		4	4	>32
14	β^3h-Arg_{10}-teixobactin (**5**)		1	2	>32
14	Arg_{10},β^3h-Ile_{11}-teixobactin (**6**)		2	8	>32
15	β^3h-Ala_9,β^3h-Arg_{10}-teixobactin (**7**)		>32	>32	>32
15	β^3h-Ala_9,Arg_{10},β^3h-Ile_{11}-teixobactin (**8**)		16	8	>32
15	β^3h-Arg_{10},β^3h-Ile_{11}-teixobactin (**9**)		1	0.5	>32
16	β^3h-Ala_9,β^3h-Arg_{10},β^3h-Ile_{11}-teixobactin (**10**)		2	4	>32
	teixobactin	0.25	0.25	0.25-0.5	>32
	vancomycin	0.25	0.25	0.5	>32

Conclusion

Lactam analogues of teixobactin containing aza-threonine at position 8 are readily prepared by solid-phase synthesis, with conversion of the corresponding diastereomeric threonine analogue to the aza-threonine analogue by mesylation, azide SN2 displacement, and Staudinger reduction with triphenylphosphine-2-carboxamide. Teixobactin analogues containing all four diastereomers of aza-threonine can be prepared by this route. Replacement of the lactone ring oxygen with an NH group substantially increases antibiotic activity, with D-aza-Thr_8,Arg_{10}-teixobactin (**2a**) exhibiting 2–8 fold greater antibiotic activity than Arg_{10}-teixobactin (**1a**). Polysorbate 80 exhibits a dramatic effect on the antibiotic activity of teixobactin and teixobactin analogues; D-aza-Thr_8,Arg_{10}-teixobactin exhibits an MIC of 0.008 μg/mL against *S. aureus* in the presence of 0.002% polysorbate 80.

X-ray crystallography reveals that the additional NH group of azateixobactin analogue **3a** hydrogen bonds to a bound chloride anion and supports a model in which azateixobactin analogues achieve enhanced antibiotic activity by better binding to the anionic pyrophosphate group of lipid II and related cell-wall precursors. The X-ray crystallographic structure further

supports a model in which the formation of hydrogen-bonded dimers or amyloid-like higher order assemblies is central to antibiotic activity, with two molecules of teixobactin or a teixobactin analogue coordinating to the bound anion. Although ring-expanded teixobactin analogues were hypothesized to better accommodate the pyrophosphate group of lipid II and related cell-wall precursors, teixobactin analogues containing β^3-homo amino acids exhibited no greater antibiotic activity. Collectively, these studies illustrate how chemical synthesis, X-ray crystallography, and antibiotic activity assays may be used together to help elucidate teixobactin. We anticipate that these studies will facilitate the design of teixobactin analogues with improved properties that are useful in the clinic.

References and Notes

1 Ling, L. L.; Schneider, T.; Peoples, A. J.; Spoering, A. L.; Engels, I.; Conlon, B. P.; Mueller, A.; Schäberle, T. F.; Hughes, D. E.; Epstein, S.; Jones, M.; Lazarides, L.; Steadman, V. A.; Cohen, D. R.; Felix, C. R.; Fetterman, K. A.; Millett, W. P.; Nitti, A. G.; Zullo, A. M.; Chen, C.; Lewis, K. A new antibiotic kills pathogens without detectable resistance. *Nature* **2015**, *517*, 455–459.

2 Homma, T.; Nuxoll, A.; Gandt, A. B.; Ebner, P.; Engels, I.; Schneider, T.; Götz, F.; Lewis, K.; Conlon, B. P. Dual Targeting of Cell Wall Precursors by Teixobactin Leads to Cell Lysis. *Antimicrob Agents Chemother.* **2016**, *60*, 6510–6517.

3 Breukink, E.; de Kruijff, B. Lipid II as a target for antibiotics. *Nat. Rev. Drug Discov.* **2006**, *5*, 321–323.

4 Atkinson, D. J.; Naysmith, B. J.; Furkert, D. P.; Brimble, M. A. Enduracididine, a rare amino acid component of peptide antibiotics: Natural products and synthesis. *Beilstein J. Org. Chem.* **2016**, *12*, 2325–2342.

5 Yang, H; Wierzbicki, M.; Du Bois, D. R.; Nowick, J. S. X-ray Crystallographic Structure of a Teixobactin Derivative Reveals Amyloid-like Assembly. *J. Am. Chem. Soc.* **2018**, *140*, 14028–14032.

6 Zong, Y.; Fang, F.; Meyer, K. J.; Wang, L.; Ni, Z.; Gao, H.; Lewis, K.; Zhang, J.; Rao, Y. Gram-scale total synthesis of teixobactin promoting binding mode study and discovery of more potent antibiotics. *Nat. Commun.* **2019**, *10*, 3268.

7 For related studies Ramoplanin see the reference: (1) Nam, J.; Shin, D.; Rew, Y.; Boger, D. L. Alanine Scan of [L-Dap2]Ramoplanin A2 Aglycon: Assessment of the Importance of Each Residue. J. *Am. Chem. Soc.* **2007**, *129*, 8747–8755. (2) Xie, J.; Okano, A.; Pierce, J. G.; James, R. C.; Stamm, S.; Crane, C. M.; Boger, D. L. Total Synthesis of [Ψ[C(=S)NH]Tpg^4]Vancomycin Aglycon, [Ψ[C(=NH)NH]Tpg^4]Vancomycin Aglycon, and Related Key Compounds: Reengineering Vancomycin for Dual D-Ala-D-Ala and D-Ala-D-Lac Binding. *J. Am. Chem. Soc.* **2012**, *134*, 1284−1297.

8 Yang, H.; Chen, K. H.; Nowick, J. S. Elucidation of the Teixobactin Pharmacophore. *ACS Chem. Biol.* **2016**, *11*, 1823−1826.

9 Izzo, I.; Acosta, G. A.; Tulla-Puche, J.; Cupido, T.; Martin-Lopez, M. J.; Cuevas, C.; Albericio, F. Solid-Phase Synthesis of Aza-Kahalalide F Analogues: (2R,3R)-2-Amino-3-azidobutanoic Acid as Precursor of the Aza-Threonine. *Eur. J. Org. Chem.* **2010**, 2536–2543.

10 Bartra, M.; Romea, P. Urpí, F.; Vilarrasa, J. A Fast Procedure for the Reduction of Azides and Nitro Compounds Based on the Reducing Ability of Sn(SR)3- Species. *Tetrahedron* **1990**, *46*, 587−594.

11 Saneyoshi, H.; Ochikubo, T.; Mashimo, T.; Hatano, K.; Ito, Y.; Abe, H. Triphenylphosphinecarboxamide: An Effective Reagent for the Reduction of Azides and Its Application to Nucleic Acid Detection. *Org. Lett.* **2014**, *16*, 30–33.

12 Yang, H.; Du Bois, D. R.; Ziller, J. W.; Nowick, J. S. X-ray Crystallographic Structure of a Teixobactin Analogue Reveals Key Interactions of the Teixobactin Pharmacophore. *Chem. Commun.* **2017**, *53*, 2772−2775.

13 Zong et al. reported a lactam derivative of Lys10-teixobactin bearing D-aza-threonine at position 8 and bearing biphenyl derivative of phenylalanine at position 1 exhibiting antibiotic activity comparable to natural teixobactin. [Zong, Y.; Sun, X.; Gao, H.; Meyer, K. J.; Lewis, K.; Rao, Y. Developing equipotent teixobactin analogues against drug-resistant bacteria and discovering a hydrophobic interaction between lipid II and teixobactin. *J. Med. Chem.* **2018**, *61*, 3409–3421.

14 Similar enhancements in the activity of teixobactin analogues have been observed by Parmer et al.: Parmar, A.; Iyer, A.; Prior, S. H.; Lloyd, D. G.; Leng Goh, E. T.; Vincent, C. S.; Palmai-Pallag, T.; Bachrati, C. Z.; Breukink, E.; Madder, A.; Lakshminarayanan, R.; Taylor, E. J.; Singh, I. Teixobactin analogues reveal enduracididine to be non-essential for highly potent antibacterial activity and lipid II binding. *Chem. Sci.* **2017**, *8*, 8183−8192.

15 Arhin, F. F.; Sarmiento, I.; Belley, A.; McKay, G. A.; Draghi, D. C.; Grober, P.; Sahm, D. F.; Parr, T. R. Jr.; Moeck, G. Effect of Polysorbate 80 on Oritavancin Binding to Plastic Surfaces: Implications for Susceptibility Testing. *Antimicrob. Agents Chemother*. **2008**, *52*, 1597–1603.

16 Chen, K.H.; Le, S. P.; Han, X.; Frias, J. M.; Nowick, J. S. Alanine Scan Reveals Modifiable Residues in Teixobactin. *Chem. Commun.* **2017**, *53*, 11357–11359.

17 As we had previously observed for *N*-Me-D-Phe$^{I}_{1}$,*N*-Me-D-Gln$_4$,Arg$_{10}$-teixobactin [PDB 6E00, ref 5], the *N*-methyl group substantially decreased the antibiotic activity. The MIC of **3a** was 32 μg/mL against *S. epidermidis* and *B. subtilis* in the absence of polysorbate 80.

18 Kabsch, W. XDS. *Acta Crystallogr., Sect. D: Biol. Crystallogr.* **2010**, *66*, 125−132.

19 Foadi, J.; Aller, P.; Alguel, Y.; Cameron, A.; Axford, D.; Owen, R. L.; Armour, W.; Waterman, D. G.; Iwata, S.; Evans, G. Clustering procedures for the optimal selection of data sets from multiple crystals in macromolecular crystallography. *Acta Crystallogr., Sect. D: Biol. Crystallogr.* **2013**, *69*, 1617−1632.

20 Adams, P. D.; Afonine, P.V.; Bunkoczi, G.; Chen, V. B.; Davis, I. W.; Echols, N.; Headd, J. J.; Hung, L. W.; Kapral, G. J.; Grosse-Kunstleve, R. W.; McCoy, A. J.; Moriarty, N. W.; Oeffner, R.; Read, R. J.; Richardson, D. C.; Richardson, J. S.; Terwilliger, T. C.; Zwart, P. H.

PHENIX: a comprehensive Python-based system for macromolecular structure solution. *Acta Crystallogr., Sect. D: Biol. Crystallogr.* **2010**, *66*, 213−221.

21 This observed binding site is very similar to our previously reported X-ray crystallographic structure of a truncated macrolactone teixobactin binding a chloride anion [ref 12].

22 Breukink, E.; de Kruijff, B. Lipid II as a target for antibiotics. *Nat. Rev. Drug Discov.* **2006**, *5*, 321–323.

23 Cavalleri, B.; Pagani, H.; Volpe, G.; Selva, E.; Parenti, F. RAMOPLANIN (A-16686), A NEW GLYCOLIPODEPSIPEPTIDE ANTIBIOTIC. *J. Antibiot.* **1984**, *37*, 309–317.

24 (a) Bonner, D. P.; O'Sullivan, J.; Tanaka, S. K.; Clark, J. M.; Whitney, R. R. *J. Antibiot.* **1988**, *41*, 1745−1751. (b) Kato, T.; Hinoo, H.; Terui, Y.; Kikuchi, J.; Shoji, J. *J. Antibiot.* **1988**, *41*, 719−725. (c) Shoji, J.; Hinoo, H.; Matsumoto, K.; Hattori, T.; Yoshida, T.; Matsuura, S.; Kondo, E. *J. Antibiot.* **1988**, *41*, 713−718.

25 Shoji, J.; Hinoo, H.; Katayama, T.; Nakagawa, Y.; Ikenishi, Y.; Iwatani, K.; Yoshida, T. Structures of New Peptide Antibiotics, Plusbacins A1~A4 and B1~B4. *J. Antibiot.* **1992**, *45*, 824–831.

Supporting Information

Table of contents

Supplemental figures and table

Figure S5.1. Crude HPLC traces of Boc-Ala-D-aza-Thr(CONH-Ile11-Fmoc)-Gln(Trt)-OH.

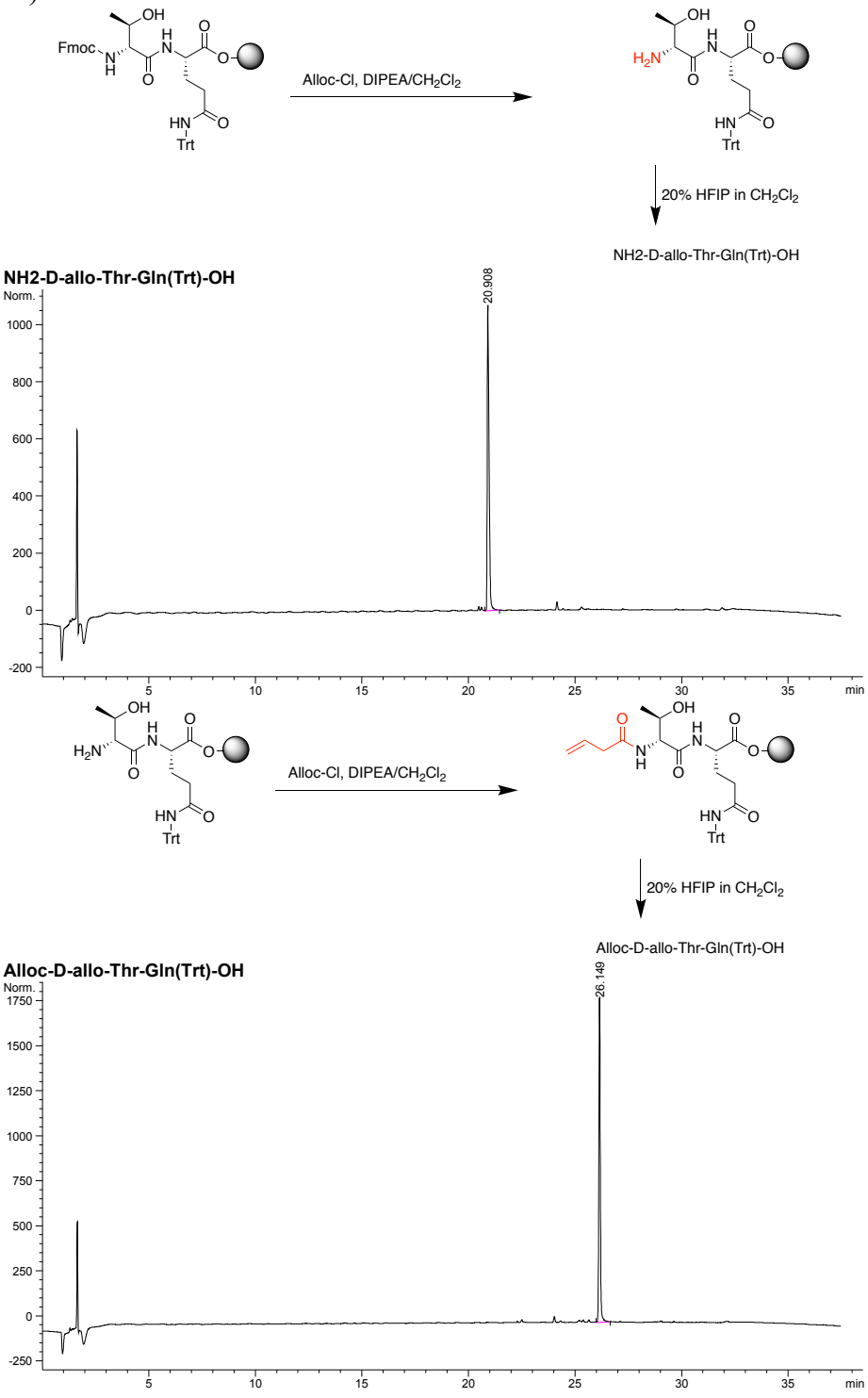

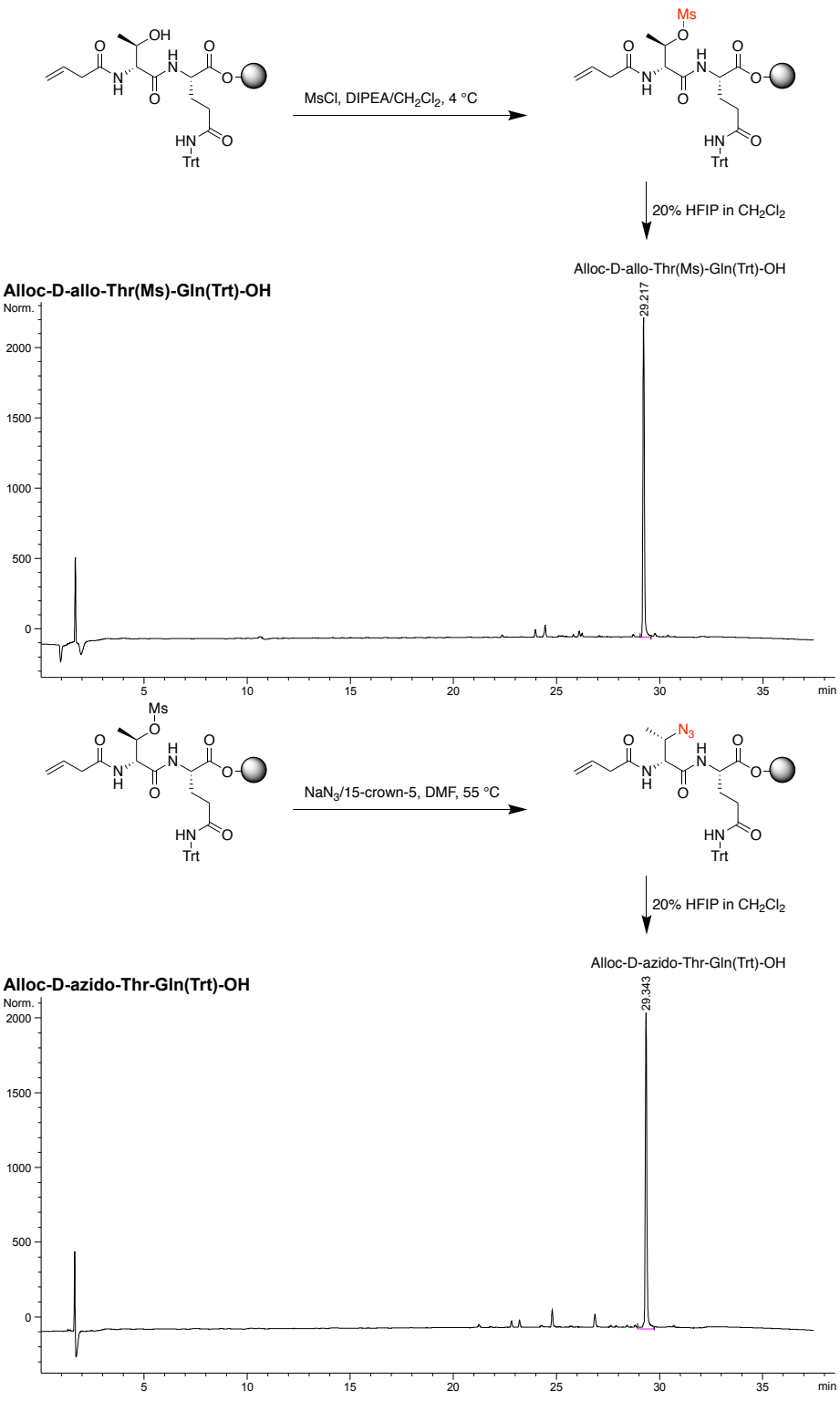
MsCl, DIPEA/CH2Cl2, 4 °C
20% HFIP in CH2Cl2
Alloc-D-allo-Thr(Ms)-Gln(Trt)-OH
Alloc-D-allo-Thr(Ms)-Gln(Trt)-OH
Norm.
29.217
min
NaN3/15-crown-5, DMF, 55 °C
20% HFIP in CH2Cl2
Alloc-D-azido-Thr-Gln(Trt)-OH
Alloc-D-azido-Thr-Gln(Trt)-OH
Norm.
29.343
min

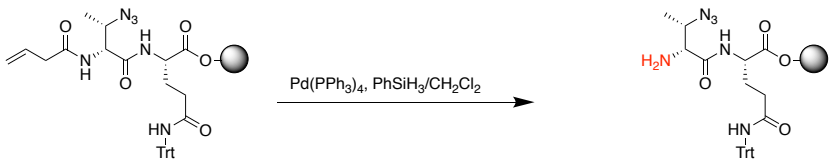

20% HFIP in CH_2Cl_2

NH_2-D-azido-Thr-Gln(Trt)-OH

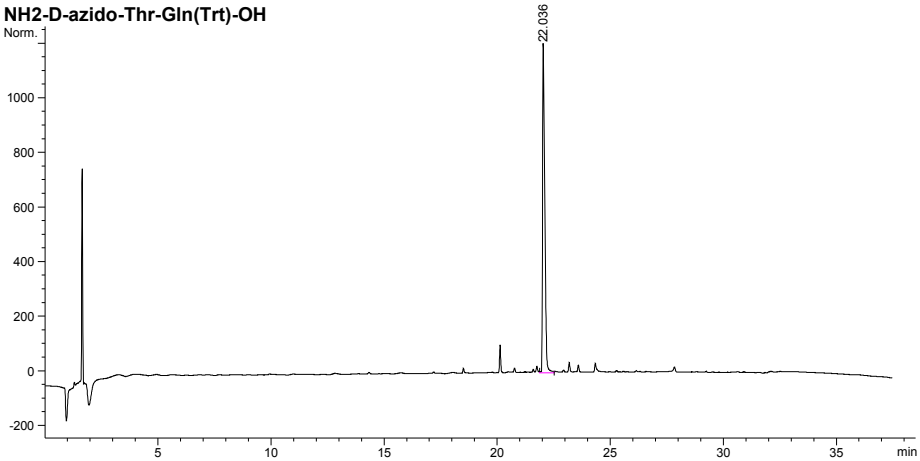

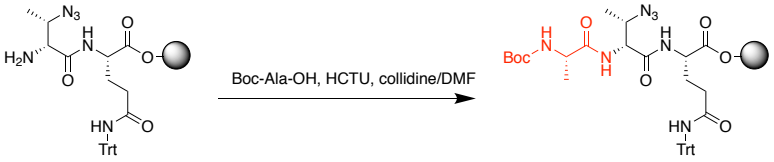

20% HFIP in CH_2Cl_2

Boc-Ala-D-azido-Thr-Gln(Trt)-OH

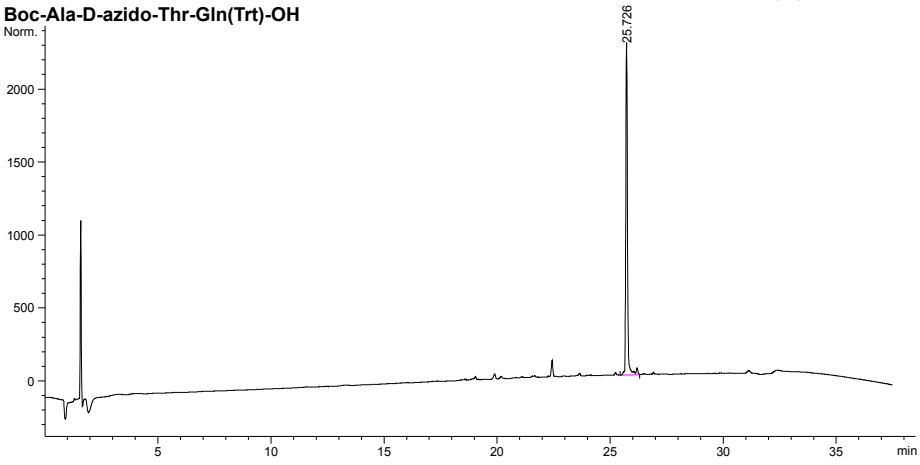

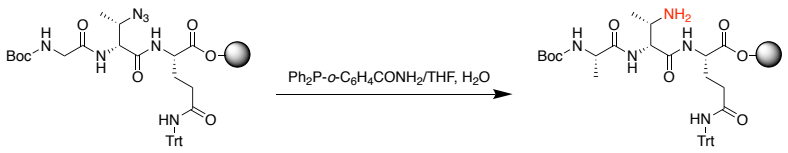

Boc-Ala-D-aza-Thr-Gln(Trt)-OH

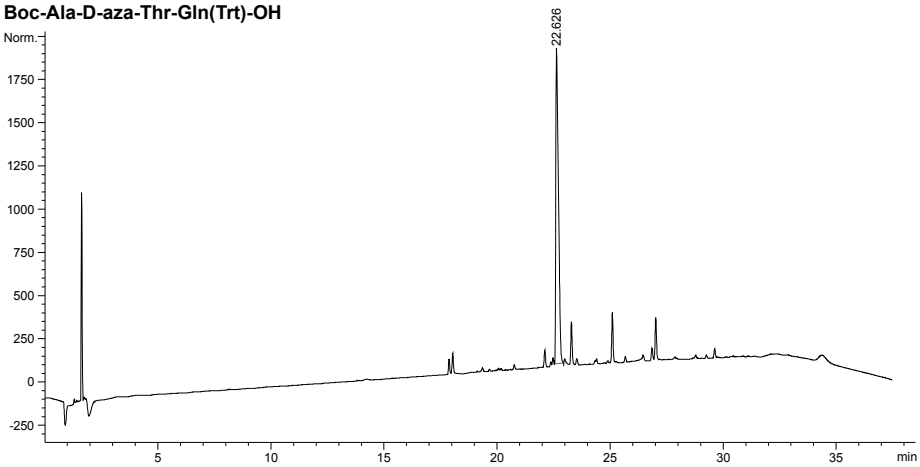

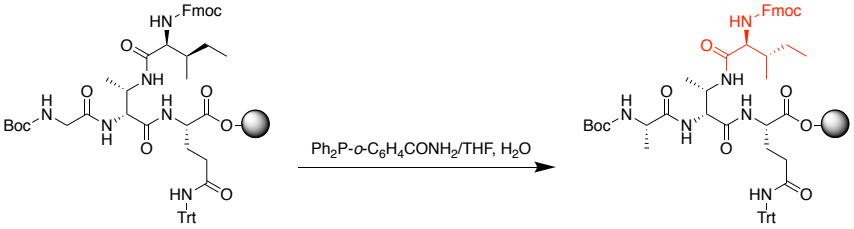

Boc-Ala-D-aza-Thr(CONH-Ile-NH-Fmoc)Gln(Trt)-OH

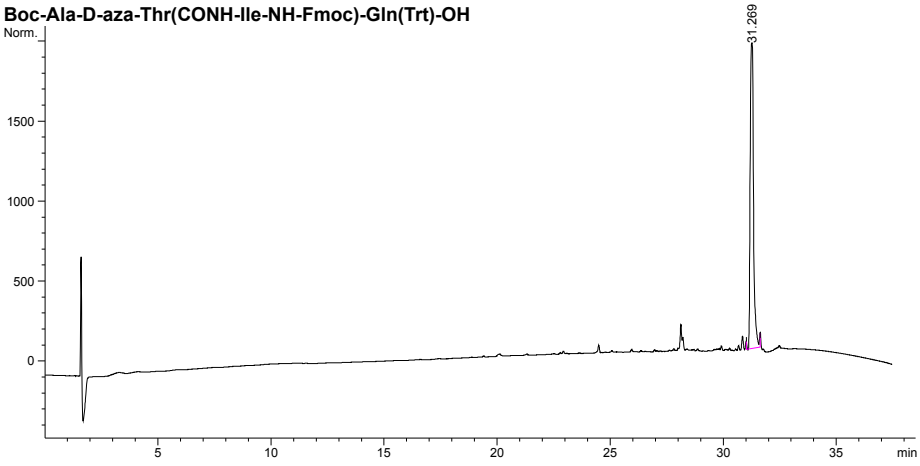

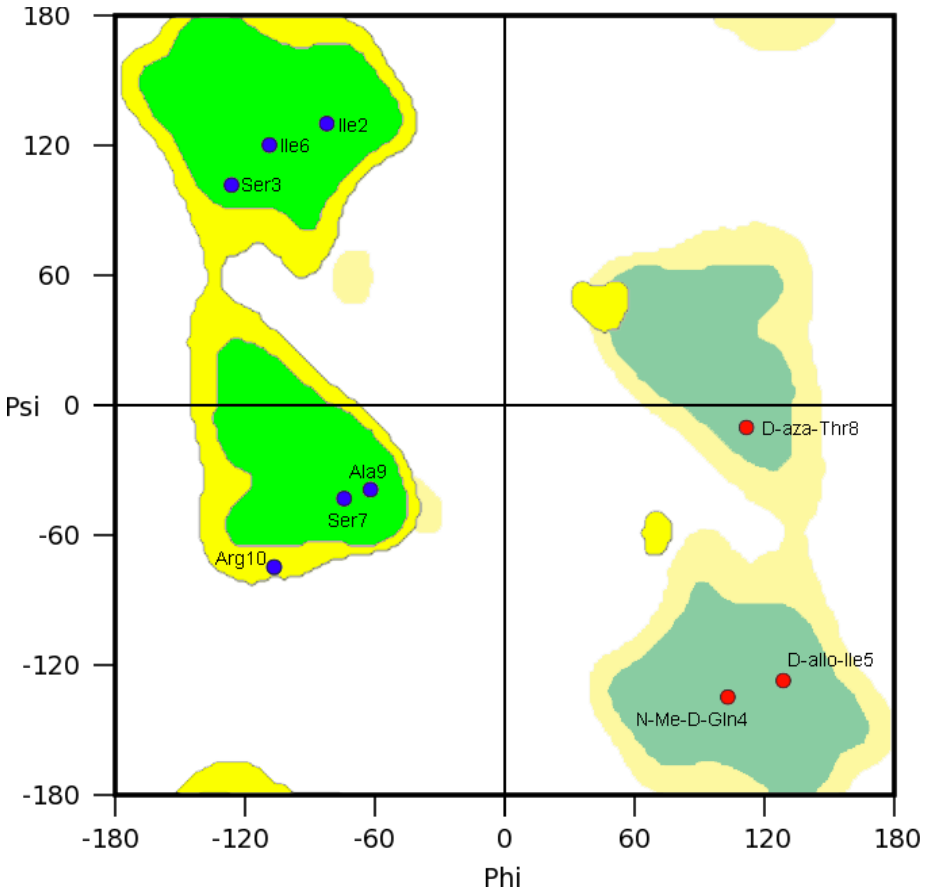

Figure S5.2. Ramachandran plot illustrating the ϕ and φ angles of residues 2–10 of *N*-Me-D-Gln$_4$,D-aza-Thr$_8$,Arg$_{10}$-teixobactin (**2a**). The green regions correspond to preferred dihedral angles for L-peptides and proteins; the yellow regions correspond to allowed regions for L-peptides and proteins; the pastel green and pastel yellow regions correspond to preferred and allowed dihedral angles for D-peptides and proteins.

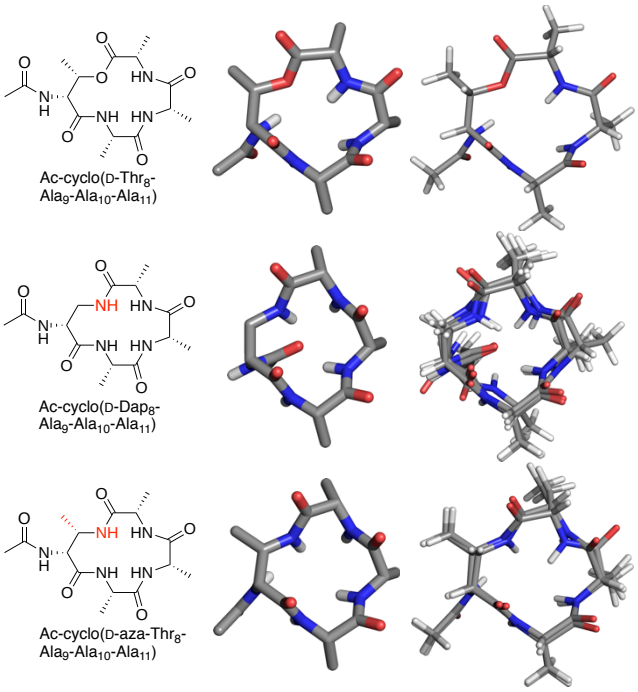

Figure S5.3. Molecular models of low-energy conformers of macrocycles from teixobactin and aza-teixobactin analogues. The models were generated by conformational searching in MacroModel using the MMFFs force field and GB/SA water solvation. Conformers represent the global minimum and all local-energy conformers within 5.0 kJ/mol of the global minimum.

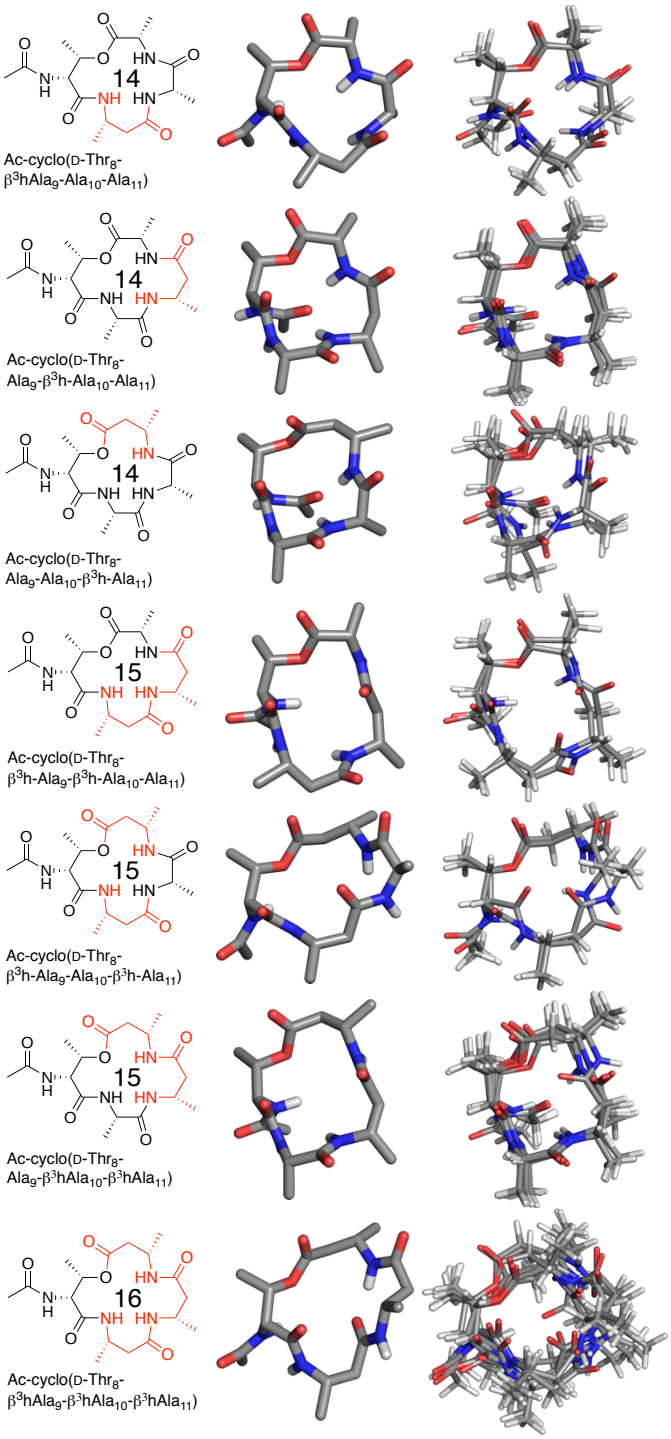

Figure S5.4. Molecular models of low-energy conformers of macrocycles from ring-expanded macrolactone teixobactin analogues containing β-homo alanines. The models were generated by conformational searching in MacroModel using the MMFFs force field and GB/SA water solvation. Conformers represent the global minimum and all local-energy conformers within 5.0 kJ/mol of the global minimum.

Table S5.1. MIC values of teixobactin homologues in µg/mL with 0.002% polysorbate 80.

Ring size		*Staphylococcus aureus* ATCC 29213	*Staphylococcus epidermidis* ATCC 14990	*Bacillus subtilis* ATCC 6051	*Escherichia coli* ATCC 10798
13	Arg_{10}-teixobactin (**1a**)	0.06	0.13	0.06	>8
14	β^3h-Ala,Arg_{10}-teixobactin (**4**)		4		>8
14	β^3h-Arg_{10}-teixobactin (**5**)		0.13		>8
14	Arg_{10},β^3h-Ile_{11}-teixobactin (**6**)		2		>8
15	β^3h-Ala_9,β^3h-Arg_{10}-teixobactin (**7**)		>8		>8
15	β^3h-Ala_9,Arg_{10},β^3h-Ile_{11}-teixobactin (**8**)		>8		>8
15	β^3h-Arg_{10},β^3h-Ile_{11}-teixobactin (**9**)		0.13		>8
16	β^3h-Ala_9,β^3h-Arg_{10},β^3h-Ile_{11}-teixobactin (**10**)		2		>8
	teixobactin	<0.008	<0.008	<0.008	>8
	vancomycin	0.125	0.25	0.25	>8

Materials and Methods

General information

Methylene chloride (CH_2Cl_2) was passed through alumina under argon prior to use. Amine-free *N*,*N*-dimethylformamide (DMF) was purchased from Alfa Aesar. Fmoc-D-*allo*-Ile-OH was purchased from Santa Cruz Biotechnology. Fmoc-*N*-Me-D-Gln(Trt)-OH was purchased from ChemPep. Other protected amino acids were purchased from CHEM-IMPEX. 2-(Diphenylphosphino)benzoic acid was purchased from Arctom chemicals. Preparative reverse-phase HPLC was performed on a Rainin Dynamax instrument equipped with an Agilent Zorbax SB-C18 column. Analytical reverse-phase HPLC was performed on an Agilent 1260 Infinity II instrument equipped with a Phenomonex Aeris PEPTIDE 2.6μ XB-C18 column. HPLC grade acetonitrile (MeCN) and deionized water (18 MΩ) containing 0.1% trifluoroacetic acid (TFA) were used as solvents for both preparative and analytical reverse-phase HPLC. Deionized water (18 MΩ) was obtained from a Barnstead NANOpure Diamond water purification system. Teixobactin analogues **2a–10** were prepared and studied as the trifluoroacetate salts.

Synthesis of D-aza-Thr$_8$,Arg$_{10}$-teixobactin (3a)

Resin Loading. 2-Chlorotrityl chloride resin (300 mg, 1.2 mmol/g) was added to a 10-mL Bio-Rad Poly-Prep chromatography column. The resin was suspended in dry CH_2Cl_2 (5 mL) and allowed to swell for 15 minutes. The CH_2Cl_2 was dispensed with a flow of nitrogen. The resin was loaded with a solution of Fmoc-Ala-OH (90 mg, 0.29 mmol, 2 equiv) and 2,4,6-collidine (300 μL) in dry CH_2Cl_2 (7 mL) and rocked for 4 hours.

Resin Capping. The solution was dispensed with a flow of nitrogen and washed with dry CH_2Cl_2 (3x). A mixture of CH_2Cl_2 (5 mL), MeOH (0.8 mL), and DIPEA (0.4 mL) was made and

poured into the Poly-Prep column containing the resin and rocked for 1 h to cap any unreacted sites in the resin. The solution was dispensed with a flow of nitrogen and washed with dry CH_2Cl_2 (3x). The resin was washed with MeOH and blown with nitrogen until dry resin was observed.

Loading Check. Approximately 1 mg of the dry resin was weighed out into a scintillation vial and 20% piperidine in DMF (3 mL) was added. The vial was rocked for 30 minutes. The mixture was filtered using a Pasteur pipet plugged with glass wool. The UV/Vis spectrometer was blanked at 290 nm with a cuvette filled with 20% piperidine in DMF. The absorbance of the filtered mixture was measured [1.4 mg of resin weighed; A_{290} = 1.1234; 0.15 mmol loading].

Fmoc deprotection. The loaded resin was transferred to a solid-phase peptide hand coupling vessel. The resin was washed with dry CH_2Cl (3x) and then dry DMF (3x). To the reaction vessel, 20% piperidine in dry DMF (5 mL) was added. Using a nitrogen flow to bubble the hand coupling vessel, the reaction was mixed for 20 minutes. The resin was washed with dry DMF (3x).

Coupling Fmoc-D-allo-Thr-OH with HCTU. Based on loading, Fmoc-D-*allo*-Thr-OH (105 mg, 0.30 mmol, 2 equiv) and HCTU (121 mg, 0.30 mmol, 2 equiv) were weighed out and dissolved in 20% collidine in dry DMF. This solution was added to the reaction vessel containing the deprotected peptide on resin. Using a nitrogen flow to bubble the hand coupling vessel, the reaction was mixed for 4 h. The resin was washed with dry DMF (3x).

Fmoc deprotection. To the reaction vessel, 20% piperidine in dry DMF (5 mL) was added. Using a nitrogen flow to bubble the hand coupling vessel, the reaction was mixed for 20 minutes. The resin was washed with dry DMF (3x).

Alloc protection. The resin was transferred to a Poly-Prep column with dry DMF and the solution was dispensed with a flow of nitrogen. The resin was washed with dry CH_2Cl_2 (3x). To resin in Poly-Prep column, dry CH_2Cl_2 (5 mL), DIPEA (38 µL, 0.23 mmol, 1.5 equiv) and ally chloroformate (23 µL, 0.23 mmol, 1.5 equiv) were added sequentially then capped and mixed on a rocker for 1 h. The resin was washed with dry CH_2Cl (3x).

Mesylation. Dry CH_2Cl_2 (6 mL) was added to the resin in Poly-Prep column and then capped and rocked in a cold room (4 °C) for 15 min. DIPEA (254 µL, 1.5 mmol, 10 equiv) was directly added to the solution in the Poly-Prep column was rocked in a cold room (4 °C) for additional 15 min. Methanesulfonyl chloride (113 µL, 1.5 mmol, 10 equiv) was directly added to the solution in the Poly-Prep column was rocked in a cold room (4 °C) for additional 15 min. The resin was washed with dry CH_2Cl_2 (3x) then with dry DMF (3x). The resin was transferred to the hand coupling vessel.

S_N2 with NaN_3. NaN_3 (474 mg, 7.5 mmol, 50 equiv) was carefully weighed out using the back of a glass Pasteur pipette into a glass test tube (to avoid possible explosive of NaN_3 with metal or acid). The weighed out NaN_3 was transferred to the resin in the hand coupling vessel containing resin. Dry DMF (1 mL) and 15-crown-5 (1 mL) were added to the hand coupling vessel. [NaN_3 is super saturated in the solvent mixture] A tube with a continuous water flow at 55 °C was wrapped around the hand coupling vessel to provide heating. Using a gentle nitrogen flow, the mixture was bubbled for 12 h at 55 °C. The resin was washed with 10 mL of 20% H_2O in THF (5x) to remove any excess NaN_3. The resin was transferred to a Poly-Prep column with dry DMF and then washed with dry CH_2Cl_2 (3x).

Alloc deprotection. A mixture of CH_2Cl_2 (5 mL), tetrakis(triphenylphosphine)palladium(0) (16.9 mg, 0.015 mmol, 0.1 equiv) and phenylsilane

(360 μL, 3 mmol, 20 equiv) was added to the resin and rocked for 30 minutes. The resin was washed with dry CH_2Cl_2 (3x) then with dry DMF (3x) and transferred to a hand coupling vessel.

Peptide coupling. The linear peptide was synthesized through the following cycles: *i*. coupling of amino acid (0.60 mmol, 4 equiv) with HCTU (241 mg, 0.60 mmol, 4 equiv) in 20% (v/v) 2,4,6-vollidine in dry DMF (3 mL) for 30 min, ii. resin washing with dry DMF (3x), *iii*. Fmoc deprotection with 20% (v/v) piperidine in dry DMF (3 mL) for 20 min, and *iv*. resin washing with dry DMF (3x). For D-to-L and L-to-D amino acid couplings, the reaction time in step *i* was increased to 1 h. After completing the linear synthesis, the resin was transferred to a 10-mL Bio-Rad Poly-Prep chromatography column. The resin was then washed with dry DMF (3x) and then dry THF (3x).

Azide reduction. Triphenylphosphine-2-carboxamide[1] (223 mg, 0.45 mmol, 5 equiv) in THF (5 mL) was added to the resin in a Poly-Prep chromatography column and rocked for 4 h. The solution was dispensed with a flow of nitrogen and 20% H_2O in THF (5 mL) was added and rocked for 4 h. The resin was washed with dry DMF (3x) and transferred to a hand coupling vessel using DMF.

Peptide synthesis. The coupling and Fmoc deprotection of Ile_{11} and Arg_{10} was performed as described above. After Fmoc deprotection of Arg_{10}, the resin containing branched linear peptide was transferred to 10-mL Bio-Rad Poly-Prep chromatography column using DMF. The resin was washed with dry DMF (3x) and then with dry CH_2Cl_2 (3x).

Cleavage of the branched linear peptide from the resin. To cleave the peptide, the resin was treated with 20% hexafluoroisopropanol in dry CH_2Cl_2 (7 mL) followed by gentle agitation on a rocker for 30 min. The filtrate was collected in a round-bottom flask. The resin was washed with a second aliquot of 20% hexafluoroisopropanol (7 mL). The filtrates were combined and

concentrated under reduced pressure to afford a clear oil. The oil was placed under vacuum (≤ 100 mTorr) to remove any residual solvents.

Macrolactamization. To the round-bottom flask containing cleaved peptide, a mixture of HBTU (332 mg, 0.9 mmol, 6 equiv) and HOBT (118 mg, 0.9 mmol, 6 equiv) in dry DMF (50 mL) was added and stirred for 15 min under nitrogen. Diisopropylamine (153 μL, 0.9 mmol, 6 equiv) was added to the stirring solution and then stirred 12 h under nitrogen. The solution was evaporated by rotary evaporator and the residue was dried under vacuum (≤ 100 mTorr) to give pale yellow pellet.

Global Deprotection. A solution of TFA (9 mL), H_2O (0.5 mL), and TIPS (0.5 mL) was added to the round-bottom flask containing cyclized peptide and stirred for 1 h under nitrogen. evaporated by rotary evaporator and the residue was dried under vacuum (≤ 100 mTorr).

Purification. The globally deprotected peptide was dissolved in approximately 35% CH_3CN in H_2O (10 mL) and centrifuged at 14,000 rpm for 5 min. the solution was filtered through a 0.20-μm nylon filter. The peptide was purified by reverse-phase HPLC with H_2O/CH_3CN (gradient elution of 20-95% CH_3CN with 0.1% TFA). Pure fractions analyzed by analytical HPLC and electrospray ionization (ESI) mass spectrometry were combined and lyophilized. D-aza-Thr_8,Arg_{10}-teixobactin (**2a**) was isolated as trifluoroacetic acid (TFA) salt of a 13.5 mg white powder with ≥95% purity. Other related aza-threonine teixobactin analogues (**2b–2d**) were prepared in a similar procedure.

For ring-expanded teixobactin analogues containing β^3h-amino acids (**4–10**), were synthesized as the trifluoroacetate salts using the procedures we have previously reported.[2] Dry DMF was used instead of a mixture of $CH_3CN/THF/CH_2Cl_2$ for the cyclization step.

Minimum inhibitory concentration (MIC) assay of teixobactin analogue

MIC assays of teixobactin and teixobactin analogues (**2a–10**) were performed using the procedure we have previously reported.[2,3] The procedure in this section is adapted from and in some cases taken verbatim from references 2 and 3.

MIC assays of teixobactin and teixobactin analogues (**2a–10**) were determined by using a broth microdilution method according to CLSI.[4] *Staphylococcus aureus* (ATCC 29213), *Staphylococcus epidermidis* (ATCC 14990), *Bacillus subtilis* (ATCC 6051) and *Escherichia coli* (ATCC 10798) were acquired as freeze-dried powders from ATCC.

Preparation of bacterial plate stocks. A portion of freeze-dried bacteria powder was removed with a sterile loop and suspended in 5 mL of Mueller-Hinton broth in a 14-mL polypropylene round-bottom culture tube. The mixture was incubated at 37 °C while shaking overnight. The mixture was streaked on Mueller-Hinton agar plates, and the plates were incubated at 37 °C overnight to allow colonies to grow. The plates were wrapped with Parafilm and stored for subsequent experiments.

Determination of bacterial concentration (CFU/mL). Five colonies from the bacterial plate stocks were transferred to a single 14-mL polypropylene round-bottom tube containing Mueller-Hinton broth (2 mL) and the mixture was incubated at 37 °C while shaking. As the turbidity of the cell suspension mixture visually increased, a 200-µL aliquot was transferred to a 96-well plate for OD_{600} measurement. The cell suspension mixture was diluted with Mueller-Hinton broth to an OD_{600} of 0.075 as measured for a 200-µL sample in a 96-well plate (equivalent to a 0.5 McFarland standard). A 10-µL aliquot of the diluted cell suspension was diluted 1:1000 with Mueller-Hinton broth. A 10-µL aliquot of the 1:1000 diluted cell suspension mixture was further diluted 1:200 with Mueller-Hinton broth. A 100-µL aliquot of the resulting

mixture was then streaked on a Mueller-Hinton agar plate (repeated four times). The agar plates were incubated at 37 °C overnight. The number of colonies on each agar plate was counted, and the average of four plates was used to back calculate the bacterial concentration (CFU/mL) at an OD_{600} of 0.075 as measured for a 200-µL sample in a 96-well plate (equivalent to a 0.5 McFarland standard).

Table S5.2. Bacterial concentration determination.[2,3]

Bacteria	Average number of colonies per plate	Concentration at a 0.5 McFarland standard[a]
Staphylococcus aureus ATCC 29213	214	4.3 x 10^8 CFU/mL
Streptococcus salivarius ATCC 13419	25	5 x 10^7 CFU/mL
Bacillus subtilis ATCC 6051	25	5 x 10^7 CFU/mL
Escherichia coli ATCC 10798	24	4.8 x 10^7 CFU/mL

[a] OD_{600} of 0.075 as measured for a 200-µL sample in a 96-well plate

Preparing the peptide homologue stock. Solutions of D-aza-Thr_8,Arg_{10}-teixobactin (**2a**), other teixobactin homologues (**2b–10**), teixobactin and vancomycin were prepared gravimetrically by dissolving an appropriate amount of peptide in an appropriate volume of sterile DMSO to make 20 mg/mL stock solutions. The stock solutions were stored at -20 °C for subsequent experiments.

Preparing the minimum inhibitory concentration (MIC) assays. An aliquot of the 20 mg/mL peptide homologue stock solutions was diluted to 64 µg/mL with Mueller-Hinton broth. A 200-µL aliquot of the 64 µg/mL solution was transferred to a 96-well plate. Two-fold serial dilutions were made with Mueller-Hinton broth across a 96-well plate to achieve a final volume

of 100 µL in each well. The 100-µL serial diluted solutions had the following concentrations: 64, 32, 16, 8, 4, 2, 1, 0.5, 0.25, 0.125, and 0.06125 µg/mL.

Performing the minimum inhibitory concentration (MIC) assays. Five colonies from the bacterial plate stocks were selected and transferred to a single 14-mL polypropylene round-bottom tube that contained Mueller-Hinton broth (2 mL) and the mixture was incubated at 37 °C while shaking. As the turbidity of the cell suspension mixture visually increased, the mixture was diluted with Mueller-Hinton broth to OD_{600} of 0.075 as measured in a 96-well plate (equivalent to a 0.5 McFarland standard). Based on the previously determined CFU/mL (Table S2), the diluted mixture was further diluted to 1 x 10^6 CFU/mL with Mueller-Hinton broth. A 100-µL aliquot of the 1 x 10^6 CFU/mL bacterial solution was added to each well in 96-well plates, resulting final bacteria concentration of 5 x 10^5 CFU/mL in each well. As 100-µL of bacteria were added to each well, peptide homologue solution was also diluted down to the following concentrations: 32, 16, 8, 4, 2, 1, 0.5, 0.25, 0.125, 0.0625, and 0.03125 µg/mL. The plate was covered with a lid and incubated at 37 °C for 16 h. The OD_{600} was measured using a 96-well UV/Vis plate reader (MultiSkan GO, Thermo Scientific). The MIC values were taken as the lowest concentration that had no bacteria growth. Each MIC assay was run in duplicate in three independent runs to ensure reproducibility.

Performing the minimum inhibitory concentration (MIC) assays with Mueller-Hinton broth containing 0.002% polysorbate 80. Mueller-Hinton broth containing 0.002% (v/v) polysorbate 80 was autoclaved and used to dilute the 20 mg/mL DMSO peptide stock solution and the bacteria culture.

Crystallization of *N*-Me-D-Gln$_4$,D-aza-Thr$_8$,Arg$_{10}$-teixobactin (3a)[5]

N-Me-D-Gln$_4$,D-aza-Thr$_8$,Arg$_{10}$-teixobactin (**3a**) was dissolved in 0.2 micron syringe filtered NANOpure H_2O (10 mg/mL). Crystallization conditions were screened by screening in a 96-well plate format using three crystallization kits from Hampton Research (PEG/Ion, Index, and Crystal Screen). Each well was loaded with 100 µL of a different mother liquor solution from the kits. The hanging drops were set up using a TTP Labtech Mosquito® liquid handling instrument. Hanging drops were made by combining an appropriate volume of *N*-Me-D-Gln$_4$,D-aza-Thr$_8$,Arg$_{10}$-teixobactin (4a) with an appropriate volume of well solution to create three 150-nL hanging drops with 1:1, 1:2, and 2:1 peptide:well solution. Hexagonal prism -shaped crystals grew in all conditions that contained polyethylene glycol (PEG) and chloride salts.

Crystal growth was optimized using conditions containing HEPES Na, PEG 400 and $CaCl_2$. In the optimization, the HEPES Na (pH 5.5-8.0), $CaCl_2$, and PEG 400 concentrations were varied across the 4x6 matrix of a Hampton VDX 24-well plate to afford crystals suitable for X-ray diffraction. The hanging drops for these optimizations were prepared on glass slides by combining 1 or 2 µL of teixobactin solution with 1 or 2 µL of well solution in ratios of 1:1, 2:1, and 1:2. Crystals that formed were checked for diffraction using a Rigaku Micromax-007 HF diffractometer with a Cu anode at 1.54 Å. As a result of the optimization, 0.16 M $CaCl_2$, 0.1 M HEPES Na pH 7.00, and 24% PEG 400 afforded crystals suitable for X-ray diffraction.

X-ray crystallographic data collection, data processing, and structure determination

Data collection was performed with the BOS/B3 software at Advanced Light Source (ALS) using beamline 8.2.2 at a wavelength of 1.771190 Å (7000 eV). The rotation method was employed and three sets of 360 images each were collected at a 1.0º rotation interval (a total of three complete 360º rotations). The three sets were processed with XDS[6], and the resulting datasets were merged with BLEND[7]. The structure was solved with SAD phasing implemented in the Hybrid Substructure Search (HySS)[8] module of the Phenix suite[9]. Chloride atom was used as sources of the anomalous signal. The initial electron density maps were generated using the substructure coordinates as initial positions in Autosol[10]. The structure was then refined with Phenix.refine[11] under Phenix using Coot[12] for model building. All B-factors were refined isotropically and riding hydrogen atoms coordinates were generated geometrically. The bond length, angles, and torsions restraints for unnatural amino acids (*N*-Me-D-Gln, D-aza-Thr, and D-*allo*-Ile) were generated with eLBOW[13] under Phenix.

Table S5.3. Crystallographic properties, crystallization conditions, data collection, and model refinement statistics for *N*-Me-D-Gln$_4$,D-aza-Thr$_8$,Arg$_{10}$-teixobactin (**3a**).

	N-Me-D-Gln$_4$,D-aza-Thr$_8$,Arg$_{10}$-teixobactin (**3a**)
PDB ID	6PSL
space group	$P3_221$
a, b, c (Å)	20.024, 20.024, 32.328
α, β, γ (˚)	90.0, 90.0, 120.0
peptides per asymmetric unit	1
crystallization conditions	0.16 M $CaCl_2$, 0.1 M HEPES Na pH 7.00, 24% PEG 400
Data collection	
wavelength (Å)	1.771190 Å (7000 eV)
resolution (Å)	15.28-2.10 (2.35-2.10)
total reflections	24455 (4809)
unique reflections	535 (144)
Multiplicity	45.7 (33.4)
completeness (%)	99.7 (100)
mean I/σ	78.2 (52.7)
R_{merge}	0.053 (0.066)
$R_{measure}$	0.053 (0.067)
$CC_{1/2}$	1.00 (0.999)
CC*	1.00 (1.00)
Refinement	
R_{work}	0.092 (0.12)
R_{free}	0.117 (0.19)
number of non-hydrogen atoms per ASU	94
RMS_{bonds}	0.014
RMS_{angles}	0.99
Ramachandran	
allowed (%)	100
outliers (%)	0
clashscore	0
average B-factor	8.89

HPLC and MS of teixobactin analogues (2a-10)

aza-D-Thr$_8$,Arg$_{10}$-teixobactin (**2a**)

aza-D-*allo*-Thr$_8$,Arg$_{10}$-teixobactin (**2b**)

aza-L-Thr$_8$,Arg$_{10}$-teixobactin (**2c**)

aza-L-*allo*-Thr$_8$,Arg$_{10}$-teixobactin (**2d**)

N-Me-D-Gln$_4$,aza-D-Thr$_8$,Arg$_{10}$-teixobactin (**3a**)

β^3h-Ala$_9$,Arg$_{10}$-teixobactin (**4**)

β^3h-Arg$_{10}$-teixobactin (**5**)

Arg$_{10}$,β^3h-Ile$_{11}$-teixobactin (**6**)

β^3h-Ala$_9$,β^3h-Arg$_{10}$-teixobactin (**7**)

β^3h-Ala$_9$,Arg$_{10}$,β^3h-Ile$_{11}$-teixobactin (**8**)

β^3h-Arg$_{10}$,β^3h-Ile$_{11}$-teixobactin (**9**)

β^3h-Ala$_9$,β^3h-Arg$_{10}$,β^3h-Ile$_{11}$-teixobactin (**10**)

References and Notes

1 Triphenylphosphine-2-carboxamide was synthesized using the procedure reported by Saneyoshi et al. MS (positive ion mode) calcd for C19H17NOP+ [M+H]+ m/z 306.10, found 306.12. [Saneyoshi, H.; Ochikubo, T.; Mashimo, T.; Hatano, K.; Ito, Y.; Abe, H. *Org. Lett.* **2014**, *16*, 30–33.]

2 Yang, H.; Chen, K. H.; Nowick, J. S. *ACS Chem. Biol.* **2016**, *11*, 1823–1826.

3 Chen, K.H.; Le, S. P.; Han, X.; Frias, J. M.; Nowick, J. S. *Chem. Commun.* **2017**, *53*, 11357–11359.

4 CLSI. *Methods for Dilution Antimicrobial Susceptibility Tests for Bacteria That Grow Aerobically. Approved Standard—Ninth Edition.* CLSI document M07-A9. Wayne, PA: Clinical and Laboratory Standards Institute; 2012.

5 The procedure in this section is adapted from and in some cases taken verbatim from Yang, H; Wierzbicki, M.; Du Bois, D. R.; Nowick, J. S. *J. Am. Chem. Soc.* **2018**, *140*, 14028−14032.

6 Kabsch, W. Acta *Crystallogr., Sect. D: Biol. Crystallogr.* **2010**, *66*, 125–132.

7 Foadi, J.; Aller, P.; Alguel, Y.; Cameron, A.; Axford, D.; Owen, R. L.; Armour, W.; Waterman, D. G.; Iwata, S.; Evans, G. *Acta Crystallogr., Sect. D: Biol. Crystallogr.* **2013**, *69*, 1617–1632.

8 Grosse-Kunstleve, R. W.; Adams, P. D. *Acta Crystallogr., Sect. D: Biol. Crystallogr.* **2003**, *59*, 1966–1973.

9 Adams, P. D.; Afonine, P. V.; Bunkoczi, G.; Chen, V. B.; Davis, I. W.; Echols, N.; Headd, J. J.; Hung, L. W.; Kapral, G. J.; Grosse-Kunstleve, R. W.; McCoy, A. J.; Moriarty, N. W.; Oeffner, R.; Read, R. J.; Richardson, D. C.; Richardson, J. S.; Terwilliger, T. C.; Zwart, P. H. *Acta Crystallogr., Sect. D: Biol. Crystallogr.* **2010**, *66*, 213–221.

10 Terwilliger, T. C.; Adams, P. D.; Read, R. J.; McCoy, A. J.; Moriarty, N. W.; Grosse-Kunstleve, R. W.; Afonine, P. V.; Zwart, P. H.; Hung L. W. *Acta Crystallogr., Sect. D: Biol. Crystallogr.* **2009**, *65*, 582–601.

11 Afonine, P. V.; Grosse-Kunstleve, R. W.; Echols, N.; Headd, J. J.; Moriarty, N. W.; Mustyakimov, M.; Terwilliger, T. C.; Urzhumtsev, A.; Zwart, P. H.; Adams. P. *Acta Crystallogr., Sect. D: Biol. Crystallogr.* **2012**, *68*, 352–367.

12 Emsley, P.; Lohkamp, B.; Scott, W. G.; Cowtan, K. *Acta Crystallogr., Sect. D: Biol. Crystallogr.* **2010**, *66*, 486–501.

13 Moriarty, N. W.; Grosse-Kunstleve, R. W.; Adams, P. D. *Acta Crystallogr., Sect. D: Biol. Crystallogr.* **2009**, *65*, 1074–1080.